

MIT LIBRARIES



3 9080 01444 3524

Aero

TJ778

.M41

.G24

no. 225

**EFFECTS OF INLET CONDITIONS ON
CENTRIFUGAL DIFFUSER PERFORMANCE**

by

Sabri Deniz

GTL Report #225

March 1997



GAS TURBINE LABORATORY
MASSACHUSETTS INSTITUTE OF TECHNOLOGY
CAMBRIDGE, MASSACHUSETTS

**EFFECTS OF INLET CONDITIONS ON
CENTRIFUGAL DIFFUSER PERFORMANCE**

by

Sabri Deniz

GTL Report #225

March 1997

This research was sponsored by Kobe Steel Ltd., Japan.

Abstract

This report examines the influence of inlet flow conditions, including Mach number, flow angle, blockage, and axial flow non-uniformity, on the performance and operating range of a straight channel centrifugal compressor diffuser. The research was carried out in a unique facility specifically developed to provide the diffuser with a controlled inlet flow. The tests were carried out for inlet Mach number up to values greater than unity and for a range of inlet flow angles up to the onset of rotating stall.

It was found that expressing the overall diffuser pressure recovery coefficient, defined using availability or mass averaged inlet total pressure, as a function of momentum averaged diffuser inlet flow angle yields a relationship which is essentially independent of diffuser inlet flow distortion, blockage, or Mach number. Further, the operating range of the diffuser was limited by the onset of rotating stall at a momentum averaged diffuser inlet flow angle ($\alpha_{\text{crit}} = 70.5^\circ \pm 0.5^\circ$), which was also independent of the inlet flow field axial distortion and Mach number.

The straight channel diffuser was designed to be comparable to a previously tested discrete passage diffuser and the performance of the two was compared; the overall pressure recovery of the former was found to be roughly 10% higher than that of the latter. Both diffuser types, straight channel and discrete passage diffuser showed similar behavior regarding the insensitivity of the performance and operating range to inlet flow axial non-uniformities and Mach number.

The report also presents information on recent developments in the area of centrifugal compressor diffusers together with a detailed review of the open literature.

Acknowledgments

Primarily, I would like to thank Professor Edward M. Greitzer, the former Director of the Gas Turbine Laboratory, for his guidance, motivation and for the helpful discussions. Working at MIT was a valuable and productive experience; I learned a lot and enjoyed my stay at the GTL very much.

Special thanks to Professor Nicholas A. Cumpsty from Whittle Laboratory, University of Cambridge, England for his advice and suggestions and to Professor Georg Gyarmathy from Turbomachinery Laboratory, Swiss Federal Institute of Technology-Zurich, Switzerland for his comments and support during my visits and conferences in Switzerland.

I also thank Dr. Gerald Guenette for his expert advice and Dr. Choon Tan for the attention and comments he provided.

The experimental facility was designed by Dr. Victor Filipenco. I wish to express my appreciation to him and to Mr. Mark Johnston for providing information that was needed for running the test rig.

The Gas Turbine Laboratory provided the framework to pursue this research. On the administrative side I wish to thank Holly Anderson, Robin Courchesne, Diana Park, and Lori Martinez, and on the facility side I thank Viktor Dubrowski, James Letendre and Bill Ames.

This research was supported by Kobe Steel Ltd. , Japan. The comments and suggestions of Dr. Fumitaka Kano, former Manager of Fluid Machinery, Mr. Yoshiteru Fukao, Manager, Turbomachinery and Mr. Takeshi Inaba, Engineer are gratefully appreciated.

I would also like to express my appreciation to Dr. Richard Alverson and Mr. David Sagre of Allison Engine Company for providing very helpful design recommendations for the design of the investigated diffuser and to Mr. Peter Tramm for his support of these efforts.

The first year of my stay at MIT was made possible by a scholarship of the Commission of the Swiss National Foundation for the Furtherance of Scientific Research. This support is gratefully acknowledged.

Last but not least, the support and encouragement of a special person in my life, Aslı during my research at MIT deserves special thanks.

Table of Contents

Abstract	I
Acknowledgments	III
Table of Contents	V
List of Figures	IX
List of Tables	XV
Nomenclature	XVII
1 Introduction and Background	1
1.1 Introduction	1
1.2 Background and Previous Research	2
1.2.1 Flow in Diffusers	2
1.2.2 Radial Diffuser Types	10
1.2.2.1 Vaned Diffuser Components	18
1.2.3 Flow Instabilities in Radial Diffusers	19
1.2.3.1 Vaneless Diffuser and Flow Instabilities	21
1.2.3.2 Vaned Diffuser and Flow Instabilities	22
1.2.3.3 Some Practices for Vaned Diffusers to Achieve a Larger Flow Range	29
1.2.4 Flow at the Impeller Exit	36
1.2.5 CFD Calculations for Centrifugal Compressor Diffusers	42
1.2.6 Radial Diffuser Investigations Important for the Present Study	49
1.3 Objectives of the Present Study	58
2 Facility and Experimental Apparatus	69
2.1 Overall Facility Description	69
2.2 Straight Channel Diffuser	70
2.3 Instrumentation	71
2.3.1 Total Pressure/Flow Angle Probe	72
2.3.2 Pressure Transducers	73
2.3.3 Temperature Measurements	74
2.3.4 Mass Flow Meter and Tachometer	75
2.3.5 Data Acquisition System	75

2.3.5a Data Acquisition Hardware	75
2.3.5b Data Acquisition Software	76
2.3.6 Operation of the Facility	76
2.4 Facility Modifications for the Straight Channel Diffuser Tests	77
3 Performance Parameters and Test Plan	89
3.1 Measured and Derived Quantities	89
3.1.1 Operating Point Definition	89
3.1.1.1 Impeller Rotor Speed	89
3.1.1.2 Venturi Mass Flow Rate	89
3.1.1.3 Impeller Performance Ratio	90
3.1.2 Total-Pressure/Flow-Angle Traverse Probe Data	92
3.1.2.1 Mach Number at the Diffuser Inlet	92
3.1.2.2 Static Temperature at the Diffuser Inlet	93
3.1.2.3 Mass Flow Continuity Verification	93
3.1.3 Diffuser Performance Parameters	94
3.1.3.1 Performance Parameters for Pressure Recovery	94
3.1.3.2 Diffuser Inlet Average and Distortion Flow Field Parameters	96
3.1.3.2.1 Total Pressure at the Diffuser Inlet	96
3.1.3.2.2 Calculation of Ideal Pressure Recovery	100
3.1.3.2.3 Flow Angle at the Diffuser Inlet	100
3.1.3.2.4 Inlet Blockage, Mass, Momentum, and Kinetic Energy Deficit and Skew Parameters	101
3.1.4 Static Pressure Measurements at Different Locations	103
3.2 Scope of Experiments	105
4 Experimental Results	111
4.1 Baseline Inlet Flow-Field Data	111
(Data Without Air Injection-Suction)	
4.2 Influence of Inlet Flow Conditions	114
(Data With Air Injection-Suction)	
4.2.1 Effect of Inlet Parameters	115
4.2.2 Static Pressure Rise in Diffuser Channel	117
4.2.3 Different Definitions of Diffuser Pressure Recovery	

Coefficient	118
4.2.4 Stall Onset Observation	119
4.3 Comparison With Discrete Passage Diffuser Results	120
4.4 Comparisons with Other Vaned Diffuser Investigations	123
5 Summary, Conclusions and Recommendations for Future Research	163
5.1 Summary and Conclusions	163
5.2 Recommendations for Future Research	164
References	169
Appendix	191
A.1 Result Summary Tables	193
A.2 Mass Flow Continuity Control	201
A.3 Circumferential Distortion at the Straight Channel Diffuser Inlet and Exit	203
A.4 Influence of Throat Blockage on Radial Diffuser Performance	207
A.5 Static Pressure Distribution in Quasi-Vaneless Space	225

List of Figures

Fig. 1.1	Flow regimes in single channel two-dimensional diffusers	60
Fig. 1.2	Vaned diffuser types	61
Fig. 1.3	General pipe diffuser geometry	62
Fig. 1.4	Straight channel diffuser geometry	63
Fig. 1.5	Stability parameter for overall centrifugal compressor stage and for each individual stage component	64
Fig. 1.6	Diffuser divergence angle versus (a) efficiency and versus (b) stable flow range. Comparison of the diffuser geometries from (a) and (b) with the single channel diffuser data	65
Fig. 1.7	Centrifugal compressor operating range as a function of channel diffuser $\Delta 2\theta$ for different vaned and pipe diffusers	66
Fig. 1.8	Meridional velocity distribution at a centrifugal compressor impeller exit	67
Fig. 1.9	(a) Measured and calculated impeller pressure ratio versus mass flow rate and (b) measured and calculated meridional velocity distribution at a centrifugal compressor impeller exit for different mass flow rates	68
Fig. 2.1	Swirl generator/Diffuser test section assembly and flow system schematic	80
Fig. 2.2	Swirl generator mechanical concept schematic	81
Fig. 2.3	Swirl generator blading	82
Fig. 2.4	Schematic of the velocity profile control slots and flow passage arrangement	83
Fig. 2.5	Straight channel diffuser channel static pressure tap locations ..	84
Fig. 2.6a	Straight channel diffuser rear wall pressure taps	85
Fig. 2.6b	Straight channel diffuser front wall pressure taps	86
Fig. 2.7	Modification of the diffuser test facility and vaned diffuser mechanical detail	87
Fig. 4.1	Constant speed characteristics, (a) Atmosphere to diffuser inlet pressure ratio versus corrected mass flow, (b) Atmosphere to diffuser exit pressure ratio versus corrected mass flow	125
Fig. 4.2	Performance map in terms of non-dimensional flow coefficient versus diffuser pressure rise	126

Fig. 4.3	(a) Flow angle, (b) absolute Mach number axial distributions at the diffuser inlet, no injection/suction, different corrected impeller speeds	127
Fig. 4.4	Mass averaged overall straight channel diffuser pressure recovery as a function of the diffuser inlet momentum averaged flow angle, no injection/suction, different corrected impeller speeds	128
Fig. 4.5	Mass averaged overall straight channel diffuser pressure recovery as a function of the diffuser inlet absolute Mach number, no injection/suction, different corrected impeller speeds	129
Fig. 4.6	Mass averaged overall straight channel diffuser pressure recovery as a function of the diffuser inlet blockage, no injection/suction, different corrected impeller speeds	130
Fig. 4.7	Mass averaged overall straight channel diffuser pressure recovery as a function of the diffuser inlet flow angle non-uniformity, no injection/suction, different corrected impeller speeds	131
Fig. 4.8	Mass averaged overall straight channel diffuser pressure recovery as a function of the diffuser inlet mass flow non-uniformity, no injection/suction, different corrected impeller speeds	132
Fig. 4.9	Static pressure distribution along the centerline of a diffuser channel for different corrected impeller speeds and plenum pressure ratios	133
Fig. 4.10	Static pressure distribution along the centerline of a diffuser channel for different plenum pressure ratios and for a corrected impeller speed	134
Fig. 4.11	(a) Flow angle and (b) absolute Mach number axial distributions at the diffuser inlet, with injection/suction (Series II/Profile A/N = 2000 RPM)	135
Fig. 4.12	(a) Flow angle and (b) absolute Mach number axial distributions at the diffuser inlet, with injection/suction (Series II/Profile B/N = 2000 RPM)	136
Fig. 4.13	(a) Flow angle and (b) absolute Mach number axial distributions at the diffuser inlet, with injection/suction (Series II/Profile A/N = 5000 RPM)	137
Fig. 4.14	(a) Flow angle and (b) absolute Mach number axial distributions at the diffuser inlet, with injection/suction (Series II/Profile B/N = 5000 RPM)	138

Fig. 4.15	Flow angle axial distributions at the diffuser inlet, with injection/suction (Series III/Profile A/N = 2000 RPM)	139
Fig. 4.16	(a) Flow angle and (b) absolute Mach number axial distributions at the diffuser inlet, with injection/suction (Series IV/Profile A/N = 2000 RPM)	140
Fig. 4.17	(a) Flow angle and (b) absolute Mach number axial distributions at the diffuser inlet, with injection/suction (Series IV/Profile B/N = 6000 RPM)	141
Fig. 4.18	(a) Flow angle and (b) absolute Mach number axial distributions at the diffuser inlet, with injection/suction (Series IV/Profile C/N = 4000 RPM)	142
Fig. 4.19	Mass averaged overall straight channel diffuser pressure recovery as a function of the diffuser inlet momentum averaged flow angle, with and without injection/suction	143
Fig. 4.20	Mass averaged overall straight channel diffuser pressure recovery as a function of the diffuser inlet absolute Mach number, with and without injection/suction	144
Fig. 4.21	Mass averaged overall straight channel diffuser pressure recovery as a function of diffuser inlet Reynolds number, with and without injection/suction	145
Fig. 4.22	Mass averaged overall straight channel diffuser pressure recovery as a function of the diffuser inlet blockage, with and without injection/suction	146
Fig. 4.23	Mass averaged overall straight channel diffuser pressure recovery as a function of the diffuser inlet flow angle non-uniformity, with and without injection/suction	147
Fig. 4.24	Mass averaged overall straight channel diffuser pressure recovery as a function of the diffuser inlet mass flow non-uniformity, with and without injection/suction	148
Fig. 4.25	Mass averaged overall straight channel diffuser pressure recovery as a function of the diffuser inlet absolute Mach number, represented for constant inlet flow angles	149
Fig. 4.26	Mass averaged overall straight channel diffuser pressure recovery as a function of the diffuser inlet blockage, represented for constant inlet flow angles	150

Fig. 4.27	Mass averaged overall straight channel diffuser pressure recovery as a function of the diffuser inlet flow angle non-uniformity, represented for constant inlet flow angles	151
Fig. 4.28	Mass averaged overall straight channel diffuser pressure recovery as a function of the diffuser inlet mass flow non-uniformity, represented for constant inlet flow angles	152
Fig. 4.29	Static pressure distribution along the centerline of a diffuser channel for a corrected impeller speed $N = 6000$ RPM with injection/suction	153
Fig. 4.30	Static pressure distribution along the centerline of a diffuser channel for a corrected impeller speed $N = 4000$ RPM with injection/suction	154
Fig. 4.31	Static pressure distribution along the centerline of a diffuser channel for a corrected impeller speed $N = 2000$ RPM with injection/suction	155
Fig. 4.32a	Different definitions of overall diffuser pressure recovery coefficient as a function of the diffuser inlet momentum averaged flow angle for corrected impeller speed $N = 4000$ RPM, no injection/suction	156
Fig. 4.32b	Different definitions of overall diffuser pressure recovery coefficient as a function of the diffuser inlet momentum averaged flow angle for corrected impeller speed $N = 2000$ RPM, with injection/suction	157
Fig. 4.32c	Different definitions of overall diffuser pressure recovery coefficient as a function of the diffuser inlet momentum averaged flow angle for corrected impeller speed $N = 6000$ RPM, with injection/suction	158
Fig. 4.33	Discrete passage diffuser geometry	159
Fig. 4.34	Comparison of overall diffuser pressure recovery coefficient between discrete passage and straight channel diffusers	160
Fig. 4.35	Static pressure distribution along discrete passage diffuser centerline with low and high diffuser inlet flow distortion	161
Fig. 4.36	Pressure recovery of cambered vane diffuser as a function of the diffuser inlet flow angle for two diffuser divergence angles ...	162
Fig. A2.1	Mass flow continuity control for different corrected impeller speeds	202

Fig. A3.1	Static pressure circumferential distribution at impeller exit at (a) rear wall and (b) front wall for different corrected impeller speeds	204
Fig. A3.2	Static pressure circumferential distribution at diffuser exit at (a) rear wall and (b) front wall for different corrected impeller speeds	205
Fig. A4.1	Diffuser throat blockage versus pressure rise coefficient from impeller exit to throat	215
Fig. A4.2	Correlations of throat blockage versus pressure recovery from vane leading edge to throat	215
Fig. A4.3	Maximum pressure recovery of conical and square throat, two dimensional diffusers versus blockage	216
Fig. A4.4	Channel diffuser pressure recovery versus throat blockage compared with single channel diffuser data	217
Fig. A4.5	Channel diffuser pressure recovery versus throat blockage for different cambered vane diffuser geometries compared with single channel diffuser data	218
Fig. A4.6	Channel diffuser pressure recovery versus throat blockage for different design cases, builds and vaned diffusers, compared with single channel diffuser data	219
Fig. A4.7	Correlations of throat blockage versus pressure recovery from leading edge to throat for different straight channel diffusers ...	220
Fig. A4.8	Straight channel diffuser channel part pressure recovery based on diffuser inlet total pressure versus throat blockage for different corrected impeller speeds and inlet distortion levels, compared with single channel diffuser data	221
Fig. A4.9	Straight channel diffuser channel part pressure recovery based on computed throat total pressure versus throat blockage for different corrected impeller speeds and inlet distortion levels, compared with single channel diffuser data	222
Fig. A4.10	Mass averaged straight channel diffuser pressure recovery from leading edge to throat as a function of momentum averaged diffuser inlet flow angle for different corrected impeller speeds and inlet distortion levels	223

Fig. A5.1 Static pressure distribution in the quasi-vaneless space (for straight channel diffuser) for three corrected impeller speeds and increasing diffuser inlet flow angles, no injection/suction .. 227

Fig. A5.2 Static pressure distribution in the quasi-vaneless space (for discrete passage diffuser) for three corrected impeller speeds at the rotating stall threshold with undistorted and distorted inlet flow 228

List of Tables

Table 2.1	Facility dimensions summary	78
Table 2.2	Parameters for straight channel- and discrete passage diffuser ..	78
Table 2.3	Diffuser channel static pressure tap location coordinates	79
Table 3.1	Filipenco's [1991] distortion parameter definitions	108
Table 3.2	Test plan with the diffuser inlet flow field parameter range obtained	109
Table A1.1	Data for straight channel diffuser	194

Nomenclature

Symbols

a	[m/s]	acoustic-wave propagation speed
A	[m]	area
AR	[-]	area ratio (diffuser exit area over the area at throat)
AS	[-]	aspect ratio ($=b/W_t$)
B	[-]	blockage (defined in Eq. 3.44)
b	[m]	diffuser depth
C_m	[m/s]	meridional velocity
C_p	[-]	pressure recovery coefficient (defined in Eq. 3.13)
$C_{p\psi}$	[-]	pressure recovery coefficient based on availability-averaged diffuser inlet dynamic pressure (defined in Eq. 3.25)
C_{pa}	[-]	pressure recovery coefficient based on maximum dynamic pressure at diffuser inlet (defined in Eq. 3.23)
C_{pb}	[-]	pressure recovery coefficient based on the area averaged diffuser inlet dynamic pressure (defined in Eq. 3.22)
C_{pc}	[-]	pressure recovery coefficient based on the area averaged diffuser inlet velocity (defined in Eq. 3.20)
D	[m]	diameter
D_p	[-]	diffuser pressure rise coefficient (defined in Eq. 3.49)
L	[m]	length of the diffuser channel
LWR	[-]	length to width ratio of a diffuser channel ($=L/W_t$)
\dot{m}	[kg/s]	mass flow rate
M	[-]	Mach number ($=V/a$)
N	[RPM]	rotor rotational speed (revolutions per minute)
P	[Pa]	pressure
P_s	[Pa]	static pressure
P_t	[Pa]	total pressure
$P_{t\psi}$	[Pa]	availability-averaged total pressure (defined in Eq. 3.24)
r	[m]	radius or radial coordinate, orthogonal to x and θ
R	[KJ/kgK]	gas constant for air in equation of state $Pv = RT$

Re	[-]	Reynolds number	(= Vb/ν)
SP	[-]	stability parameter	
t	[s]	time	
T	[°K]	temperature	
U	[m/s]	meridional velocity	(= $\pi DN/60$)
V	[m/s]	magnitude of total velocity	
W_t	[m]	width of the diffuser throat	
x		linear coordinate in axial direction of machine	
Z_b	[-]	number of impeller blades	
Z_v	[-]	number of diffuser vanes	
z		local coordinate normal to duct wall	
α	[°]	flow angle, relative to radial or meridional direction,	
α_n	[-]	flow angle non-uniformity (defined in Eq. 3.42)	
α_s	[-]	flow angle skew (defined in Eq. 3.43)	
β	[°]	wedge angle of the diffuser vane	
γ	[-]	ratio of specific heats,	
η	[-]	effectiveness	
φ	[-]	dimensionless flow number (defined in Eq. 3.48)	
θ		angular coordinate, orthogonal to x and r, positive in rotor rotation direction	
2θ	[°]	diffuser channel divergence angle	
ν	[m ² /s]	kinematic viscosity	
ζ		local linear coordinate normal to diffuser channel centerline (orthogonal to x and ξ) (see Figure 2.5)	
ξ		distance along diffuser channel centerline, measured from point of tangency of centerline to base circle (see Figure 2.5)	
ξ_{ke}	[-]	kinetic-energy-flux skew (defined in Table 3.1)	
ξ_m	[-]	mass-flux skew (defined in Table 3.1)	
ξ_p	[-]	momentum-flux skew (defined in Table 3.1)	
Π_s	[-]	total-to-static pressure ratio (defined in Eq. 3.3)	
Π_{tt}	[-]	total-to-total pressure ratio (defined in Eq. 3.4)	
ρ	[kg/m ³]	density	
σ_{ke}	[-]	kinetic-energy-flux deficit (defined in Table 3.1)	

σ_m	[-]	mass-flux deficit (defined in Table 3.1)
σ_p	[-]	momentum-flux deficit (defined in Table 3.1)
ψ_d	[-]	circumferential static pressure distortion parameter (defined in Eq. 3.45)

Subscripts

amb	ambient conditions
crit	critical
corr	corrected
diff	diffuser
id	ideal
LE	leading edge
max	maximum
r	in radial direction or radial component
ref	reference condition
s	static
t	total condition; tangential component
th	at diffuser throat
x	in x-direction or x-component
θ	in θ -direction (circumferential) or θ -component
0	at impeller (swirl generator) inlet
1'	at impeller (swirl generator) exit or same as vaneless-space-begin
1	at diffuser inlet or same as vaneless space-end
2	at diffuser exit
3	at main collector/plenum

CHAPTER 1

Introduction and Background

1.1 Introduction

The centrifugal compressor is a widely-utilized device with an application spectrum covering turbochargers, aircraft engines, process and refinery industries, the refrigeration industry, and small stationary gas turbines. Centrifugal pumps have perhaps an even wider range of applications. An important component of these centrifugal turbomachines is the radial diffuser, the purpose of which is to reduce the absolute velocity of the flow leaving the impeller. Users of centrifugal compressors or pumps generally would not like a high kinetic energy level at the impeller exit (which is, depending on the machine approximately 30 - 50% of the total energy input) and seek a high pressure rise for the stage. The kinetic energy at the impeller exit must be therefore efficiently recovered within a diffuser, which serves to convert kinetic energy into a static pressure rise with an increase in flow area.

The diffuser plays an important role in establishing the overall efficiency and pressure rise of a centrifugal compressor stage. In addition, depending on the design of the impeller and its matching to the diffuser, the diffuser can be the key component limiting the operating range of the compressor between choke and stall.

Despite the facts that the diffuser may appear to be one of the simplest flow elements -with regard to geometry-, and the impact of the diffuser is well known and appreciated, the flow in diffusers of radial turbomachines is not yet sufficiently understood for many design and development purposes and a universal design method has not been established. This is due not only to the complex three-dimensional (3D) flow pattern at the impeller exit or diffuser inlet, but also because the conditions of the impeller discharge flow vary from one impeller to another and there are many design parameters to consider.

The goal of the centrifugal compressor diffuser designer is to be able to predict the fluid dynamic characteristics of a diffuser configuration as a function of the flow field entering the diffuser (i.e. that provided by the impeller) to optimize the impeller-diffuser combination. Most design techniques have been two dimensional, assuming a uniform flow in the spanwise direction and accounting for main-stream and normal flow property variations. As pointed out for example by Wilson [1984], however, the flow at the exit of a centrifugal compressor impeller can be distorted (see Section 1.2.4), in both space and time. The state of the art is that empirical and experimental information is required to obtain a good diffuser-impeller combination. It is also not always evident how diffuser performance data can be used to predict the fluid dynamic behavior of a diffuser operating with a different centrifugal compressor impeller. Testing of a specific impeller-diffuser combination establishes the performance characteristics of that particular combination, but generalization about the diffuser behavior is difficult (Filipenco [1991]).

This study examines the influence of inlet conditions on the performance of radial diffusers used in the high performance centrifugal compressors. Specifically it addresses the influence of Mach number, flow angle, axial velocity distribution, flow non-uniformity, and fluid dynamic blockage on radial diffuser performance and stability.

1.2 Background and Previous Research

This section gives an overview of the flow mechanisms in diffusers, an analysis of some important parameters, and a discussion of previous related research on radial diffusers. In addition to impeller exit flow, flow instabilities, diffuser performance, and the ability of current numerical calculations for radial diffusers are discussed.

1.2.1 Flow in Diffusers

Diffusers have been employed for a long time as devices to convert kinetic energy into a static pressure rise in different fluid systems. Diffuser technology is

one of the most comprehensively studied aspects of turbomachinery. Basic diffuser technology is summarized in references such as by Japikse [1996], Japikse [1984a], and Runstadler et al. [1975]. Most of the diffuser studies in these publications and others in the open literature have focused on single (individual) diffuser channels. It was assumed that the laboratory data available for single channel diffusers might be applied directly to industrial compressor diffuser design, and that the actual centrifugal compressor stage would show results in agreement with the laboratory single channel diffuser testing. Kline et al. [1959], Kline & Johnston [1986] and Reneau et al. [1967] give overviews of major single channel diffuser research results. These showed the influence of the diffuser parameters on performance using so-called diffuser design maps. An example of a diffuser map is given in Figure 1.1 from Reneau et al. [1967]. Four different flow regimes in the single channel diffusers are observed depending on the diffuser geometry:

- No Stall
- Appreciable Stall
- Full Developed Stall
- Jet Flow

The specification of a wide variety of parameters is essential to analyze the flow and performance of the diffusers. To define diffuser performance, the pressure recovery coefficient C_p (actual or ideal) is the most frequently used parameter. This is a simple way of conceptualizing the main purpose of a diffuser. C_p is defined as the static pressure rise through the diffuser divided by the inlet dynamic head (see Eq. 3.13). Diffuser maps available in the open literature (e.g. Japikse [1984a]) aid the diffuser designer in rapidly determining the possible level of static pressure recovery subject to the principal geometric parameters. Unfortunately, each diffuser map is restricted to a specific level of fluid dynamic parameters, such as inlet blockage or Mach number (Runstadler & Dolan [1973]). Some parameters, such as the diffuser geometry, are under the designer's control, but others are set by the downstream and upstream flow elements. To optimize the design, one must have a knowledge of the effect of the geometrical and fluid dynamic parameters on pressure recovery performance.

The main geometrical parameters for diffusers are:

- Diffuser divergence angle 2θ
- Area ratio $AR = A_{\text{diffuser exit}}/A_{\text{diffuser inlet}}$
- Aspect ratio $AS = \text{depth}/\text{width}$ (at the diffuser inlet)
- Length to width ratio (non-dimensional length) LWR
- Shape of the cross section (conical or rectangular)

Not all of these geometrical parameters are independent. There is a fixed relationship between the area ratio and the other geometric parameters as follows:

$$AR = 1 + 2 LWR \tan\theta \quad (1.1)$$

The fluid dynamic parameters are:

- Flow angle α
- Mach number M
- Blockage B
- Velocity Distribution
- Turbulence
- Reynolds number Re
- Surfaces condition

Based on the work of many investigators, it was concluded by Japikse [1987] that three critical fluid dynamic parameters must be known to specify the performance of a diffuser (plus a wide variety of geometric parameters as well). The three include the inlet blockage, the shape of the velocity profile entering the diffuser, and the turbulence scale and intensity at the diffuser inlet.

The blockage is simply the displacement thickness of the boundary layer in the diffuser inlet flow area. It represents the amount of effective flow area reduction that the boundary layer causes. The importance of displacement thickness on diffuser performance was first documented by Reneau et al. [1967]; the idea was generalized into the "blockage" concept and quantified (see Eq. 3.44) by Sovran &

Klomp [1967]. The influence of blockage on pressure recovery has been extensively investigated for single channel diffusers and substantial tables of data are available. For example, Runstadler & Dean [1969] investigated the performance of flat wall-channel type diffusers as a function of diffuser geometry over a range of diffuser inlet Mach numbers from 0.2 to 1.0 and boundary layer blockage from ~1 to ~14 %. In their study, the inlet flow field consisted of a potential core surrounded by the wall boundary layer.

According to Kline & Johnston [1986] it is important to distinguish between the effects of inlet boundary layer (or blockage) on flow regime and on pressure recovery, as they are quite different. For single channel diffusers the line of maximum pressure recovery (and the limit of appreciable stall) was measured to be independent of inlet blockage (Reneau et al. [1967]). This was also seen in the theoretical calculations of Senoo & Nishi [1977a, b]. These calculations showed that the interaction between boundary layer and core flow has a stabilizing effect on the boundary layer development and eventual flow separation.

Although the velocity profile entering the diffuser is presumed as another critical parameter, no general convention has been developed to specify the inlet velocity profile to a diffuser. Different inlet profiles, simple skewed and/or highly distorted have been considered and reported in the open literature for single channel diffusers. A detailed study was carried out by Wolf & Johnston [1969], whose main results can be summarized as follows:

- a) Distorted mean-velocity profiles at diffuser inlet influenced the flow development, separation, stall and therefore flow regimes in diffuser.
- b) Distorted mean-velocity inlet profiles generally decreased diffuser pressure recovery, although certain distorted asymmetrical velocity profiles caused higher pressure recovery than the uniform velocity distribution at the diffuser inlet. A slightly distorted wake-type inlet profile may be beneficial for performance according to Wolf & Johnston [1969].
- c) The inviscid forces in diffusers were pressure-profile distorters; that is, given a transverse velocity difference or gradient at the inlet, the inviscid forces in a diffusing passage tended to increase the transverse differences in velocity.

Other studies (Al-Mudhafar et al. [1982], Bhinder et al. [1984], Jesionek & Wyszynski [1979], Masuda et al. [1971], McDonald et al. [1971], Waitman et al. [1961]) investigated the effects of non-uniform diffuser inlet conditions on single channel diffuser performance.

The results of an experimental study on the influence of severely distorted velocity profiles on the performance of a single channel straight two-dimensional diffuser are reported by Al-Mudhafar et al. [1982]. The diffuser pressure recovery progressively deteriorated (up to 50%) as the inlet velocity was distorted. The effect of inlet distortion on the performance of a low aspect ratio single channel two-dimensional plane wall diffuser was investigated by Bhinder et al. [1984]. The performance of the diffuser was nearly independent of mean inlet Mach and Reynolds numbers. The inlet distortion was quantified by a distortion parameter, λ (defines the inlet velocity profiles quantitatively), which was found to correlate well with the pressure recovery. The diffuser pressure recovery decreased with increasing inlet distortion. Another experimental study on the effects of distortions of inlet velocity profiles on performance in subsonic curved diffusers is reported by Jesionek & Wyszynski [1979]. The curved diffuser flow measurements indicated pronounced effects of curvature on pressure and velocity distributions. Diffuser pressure recovery coefficient and effectiveness were found to be strongly dependent on the type of the inlet velocity distributions.

Properties of uniform shear flow in single channel rectangular parallel walled diffusers were investigated by Masuda et al. [1971]. The effect of non-uniform free stream velocity profile on diffuser pressure recovery was to increase both total pressure losses and amount of momentum change in diffuser. When the divergence angle of the diffuser was small ($2\theta < 8^\circ$), the latter effect was so great that the diffuser static pressure rose compared to the pressure recovery with uniform inlet velocity profile.

McDonald et al. [1971] investigated the effect of swirling inlet flow on the performance of single channel conical diffusers. The effect of inlet swirl was correlated with the flow regime with axial inlet flow (e.g. inlet flow without swirl). Swirling inlet flow did not affect performance of diffusers which were

unseparated or only slightly separated with pure axial inlet flow. For diffusers, which were moderately or badly separated for pure axial inlet flow, swirling inlet flow caused large performance increases based on total inlet kinetic energy indicating that optimum diffuser performance for swirling flow may be higher than that for axial inlet flow. Waitman et al. [1961] investigated effects of inlet conditions on performance of single channel subsonic diffusers. Pressure recovery increased with increasing turbulence level at diffuser inlet. Diffuser pressure recovery was also a function of inlet boundary layer conditions. Reductions in pressure recovery occurred if the inlet boundary layer was thickened.

Klein [1981] reviewed the data (about thirty publications) on inlet conditions on single channel conical diffuser performance and discussed the effects of inlet boundary layer blockage, inlet shape parameter, turbulence and Reynolds number. A comparison of results between different sources was complicated by the variety of definitions of performance parameters and averaging methods. He also found many inconsistencies and confusing results between different sources of data he discussed. For example, the curves from different sources showing diffuser performance against inlet blockage revealed discrepancies: some of these curves decreased continuously with increasing blockage, others dropped sharply initially (up to $B \approx 0.05$) and then remained constant over a blockage range, which is typical for centrifugal compressor diffuser applications.

The influence of turbulence at the diffuser inlet is less investigated than the other fluid dynamic parameters. A chart of diffuser performance as a function of inlet turbulence parameters by Hoffman [1981] showed that the pressure recovery of single channel diffuser depends both on turbulence intensity and turbulence scale. Increases of the diffuser's static pressure recovery coefficient of 11.3 and 23.9% at included diffuser divergence angles of 12° and 20° respectively were obtained when the value of the inlet integral free-stream scale turbulence in the flow direction was at least 7.2 times larger than the inlet boundary layer displacement thickness and when the inlet total free-stream turbulence intensity was at least 3.5 %. It is hypothesized that a larger scale of turbulence transmits the free-stream energy to the walls more effectively and, when coupled with large turbulence intensities, are mechanisms which act to delay separation within

the diffuser. Hoffman & Gonzales [1984] found that the pressure recovery coefficient of a two-dimensional single channel diffuser was increased by 10% for the diffuser divergence angle $2\theta = 9^\circ$ and by 22% for the diffuser divergence angle $2\theta = 20^\circ$ with the inlet free stream turbulence, having turbulence intensity greater than 3.5% and integral scale of turbulence in the flow direction 5 times greater than the inlet boundary layer displacement thickness.

During the early years of diffuser research the Mach number at the diffuser inlet was thought to be critical. As shown by Japikse [1984b] this early belief was erroneous and it was based on incomplete measurements. It was established e.g. by Runstadler et al. [1975] that one must pass a diffuser throat Mach number of 1.0 before developing any significant dependence on Mach number (Japikse [1984b]). In cases of transonic and supersonic inlet flow, normal shock waves are observed in front of the leading edge of the vanes for different type of vaned diffusers (Dean [1971], Verdonk [1978a], Japikse [1980]). Normal shock is a good mean to achieve a large pressure rise within a short distance (Japikse [1984b]). The major disadvantage at a high Mach number is the narrow flow range of the compressor stage.

Single channel diffusers are characterized by a Reynolds number based on an inlet hydraulic diameter. For typical turbomachine flows, the flow is in the fully turbulent regime so the Reynolds number has a weak influence. For single channel diffusers, Russo & Blair [1981] examined the influence of Reynolds number on the pressure recovery coefficient keeping the inlet blockage constant. They found that Reynolds number did not remarkably affect the diffuser performance for $Re > 4 \cdot 10^5$.

The flow regimes, phenomena, and influence of geometrical and fluid dynamic parameters have been well described for single channel diffusers in the open literature. For centrifugal compressor diffusers, the situation is less well mapped and understood, because centrifugal compressor diffusers exhibit additional fluid dynamic features. The main differences between single channel and centrifugal compressors (vaned) diffusers can be summarized as follows:

1) There are more parameters to be considered for the diffusers of centrifugal compressors than for single channel diffusers. The main additional parameters are:

- vane number
- vaneless space radius ratio (the radius to the leading edge of the diffuser vane divided by the impeller tip radius)
- geometry (shape) and sharpness of the vane leading edges
- contouring of the vaneless space and sidewall divergence
- downstream conditions (volute, plenum etc.)

The number of diffuser vanes seems to influence the performance and flow range of the radial diffusers, but the reason for this is either not understood (or at least not published, Cumpsty [1989]). Dean [1974] suggested that the number of vanes employed in straight channel and vane island diffusers in contemporary practice varies from 8 to 60. According to Dean [1973] the choice of the number of vanes depends upon impeller discharge Mach number. Near and below Mach numbers of unity, a large number of vanes may be beneficial; at higher Mach numbers, smaller vane numbers are recommended. As the vane number is reduced, the aspect ratio of the diffuser throat drifts away from the optimal value of 1, on the basis of the impact of throat aspect ratio on maximum channel diffuser pressure recovery. Design calculations showed a significant penalty for throat AS < 0.5 or > 2.0. Based on an experimental investigation, Yoshinaga et al. [1980] suggested a maximum number of diffuser vanes as 27 for high performance. No significant difference was found in compressor flow range with vane number variation between 13 and 41 by Rodgers [1982a].

The vane leading edge radius of curvature, r_{LE} , affects the useful life of the vanes in a centrifugal compressor diffuser. From this standpoint, a blunt vane (large radius of curvature of the leading edge) is desirable, whereas from a fluid dynamic viewpoint, a sharp vane is most often desired (Baghdadi [1973]). Great care sometimes is given to the design of the vane shape, but there is little evidence that this has a significant effect on the flow in the diffuser (Cumpsty [1989]). The influence of diffuser vane leading edge geometry, particularly the influence of pressure face angle and quasi-vaneless space suction surface profile,

on the performance of a centrifugal compressor was investigated by Clements & Artt [1989]. They found that compressor performance was virtually unaffected by changes in pressure face angle, whilst being sensitive to changes in quasi-vaneless space suction surface profile. Straight channel diffusers produced higher stage efficiencies than any diffuser with a concave suction surface profile between the leading edge and throat.

2) Inlet conditions for a centrifugal compressor diffuser are determined by the impeller and are highly distorted. They also depend on the impeller operating point. The interaction between impeller and diffuser implies that the knowledge about the influence of blockage or inlet velocity distribution for single channel diffusers may not be directly applicable to centrifugal compressor diffusers.

3) The centrifugal compressor diffuser consists of an array of several diffuser channels acting in parallel. Phenomena which are not observed with a single channel diffuser can occur due to the fluid dynamic interactions of the channels. Such phenomena can not be simulated using a single channel diffuser.

4) Centrifugal compressor diffusers have a vaneless space and a quasi-vaneless space. Data obtained using a single diffuser channel do not give information on the flow mechanisms within the vaneless or quasi-vaneless spaces. Previous investigators suggested that the flow phenomena in these regions are critical factors regarding the overall stage stability (Hunziker & Gyarmathy [1993]) and pressure recovery (e.g. Elder & Gill [1985], Inoue & Cumpsty [1984]).

1.2.2 Radial Diffuser Types

Radial diffusers of many different configurations have been applied to centrifugal compressors. These can be grouped into two general classes: vaneless diffusers and vaned diffusers. The highest-performance compressors make use of vaned diffusers as they have a smaller exit-radius for a given level of diffusion and generally exhibit a higher pressure rise than the vaneless type, in spite of operating over a relatively narrower flow range. As pointed out by Dean [1973], a vaned diffuser typically demonstrates higher pressure rise (often by as much as

20 % in pressure recovery and 10 % in stage efficiency) compared to a vaneless diffuser. However, the operating range is smaller. Vaneless diffusers often demonstrate a flow range of 50% from match point to surge while the vaned diffusers show about 25% range. The choice of diffuser type can, therefore, depend on the relative importance of flow range versus stage efficiency. Centrifugal compressors for process applications are generally operated at low pressure levels because a wide flow range is required and these compressors are often equipped with vaneless diffusers. Conversely, high performance levels are required for diffusers in gas turbine engines and the compressors are generally equipped with vaned diffusers. The current design trend for all radial compressor applications is to have high efficiency in addition to wide flow range. The application of vaned diffusers has drawn increased attention.

The vaned diffuser consists of a two dimensional diverging channels (straight channel diffusers) or conical pipes (pipe or discrete-passage diffusers). Different types of vaned diffusers such as straight channel, vane island, airfoil (cambered vane), cascade type tandem airfoil, discrete passage, and pipe diffusers (Figure 1.2) are used in centrifugal compressors. The criteria for assigning the precedence of either a pipe diffuser over a channel diffuser or even an airfoil over a tandem cascade diffuser are not well established. Of the different common radial diffuser configurations, the vaneless diffuser has been the most extensively studied followed by the straight channel and cambered vane types; the least amount of data has accumulated for the pipe and discrete-passage diffusers.

The tangential velocity into the diffuser is usually about three times as large as the radial component and it is therefore the deceleration of the tangential component which provides most of the pressure rise (Cumpsty [1989]). The vaneless space diffusion process is controlled mainly by angular momentum considerations but the process is influenced by frictional viscous losses which modify the flow profile. Performance of a vaneless diffuser has been evaluated with the use of boundary layer theory or with the use of one-dimensional equations for conservation of radial and angular momentum, mass and total enthalpy. The effect of viscosity is modeled either through the use of a single skin friction coefficient (Japikse [1982], Eckardt [1977]) or through the use of both a skin friction coefficient and dissipation coefficient (Traupel [1977]). In many

cases, simple constants are used for a given flow problem; in other cases, the coefficients are evaluated as a function of Reynolds number, and in other instances the fluid dynamic inlet effects are modeled with a scaled length parameter (Traupel [1977]; Eckert & Schnell [1961]). It appears, however, that none of these analyses include the influence of impeller exit profile. The results of applications of the basic conservation equations on the flow in vaneless diffuser (considering wall friction effects) were summarized in several characteristic plots by Johnston & Dean [1966]. Later, Senoo & Kinoshita [1977] and Senoo & Nishi [1977a, b] computed the flow in a vaneless diffuser using boundary layer equations.

The straight channel type diffuser (Figure 1.2e) is used by a large number of compressor companies. It is both simple to manufacture and, yields good performance (Krain [1981 and 1984], Rodgers [1982a], Kano et al. [1982]). An optimal diffuser divergence angle for straight channel diffusers is $2\theta = 8 - 10^\circ$ according to measurements by Yoshinaga et al. [1980].

Vane-Island diffusers (Figure 1.2f) for high Mach numbers at diffuser inlet are a special form of straight channel diffusers with smaller vane numbers and a concave geometry of suction side of the vane surface at the inlet (Conrad et al. [1980], Verdonk [1978a], Jiang & Yang [1982]).

Curved channel (cambered vane) diffusers (Figure 1.2a, b) consist of airfoils or blades, instead of vanes. A limitation of curved channel diffusers is that a secondary flow can develop along the side walls, because of the curved nature of the channel. Despite this disadvantage, the investigations by Kenny [1972], Jansen [1982], Stein [1986], and Hunziker [1993] showed similar performance levels to the ones by straight channel diffusers.

Tandem cascade diffusers (Figure 1.2c) have also been used in turbomachinery industry. A well documented and successful design procedure for the tandem cascade diffusers has not been developed, except for the recent publication by Japikse [1996]. The proper application of airfoils in a cascade configuration is well recognized for axial compressor and turbine design. Several references (e.g.

Senoo et al. [1983] and Senoo [1984c]) presented information on tandem cascade diffusers, but there is sparse industrial verification in the open literature.

An advantage of a multiple cascade system is that it can accomplish the same diffusion as a single cambered vane but with half the diffusion factor per row according to Pampreen [1972]. Pampreen [1972] hypothesized that a cascade diffuser can be designed more compactly and could perform better than a conventional diffuser for identical inlet and exit conditions, with less loss and a larger operating range. He studied the operating characteristics of different multiple cascade diffusers. Various blade shapes and positions were tested for their efficiency and pressure ratio. Pampreen [1972] concluded that the maximum losses of the multiple cascade diffuser were about 10% less than those of the conventional vaned diffuser. He made a comparison between a three-row cascade diffuser and a single-row channel diffuser and claimed that the cascade diffuser was superior. Wider operating range was found for the multiple cascade diffuser than for the channel diffuser. In addition, higher efficiency was reported for the tandem cascade diffuser. The compared channel diffuser design parameters in Pampreen's investigations were not well specified and it is difficult to determine whether or not this type of vaned diffuser represents state-of-the-art performance (Japikse [1987]). Disadvantages of tandem cascade diffuser appear to be complexity of design, higher costs of manufacture, and relative scarcity of design data.

The approach to cascade airfoil diffuser design was initiated, because a coherent and substantive data base of NACA cascade airfoil information was available at a very early time. In tandem airfoil diffuser design, it has been suggested that the use of the NACA airfoil data is valid for setting the basic airfoil geometries and obtaining the correct flow turning within a reasonable but unknown degree of accuracy. However, the estimated losses have been found to be almost an order of magnitude too low and a multiplier of seven or eight times the basic loss level from the cascade data correlations has been recommended for design (Japikse [1996]).

Further work on tandem diffusers has been presented by Senoo et al. [1983], who theoretically and experimentally examined the effect of cascading two airfoil

type diffuser blades. The front row of the cascade was designed for low flow rates and the back row was designed for high flow rates. Senoo et al. [1983] found that the tandem cascade diffuser possessed a wide range of stable operation and produced better pressure recovery than a similar vaneless diffuser. Rodgers [1993] also investigated different tandem cascade geometries on a small, high specific speed transonic centrifugal compressor stage and made comparisons between tandem cascade- and straight channel diffusers in terms of both flow range and pressure recovery. Tests showed the importance of the first tandem row on overall compressor performance, and demonstrated higher flow range at the expense of slightly reduced efficiency (1.5% reduction in peak overall efficiency), as compared to an optimum channel type diffuser, tested at the same compressor stage.

It is generally believed that vaned diffusers reduce the operating range of the compressor stage by throat choking at high flow rates and stalling at low flow rates. In an attempt to overcome this deficiency of the vaned diffusers or in other words to eliminate the throat in vaned diffusers, the concept of low solidity vaned diffusers (LSVD) was introduced by Senoo et al. [1983], and Senoo et al. [1989]. The primary feature of the design is that LSVD does not include a throat between its blades. LSVD has been used in the process and refrigeration industry, where a wide operating range of the compressor is important. According to Senoo's results, the low solidity vaned diffuser has almost the same operating range as a vaneless diffuser, but the static pressure recovery coefficient is significantly higher than a vaneless diffuser. This result was confirmed by Haak et al. [1995], who compared a centrifugal compressor stage with vaneless and single cascade low solidity vaned diffuser and called LSVD a compromise between vaneless and vaned diffusers. Osborne & Sorokes [1988] conducted further experiments using design procedures derived from Senoo with simple flat vane construction and obtained results similar to those by Senoo. Hayami et al. [1989] investigated low solidity cascade diffusers and compared the performance with data of the same compressor with vaneless diffuser. A wider flow range as well as a higher pressure ratio and a higher efficiency, than vaneless diffusers were demonstrated even when the inflow Mach number to the cascade diffuser was over unity.

Harada & Goto [1993] experimentally and numerically investigated the performances of single and tandem low solidity vaned diffusers and compared them to those of vaneless diffusers. Both the single and tandem low solidity vaned diffusers performed better than the vaneless diffusers. The tandem low solidity vaned diffuser showed an increase in pressure recovery coefficient of greater than 15% at the design point, and an increase greater than 40% at the lower flow rate, as compared with the pressure recovery of vaneless diffuser. The total-to-static overall compressor stage efficiency was improved by 4% to 10% from 100% to 70% flow rate by using a low solidity tandem diffuser. All the investigations of low solidity vaned diffuser showed better performance compared to a vaneless diffuser without a loss in operating range. Unfortunately, there is little data available in the open literature for direct performance comparisons between low solidity vaned diffuser and other vaned diffusers such as straight channel diffuser or cambered vane diffuser. The maximal achieved mass - averaged diffuser pressure recovery was 0.70 - 0.72 for the single row low solidity vaned diffuser and slightly higher for tandem low solidity diffuser by Harada & Goto [1993]. Sorokes & Welch [1991] and [1992] provided a comprehensive set of low solidity vaned diffuser data showing the effects of various setting angles on both diffuser performance and overall stage performance.

Hohlweg et al. [1993] compared performance and flow range, stage efficiency of low solidity vaned diffusers to those of conventional thin vaned diffusers. In the experiments with a high Mach number industrial compressor, the conventional vaned diffuser achieved a minimum of 2.6% efficiency higher at the design flow than that for the closest low solidity vaned diffuser. On the other hand, the low solidity vaned diffuser attained 4.9% efficiency gain over the vaneless diffuser. In the experiments with a low Mach number process compressor, the low solidity vaned diffuser achieved essentially the same design point efficiency level as conventional vaned diffuser. Recently, a vaneless, a conventional vaned and two low solidity vaned diffusers were tested by Amineni et al. [1996] and the results were compared in terms of the effect of diffuser systems on the stage performance, the maximum efficiency and the operating range of the compressor. For high Mach number ($M = 1.02$ at diffuser inlet) the vaned diffuser maximum flow rate was 16% less than the vaneless diffuser and LSVDs,

indicating that the maximum flow rate through the compressor was controlled by vaned diffuser throat choking. The LSVDs investigated by Amineni et al. [1996] had an operating range in between vaned and vaneless diffusers. In all cases the best efficiency was performed with vaned diffuser.

Pipe diffusers have largely been developed by Kenny [1972]. In this configuration the vanes and channels are replaced by discrete pipes lying with their axes tangential to the impeller tip circle in the plane of the vaneless space (Figure 1.3). Although the pipe diffusers are used in centrifugal compressor industry, little data about design and performance exist in the open literature. There is also a lack of knowledge about flow mechanisms inside the pipe diffusers to provide a systematic approach for diffuser design.

The discrete-passage diffuser was developed by General Electric Company (see Figure 4.33) Detailed experimental investigations on discrete-passage diffusers have been carried out at MIT Gas Turbine Laboratory over the past several years and are reported by Filipenco [1991], and Johnston [1993].

The circular cross section of the pipes or passages at diffuser throat is considered to allow pipe or discrete passage diffusers to swallow a highly non-uniform flow better than the vaned diffusers. As pointed out by Kerrebrock [1989], the swept-back nature of the diffuser leading edges may account for the relatively good transonic performance of this type of radial diffuser. Many arguments have been made on the advantages and disadvantages of both pipe and discrete passage and vaned diffusers e.g. Klassen [1973]. For example, according to Elder & Forster [1987], pipe diffusers have a leading edge with inlet blade angles which become more tangential at the side walls than in the central region. This suggests that the pipe diffuser has some advantage in accommodating the hub to shroud axial velocity profile. An alleged advantage of the pipe diffuser, over the cambered vane diffuser is the lower throat blockage at a given leading edge to diffuser throat static pressure rise (Kenny [1972]). Kenny compared curves of pressure recovery for a pipe diffuser and a cambered vane diffuser, and showed superior performance of the pipe diffuser for a given level of blockage at the throat. The lower throat blockage of the pipe diffuser suggests a smaller

geometric throat for the same flow rate, and consequently, a more compact diffusing system as well as higher effectiveness according to Kenny [1972].

According to Japikse [1996] the performance levels of pipe diffusers are at the same level or occasionally slightly better than, those of vaned channel diffusers (Straight channel or cambered vane). Dean [1973] claimed that pipe diffusers seem to give better peak recovery (2 - 3 points higher), but often shorter range than the vaned channel diffusers. The reason for the higher performance of pipe diffuser is believed to lie in the entry configuration, which should help controlling boundary layer flow and especially back flow, rather than in the conical channel compared to flat, straight centerline types. Blair & Russo [1980] tested passage diffusers in a non-rotating "static blow test" apparatus. Diffuser static pressure recovery coefficients of 0.79 - 0.82 at throat blockages of 2 - 3% for an inlet Mach number of 0.7 - 0.8 were obtained by Blair & Russo [1980]. But this diffuser performance was evaluated from single passage diffuser tests.

Comparative tests of straight channel and pipe diffusers were completed by Rodgers & Saphiro [1972] on a compressor designed for a pressure ratio of 6.0. Both diffusers had the same throat area and the pipe diffuser had 29 pipes and the straight channel diffuser had 21 vanes. The results of the tests indicated slightly higher overall diffuser pressure recoveries for the straight channel diffuser (peak pressure recovery for the straight channel diffuser was 0.69 and for the pipe diffuser 0.67), as well as higher flow range (ca. 5%) between choke and stall.

There are also other diffuser arrangements which have been developed to reduce pressure losses associated with the diffusion process and to increase the stable operating ranges of centrifugal compressors. One method is the replacement of the vaneless diffuser section with a free rotating vaneless diffuser (Rodgers & Mnew [1975]), which tends to smooth out the distorted entry flow profiles. It is claimed that application of rotating vaneless diffuser induces an increased flow range and higher performance as shown by Rodgers [1978]. However, this could be achieved only at the cost of a complicated geometry. Ribaud & Fradin [1989] also investigated rotating vaneless diffuser. The free rotation of the vaneless

diffuser reduced the friction losses by about 70%. The structure of the flow at the impeller outlet influenced the efficiency of the rotating vaneless diffuser.

1.2.2.1 Vaned Diffuser Components

It is very common and also useful to divide the vaned diffuser in three parts (or subcomponents) (Figure 1.4):

- 1) Vaneless Space (or Diffuser): The diffuser part between impeller exit and leading edge of the diffuser
- 2) Quasi-Vaneless Space: The diffuser part between the diffuser leading edge and the diffuser throat
- 3) Channel Diffuser: The diffuser part from diffuser throat to diffuser exit

The vaneless space takes advantage of the property of a vaneless diffuser that a supersonic flow at the impeller exit can diffuse to subsonic flow without the possibility of shocks. Mechanical constraints also lead to the necessity for a vaneless region. The optimum length of the vaneless space (vaneless space radius ratio) has not been systematically studied in terms of fundamental flow variables, but seems to be a significant design factor, for performance, flow range, noise, blade oscillations and structural integrity (Cumpsty [1989]). Generally, increasing vaneless space gives wider flow range and reduction of noise and oscillations, but it also means lower pressure rise and efficiency. In the open literature one can find different values for an optimum vaneless space radius ratio. A number of researchers have suggested various optimal values for the vaneless space radius ratio as summarized in the following:

<u>Reference</u>	<u>Vaneless Space Radius Ratio</u>
Came & Herbert [1980]	1.05
Clements & Artt [1989]	1.06 - 1.10
Rodgers [1982a]	1.125
Japikse [1986]	1.125
Jiang & Yang [1982]	1.15 - 1.20

Detailed investigations of the flow in the quasi-vaneless space have been carried out by Krain [1981], Elder & Gill [1985], Stein [1986] and Casey et al. [1995a].

The channel part of the vaned diffuser is the part being most similar to the single channel diffusers although few detailed measurements of flow fields in channel parts of vaned diffusers are available. The pressure rise at the diffuser walls were measured, e.g. by Jansen [1982], Kano et al. [1982], Stein [1986], and Hunziker & Gyarmathy [1993]. At the inlet region of channel part of vaned diffusers, Stein [1986] measured unsteady pressures and Casey et al. [1995a] measured velocities. They found similar distributions for different impeller blade positions. The time-dependent distributions of the incoming flow appeared to have little influence on the pressure recovery in the channel part of the vaned diffuser.

1.2.3 Flow Instabilities in Radial Diffusers

In addition to high design-point-efficiency, compressor applications require operation over a range of flows. The maximum flow is set by the occurrence of choking in any flow component of the compressor while the lower limit is the onset of local and/or global instability such as rotating stall or surge, Greitzer [1981]. Choking dictates the sizing of the compressor for a specific application. The onset of flow instability makes designing more difficult, because it is not completely understood in terms of flow processes occurring within the individual compressor components. However, the radial diffuser appears to play a major role in setting the operating flow range of high performance centrifugal compressors.

One type of flow instability for compressors is rotating stall, where one or more "stall cells", which are patches of low or reversed flow, propagate around the circumference of the compressor. The speed of the cells is typically a fraction (from 10 to 30%) of the impeller speed in a centrifugal compressor stage. In fully developed rotating stall, the overall flow through the machine is constant in time, with the stall cells merely serving to redistribute the flow around the annulus. The formation of these rotating stall cells is the result of an instability of the axisymmetric flow in the machine, in which small circumferential non-

uniformities grow into finite amplitude disturbances. Rotating stall can thus be regarded as a local component instability, in the sense that it is associated with an individual component rather than with the overall compression system (Greitzer [1976a, b]).

There is another type of instability known as surge, that is often associated with stall in centrifugal compressor diffusers. Surge is a global instability involving an oscillation of the overall flow in the machine. The frequencies of surge are set by the system geometry rather than by those of the individual components. The frequencies are therefore relatively independent of impeller speed and tend to be an order or more lower than those of rotating stall. Surge can be divided into two categories. Mild surge means periodic oscillations of the mass flow through the compressor without flow reversal. Deep surge means high amplitude, low frequency flow fluctuations with intermittent back flow through the stage. The transition from mild surge to deep surge in a centrifugal compressor with a vaned diffuser was investigated in detail by Ribí & Gyarmathy [1993].

The stable flow range of a centrifugal compressor is generally thought to be limited by surge, but the initiation point of rotating stall can also be the key item, due to the coupling that exists between the two modes of instability. Although several authors believe that rotating stall cannot be the major mechanism for the onset of surge due to the greatly differing frequencies between rotating stall and surge, for an axial compressor, the existing data show that the local instability, rotating stall, can act essentially as a trigger for the global instability (Greitzer [1980]). For centrifugal compressors, the situation is less clear, because the amount of detailed time resolved data on the initiation of instability is much less than that for axial compressors. The occurrence of flow instability not only limits the operating range of compressors, but it may also prevent the attainment of maximum efficiency which often lies at or close to the surge line.

The origin of the flow instability can be any component of centrifugal compressor. Impellers, as well as vaneless or vaned diffusers, or an unsteady interaction between impeller and diffuser, can cause rotating stall. It is sometimes difficult to detect which component is the origin of the instability and which modifications should be made to stabilize the flow. A clear distinction

between impeller and diffuser rotating stall is not always possible and both phenomena sometimes exist simultaneously or alternately. Zones of stable operation and mild surge regions have also been observed between the onset of rotating stall and deep surge. It is believed that the diffuser generally controls the flow range and that stable flow range of the centrifugal compressor can be increased by a modification of the diffuser characteristics, but the stalling element cannot always be regarded as being the diffuser. In addition, the choice of parameters to correlate the onset of centrifugal compressor instability (e.g. diffusion factor, velocity ratio, static pressure rise in the quasi-vaneless space of vaned diffuser) is still under considerable debate as are the unsteady physical phenomena that characterize the stall process.

1.2.3.1 Vaneless Diffuser and Flow Instabilities

A large number of investigations of flow instabilities in vaneless diffusers are available in the open literature, including experiments and modeling of the instabilities. Related discussions on the origin of the flow instability and the influences of the impeller exit flow, especially flow angle, on the instability are also common to the instability phenomena in centrifugal compressor vaned diffusers. For a centrifugal compressor stage with vaneless diffuser, impeller stall (Lennemann & Howard [1970], Mizuki et al. [1976], Rodgers [1977a], Senoo et al. [1979], Kosuge et al. [1982]) as well as vaneless diffuser rotating stall (Jansen [1964a, b], Abdelhamid & Bertrand [1980], Abdelhamid [1981], Senoo & Kinoshita [1978], Ligrani & Van den Braembussche [1982], Frigne & Van den Braembussche [1984], and Abdelhamid [1980]) have been reported. Some authors (Jansen [1964a, b]) have related vaneless diffuser rotating stall to the effects of boundary layer separation and/or local reverse flow while other authors (Abdelhamid [1980]) explained it by a fluid dynamic instability of the diffuser core flow.

Vaneless diffuser flow field traverses obtained by Yoshinaga et al. [1980] showed the existence of reverse flow near the shroud. Similar regions of reverse flow were also observed by Rodgers [1982b] and Benvenuti [1978]. Senoo & Nishi [1977b] developed a theory which stated that reverse flow is related to the

diffuser inlet flow angle and diffuser depth, b . The presentation by Frigne & Van den Braembussche [1984] correlated the onset of vaneless diffuser rotating stall with critical inlet flow angle, α_{crit} . Stall of different nature and origin may appear in one stage depending upon impeller speed and fluid dynamic parameters (Frigne & Van den Braembussche [1984]). Abdelhamid [1980] showed that depending on the impeller-diffuser interaction, two types of vaneless diffuser rotating stall are possible. Further Abdelhamid [1983] demonstrated in his experiments that both types of vaneless diffuser rotating stall can exist at the same centrifugal compressor stage.

1.2.3.2 Vaned Diffuser and Flow Instabilities

The flow instabilities in centrifugal compressor with vaned diffusers are less investigated than the instabilities in vaneless diffusers. In terms of rotating stall, most of the observations and experiments refer to axial compressors and the ability to predict surge for centrifugal compressors is substantially behind the technology base for axial compressors (Japikse [1996]).

Surge (mild surge) in a high pressure ratio centrifugal compressor with vaned diffuser was investigated by Toyama et al. [1977] and the results of high-frequency response measurements during surge operation were presented. Special emphasis was given to the flow development in diffuser inlet region and its relation to the onset of surge. One important conclusion was that surge of the test compressor was triggered by the diffuser flow. At the initiation point of surge, the stagnation pressure loss in the diffuser inlet region increased, however, gross separation of the diffuser inlet boundary layer was not observed before surge. No evidence of rotating stall was found, and surge was triggered by excessive diffusion in the vaneless and quasi-vaneless space at the inlet region of vaned diffuser (when the instantaneous value of diffuser inlet pressure recovery coefficient from impeller exit to diffuser throat reached approximately 0.40 - 0.45). Dean & Young [1977], Dean [1974], and Kenny [1972] asserted that surge is caused by a breakdown of the flow in the vaned diffuser.

The work of Jansen et al. [1980] provided some analytical basis for overall unsteady flow during instability in the centrifugal compressors. This work was a thorough examination of surge cycles in a small high speed centrifugal compressor. Time dependent inlet and outlet flow measurements were conducted with a turbocharger compressor equipped with a vaned diffuser to determine the time dependent mass flow rate, pressure, and flow direction during surge cycles at two different impeller speeds. The data were compared against predictions from Greitzer's [1976a, b] model which uses first-order ordinary non-linear lumped parameter differential equations.

The transition from mild surge to deep surge in a centrifugal compressor with a cambered vane diffuser was investigated by Ribi & Gyarmathy [1993] for different vaned diffuser geometries and different operating points in the compressor map. Depending on impeller tip Mach number mild surge or rotating stall was seen before deep surge. An intermittent mass flow reduction during mild surge provoked impeller rotating stall and then triggered the transition to deep surge. The instantaneous behavior of the same centrifugal compressor stage during mild surge was investigated by Ribi & Gyarmathy [1995]. By subdividing the time-dependent pressure rise into the contributions of the stage components (impeller plus inlet duct, diffuser and collecting chamber), an analysis of the instantaneous behavior of each component was performed. The results revealed that the impeller responded to the pulsations in a quasi steady way, but large deviations from the quasi steady behavior occurred in the vaned diffuser.

It is currently an open question whether rotating stall has a role in surge for centrifugal compressors. Rotating stall occurs in centrifugal compressors and evidence of rotating stall has been found in both the impeller and diffuser by Kämmer & Rautenberg [1982] and by Abdelhamid et al. [1987]. Amann & Nordenson [1961] believed a diffuser rotating stall is responsible for the flow breakdown in the stage. However, the time resolved measurements of the flow in a centrifugal compressor entering surge made by Toyama et al. [1977] and by Dean & Young [1977] did not show rotating stall prior to the observed surge. One difficulty in arriving at a general description of centrifugal compressor

instability is that the speeds, the overall system, and the compressor geometries cover a wider range than those of axial compressors.

Unsteady pressure and blade vibration measurements were carried out by Jin et al. [1992] and [1994] on a centrifugal compressor stage with different impeller and diffuser geometries. The excitation and blade vibrations during surge for the vaned diffuser were stronger than those for vaneless diffuser.

Fink et al. [1991] investigated surge in a radial turbocharger compressor equipped with vaneless diffuser. The main conclusion was that the element most responsible for surge initiation in this compressor was the impeller. Although the vaneless diffuser was a destabilizing element (due to its positive characteristic slope), its characteristic slope was nearly constant near the surge line and it was not the component whose performance change initiated instability and surge. A lumped parameter model for the modeling of the overall system behavior and the surge, was also developed by Fink et al. [1991].

Greitzer [1981] reviewed the literature concerning different types of instabilities and provided a criteria for the static and dynamic instability of the system comprising of the compressor, the piping and the user. Based on the physical mechanisms for dynamic instability various active and passive control concepts have been proposed and realized for centrifugal compressor stages (Pinsley et al. [1991], Gysling et al. [1991], and Simon et al. [1992]). An active control scheme to control rotating stall in a centrifugal compressor in a manner similar to that applied to axial machines was investigated by Lawless & Fleeter [1993b].

There are only a few investigations covering rotating stall in vaned diffusers of centrifugal compressors (Ogata & Ariga [1995], Hunziker & Gyarmathy [1993], Lawless & Fleeter [1993a], Filipenco [1991], Haupt et al. [1988], and Abdelhamid et al. [1987]).

Flow visualizations by Le Manarch & Robert [1958] showed impeller rotating stall initiated by the vaned diffuser rotating stall. One stall cell was rotating at 20% of the impeller speed. The stall cell consisted of a vortex at impeller exit and created return flow along the blade pressure side. This impeller exit flow

perturbation was initiated by the unsteady flow in the vaned diffuser and did not exist for a vaneless diffuser.

Investigations of rotating stall in a high performance centrifugal compressor with vaned (cambered vanes) diffuser was carried out by Abdelhamid et al. [1987]. Two types of rotating stall were observed. At low compressor speeds ($N < 13600$ RPM) there were three cells with a rotation speed of approximately 5-6% of the impeller speed. For higher speeds ($N > 13600$ RPM) the rotating pattern changed to two cells and rotated at approximately 16 - 20% of impeller speed. The maximal relative magnitude of flow oscillations was observed in the quasi-vaneless space. Abdelhamid et al. [1987] stated that the deterioration of flow conditions in the diffuser inlet with decreased flow angle at impeller exit is to be a significant destabilizing factor leading the onset of the instability and flow oscillations.

Haupt et al. [1988] investigated the influence of different vaned diffuser types (straight channel, cambered vane and twisted diffusers) on rotating stall onset. Rotating non-uniform flow patterns were found in a wide range of operating speeds before the occurrence of surge. The number of cells was dependent on the operating conditions and varied from two to four. A comparison of unsteady flow characteristics of the straight channel and cambered vane diffuser showed similarity in the spatial distribution of the unsteady pressure field, in the frequencies of fluctuations, and in the rotation speed of the observed non-uniform patterns for both diffusers. In both of the investigated vaned diffusers, flow visualization techniques revealed the occurrence of reversed flow near the shroud wall of the impeller. The use of the two different radial diffusers interacting with the same impeller and collecting chamber, resulted in differences in the compressor characteristics. The surge line was shifted towards higher mass flow rates for the configuration with the straight channel diffuser compared to cambered vane type.

Lawless & Fleeter [1993a] performed an experimental study in a centrifugal compressor with three different vaned diffuser geometries to identify spatially coherent pressure waves which would serve as precursors to the development of an instability. The rotating stall patterns observed in the compressor

demonstrated propagation rates near impeller speed, and had from one to four cells. These instabilities were described as impeller stall by the authors, although the conditions appeared to arise simultaneously both in the diffuser and impeller and were typically of similar magnitude in both locations. The rotating stall behavior of the low speed centrifugal compressor with vaned diffuser used in the investigation by Lawless & Fleeter [1993a] exhibited a more extensive variety of spatial modes than those reported in low speed axial compressor investigations. Although exhibiting the same fundamental type of instabilities, centrifugal compressors are characterized by a much broader spectrum of unstable behavior than their axial counterpart.

Hunziker & Gyarmathy [1993] tested a centrifugal compressor with three different cambered vane diffusers. In their compressor the stability limit occurred at the flow rate corresponding to the maximum pressure rise of the overall stage. Mild surge occurred at the flow rate giving the maximum overall stage pressure rise characteristic (zero slope), in compliance with linearized stability theory.

To assess the influence of different centrifugal compressor components on the stability of the stages, Dean [1974] proposed a stability parameter, SP . The analysis of the pressure rise characteristics of each individual stage component (impeller, vaneless space, channel part of diffuser) gives a guide to the contribution of each. The slopes of the pressure rise characteristics of individual components indicate the strength of their stabilizing and destabilizing effect. The total pressure ratio of the stage can be written as a product of pressure ratios of individual components and therefore the stability parameter, SP , as a sum of the stability parameter of individual components. The influence of individual stage components on the stability can thus be shown in a graph as a function of mass flow rate (Figure 1.5 from Dean [1974]). In this figure positively sloped curves indicate instability. Of particular interest is the identification of those components or subcomponents, which contribute to a positively sloped characteristic, and of those stabilizing components which have a strongly negative slope. The impeller itself has a neutral behavior and the diffuser inlet region (vaneless diffuser + quasi-vaneless space) shows a strong stabilizing effect over a wide flow range. This effect decreases as the flow rate is reduced.

According to Figure 1.5 the unstable component of the stage is the channel part of the vaned diffuser.

Figure 1.5 also indicates the importance of the vaneless space for the stability of the overall stage. Larger vaneless space radius ratio means a smaller upstream influence of diffuser vanes with a favorable effect on stability range. However, a larger vaneless space results in higher friction losses, lower efficiency, and higher throat blockage because of boundary layer development. Dean [1973] claimed that a larger radius ratio does not lead to better performance and Kenny [1972] obtained large operating range and good performance with the diffuser leading edge close to the impeller exit. According to Haseman et al [1991], increasing the vaneless space radius ratio from 1.125 to 1.20 at the same impeller-diffuser configuration reduced the blade vibrations which were caused by rotating stall. Yoshida et al. [1991] also studied the influence of vaneless space on the stability of a vaned diffuser. The results indicated a shift of the stability limit to smaller mass flow rates when the vaneless space is reduced.

Experimental data by Japikse [1980] indicated an influence of diffuser vane number on stability range. Decreasing the number of vanes lowered the surge limit at the cost of a two percent loss in stage total pressure rise.

The stall limit of vaned diffusers is usually correlated either to the diffusion ratio from the leading edge to the throat or to the incidence angle of flow relative to the camber line of the vane or the blade suction surface (Senoo [1984a]). The incidence angle has the same physical meaning as the flow angle for fixed diffuser vanes.

The experiments with vaned diffusers in the open literature show a high pressure rise at the diffuser inlet region (in the quasi-vaneless space between diffuser leading edge and throat). According to some investigators the reason for the flow instability is this high pressure rise from the diffuser leading edge to the throat. Often the quasi-vaneless space is stated as the most critical element of a centrifugal compressor stage where the flow breaks down if a critical level of diffusion or a critical value of pressure recovery is exceeded (Kenny [1972] Toyama et al. [1977], Came & Herbert [1980], and Elder & Gill [1985]). These

investigators correlated the pressure recovery at the diffuser inlet region with the onset of the instability and gave critical values of pressure recovery, $(C_{p1-th})_{crit}$ (in most cases pressure recovery from diffuser leading edge to diffuser throat, but in some cases from impeller exit to diffuser throat, that includes pressure rise in vaneless space) for the onset of instabilities:

<u>Reference</u>	<u>$C_{p(1-th)}_{crit}$</u>
Kenny [1972]	0.45
Dean & Young [1977]	0.40
Toyama et al. [1977]	0.40 to 0.45
Rodgers [1982a]	0.30
Clements [1987]	0.35
Stein & Rautenberg [1988]	0.35
Rodgers [1993] (straight channel diffuser)	0.36
Rodgers [1993] (cascade diffuser)	0.41

The throat area of vaned diffuser is designed to pass the maximum flow rate with some margin. According to Elder & Forster [1987] the reason for centrifugal compressor instability is the high pressure rise or over-diffusion in quasi-vaneless space which is thought to generate surge, especially in high pressure ratio units. For compressor stages with vaned channel diffusers Elder & Gill [1985] collected data for stall in the vaneless and quasi-vaneless region of the channel diffusers and presented a correlation, which gives the stalling value of pressure recovery $(C_{p1-th})_{crit}$ in the vaneless and quasi-vaneless space versus the 'wetted' perimeter area (A_w) divided by the geometric throat area (A_g) times the rotor blade number (Z_b). This criterion for defining the diffusion, the ratio 'wetted surface area of the quasi-vaneless space/geometric throat area' ($= A_w/A_g$) was initially suggested by Came & Herbert [1980]. Elder & Gill [1985] added an additional parameter to this parameter, namely the blade number and found a better correlation.

The idea of a critical value of pressure recovery from diffuser leading edge to throat is not able to explain surge line shifts caused by changes in the diffuser channel geometry (Japikse [1980], Clements & Artt [1987a]). The discrepancy

between different investigations for $C_{p(1-th)crit}$ also implies that the correlation between stall onset and pressure rise at the diffuser inlet region is not adequate for design. Japikse [1984b] tested different compressor stages, which were designed by several designers and equipped with vaned diffusers. He found values of critical pressure recovery at the diffuser inlet region as 0.1 to 0.35. In other centrifugal compressor stages he observed values as high as 0.45. He concluded that the criterion of critical pressure recovery at the diffuser inlet region is quite approximate and there is no one critical value which can be used in all design work.

Diffuser leading edge incidence angle relative to the vane suction surface was introduced by Reeves [1977a] as a factor affecting stall and surge. If wedge type vanes are used (straight channel diffuser) and the divergence angle of diffuser channel is constant, the wedge angle becomes larger as the number of the vanes is reduced. As a result the direction of the suction surface becomes closer to the tangential direction for a given stagger angle of the channel. Therefore, if the incidence angle relative to the suction surface is the main parameter for stall, the flow range for a vaned diffuser is increased as the number of the vanes is reduced. Reeves [1977b] correlated the flow range of pipe diffusers to the diffuser leading edge Mach number and the incidence angle relative to the bisector of the wedge at the choke flow rate.

1.2.3.3 Some Practices for Vaned Diffusers to Achieve a Larger Flow Range

In this section we summarize some techniques used to increase flow range. There is an increasing interest in the implementation of active control schemes to extend the operating range of compressors. The effective design of control laws requires a detailed understanding of stall inception dynamics. In that one must know what the mode, or the nature of instability is. This includes the frequency content of this disturbance mode, the growth rates, and the spatial structure, because all of these items are needed to define a proper control strategy. Experimental investigation should include both local and global time resolved features of the flow field, as well as steady-state information.

The maximum efficiency of radial flow centrifugal compressors usually occurs too close to the surge line and the desirability to match engine operation close to this peak efficiency can lead to insufficient flow margin. Techniques to reduce the surge flow limit without adversely affecting compressor performance at the design point are clearly desirable. Variable geometry devices meet this requirement as they can remain inactive when design point peak efficiency is required and can be only used when surge is imminent.

Adjustable diffuser vanes (or blades) have been used to increase flow range so that the incoming flow angle can adapt to vaned diffuser and rematch the diffuser to the changed inlet flow condition. Since the onset of the instability is mainly determined by diffuser inlet flow angle, adjustable diffuser vanes can increase the flow range of the stage. Applications of adjustable diffuser vanes can be found in Rodgers [1968] and [1977b], Harp & Oatway [1979], Berenji & Raffa [1979], Simon et al. [1987], Casey & Marti [1986]. Current research is also going on at the University of Hannover in a centrifugal compressor facility with adjustable diffuser vanes.

A compressor with an adjustable vaned diffuser may be operated safely in part load conditions and smoothly over the range in which a compressor with a vaneless diffuser could perform with rotating stall instabilities. In addition, adjustable vaned diffuser adjusts to a higher static pressure ratio compared with a vaneless diffuser. Improved flow range (ca. 10%) could be observed by Rodgers [1977b], but the leakage penalty around the variable geometry diffuser vanes was also clear. Very tight clearances are necessary between the adjustable vanes and the sidewalls in order to control the leakage losses. A trade-off must be made between the advantage gained versus the cost and also versus the penalties associated with leakage around freely moving vane elements.

Flow regulation through single stage centrifugal compressor is most effectively achieved by the use favorable IGV's (Inlet Guide Vanes) and variable diffusers. Combined variable IGV's and diffuser vanes provided minimum efficiency penalty with flow reduction (Rodgers [1968]). An extensive study with IGV's and variable diffuser vanes was reported by Simon et al. [1987]. The working range of centrifugal compressors could be distinctly expanded by adjusting the diffuser

vanes according to the investigations by Simon et al. [1987]. Simultaneous adjustment of inlet guide vanes and diffuser vanes enables an increase in efficiency over the entire operating range compared with regulation of only inlet guide vanes or diffuser vanes (Simon et al. [1987]). Compared with the stage equipped only with adjustable inlet guide vanes, the efficiency gained in the case of matched adjustment of the inlet guide vanes with diffuser vanes amounted to 2% at the reference point (and up to 6% along the speed line at the reference point).

Using IGV's increases impeller and inducer flow stability allowing the downstream diffuser to operate slightly into its positive incidence zone, even though the diffuser static pressure rise versus flow characteristic exhibits a positive slope according to Rodgers [1990]. He tested a centrifugal compressor with a vaned diffuser and adjustable inlet guide vanes and showed that the high speed surge margin was extended by regulation of the IGV's, even though the vaned diffuser was operating stalled. For this test compressor, the high speed surge line was triggered by inducer stall and thus IGV regulation increased impeller stability. With this regulation it was possible to provide the net compression system stability remained negatively sloped. These results conflict with some other lower Mach number compressors where the vaned diffuser would dominate surge and IGV regulation was similar to the effect changing speed, without a significant shift in surge line. Rodger's investigations indicated that at inducer tip relative Mach numbers greater than unity, the surge line corresponded to the expected position of inducer stall. It was observed that the high speed surge line was triggered by inducer stall and low speed surge line was triggered by diffuser stall.

Two variable geometry techniques, variable prewhirl guide vanes and variable vaneless diffuser passage height, were applied to small turbocharger compressors by Whitfield et al [1976]. To improve the operating range of a centrifugal compressor, variable inlet and diffuser vanes were used on a compressor with a pressure ratio of 2.5 by Harada [1996]. Low solidity cascade vanes were used for the diffuser. By adjusting the diffuser vanes to the most suitable flow angle, pressure fluctuations caused by the unstable flow in the diffuser during low flow rate operation of the compressor could be suppressed.

The compressor could be operated nearly up to the shut-off flow rate without any indication of surge. According to Harada's investigation when the pressure ratio of the compressor is below 2.5 and the pressure fluctuation in the diffuser at low flow rate is suppressed by using adjustable diffuser vanes, the compressor can be operated under surge-free conditions even when the impeller stalls. In this investigation impeller stall occurred when the relative velocity ratio, inlet to exit of the impeller, exceeded a critical value, which depends on impeller speed.

Theoretical analyses and experimental results were reported for two unique variable geometry techniques used with pipe diffusers by Salvage [1996] to enhance off-design performance. The circular section of the pipe diffuser makes varying its geometry difficult. Adjusting the direction of the flow seems more appropriate for pipe diffusers. One technique applied (split-ring diffuser), mechanically closes the diffuser throat in an unusual manner. The other (recirculation diffuser) allows flow recirculation to close the diffuser throat artificially while attempting to improve diffuser inlet flow characteristics. In the case of the split-ring diffuser the pipe diffuser is divided into two concentric rings, one of which is rotated with respect to the other. In the second technique, a portion of the fluid from the collector re-entered the impeller exit flow stream via a recirculation. The recirculating flow tended to fill the diffuser passage even as impeller flow is reduced. Results showed that surge margin may be improved by either method against the baseline compressor data. The surge margin improvement depended on the IGV settings, and flow recirculation may offer efficiency according to Salvage [1996]. However, Mechanical implementation, device control challenges and problems of leakage remain.

Another approach for increasing operating range is suction of low momentum flow at the suction side of the vanes in the quasi-vaneless space or at the throat. This increases mass flow range near the surge line as well as near choke according to Rodgers [1982a]. Another technique for enhancing the surge margin is linking of the diffuser throats by a communicating manifold. This equalizes the pressures in the diffuser throats and hence prevents diffuser from reaching its limiting (stalling) condition and extending the range to the stall of the diffuser. Raw [1986] applied side walls (hub and shroud) injection and/or suction at the diffuser throat and obtained an increase in flow range.

Several investigators have considered special treatments of the inlet region in order to improve the stage performance. The first technique is a twisted diffuser vane leading edge to conform the hub to shroud distribution of flow velocity and angle, leaving the impeller and entering the diffuser. Bammert et al. [1983] demonstrated that a diffuser vane inlet geometry (twisted diffuser), which is better adapted to the hub to shroud local flow conditions, can improve the centrifugal compressor range and efficiency at the speed line for which the diffuser has been optimized. Bammert et al. [1983] tested a cambered vane, a straight channel and a twisted diffuser at the same compressor stage. The three diffusers had the same design point but were geometrically dissimilar. The compressor with the twisted diffuser had better efficiency and higher pressure ratio. For higher speeds the region of operation was wider than for straight channel and cambered vane diffusers.

The geometry (shape) and sharpness of the leading edge of the radial diffuser vanes can influence the stable flow range of the centrifugal compressor. Jansen [1982] achieved a broader mass flow range with twisted diffusers, although the results of Fischer [1986] did not confirm the ones of Jansen. Another method is to use notches in the leading edge of the radial diffuser vanes. Detailed studies to investigate the effect of vane leading edge shapes and notches on the diffuser performance were carried out by Yoshinaga et al. [1980]. For this purpose the leading edges of vanes were cut out (triangular and rectangular). The vane with rectangular cut resulted in lower stage efficiency and operating range, while the vane with the triangular cut resulted in an improvement in stage efficiency of one or two points, without influencing the operating range. Another example for the vaned diffuser leading edge modification was proposed by Sulzer-Escher Wyss [1976] (This reference is taken from Hunziker [1993]). With a modification at the leading edge of the vaned diffuser there was an increase of stable flow range without changing the stage efficiency. Different shapes particularly at the diffuser inlet were found to have an effect on surge limit as also reported by Whitefield et al. [1976]. Unfortunately, it is difficult to generalize the results by Kenny [1972], Yoshinaga et al. [1980], Whitefield et al. [1976], and Sulzer-Escher Wyss [1976] and to give a systematic concept or guidelines for the modification of diffuser leading edge.

Analogous to axial compressors, casing treatments has also been used in centrifugal compressors to extend the stable operation range. One application of casing treatment at a radial impeller inlet, exit and in the vaned diffuser is reported by Jansen et al. [1980]. Casing treatment at impeller exit and vaned diffuser wall treatment with radial slots in the external hub section gave unsatisfactory results in terms of moving surge limit, but the flow rate at choking was increased. The measurements with wall treatments, showed an increase of the operating range rather in choke flow than at the surge line, with a drop in efficiency of up to 4%. The mechanical excitations experienced in this technique were also too high for practical centrifugal compressor design.

A successful diffuser casing treatment was proposed by Amann et al. [1975] for a vaned diffuser centrifugal compressor. A circumferential slot, connected to annular chamber at impeller exit (in vaneless space) was effective in suppressing surge. A more uniform circumferential pressure distribution with lower pulsation levels and pressure peaks was observed with this treatment.

A last example from this category is from Ribaud & Avram [1982] who used slots at the vaned diffuser inlet or at the throat which are connected to an annular plenum. This plenum was connected to the inlet duct through a throttle valve to regulate the amount of flow sucked out of the diffuser. With the valve closed, the pressure rise, efficiency and range improved compared to the original geometry without the apertures. Part of this performance improvement was lost when some percentage of the flow was allowed to return to the inlet duct. With the same efficiency and stage pressure ratio, the flow margin obtained was twice as that obtained without opening the throat slots.

Another aspect to be considered is the shape of vane surfaces in the radial diffuser inlet region. Most investigators prefer using straight wedge-type diffusers for the channel. By contrast, some investigators (Dean et al. [1970], Verdonk [1978b], Dolan & Runstadler [1973]) have contoured the leading edge so as to permit more gradual control of the flow entering the diffuser inlet, in the belief that this is important in the transonic flow regime. The investigations by Rodgers [1982a], Japikse & Osborne [1986a, b], and Clements & Artt [1987b] on straight channel diffusers showed that diffusers with a straight suction side at

the inlet (in quasi-vaneless space) have broader mass flow range than the concave suction side profiles. It is not possible to find definitive information that argues which system is superior at any particular Mach number level and this design feature remains to a subjective choice of designer according to Japikse [1996].

Clements & Artt [1987a] and Clements [1987] showed that there is a correlation between the stable flow range of the centrifugal compressor stage and the divergence angle, 2θ , of the channel diffuser part for a constant diffuser throat area (Figure 1.6a and b from Clements & Artt [1987]). These figures show an increasing efficiency (pressure recovery) with increasing diffuser divergence angle 2θ of the channel part (a), however, the stable flow range decreases with increasing diffuser divergence angle 2θ .

Came & Bellamey [1982], Japikse [1984b] and Van den Braembussche [1984] summarized the experiences of different compressor manufacturers and investigations on stall and surge margin of centrifugal compressor diffusers: Vaned diffusers designed for high pressure recovery (choice of channel diffuser divergence angle 2θ) have often smaller flow range and diffusers with less pressure recovery have broader flow ranges.

In addition, Japikse [1984b] showed a correlation between the stability limit of centrifugal compressors (flow range) and flow separation in the single channel diffusers, which depends on the diffuser divergence angle, 2θ . Stalling of the channel diffuser can play an important role in the eventual stalling and surging of an entire stage. Consequently, one characteristic that has been used is to correlate the stage range with the measure of the channel diffuser $\Delta 2\theta$, a hypothesis which was first suggested by Dean [1974]. Japikse first calculated the difference between radial channel diffuser divergence angle, 2θ , and maximum diffuser divergence angle of single channel diffusers without separation, $2\theta_{\max}$, and plotted this angle-difference, $\Delta 2\theta$, versus mass flow range of different radial compressor stages (Figure 1. 7). From this figure it may be observed that stable operating range decreases as $\Delta 2\theta$ is reduced in the direction of the ridge of the transitory stall or best performance of single channel diffuser. Negative $\Delta 2\theta$ means that the unit was designed with a conservative offset between the

divergence angle of the diffuser and the ridge of peak recovery at the design point conditions. It can also be noted in this figure that several points failed to follow the trends shown. All of the stages, which are exceptions to the channel diffuser stability criterion in this figure were found to embody additional phenomenon which provided extra stability according to Japikse [1984b]. All of these stages involved transonic flow conditions at the diffuser leading edge. For these cases, a strong shock system was identified and the stabilization which resulted from the shock system and the additional pressure rise, contributed to enhanced stable operating range. However, in each case the shock system created additional losses and, in several cases, mechanical damage was found on rotating components (Japikse [1984b]).

A number of other practices can be added to the list of above stated modifications for the increasing operating range of centrifugal compressors equipped with vaned diffusers (Botros & Henderson [1994] reviewed the current state of technology in surge control of centrifugal compressors). However, many of these result in an efficiency decrease when the range has been increased. To avoid surge and stall, the most appropriate design of the impeller and diffuser requires that both components are correctly matched. Recently active control techniques have been employed with success to suppress the flow instabilities in form of rotating stall and/or surge in axial and centrifugal compressors and there is an increasing interest in the implementation of active control techniques to extend the operating range of centrifugal compressors with vaned diffusers.

1.2.4 Flow at the Impeller Exit

The most important uncertainty in the centrifugal compressor design experience is the description of the flow process at the impeller exit and in the diffuser inlet according to Dean [1973]. Experimental and computational investigations on the development of flow within the impeller channel have provided some insight into the origin of the impeller exit flow non-uniformities. Discussions on the developing flow from a centrifugal impeller into radial diffusers can be found by Eckardt [1977], Krain [1984], Elder & Forster [1987], Inoue & Cumpsty [1984], Hathaway et al. [1993]. In each case, there is evidence of significant distortion,

relative to the impeller in both hub to shroud (axial) and blade to blade (circumferential) planes which causes unsteady flow in the vaned diffuser inlet region. Several experimental investigations pointed out the flow non-uniformity at the impeller exit and at the diffuser inlet, but the effect of the inlet flow field distortion on the vaned diffuser and on the overall compressor performance is not sufficiently investigated. It is generally believed that the impeller exit flow non-uniformities and the resulting unsteady impeller-diffuser flow interaction could have a significant influence on the performance of the compressor stage. The underlying fluid dynamics, however, are not understood well enough to permit the development of rational guidelines for selecting the impeller and diffuser fluid dynamic design parameters for optimal performance. If the details of the flow through the impeller-diffuser stage are clearly understood, appropriate design steps can be taken to improve sizing of the components, to achieve more effective matching, and to increase stage efficiency and stability margin (Filipenco [1991]).

The flow character at a centrifugal compressor impeller exit, which differs considerably from a potential- theoretical profile, is very often called a jet - wake pattern. The "jet" is the flow with high meridional velocity which is primarily present in the hub/pressure side area. The "wake" is the flow in the shroud/suction side area that has a low meridional velocity. Dean & Senoo [1960] and Dean [1971] first described the process downstream of the impeller in a vaneless diffuser with the jet-wake model. The idea of a jet-wake flow was popularized with an analytical description of the jet-wake process for an centrifugal impeller by Johnston & Dean [1966]. In 1977, Eckardt published the results of detailed measurements at different planes of a centrifugal compressor impeller. (See Fig. 1.8 from Eckardt [1977]). The presence of secondary flows, tip clearance leakage and shroud boundary layers were found to develop into a low momentum zone (wake) at the impeller exit. Navier Stokes computations of the Eckardt's impeller were performed by Moore & Moore [1980] and qualitative indications of the formation of a wake-type region could be identified.

The flow distribution at the impeller exit depends also on the operating point of the compressor stage. Figure 1.9 from Dalbert [1993] shows the measured (Laser-Two Focus Velocimeter) and calculated (with the Dawes code) velocity

distributions at the exit of a centrifugal compressor impeller for three operating points (near surge, design point and near choke).

A jet-wake flow pattern has been observed in the discharge flow of a centrifugal compressor impeller by many researchers (McDonald et al. [1971], Mizuki et al. [1975], Olivari & Salaspini [1975]). However, the wake has been detected at different positions in the exit plane of the impeller. Investigations by Kämmer [1984], and Ribaud [1987] indicated a back flow region from the diffuser to the impeller at the front wall (shroud) for reduced mass flow rates. For some operating conditions was the back flow region near the rear wall (hub) and the reason of this change was not clear or well understood. Impeller shroud boundary layer separation and secondary flow were observed to lead to the formation of a wake in the suction side/shroud corner region at the impeller exit by Johnson & Moore [1983a, b]. In the experiments of Kano et al. [1982] low momentum flow accumulated at the corner of the shroud and the blade suction side of the impeller. In some studies, for example by Fisher & Inoue [1981], the presence of a distinct low momentum zone, called the wake by previous investigators, is more difficult to identify. Hamkins & Flack [1987] made laser measurements in an unshrouded pump impeller showing a jet/wake development which is almost contrary to the flow character of the Eckardt's impeller, i.e. the wake development was found close to the pressure side.

The location of the wake is known to be influenced by flow rate and impeller speed as well as impeller geometry, but even today design techniques cannot predict accurately either the wake size and/or the location of the wake. According to the analysis by Johnson & Moore [1983a, b] at the impeller exit, the wake is located on the suction surface in the 'below design' flow, near the suction-surface/shroud corner in the 'design' flow and on the shroud 'above design' flow. It is concluded by Johnson & Moore [1983a, b] that the relative magnitudes of the secondary flows due to curvature and due to rotation generated in the axial-to-radial bend are responsible for the wake's position. Laser 2Focus measurements of the flow at the exit of modern unshrouded centrifugal impellers with backswept blades yield a more uniform velocity profile compared to former measurements of Eckardt on impellers with radial blading (Rohne & Banzhaf [1990]). Hah & Krain [1989] experimentally and

numerically investigated a 4.7:1 pressure ratio high efficiency, backswept impeller. They found comparatively smooth impeller discharge velocity profiles at all operating conditions (design point, near choke and surge) differing widely from the jet/wake type pattern.

According to Japikse [1987] the concept of a jet-wake structure is now less clear in the cases of well designed impellers and impellers with substantial backsweep. Japikse recognized rather the existence of an isentropic core (in the vast majority of compressor and pump studies) and various stream tubes of lower momentum fluid which is caused by secondary flows, shroud and wall boundary layers, tip clearance etc. There is no difficulty with the "jet" concept; the problem is with the term "wake" where many impeller flow fields may not show a distinct "wake"-like character but rather can be better characterized as low momentum secondary flows (Japikse [1987]).

The development of a low energy, low momentum region close to the shroud wall, associated with a high velocity region near the pressure surface, has been confirmed in centrifugal compressors using the Navier-Stokes calculations by Hirsch et al. [1996a, b]. Indications were implying that the main mechanism for the accumulation of low energy fluid in the shroud area is the radial transport of boundary layer material along the blade surface. Its location results from a balance between secondary and tip leakage flows and is not necessarily connected to boundary layer separation.

Eckardt [1977] also measured the static pressure distribution at the vaneless diffuser inlet region. The decrease in static pressure gradients with increasing vaneless space radius ratio was noticeable in the axial as well as in the circumferential directions. The radial development of the measured velocity distributions indicated a mixing within the flow at the vaneless space. The mixing process in vaneless space can lead to losses amounting to as much as 10 points stage efficiency in some compressors according to Dean [1973]. Moore & Moore [1980] found that more than half of the entropy rise in Eckardt's test compressor occurred in the vaneless diffuser.

According to Rodgers [1982b], the velocity profile at the diffuser inlet does not influence the pressure recovery in the vaneless diffuser. On the other hand, the experimental investigation by Reddy [1990] on a vortex nozzle-vaneless diffuser test rig indicated that the inlet flow distortion does have significant effect on vaneless diffuser pressure recovery due to high mixing losses. The mass weighted diffuser pressure recovery coefficient decreased from 0.45 to 0.25 with the increase in inlet distortion coefficient, B_f , from 1.0 to 1.15. (Unfortunately, the definition of the inlet distortion coefficient, B_f , is not given in this paper.)

The detailed impeller exit flow measurements by Eckardt [1977] were carried out in a compressor stage with vaneless diffuser. Krain [1984] presented velocity and pressure distribution measurements in a centrifugal compressor stage with a vaned diffuser (straight channel type). The distorted impeller discharge flow character caused a non-uniform flow incidence angle distribution at the diffuser vane leading edge resulting in an impeller-diffuser interaction. A flow angle difference between hub and shroud of up to 27° was present at the diffuser vane leading edge. The measurements in the quasi-vaneless diffuser area showed that the impeller produced a continuous variation of the flow direction within the whole flow channel. A similar flow pattern as observed in quasi-vaneless area was observed at the diffuser throat, but shifted in time. This time shift was equivalent to the time a particle needs to pass from quasi-vaneless area to throat. According to this result, the diffuser inlet flow is highly unsteady and skewed, even within the diffuser throat where steady state conditions are presumed. Often the design of the diffuser channel is based on design procedures that assume steady state condition within the diffuser throat. Therefore the diffuser design may fail if the diffuser is coupled with an impeller that discharges a highly unsteady flow pattern, according to Krain's [1984] conclusion.

The measurements by Krain [1984] and Casey et al. [1995a] showed that impeller exit flow is balanced out after the throat, in the channel part of the vaned diffuser, indicating a mixing process at the diffuser inlet region (in vaneless and quasi-vaneless spaces). To analyze mixing process, which is connected with total pressure losses, in vaneless diffusers some theoretical models have been developed. Most theoretical models for the vaneless space flow assume that the non-uniform impeller exit flow mixes out instantaneously to a uniform flow. The

theories by Dean & Senoo [1960] and Johnston & Dean [1966] try to model the mixing process in vaneless diffuser. According to these theories the end of the mixing zone is at the radius ratio $r/r_{\text{impeller exit}} = 1.15$. But the experiments by Hass [1976], Eckardt [1977] showed fluctuations of the velocity vector in direction and magnitude at the diffuser inlet and actual mixing of the flow continued longer. The spatial development of the radial velocity after the impeller exit showed, that the flow for the radius ratio $r/r_{\text{impeller exit}} = 1.15$ was circumferentially almost uniform, however the axial non-uniformity was nearly the same as the impeller exit. The flow at the vaned diffuser inlet did not show high unsteadiness, but was non-uniform in axial direction both for the velocity and flow angle (Jansen [1982]).

In an investigation of the influence of circumferential non-uniformities in the impeller exit flow on radial diffuser performance, Baghdadi [1973] compared the performance and stability of a radial wedge (straight channel)-type diffuser on the basis of measurements obtained using the vortex-nozzle swirling flow generator (Baghdadi & McDonald [1975], Baghdadi [1976]) with those obtained using an actual centrifugal impeller. The radial diffuser performance and stability for the two cases were found to "agree within the range of experimental accuracy". Since the vortex nozzle produced a circumferentially uniform flow while the impeller produced a jet-wake type flow at the diffuser inlet, it was concluded that the diffuser performance is insensitive to the jet-wake structure of the impeller exit flow. It was suggested that a combination of rapid mixing and the high frequency of the unsteadiness were responsible for this insensitivity of diffuser to the circumferential non-uniformities at the inlet.

It was also observed by Inoue & Cumpsty [1984] that the circumferential distortion from the impeller was attenuated very rapidly in the inlet region of the diffuser vanes and had only minor effects on the flow inside the vaned diffuser passage. Recently the CFD (Computational Fluid Dynamics) calculations on vaned diffuser carried out by Dawes [1994] showed similar results, i.e. insensitivity of diffuser performance on circumferential inlet distortion. All these experiments suggest that the (unsteady) circumferential asymmetry perceived by the diffuser due to impeller exit conditions does not seem to affect the

performance of the downstream diffuser, although it is important as a vibration exciter and as a source of noise (Cumpsty [1989]).

For sensing of the fluctuations at the impeller exit flow field Stein [1986] carried out time resolved pressure, velocity and flow angle measurements at the impeller exit for different impeller-diffuser positions. These measurements did not show any remarkable influence of unsteady effects on the diffuser pressure recovery. A strong mixing zone with high pressure losses existed in the vaneless space, similar to vaneless diffuser investigations. Flow angle fluctuations could be measured at the throat of the diffuser, but the influence of these fluctuations on the flow field and pressure recovery of the channel diffuser part was found to be small by Stein [1986].

1.2.5 CFD Calculations for Centrifugal Compressor Diffusers

For a long time for flow calculations in centrifugal compressor diffusers and for performance predictions, boundary layer calculation methods have been applied (Kline & Johnston [1986]). An example of boundary layer calculations for the inlet region (from impeller exit to throat) of vaned diffusers is presented by Conrad et al. [1980]. In this paper the vaned diffuser inlet region was designed using a two-dimensional, potential flow/boundary layer calculation procedure. Calculations for the overall performance of single channel diffusers using boundary layer computational techniques have also been done (Bardina et al. [1981], Wysocki & Kazimierski [1986]). Pressure recovery of single channel diffusers operating over a wide variety of AR and LWR was obtained by Bardina et al. [1981] including the transitory stall regimes. The studies carried out for single channel diffusers demonstrated that the performance of single channel diffuser can be predicted using boundary layer theory (Johnston [1986]). The prediction of the onset of stall and the line of appreciable stall have also been computed.

It appears that fundamental boundary layer calculations can work well for the diffuser inlet portion of vaned diffusers if impellers yield a fairly simple and clear inlet flow to the diffuser. However, it seems improbable that boundary

layer calculations, even with further modification to account for inlet velocity profile and vorticity, could model the wide variety of practical examples of impeller exit flows. The work by Senoo & Nishi [1977a] has been extended to include the influence of inlet distortion providing the most complete utilization of boundary layer theory for a centrifugal compressor diffuser performance problem. Mean difficulty in utilizing this procedure by Senoo & Nishi [1977a] is the lack of general knowledge concerning the initial profile shape which leaves the impeller and enters the diffuser, and may depend on the operation point of the compressor (see Chapter 1.2.4).

Recent advances in numerical algorithms for solving Euler and/or Navier-Stokes equations and the availability of computational resources have made it possible to compute and analyze steady and unsteady three-dimensional flow through geometrically complex flow paths. Numerous presentations can be found in the current literature on the successes of various types of Navier-Stokes and/or Euler CFD calculations for various turbomachinery flow elements. In the design of industrial centrifugal pumps, CFD has already become a standard tool in the analysis of impellers. Dalbert et al. [1988] and Casey et al. [1990] reviewed some theoretical and experimental techniques of the design procedure used for the fluid dynamic development of centrifugal compressors.

Unfortunately the integration of CFD methods in the design process of centrifugal compressor diffusers and the application oriented optimization of such diffusers have not received much attention. The fundamental problem lies in the time-unsteady flow effects which can be critical to the performance of a high pressure recovery diffuser according to Cumpsty [1989]. The inlet boundary conditions for the diffuser calculations are given by the unsteady and three-dimensional impeller exit flow. The three-dimensional nature of this flow field can be estimated by using a simulation of the impeller flow field, but few CFD codes are available that can efficiently compute the flow field in a vaned diffuser taking into account the periodically unsteady nature of the flow from the impeller (Casey et al. [1995b]). A fully unsteady flow calculation of both the impeller and the diffuser is necessary and, although this is now technically possible, there are currently poor practical applications in industry to examine the unsteady diffuser-impeller interaction in full detail using three-dimensional

Navier Stokes simulations of an entire centrifugal compressor or pump according to Casey et al. [1995a]. Despite the difficulty of such calculations, initial attempts for the numerical simulation of this type of unsteady interaction have already appeared in the open literature, for example the three-dimensional viscous calculations in a centrifugal compressor as presented by Dawes [1994]. For industrial calculations, the diffuser is generally considered as being steady and the inlet boundary conditions are taken as a time-average of the impeller exit flow conditions (Dalbert et al. [1993]).

In addition to the complex inlet conditions, the decelerating nature of the flow in a diffuser is still a difficult problem for current Navier-Stokes solvers as it is known that the standard k - ϵ turbulence model has a number of severe weaknesses in adverse pressure gradients. This is exacerbated by the fact that the diffuser designer is interested in obtaining peak performance from the diffuser and this occurs very close to the condition where unsteady flow separation begins according to the single channel diffuser investigations. Thus, even at the design point the flow in a well-designed diffuser is on the verge of separation and difficult to calculate, and at off-design operating points flow separations are even more likely (Casey et al. [1995b]). But a treatment of the flow in the vaneless or vaned diffuser, on the basis of inviscid flow or inviscid core flow with boundary layers on the walls is not satisfactory for today's centrifugal compressor diffuser design and the calculation of the flow in the vaned diffuser should not be beyond the capacity of modern 3D viscous methods (Cumpsty [1989]). With the application of CFD as a design tool of radial diffusers, the costs could be reduced remarkably.

A time-resolved simulation of the Krain's [1984] stage (centrifugal impeller and straight channel vaned diffuser) was performed by Dawes [1994] using a time-accurate, three-dimensional, unstructured mesh, and solution-adaptive Navier-Stokes solver. The predicted flow field, compared with the experiment, displayed a unsteady interaction especially in the neighborhood of the diffuser entry zone which experienced large periodic flow unsteadiness. Downstream of the throat, although the magnitude of this unsteadiness diminished rapidly, the flow had a highly distorted character. The distorted jet-wake flow emerging from the impeller did not appear to mix out before arriving at the diffuser vanes leading

edge as assumed in some design methods. Good qualitative agreement was achieved between the predicted and measured flow fields both in the impeller and in the entry zone of the diffuser. The calculated flow pattern in the diffuser downstream of the throat was quite similar near the shroud and at mid span, but different near the hub where a substantial hub-pressure side corner stall was predicted. Dawes [1994] also investigated the loss levels in the diffuser and concluded that little loss could be attributed directly to unsteady effects. The principle cause of the high loss levels observed in the diffuser was due to the axial (hub-shroud) distortion in flow angle at diffuser inlet which initiated a strong hub/corner stall in the calculation of Dawes [1994].

Dalbert et al. [1993] applied a three-dimensional, viscous flow code (Navier-Stokes solver) developed by Dawes [1988] to a vaned diffuser (cambered vane) of a centrifugal compressor stage which was previously tested by Hunziker [1993]. The objective was to check the ability of the CFD codes to calculate the performance of vaned diffusers and to investigate possibilities for the representation of the flow phenomena. The computations were compared with Hunziker's [1993] extensive experimental data at three different operating points (from near surge operating point to the choke). Although, the computed static pressure distributions showed a good qualitative agreement with the measurements in all three operating points, one important conclusion of the authors is that it seems questionable whether the calculation and measurement of static pressure distribution alone can give any reliable information about the fluid dynamic quality of the vaned diffuser, especially with respect to off-design points. The measured and calculated static pressure distributions do not reflect the complicated flow pattern in the vaned diffuser.

Drtina et al. [1993] performed three-dimensional, viscous, and compressible flow calculations in order to improve the performance of a radial compressor diffuser with splitter using a commercial finite-volume Navier-Stokes code (STAR-CD). Several operating points ranging from the surge limit to choke were considered. The pressure distributions predicted by the calculations as well as the overall diffuser performance showed descent consistency with experimental data. The presence of splitter blade caused a local pressure drop, thereby affecting the

pressure recovery of the diffuser. The flow was also sensitive to the position and geometry of the splitter blade in the diffuser channel.

Casey et al. [1995b] used a commercial Navier-Stokes solver (TASCflow) with k- ϵ turbulence model for the flow calculation in a vaned diffuser of a centrifugal pump. Initial calculations of a two-dimensional single channel diffuser demonstrated the ability of this Reynolds averaged Navier-Stokes code to predict the measured effects of inlet blockage and area ratio on the single channel diffuser pressure recovery. Later three steady-state calculations of the vaned diffuser of a medium specific speed pump were carried out using different inlet boundary conditions to represent the flow at the pump impeller exit. The results of these calculations were compared with LDA and pressure measurement data of the flow field (Casey et al. [1995a]). Although the Navier Stokes code was able to predict some of the important features of the 3D flow field, it was not able to accurately predict the performance of the investigated highly loaded pump diffuser (Casey et al. [1995b]). The optical and pneumatic measurements showed (Casey et al. [1995b]), that the flow in the vaned diffuser was periodically unsteady, highly turbulent and had extensive regions of flow separation, especially at off-design points. Current CFD methods are having difficulty in predicting exact diffuser performance in regions where flow separation -even at the design point- occurs. This is important because the best operating point of a diffuser is usually very close to the onset of separated flow. Another important aspect of vaned diffuser calculations is the position of the inlet boundary condition and the influence of periodic unsteadiness related to the impeller blade passing.

The unsteady flow field in the vaned diffuser of a medium specific speed centrifugal pump was recently both experimentally and numerically analyzed by Muggli et al. [1996]. The time periodic flow field in the diffuser was examined experimentally with laser doppler anemometry, laser particle tracking velocimetry and with unsteady pressure transducers. The flow was computed with a commercial Navier-Stokes CFD code, whereby the unsteady effects were simulated by a time periodic inlet profile across the diffuser inlet and represented the wakes and potential interaction from impeller. A simple possible form of unsteady calculation for examination of the unsteady flow field in the

diffuser is used, where the unsteady flow coming from the impeller was modeled by a periodic inlet profile rotating around the diffuser inlet with rotational speed of the impeller. Thereby any reverse interaction of the diffuser on the impeller flow field was neglected. Additional simplifications made in these simulations included that a representative two-dimensional section of the diffuser was simulated and also a pitch change in the impeller flow was assumed so that a representative section with two blade passages of the flow could be calculated. Despite these simplifications the simulation included both the potential interactions and the wake/blade interactions occurring in the diffuser due to the passage of the impeller across the inlet boundary of the diffuser computational domain. In order to achieve a better understanding three different comparisons were made. First, a steady flow solution with a constant mean inlet condition was compared with the time-average of the unsteady solution as a means of assessing the significance of the unsteady effects on the flow field. Second, the unsteady solution at various time intervals was compared with the time-average of the unsteady solution to identify important features of the unsteady flow field. Finally, the results of unsteady calculations were compared with the detailed time-periodic flow measurements in the vaned diffuser of the test pump. The results of unsteady simulation were in good qualitative agreement with the unsteady measurements, and both showed the passage and decay of the impeller blade wakes through the diffuser. The test data and simulations indicated that the magnitude of the periodic unsteadiness in the diffuser was strongest at impeller outlet and diminished rapidly downstream of the diffuser throat. The two-dimensional simulation with a time periodic profile to represent the wakes and the potential interaction effects from the impeller showed that many of the important phenomena involved in the impeller/diffuser interaction can be examined without the need for an unsteady impeller/diffuser simulation. There was no substantial difference between steady simulation and the time-average of the unsteady simulation in terms of the flow field and pressure rise predicted by these simulations.

Flow choking characteristics, shock wave structure between diffuser vanes and unsteady impeller/diffuser interaction of a high speed centrifugal compressor operating at low pressure ratio, and high volume flow rate conditions were analyzed using three-dimensional, unsteady numerical calculations by Yamane

& Nagashima [1995]. The calculation results were compared with the available experimental observations, whereupon a good agreement was obtained with respect to the changes in the shock wave pattern as well as the instantaneous static pressure distributions on the diffuser shroud wall along the operation line.

Teipel & Wiedermann [1984], [1986], and [1990], Jeske & Teipel [1983] and Teipel et al. [1992] carried out numerical investigations on flows in radial diffusers. In his earlier calculations Professor Teipel and his co-workers used inviscid Euler codes, whereas most of their presented work later was restricted with code development and validation. The transonic flow in a curved vane diffuser of a centrifugal compressor with high pressure ratio was calculated by Jeske & Teipel [1983] with an inviscid calculation of the pressure field in the diffuser channel and with the determination of the boundary layer flow along the diffuser blades. The numerical results were compared with experiments, and the agreement was found satisfactory by the authors.

It is assumed that the location of the splitter leading edge is crucial for the efficiency and stall behavior of the diffuser. A Euler code for calculating two-dimensional transonic flow fields in centrifugal compressor diffusers was applied by Teipel & Wiedermann [1990] to study the effect of various geometrical parameters of splitter vane diffusers such as the thickness distribution and the leading edge location of the splitter. They found a more favorable influence on the diffuser characteristic if the splitter leading edge is located downstream of the throat of the diffuser channel. However, Teipel & Wiedermann [1990] solved the Euler equations without taking the effect of viscosity into account.

Three-dimensional, inviscid, transonic flow field of the radial diffuser with twisted vanes of Jansen & Rautenberg [1982] was calculated by Teipel & Wiedermann [1986]. Comparison with the experimental data showed that the essential features of the pressure distribution in the vaned diffuser can be calculated with an inviscid three-dimensional method, but a coupling of inviscid theory and boundary layer theory did not provide a sufficient prediction of losses in diffuser channel.

Two dimensional, transonic, and viscous flow field of a centrifugal compressor diffuser (cambered vane diffuser) was calculated by Teipel et al. [1992]. The predicted diffuser pressure field and pressure recovery coefficient were in reasonable agreement with the experimental data.

1.2.6 Radial Diffuser Investigations Important for the Present Study

Most of the experimental investigations on centrifugal compressor diffusers had generally concentrated on obtaining overall diffuser performance and/or overall compressor performance maps, which included the diffusers. The detailed radial diffuser measurements on actual centrifugal compressor flows are those obtained by Krain [1984], and Kano et al. [1982] (straight channel diffuser), Hunziker [1993] (cambered vane diffuser), and Inoue & Cumpsty [1984].

The investigations described by Krain [1981] and Krain [1984] revealed a highly distorted flow pattern at the vaned diffuser inlet. The straight channel diffuser tested by Krain has 27 vanes, and the vaneless space (diffuser leading edge/impeller exit) radius ratio is 1.10. Maximum overall diffuser pressure recovery was about 87% and was largely independent of diffuser inlet Mach number. Measured maximum overall diffuser recovery was obtained for all speed lines near rotating stall, where diffuser pressure recovery dropped rapidly for constant impeller speed and increasing mass flow, resulting in a considerable overall stage pressure drop indicated in the compressor map. Krain used a laser doppler velocimeter system to obtain instantaneous velocity and flow angle profiles across a plane in the quasi-vaneless inlet region and across the throat plane. The total pressure distribution at the diffuser inlet was circumferentially smooth and raised gradually from shroud to hub. The corresponding absolute flow angle and radial velocity distributions revealed a more distorted pattern in both circumferential and axial directions. Periodic flow unsteadiness was observed in the entry zone to the vaned diffuser with temporal variations in flow angle, of the order of 10 - 15°, and spanwise variations from hub to shroud, of the order of 20 - 25°. Within the diffuser throat a variation of 13° in flow angle was observed indicating that the impeller discharge flow distortion keeps up the channel diffuser throat.

Since the meridional velocities differed from hub to shroud at the impeller exit, the inlet conditions for the succeeding diffuser varied considerably across the diffuser depth. Despite these non-uniform inlet conditions the diffuser revealed a good overall pressure recovery, which seems to be due to the enhanced mixing at diffuser inlet, as it is known to increase diffuser recovery according to the investigations of Waitman et al. [1961]. The presented data from the measurements downstream of the diffuser throat by Krain [1984] showed that despite the large periodic unsteadiness in the entry zone, levels of unsteadiness decreased rapidly downstream of the throat.

In a similar study, Inoue [1980] observed large periodic flow unsteadiness in the diffuser vane entry zone. He also found that the magnitude of this periodic unsteadiness diminished rapidly downstream of the throat so that in the channel part of the diffuser no periodic unsteadiness could be observed. In neither study did the impeller exit flow mix out before arriving at the diffuser vane leading edges. For vaneless diffusers Senoo [1984b] reported that axial distortions mixed out less rapidly than circumferential distortions and axial distortion persisted further downstream than did circumferential distortions in vaneless diffusers. According to Dawes [1994] the axial variation of flow property, especially flow angle, seems to exert a more significant influence on the diffuser performance than does the unsteady, circumferential variation in flow.

The vaned diffusers reported by Kano et al. [1982] have the shape of the NASA 65-series profile for the quasi-vaneless region and a nearly straight 2-D channel downstream of the throat. Three different impellers (A, B, and C), which have backward leaning blades, and 14 diffusers of various shapes were tested. Number of impeller blades are 18 and the divergence angle, 2θ , of vaned diffuser is approximately 19° for the a-series, and 14° for the b-series. All the investigated diffusers have 15 vanes each.

All the investigated impellers by Kano et al. [1982] had almost the same characteristics in the head coefficient and the velocity distribution at the impeller exits were non-uniform. Therefore, the peak of the time averaged meridional velocity was not located at the middle of diffuser depth, but it was shifted toward the hub side. The meridional velocity was very low at the shroud side,

though the tangential velocity was almost uniform. Kano et al. [1982] showed how the flow field around the vane leading edge and in the throat changed with flow rate and how the approach incidence influenced the overall pressure recovery. The static pressure distribution in the quasi-vaneless space varied in accordance with operating conditions and flow angle. The boundary layer blockage due to the displacement thickness at the exit of the impeller was 3.8% for impeller A, 6.6% for impeller B and 4.3% for impeller C in the design condition. The boundary layer distribution was not uniform in the quasi-vaneless space and the throat section. There was a large growth of the boundary layer on the pressure side, though it was a small amount on the suction side. A large static pressure recovery obtained in the quasi-vaneless region produced a thick boundary layer at throat. The smaller the flow rate was, the larger throat blockage became. Blockages at the throat were approximately 12% at design flow rate and 22% at lower flow rates (75% of design flow rate).

Yoshinaga et al. [1980] tested sixteen different vaned diffusers in a model compressor using pressure measurements to determine the overall behavior of the diffuser flows. Little discussion on the geometry and performance of individual diffusers was included; instead the authors suggested various general design criteria for improving compressor performance. They indicated that the leading edge shape of the vanes has considerable influence on the diffuser performance (see Chapter 1.2.3.3). In spite of the difference in inlet conditions and their configurations the optimum equivalent divergence angle for vaned diffuser was found to be 8-10°, similar to that of the single channel diffusers.

Impeller exit meridional velocity profiles were measured by Rodgers [1982a]. All measured distributions exhibited well-developed, non-uniform profiles with a trend for shroud flow migration near surge, and hub flow migration near choke. Rodgers calculated impeller tip blockage from the traverse data using the boundary displacement thickness of the absolute flow. Blockage factors at impeller tip varied from (the order of) 5% to 16% with increasing specific speed of the impeller. Because of insufficient instrumentation it was not possible to specifically isolate the effect of throat blockage on diffuser channel pressure recovery by Rodgers [1982a]. A comparison with single channel diffuser data

indicated reasonable agreement except in instances where the diffuser channel was operating near or in stall condition.

Instead of using an impeller Baghdadi & McDonald [1977] (and Baghdadi [1973]) adopted stationary radial cascade nozzles of inward flow to produce a wake-free swirling supersonic flow, then the swirling inward flow was guided outward to the test vaned diffusers. They examined the influence of inlet Mach number on the pressure recovery coefficient and on the flow range between surge and choke for three types of vaned diffusers (Wedge vane, Composite vane, and Circular Arc vane).

The flow visualization, as well as the total and static pressure measurements by Baghdadi [1973] indicated, that surge was an instability triggered by flow separation in the vaneless or quasi-vaneless space ahead of diffuser throat. The choke to surge operating range of the three diffusers tested appeared to be a function of the diffuser vane number only, according to Baghdadi & McDonald [1977]. The series of diffusers tested on the vortex nozzle rig all surged at different flow angles; yet they all had the same mean line vane angle. The static pressure characteristics of all three investigated diffusers indicated flow separation near the throat, because a static pressure decrease right at the throat occurred for surge datum points. The flow visualization, the static pressure characteristics, and the flow angle profiles all pointed to surge being due to some sort of separation occurring ahead of the diffuser throat. Separation near the diffuser throat in the quasi-vaneless or vaneless space triggered surge by producing high losses in the diffuser according to Baghdadi [1973]. Unsteady separation downstream of the diffuser throat, which was discernible in flow visualization motion pictures of the composite vane diffuser, did not trigger surge. This was explained qualitatively as being due to the higher "solidity" of the enclosed diffuser channel, which restricts the unsteadiness and prevents it from pervading the entire flow field. The geometric characteristic which correlated with the onset of surge, was the diffusion length from the diffuser inlet to the throat.

The performance results between the three diffuser types were also compared. The choke to surge flow margin achieved by the three diffusers was a function of

inlet Mach number. The relative performance advantage of one diffuser type over another was also Mach number dependent. The choke to surge flow margin plot by Baghdadi & McDonald [1975] also pointed to the dependence of the flow margin on the number of diffuser vanes.

The Baghdadi & McDonald [1977] paper attracted nine written discussions (Cumpsty [1989]). Many of these discussions addressed the stability aspects for which this facility was not mostly useful, but some criticized the nature of the experiment since it omitted the rotating jet-wake flow from the impeller and the axial profile at inlet was said to be unrepresentative. One example of this criticism is e.g. by Senoo [1984a]: "If a theoretical analysis of flow in vaned diffusers is assumed useful at all where the rotating wakes of impeller blades are disregarded, the experiment using vortex nozzles must be useful too, but the application should be limited to rough estimation of diffuser performances and to screening of various types of vaned diffusers. Even if the unsteady part of the flow due to rotation of the impeller has little effect on the performance of vaned diffusers, since it is very difficult to generate a velocity distribution which is similar to the time mean velocity distribution at the exit of an impeller, a diffuser test using vortex nozzles can not completely simulate the flow in a compressor and it does not supply quantitative information such as the choke flow rate, the maximum pressure recovery and the surge/choke flow range".

Further in the discussions on Baghdadi & McDonald's paper, many participants emphasized influences of the inlet condition of flow on the performance of the diffusers and because of the basic differences in the distorted velocity distributions between the flow of vortex nozzle and the flow out of an impeller, the results of the experimental data were not applicable to the vaned diffuser of a compressor. Especially surge is an unsteady phenomenon of the system including the diffuser and since the stability characteristic of the vortex nozzle ring was quite different from the stability characteristic of an impeller, surging of compressor could not be simulated by a vaned diffuser which was tested with vortex nozzles. Later Baghdadi [1976] applied one of three types of tested vane diffusers to a centrifugal compressor and measured the diffuser pressure recovery coefficient and the ratio of surge/choke flow rates. He claimed that the axial distribution of the time mean velocity at the exit of the impeller was very

close to that of the vortex nozzle rig and the performance of the vaned diffuser was similar to that observed in the vortex nozzle test rig. The fact that the performance of both investigations with a vortex nozzle and with a centrifugal compressor impeller was nearly identical, indicated that the diffusers were well able to cope, with the flow non-uniformity and unsteadiness from the impeller. These results beg the question as how then the diffuser is able to tolerate these wide local excursions in flow (Cumpsty [1989]).

The flow characteristics of a vaned (straight channel diffuser with 20 vanes) diffuser were determined experimentally by using a static diffuser test rig with a vortex test vehicle by Dutton et al. [1986]. Flow angle and Mach number hub to shroud distributions at the different locations of the diffuser (inlet, leading edge, throat and exit) were measured for high and low flow rates. The differences in flow angles between the shroud and the hub side at the diffuser leading edge approached up to 30° . At the throat, the flow angle distributions were more uniform than at the leading edge although the shroud side angles were still up to 20° less than the hub side flow angles. Even at the diffuser exit flow angle differences of 5 to 10° from shroud to hub were measured. The shapes of flow angle, Mach number, and static pressure profiles were relatively independent of flow rate. In the diffuser inlet region, the flow undergoes the transition from highly tangential axisymmetric jet flow to a two-dimensional channel flow. The pressure gradients in this region were strong. The flow in the diffuser channel appeared to become more and more one-dimensional as the exit is approached.

Piemsomboon et al. [1984] also used a static vortex test vehicle to produce inlet flow to a vaned diffuser. They investigated flow angle and Mach number distributions at several locations throughout the straight channel diffuser, but there was no information regarding the influence of these distributions on diffuser pressure recovery. The flow rate had little effect on the shape of the wall static pressure contours in the diffuser.

Using a swirl generator test rig, four different diffuser configurations (vaneless diffuser, a four-bladed, a six-bladed, and a eight-bladed vaned diffuser) were investigated by Brownell et al. [1987]. Of particular interest was the identification of the onset and extent of flow separation from the diffuser blades using flow

visualization. Flow separation occurred at 23%, 27% and 50% from the leading edge of the blades for the 4, 6 and 8 bladed diffusers respectively.

Inoue & Cumpsty [1984] reported tests of vaneless and different vaned diffusers using a centrifugal impeller involving flow measurements using hot wire probes and pressure transducers. The aim was to investigate the interaction between the vaned diffuser and the impeller. Unsteady measurements of velocity and wall static pressure were made at numerous positions in a vaned diffuser. Experiments were carried out at a range of flow coefficients for three diffusers with 10, 20, and 30 vane sets at each of three different vaneless space radius ratios, 1.04, 1.1 and 1.2 respectively. This investigation showed that the circumferential distortion from the impeller was attenuated very rapidly in the entrance region of the diffuser vanes and had only minor effects on the flow inside the vaned diffuser. The amount of reversed flow was greater for vaned diffusers with blades located near the impeller but it decreased with an increase in the number of blades. The instantaneous measurements of radial velocity at various radii in the vaneless diffuser indicated that the circumferential distortion of the flow did not disappear even at 1.30 vaneless space radius ratio. The distortion patterns of tangential velocity and total pressure decreased rapidly with the increasing radius, a trend attributable to the existence of energy transfer between jet and wake as described by Senoo & Ishida [1974]. The circumferential velocity leaving the impeller was about three times the main radial velocity and was more uniform. The non-uniformity out of the impeller therefore gave swing in the flow angle, but relatively small swing in the stagnation enthalpy or pressure. The shapes of the axial distortions were similar, but the magnitudes were different depending on the circumferential position of the impeller. The circumferential mean radial velocity profile in the axial direction at the inlet of a vaned diffuser was almost identical with that of a vaneless diffuser.

Stein & Rautenberg [1985] investigated two cambered vaned diffusers in a centrifugal compressor test rig. The two diffusers were identical except that the width of the vaneless space between the impeller exit and diffuser inlet was varied by 10%. The maximum efficiency of the diffuser with smaller axial width was 2% higher than that for the wider diffuser.

The performance of vane island diffusers were investigated by Rayan & Yang [1980] and Jiang & Yang [1982]. Rayan & Yang [1980] made measurements with an 8-vane configuration and found an overall diffuser pressure recovery of 0.50, which was very low for practical vaned diffuser applications. They explained the low pressure recovery of vane-island diffuser by high losses due to the highly swirling flow at the diffuser inlet. Thus the fluid particle path was long in the diffuser leading to a high total loss coefficient. Jiang & Yang [1982] investigated 14 vane configuration of vane-island diffuser and the results showed the advantage of the 14-vane over several 8-vane configurations as a 40% reduction in pressure loss coefficient.

A well documented and successful design procedure for centrifugal compressor vaned diffusers has probably never been developed according to Dalbert [1993]. Most of the published data on diffusers are restricted to comparisons of performance characteristics and the development of empirical correlations for loss and pressure recovery. Measured isobars of static pressure in diffuser channels (as shown e.g. by Yoshinaga et al. [1980] or Krain [1984]) can only provide limited information on the flow pattern in vaned diffusers. Many of the performance and flow field measurements were carried out in 'vortex rigs', as shown by Dutton et al. [1986], Brownell et al. [1987] or by Davis & Flack [1990], which can only provide limited amount of information necessary to understand the diffuser flow of a centrifugal compressor stage. The variation of the flow field at the impeller exit at different operating points is missing in these cases. Senoo et al. [1983] and Starke & Hergt [1985] showed wall flow patterns in vaned diffusers of a radial compressor stage and a centrifugal pump respectively. But even wall flow patterns cannot provide sufficient information for a thorough assessment of the diffuser flow field (Casey et al. [1995b]).

Impellers and diffusers are usually considered separately in the design process and the interaction between these two components is not taken into consideration in design calculations. For better understanding of the unsteady flow field and the nature of the interaction between the impeller and vaned diffuser, time resolved details of the unsteady flow field in a vaned diffuser of a pump were obtained as a function of the local position of the impeller blades by Casey et al [1995a]. These experiments included several measurement positions

at the diffuser and at a number of operating points along the pump characteristics. The main conclusions of this work are:

- The flow field in the investigated vaned diffuser was three dimensional and unsteady. The three-dimensionality of the flow occurred partly because of the three-dimensional nature of the impeller exit flow and partly because of the highly loaded diffuser design leading to a three-dimensional flow separation.
- The magnitude of the periodic unsteadiness in the diffuser vane was strongest at the impeller exit and diminished rapidly downstream of the diffuser throat. The magnitude of the non-periodic unsteadiness (turbulence) increased through the diffuser passage and was strongest at part-load operating points.
- The impeller blade wakes appeared in the diffuser as a pattern and negative vorticity which was convected downstream of the diffuser throat.
- Recirculating back flow from the diffuser into the impeller occurred at part-load conditions, and the extent of the back-flow was circumferentially non-uniform. The onset of the location of back flow from the diffuser into the impeller had an influence on the stability of the pump stage characteristics.

A consideration in interpreting existing diffuser data is that various investigators have correlated their data in terms of different parameters, some of which have ambiguous physical significance or make general use of the data difficult or impossible (Filipenco [1991]). In addition, much of the diffuser data published in the open literature were not based on diffuser inlet (or impeller exit) traverses. This results in an ambiguous information of the diffuser inlet conditions. Static pressure is comparatively easy to measure in most diffuser configurations using wall mounted static pressure taps. However, in order to correlate different experimental data a consistent measure of the diffuser inlet stagnation pressure must be used. In some examples in the open literature, the inlet stagnation pressure is taken to be the value at the middle of the diffuser depth (e.g. Runstadler & Dean [1969], and Runstadler et al. [1975]) while in other investigations, an area or mass averaged value is used. In some cases the inlet stagnation pressure is estimated from compressor input power and flow rate. As pointed out by Klein [1981], most of the diffuser studies are incompletely documented and many research cases did not include the necessary information for comparing one definition to another, limiting the generality of the available data. In cases such as centrifugal compressor diffuser inlet, where strong total

pressure gradients are present, it is important to emphasize that detailed measurements across the inlet, with suitable numerical averaging across the entire flow field are required, in order to establish a meaningful value of the pressure recovery coefficient or an other performance factor for a diffuser.

1.3 Objectives of the Present Study

The analysis of previous diffuser studies described in Section 1.2, in conjunction with current high-performance turbomachine design trends, suggested that the following objectives and questions, which are divided into two main parts, should be addressed in the current research:

1) Define the effects of inlet flow conditions on straight channel diffuser performance and stability:

The main part of the proposed research is the detailed investigation of a straight channel diffuser, in particular, the effect of inlet conditions, including Mach number, flow angle, boundary layer blockage, and flow non-uniformity in the axial direction, on performance and operating range.

The questions to be answered are:

- What are the pressure recovery (C_p) characteristics of a straight channel diffuser, as a function of inlet Mach number, flow angle, and blockage ?
- What is the sensitivity of the pressure-recovery coefficient of the investigated straight channel diffuser to the axial distortion of the Mach number and flow angle profiles ?

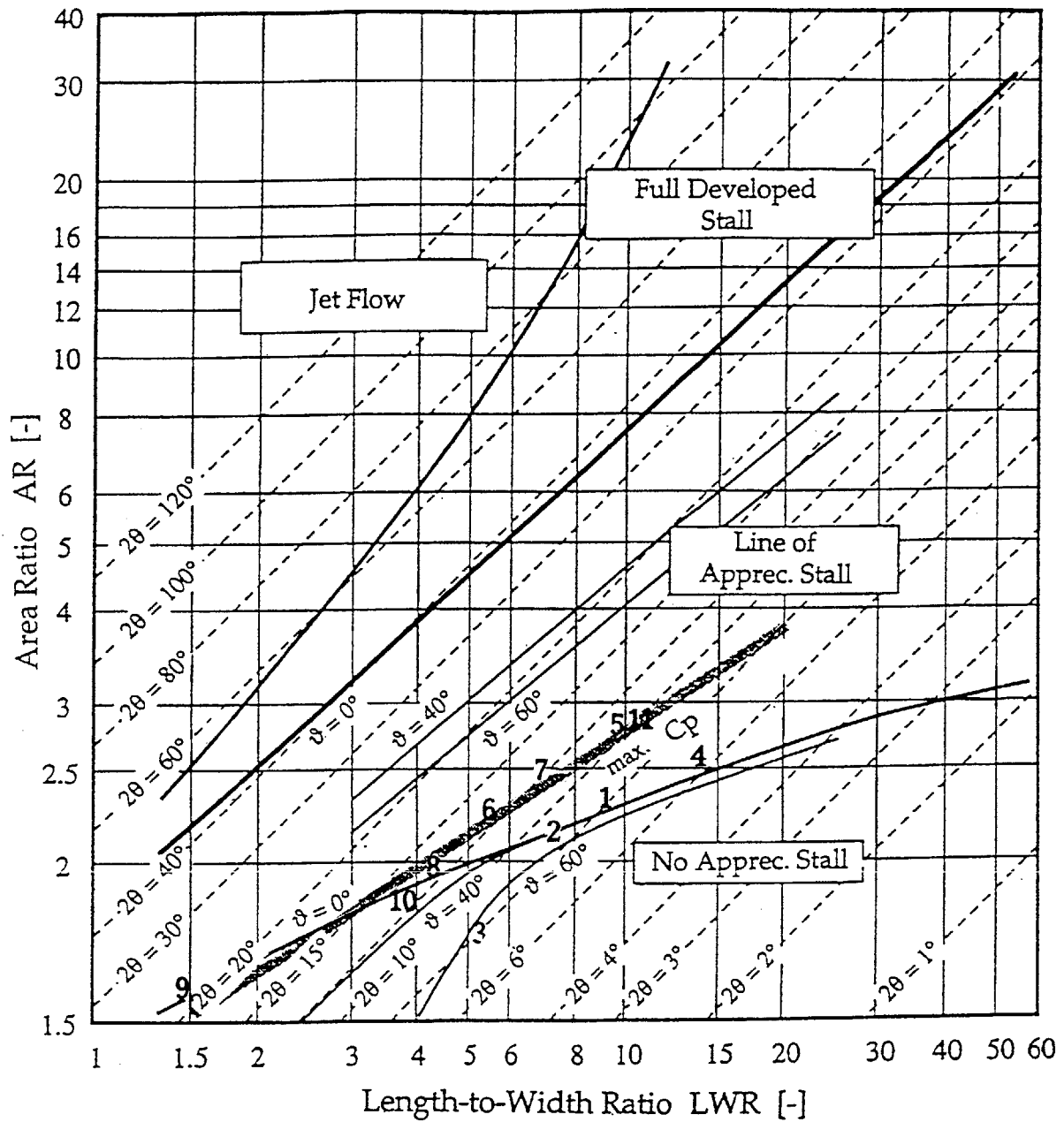
2) Compare the performance of a straight channel diffuser with that of a discrete passage diffuser:

An important objective of this research is to assess the behavior of the straight channel diffuser to those of other geometries currently being used in centrifugal compressors. One of these geometries is the discrete passage diffuser, which was

tested at the same facility and documented by Filipenco [1991] and Johnston [1993]. The basic comparisons include not only the performance of the different diffusers, but also the effects of inlet blockage and axial flow non-uniformity.

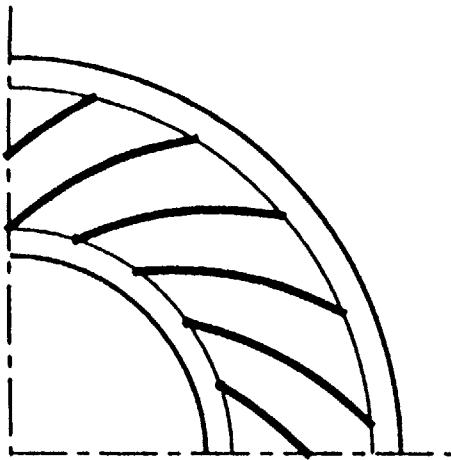
Additional questions to be answered are:

- What are the most appropriate diffuser performance characterization parameters in the general case of an axially non-uniform diffuser inlet flow-field? An intention here is to see whether the diffuser performance can be understood in terms of the same average parameters that Filipenco [1991] identified for the discrete passage diffuser.
- What are flow mechanisms in vaneless space and quasi-vaneless space ?
- What is the influence of inlet and throat blockage on radial diffuser performance?

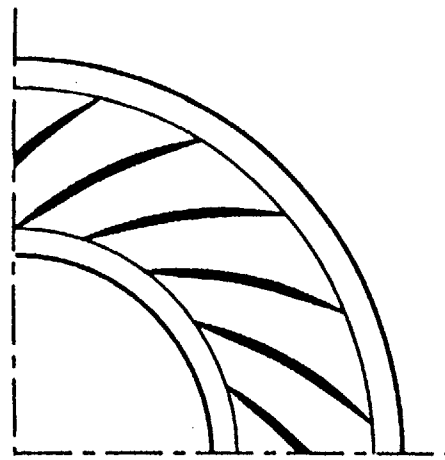


- | | |
|---|---------------------------------|
| 1- Present investigation | 7- Hunziker & Gyarmathy [1993] |
| 2- Jansen & Rautenberg [1982] | 8- Hunziker & Gyarmathy [1993] |
| 3- Jansen & Rautenberg [1982] | 9- Hunziker & Gyarmathy [1993] |
| 4- Krain [1981] | 10- Hunziker & Gyarmathy [1993] |
| 5- Haupt et al. [1988] | 11- Toyoma et al. [1977] |
| 6- Abdelhamid et al. [1987] and Stein & Rautenberg [1985] | |

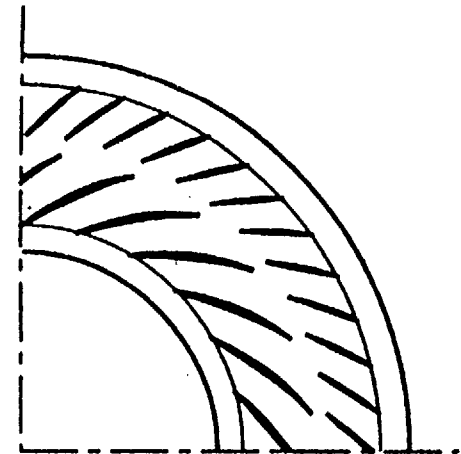
Figure 1.1 Flow regimes in single channel two-dimensional diffusers (Reneau et al. [1967]) and marked geometries of various vaned diffuser rigs from the open literature



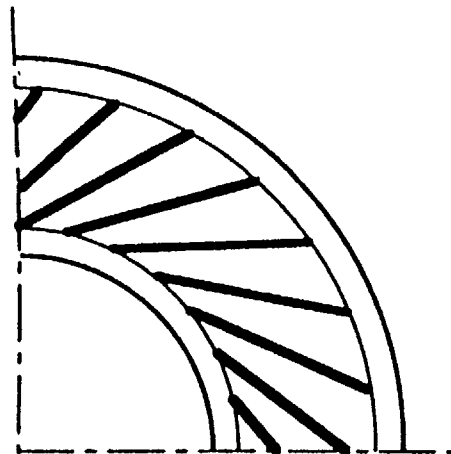
a) Curved Channel Diffuser



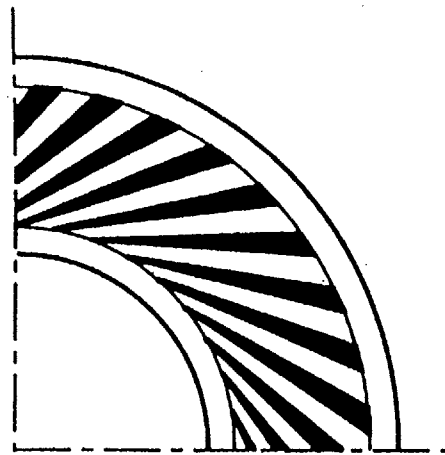
b) Cambered Vane Diffuser



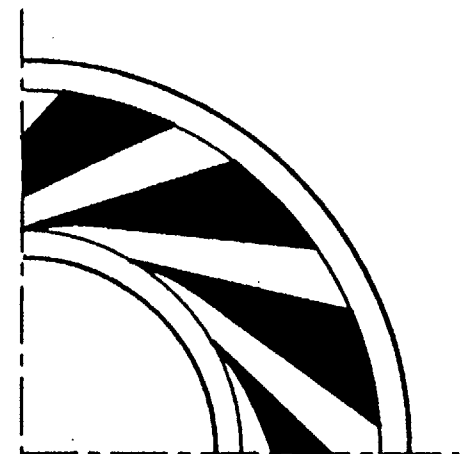
c) Multiple (Tandem) Cascade Diffuser



d) Plate Diffuser



e) Straight Channel Diffuser



f) Vane Island Diffuser

Figure 1.2 Vaned Diffuser Types (Hunziker [1993])

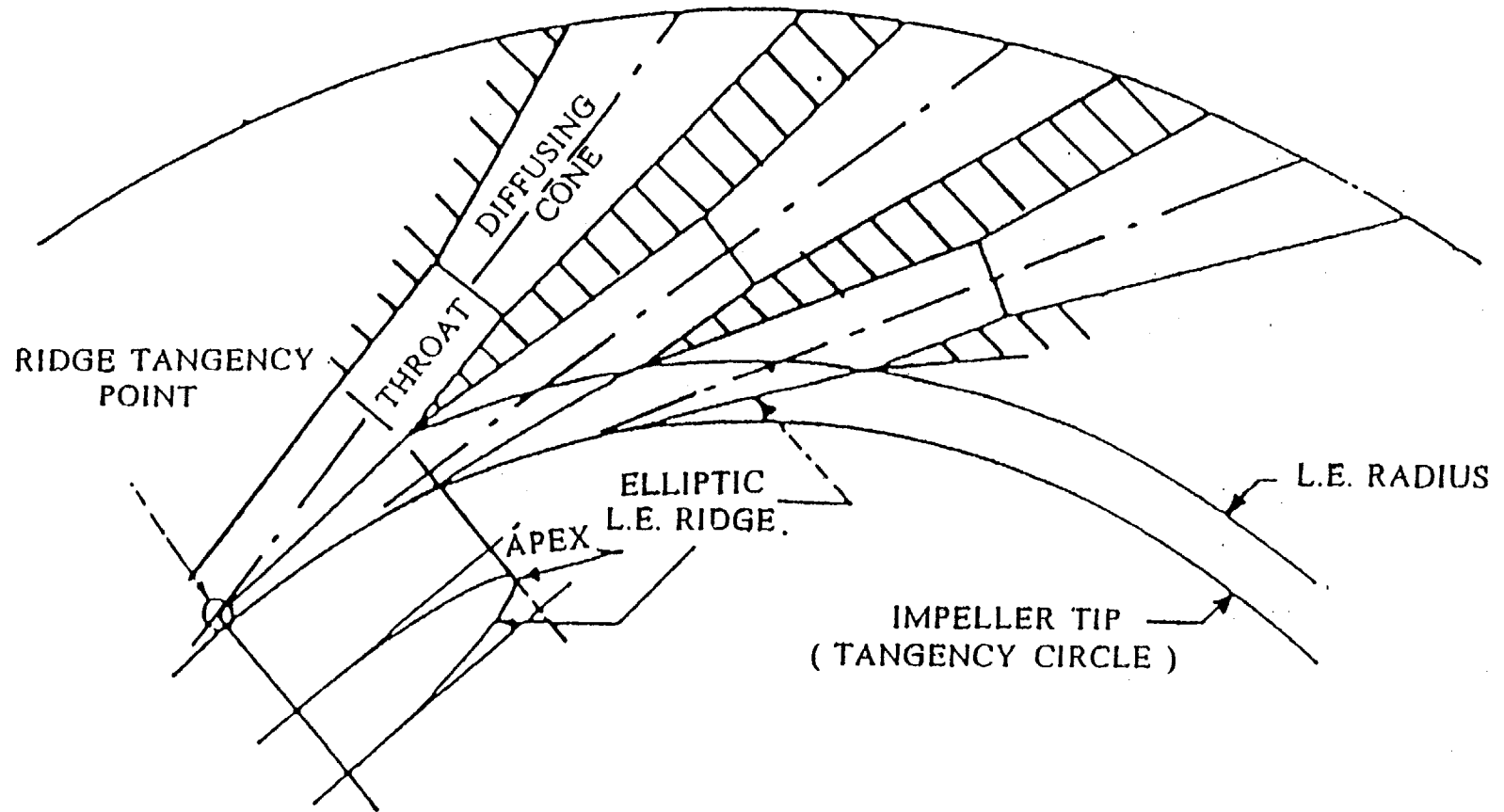


Figure 1.3 General Pipe Diffuser Geometry (Kenny [1972])

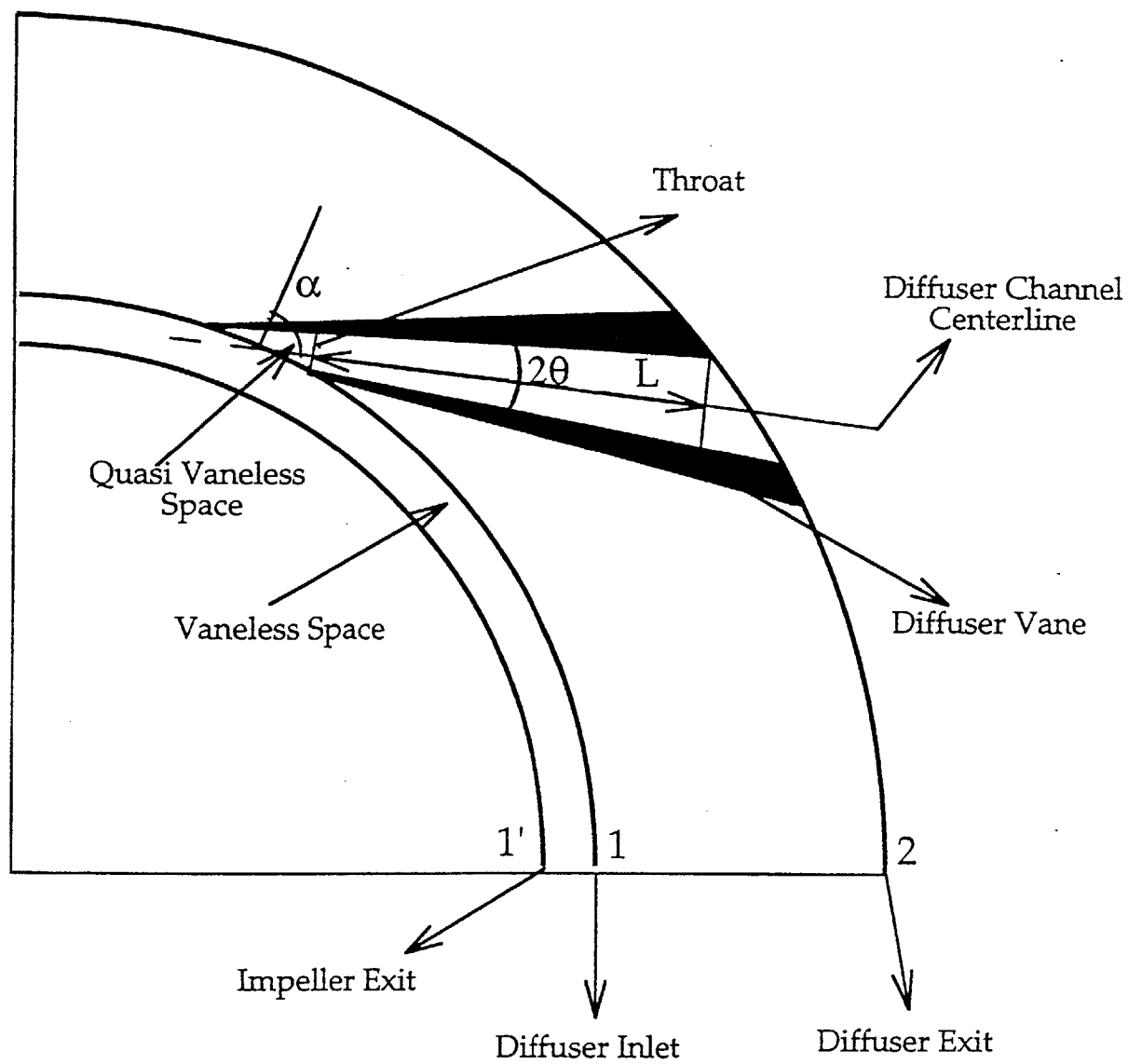


Figure 1.4 Straight-Channel Diffuser Geometry

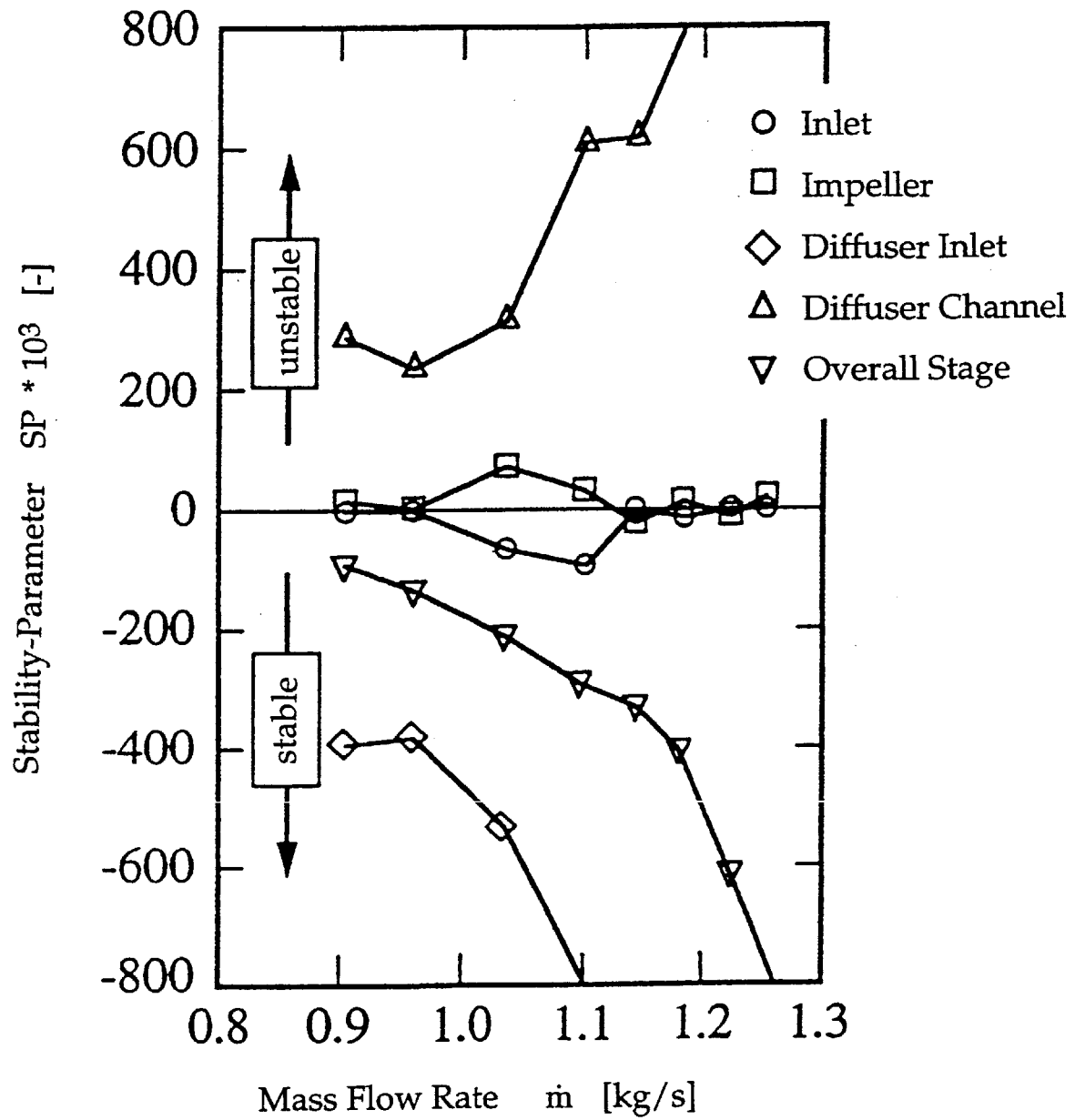


Figure 1.5 Stability-Parameter, SP, for overall centrifugal compressor stage and for each individual stage component (Dean [1974])

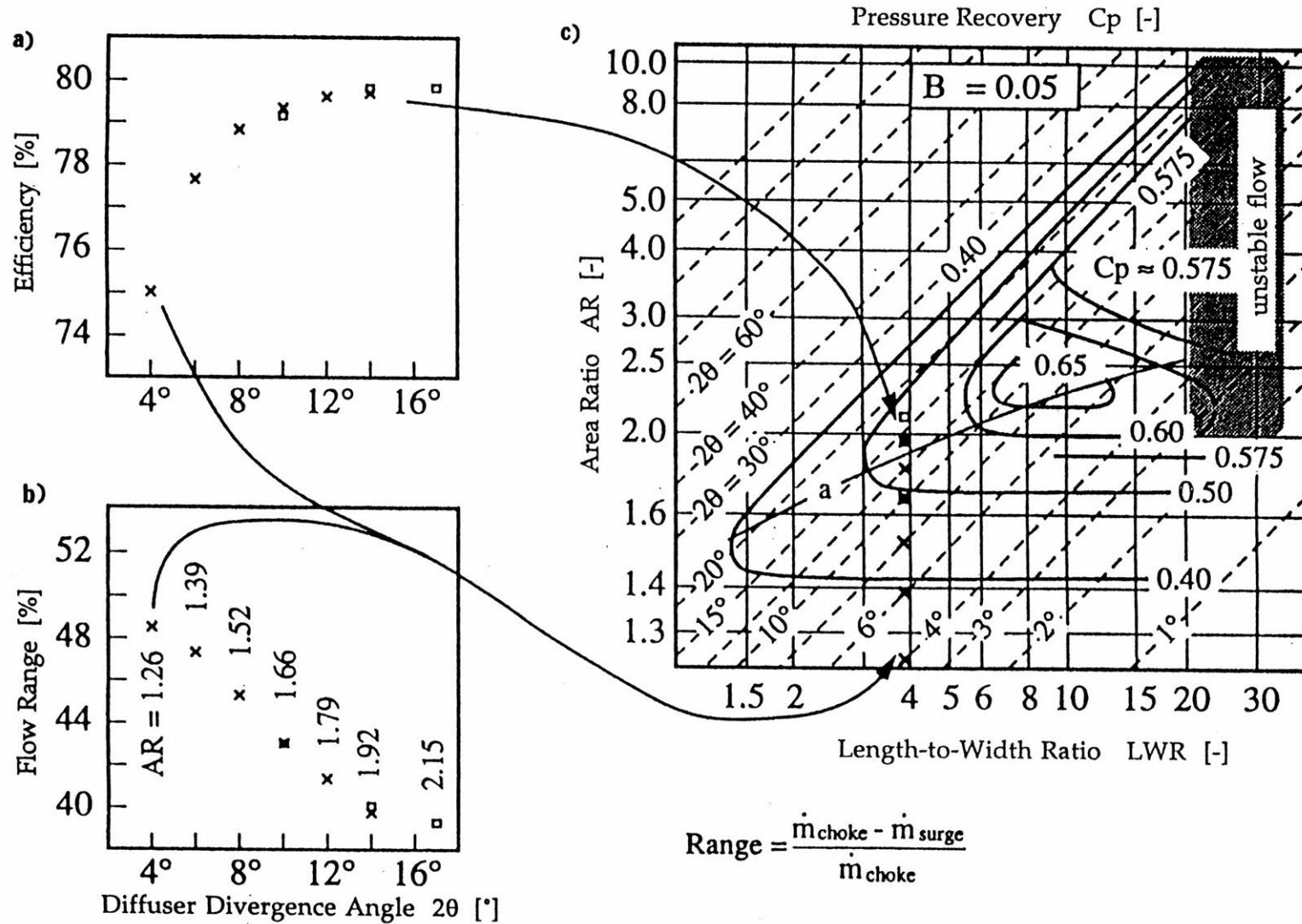
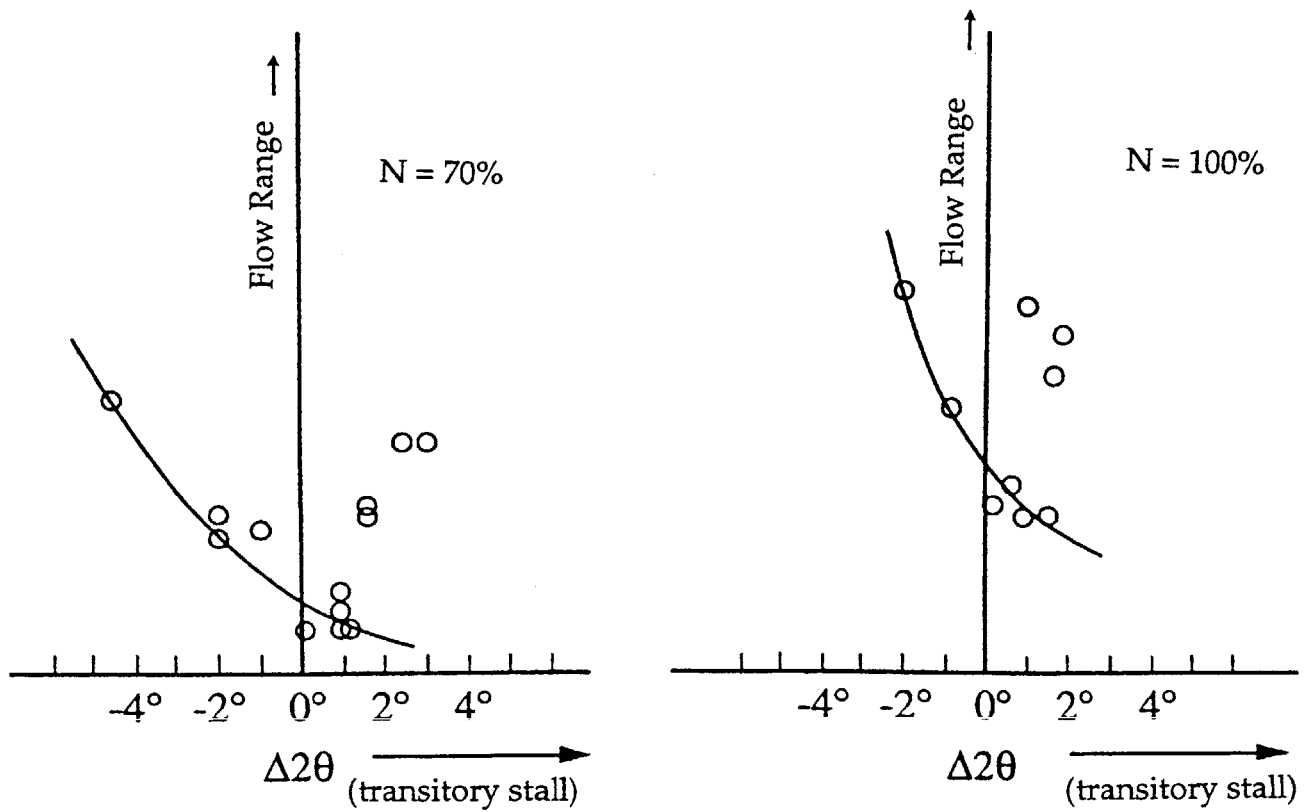
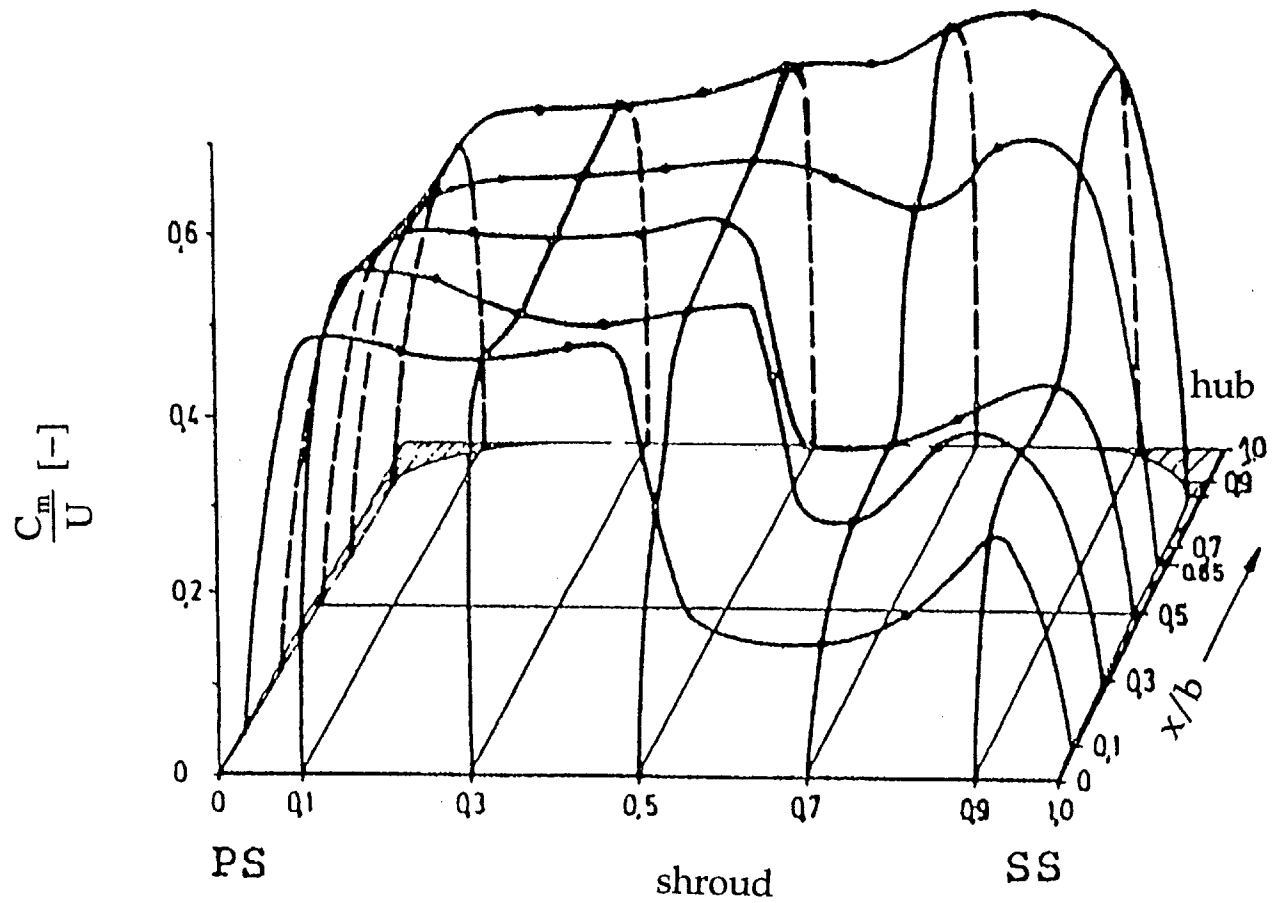


Figure 1.6 Diffuser divergence angle, 2θ , versus efficiency (a) and versus stable flow range (b) from Clements [1987]. Figure (c) shows comparison of the diffuser geometries from (a) and (b) with the single channel diffuser data of Reneau et al. [1967]



$\Delta 2\theta$ = Difference between radial channel diffuser divergence angle, 2θ , and maximum divergence angle of single channel diffusers without flow separation

Figure 1.7 Centrifugal compressor operating range as a function of channel diffuser $\Delta 2\theta$, for different vaned and pipe diffusers Japikse [1984b]



Corrected impeller speed = 14 000 RPM
 Corrected mass flow = 5.31 kg/s

Figure 1.8 Meridional velocity distribution at a centrifugal compressor impeller exit (Eckardt [1977])

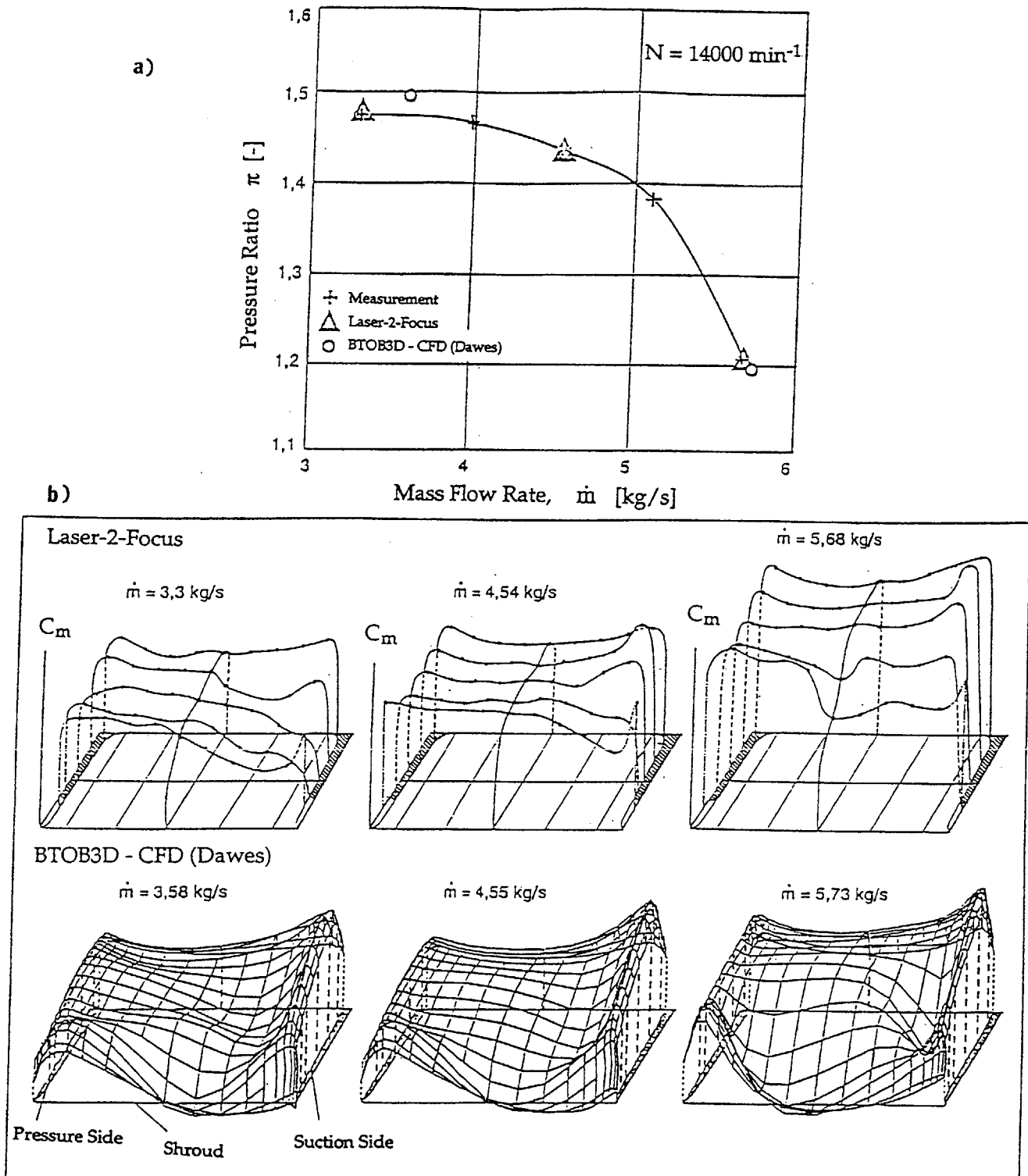


Figure 1.9 a) Measured and calculated impeller pressure ratio, π , versus mass flow rate, \dot{m} , and b) measured and calculated meridional velocity distribution at a centrifugal compressor impeller exit for different mass flow rates (Dalbert [1993])

CHAPTER 2

Facility and Experimental Apparatus

2.1 Overall Facility Description

The experimental apparatus at the MIT Gas Turbine Laboratory was designed to provide a controlled inlet flow to a centrifugal compressor diffuser. The diffuser inlet conditions accessible are Mach numbers greater than unity, flow angle of 62 - 75° and control of the boundary layer properties (e.g. inlet blockage up to $B \approx 0.35$). The facility consists of a specially designed impeller (swirl generator) which can deliver an axisymmetric, transonic flow into a test section in which different radial diffusers can be installed. Downstream of the diffuser, the flow exits to a plenum, followed by a throttle valve. The mass flow rate is monitored by the throttle valve, and a slave compressor downstream of the throttle valve can be activated to lower diffuser back pressure if needed. A venturi-type flow meter located in the rig exit pipe provides the measure of test diffuser mass flow rate. The overall facility scheme is shown in Figure 2.1 (Filipenco [1991]) and the scheme for impeller mechanical concept is shown in Figure 2.2 (Filipenco [1991]). The nominal span, b , of the impeller, vaneless space and, the diffuser was selected to be 0.009m, which was the span of a General Electric discrete-passage diffuser initially investigated in the same facility (Filipenco [1991]).

The impeller (swirl generator) has 71 lightly loaded, and high-solidity blades, which produce small wakes at the impeller exit. It is shown in Figure 2.3. There is also a static pressure drop through the blade row. The impeller exit flow has no shocks or stationary wakes and has minimal (maximum 3.0% of the average inlet dynamic pressure) circumferential non-uniformity at the exit (see Figure A 3.1 in Appendix A.3 - Impeller Exit Static Pressure Circumferential Distortion). The impeller has a negatively sloped pressure rise versus mass flow characteristic, so that no flow instabilities are encountered in the impeller over the operating range of interest (see Figure 4.1 - Constant Speed Characteristics of the Impeller). The performance of the impeller was initially determined by Filipenco [1991] using a 1.20 radius ratio vaneless diffuser.

The diffusers investigated (both discrete passage diffuser and straight channel diffuser) were mounted in the diffuser housing with a 1.10 radius ratio vaneless space between impeller exit and the diffuser inlet. The vaneless space contains the velocity profile control slots elements. The lower limit on vaneless space radius-ratio was determined by space requirements for the injection/suction slot system while the maximum allowable radius ratio was determined by flow stability and total pressure loss considerations (see Chapter 1.2) and the desire for the capability of a Mach number of unity at the test diffuser inlet. A vaneless space radius-ratio of 1.10 was selected by Filipenco [1991]. This radius-ratio complies with space requirements for the injection/suction system and according to the vaneless diffuser studies of Jansen [1964a, b], it should not cause any stability problems over the required operating range.

A unique feature of the facility is the means by which the diffuser inlet boundary layer blockage and flow distortion are controlled. There are continuous circumferential injection/suction slots immediately upstream and downstream of the impeller in stationary walls. Each slot is independently connected to a flow control system through an array of passages and manifolds, so that air can either be injected or removed from the main flow. Using a combination of injection and/or suction through these slots, a wide range of diffuser inlet blockage ($B \approx 0.02 - 0.35$) and velocity profile distortion (inlet flow angle differences up to 45° between diffuser rear and front walls) may be obtained. The baseline case (no air injection and suction) has axially symmetrical Mach number and flow angle distributions at diffuser inlet (see e.g. Figures 4.3a and b). Figure 2.4 provides a detailed view of the axial flow injection and suction manifolds.

Key dimensions of the facility are listed in Table 2.1. The details of construction and operation of the facility are described in detail by Filipenco [1991] and Johnston [1993].

2.2 Straight Channel Diffuser

The initial steps in this project were the selection, design and construction of the straight channel diffuser. The straight channel diffuser geometry is shown in Figures 2.5 and 2.6. The design of the straight channel test diffuser was started by selecting geometrical diffuser parameters (diffuser channel divergence angle, 2θ , area ratio, AR,

and length-to-width ratio, LWR), based on the diffuser map by Reneau et al. [1967] for single channel 2D-diffusers. In addition, several vaned diffuser investigations available in the open literature were taken into consideration.

An important aim of the straight channel investigations is to assess, and to compare the straight channel diffuser to the discrete passage diffuser in terms of performance and operating range. Therefore, the overall inlet conditions for the straight channel diffuser design, i.e. the mean inlet flow angle, α , the number of vanes, Z_v , vaneless space radius ratio, r_1/r_1' , were chosen to be similar to those of the discrete passage diffuser, previously tested in the same facility by Filipenco [1991]. Impeller exit radius, r_1 , and diffuser exit radius, r_2 , were chosen to be consistent with the facility dimensions. The axial depth of a diffuser channel, b , was equal to impeller exit depth.

For similarity with the previously investigated discrete passage diffuser, the straight channel diffuser throat area, A_{th} , was chosen to be the same as the discrete passage diffuser throat area. This determined the absolute dimensions of the straight channel diffuser. According to single channel diffuser investigations, for maximum diffuser pressure recovery, the optimum aspect ratio ($AS = b/W_{th}$) at the diffuser throat equals 1.0; however, setting the depth of the diffuser the same as the impeller exit depth, $b = 0.009\text{m}$, and maintaining the diffuser throat area as $W_{th} = 0.014\text{m}$ were preferred to achieving an optimum aspect ratio of 1.0.

Design parameters for the straight channel diffuser were also discussed with the Allison Engine Company (Alverson & Sagre [1994]). For the final version recommendations by Allison were used in the design. The basic parameters for the straight channel diffuser and for the discrete passage diffuser are summarized in Table 2.2.

2.3 Instrumentation

The test program includes wall static pressure measurements along the diffuser centerline, at the diffuser inlet and exit, and in the vaneless and quasi-vaneless spaces, as well as total pressure, temperature, and flow angle measurements at the diffuser inlet. These are described in the following subsections of Chapter 2.3.

2.3.1 Total-Pressure/Flow-Angle Probe

A main objective of the research program was to investigate the effect of axial distortion of the inlet flow field on diffuser performance. A means was thus needed to determine the actual diffuser inlet Mach number and flow angle profiles at various impeller operating conditions. The method used was a rotatable cylindrical single-hole total-pressure/flow angle-probe axially spanning the inlet of the test diffuser at one circumferential position ($\theta = 0^\circ$). The total-pressure/flow-angle probe was chosen by Filipenco [1991], after considering several other types of instrumentation, including hot wire velocimeters (too fragile), cone probes (require up to five separate pressure tubes, therefore too much blockage) and Kiel probes (insensitive to flow angle and too much blockage).

The single hole probe was used to minimize probe diameter and thus the effect of the probe on the diffuser inlet flow field. The probe consisted of a 0.001m diameter stainless steel tube in with a 0.23 mm diameter sensing hole radially drilled through one wall. The probe, being positioned in a cross-flow, was rotated around its axis. For the expected 60 - 75° inlet flow angle range the probe was rotated over a 40 - 115° range with a step of 5°. The maximum output pressure occurs when the sensing hole directly faces the flow and indicates the total pressure of the flow. An accurate determination of the flow angle is made by finding the centroid of the measured total pressure versus flow angle curve. The flow angle, α , was calculated by fitting a second order polynomial through a symmetrical subset of the test data. A fifth order polynomial fit, which represents the pressure distribution more accurately, was then used to calculate the maximum total pressure in the data reduction phase.

The total-pressure/flow-angle probe can be moved axially using a probe actuator and flow angle and total pressure were measured at fifteen axially-distributed points. The axial and angular positioning of the probe was achieved by means of a L.C. Smith model number BBS-1-SM-180-SM probe actuator. Rated angular positioning linearity is to within 0.1% of full angle scale (180°) and hysteresis is 0.2°. The rated traverse positioning linearity is also to within 0.1% of full scale or 0.025mm for the 25.4mm range with a hysteresis of 0.0005mm (Filipenco [1991]). All traverse/angle set points were approached from the same direction to avoid hysteresis error.

The flow angle measurement can be also used to calculate the mass flow rate and compared to the mass flow measured by the venturi-flow meter downstream of the diffuser. This provides a check on the quality of the flow angle data (see Figure A 2.1 in Appendix A.2).

2.3.2 Pressure Transducers

One channel of the diffuser was instrumented with an array of static pressure taps to measure the static pressure distribution on the different subcomponents of the diffuser as well as to calculate the diffuser pressure recovery. Figure 2.5 shows locations of the wall static pressure taps and Table 2.3 gives their coordinates.

Additional static pressure taps were placed in front and rear walls in the vaneless space at a radius ratio 1.05 relative to the impeller exit radius and at the diffuser exit to diagnose the circumferential static pressure variation. Figure 2.6a and 2.6b show the overall locations of the static pressure taps (and the total pressure probe) at the diffuser rear and front walls. The number of circumferentially distributed static pressure taps is given below:

	<u>Rear Wall (Fig. 2.6a)</u>	<u>Front Wall (Fig. 2.6b)</u>
Diffuser Inlet	10	5
Diffuser Exit	5	5

Measurements of steady state pressures at all static taps in the diffuser test rig, including the vaneless diffuser circumferential taps, the diffuser channel taps, and the main plenum pressure were carried out using of a single Druck type PDCR-23D±5 psid pressure transducer, multiplexed to the various pressure taps by means of a Scanivalve model number 48C9 pressure-transducer multiplexer. The rated combined non-linearity, hysteresis, and repeatability of this transducer is within ±0.04 % of full scale (Filipenco [1991]).

The velocity profile control system injection/suction pressures and the venturi flow meter upstream static pressure were measured by means of a Setra model number 271, ± 15 psid pressure transducer. This transducer has excellent long term stability, with a rated repeatability to within ± 0.02 % of full scale and a rated accuracy to within ± 0.05 % of full scale (Filipenco [1991]). Both the Druck and Setra pressure transducers were calibrated using a standard mercury manometer to set the applied pressure.

A Kulite model number XCS-062, ± 5 psid pressure transducer was mounted at the diffuser exit in the main collector/plenum wall to detect the rotating stall and any other unsteady pressure phenomena. This transducer has a rated combined non-linearity and hysteresis of better than ± 0.50 % of full scale and a repeatability to within ± 0.10 % of full scale. The reference pressure for the calibration of the Kulite pressure transducer was determined by means of a standard mercury manometer.

2.3.3 Temperature Measurements

Flow temperature was measured at the impeller inlet (ambient temperature), at the exit of the diffuser (at an axial location corresponding to the center plane of the diffuser), and at the exit of the venturi flow meter. The diffuser total temperature probe was located immediately downstream of the diffuser, equidistant from the rear and front walls. The Mach number was low, typically less than 0.20 so no recovery corrections were applied to the measured temperature at the diffuser exit. The flow between impeller exit and plenum was assumed to be adiabatic, with uniform stagnation temperature. The previous studies by Filipenco [1991] and Johnston [1993] indicated that the error associated with this assumption will be $\pm 0.2\%$ in the range of the investigations (500°R to 630 °R).

The diffuser exit temperature was measured by means of a shielded type E (chrome/constantan) thermocouple probe, and an Omega Engineering model number 670 digital-readout temperature display. The temperature at the exit of the venturi flow meter was measured using an Omega Engineering thermistor probe model THX-400-AP and a digital readout thermometer model 651. Ambient air temperature at the impeller inlet

was measured using a (copper/constantan) thermocouple and an Omega Engineering model number 115 digital readout thermometer.

These temperature-measurement systems are standard and can typically be used to an accuracy of $\pm 1\%$. Calibrations of the temperature sensors gave an estimated overall accuracy to within $\pm 1^\circ\text{K}$, or $<0.2\%$ over the temperature range of the investigations (Filipenco [1991]).

2.3.4 Mass Flow Meter and Tachometer

The mass flow rate through the test diffuser was determined by means of a BIF "universal venturi tube", part number 0182-10-2291, located in the test rig exit. The rated uncalibrated accuracy of the flow meter is $\pm 1.0\%$ of the true value. The mass flow rate was calculated directly, without calibration.

The impeller speed was measured by means of a Shimpo model number DT-5BC digital readout tachometer. This tachometer utilizes a built-in quartz-oscillator frequency reference resulting in a rated speed-readout-accuracy to within 0.008% of reading. The readout resolution is 0.1 RPM .

2.3.5 Data Acquisition System

2.3.5a Data Acquisition Hardware

The main hardware elements of the data acquisition systems include:

- A Dell OptiPlex XMT 590 computer with a Metrabyte-16F eight channel A/D converter board (The Dash-16F A/D converter provides a 12 bit resolution and a maximum sampling rate of 100 Khz to memory in the DMA-direct memory access-mode) and a National Instruments GPIB-PC-2A communications interface board. The board provides communications with the Scanivalve digital interface unit and the L.C. Smith probe-actuator controller.

- A pressure-transducer multiplexing unit, Scanivalve model number 48C9, and a Scanivalve digital interface unit model number SDIU-MK5. The control unit is operated automatically through the GPIB interface bus by the data acquisition software. An on-board 16-bit A/D converter converts the transducer signal conditioner output to digital form for the transmission to the data acquisition computer through the GPIB interface bus.
- A probe-actuator controller and computer interface unit, L.C. Smith model number TAC-H-SM control the stepping motor probe-actuator, which positions the probe according to software commands received through the GPIB buss from the computer.
- Signal conditioning amplifiers, Measurement Group, Instruments Division, model number 2310. These units were used as excitation for the Kulite high frequency-response pressure transducer and to amplify and to filter the transducer output.

2.3.5b Data Acquisition Software

A computer program (DATATAKE.PRO) written in ASYST programming language was used for data acquisition. The program includes options for the various test sequences including the traverse of the test section with the total-pressure/flow-angle probe, acquisition of time-resolved data from the Kulite pressure transducer and scan of selected Scanivalve channels.

Each traverse consisted of moving the total pressure/flow angle probe to the desired axial location and then rotating the probe. The axial and yaw position readings were then recorded in the computer.

2.3.6 Operation of the Facility

The operation of the test facility is done remotely. A main control panel contains the operating controls and monitoring displays for the profile-control injection/suction system, the auto-shutdown and operation monitoring system, the lubrication system,

the main plenum/collector throttle valve, and the downstream slave compressor. Readouts for the venturi flow meter flow temperature, the test section temperature, the ambient temperature, and the main plenum pressure are provided on the main control panel. A manometer for measuring the pressure drop across the venturi flow meter is wall mounted in close proximity to the panel.

2.4 Facility Modifications for the Straight-Channel Diffuser Tests

The design of a new straight channel diffuser coupled with the desire for using additional instrumentation required some modifications of the experimental facility. The main modifications included:

1) Design and construction of new diffuser-mounting flanges for rear and front sides of the test rig: The existing discrete passage diffuser was an engine part which was manufactured together with the mounting flanges. As shown in Figure 2.7, the new diffuser-mounting flanges are independent of the diffuser. This allows increased flexibility to the rig, not only for the mounting of the present straight channel diffuser, but also for future experiments.

2) Design of the diffuser walls together with the vaneless space rings as one piece: In the existing facility the diffuser and the vaneless space rings were separate pieces. The modification provided one flow surface from the impeller exit (actually from the injection/suction slots at the vaneless space) to the diffuser exit, without gaps and steps. There was also the possibility of installing additional static pressure taps in the vaneless space.

Part	Dimension
Impeller Exit Radius r_1'	0.184 m
Impeller Depth b	0.009 m
Vaneless Space Radius Ratio r_1/r_1'	1.10
Blade Number of the Impeller	71
Impeller Exit Blade Angle	64°
Impeller Inlet Blade Angle	-37.2°
Impeller Design Exit Mach Number	0.80
Total Pressure-Flow Angle Traverse Probe Diameter	0.001m
Total Pressure-Flow Angle Traverse Installed Radius	0.203 m
Exit Pipe Diameter	0.254 m
Universal Venturi Throat Diameter	0.148 m

Table 2.1 : Facility dimensions summary

	STRAIGHT CHANNEL DIFFUSER	DISCRETE PASSAGE DIFFUSER
2θ	8°	
AR	2.34	4.29
LWR	9.574	8.75
Z_v	30	30
α	69°	69°
β	4.0°	
r_1'	0.184 m	0.184 m
r_1	0.203 m	0.203 m
r_2	0.303 m	0.281 m
b	0.009 m	0.009 m
A_{th}	0.00013 m^2	0.00013 m^2
W_{th}	0.0 14 m	
L	0.138 m	0.112 m
AS	0.643	
b/r_1	0.044	0.044
r_1/r_1'	1.10	1.10
r_2/r_1'	1.64	1.52

Table 2.2 : Parameters for straight channel- and discrete passage diffuser

Tap Number	ξ [cm]	ζ [cm]	r [cm]
1	0	0	19.426
2	2.59	-0.17	"
3	3.83	-0.38	"
4	2.05	0.34	19.876
5	2.87	0.24	"
6	4.20	0	"
7	5.29	-0.27	"
8	6.21	-0.55	"
9	4.10	0.48	20.323
10	4.85	0.31	"
11	5.97	0	"
12	6.94	-0.10	"
13	7.79	-0.66	"
14	5.05	0.54	20.599
15	5.79	0.34	"
16	6.85	0	"
17	7.79	-0.36	"
18	8.55	-0.68	"
19	6.05	0.61	20.932
20	6.78	0.38	"
21	7.80	0	"
22	8.55	-0.38	20.879
23	7.05	0.69	21.313
24	7.80	0.41	"
25	8.55	0	21.224
26	7.80	0.74	21.618
27	8.55	0.43	"
28	8.55	0.79	21.948
29	9.74	0	21.730
30	10.92	0	22.289
31	12.11	0	22.893
32	13.30	0	23.543
33	14.49	0	24.234
34	15.68	0	24.963
35	16.87	0	25.725
36	18.05	0	26.520
37	19.24	0	27.343
38	20.43	0	28.192
39	21.62	0	29.065
40	22.88	0	30.018
41	22.08	0.91	"
42	23.38	-0.59	"
43	23.87	-1.21	"

Table 2.3 : Diffuser Channel Static Pressure Tap Location Coordinates (for ξ and ζ see Figure 2.5)

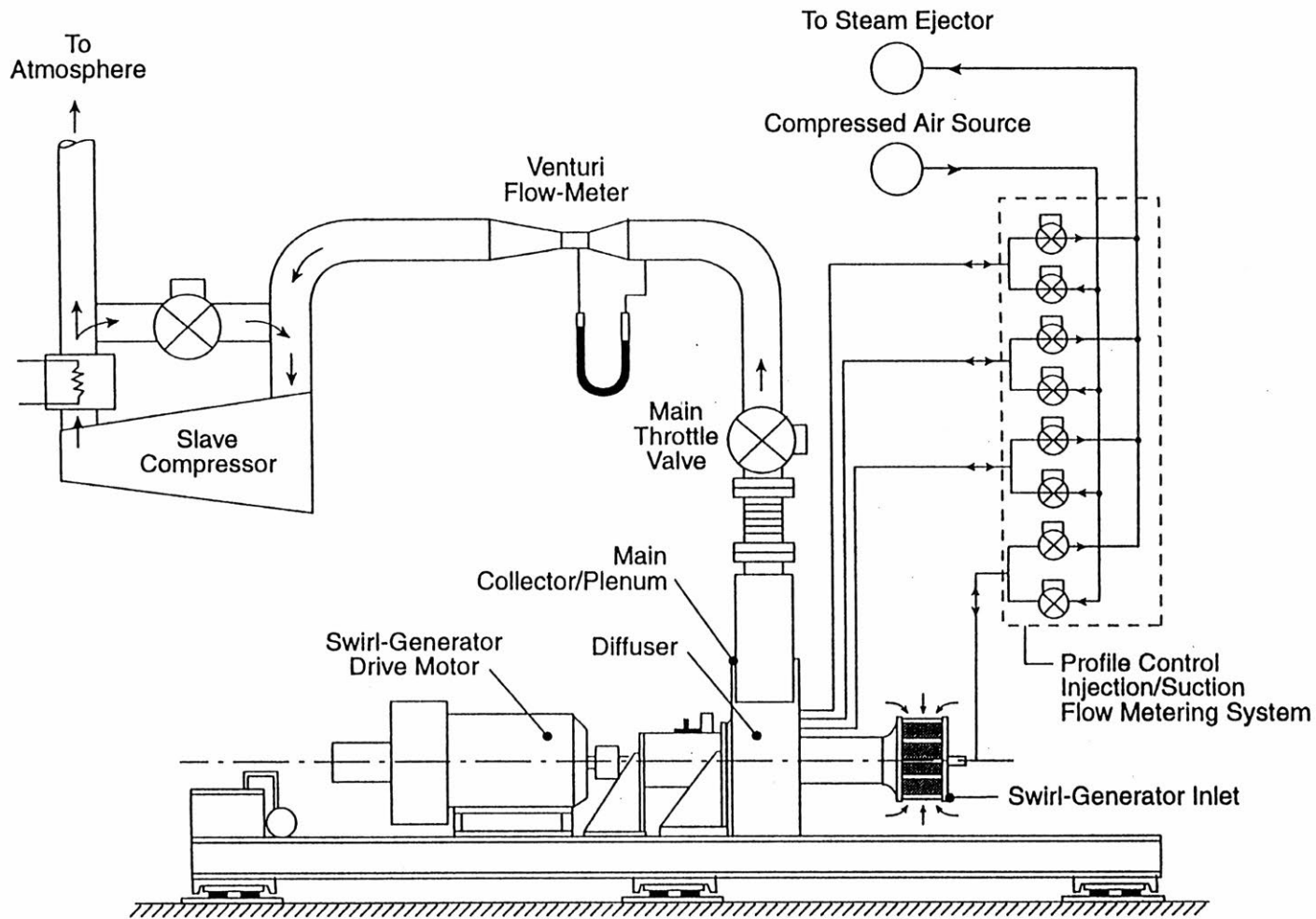


Figure 2.1 Swirl Generator/Diffuser Test-Section Assembly and Flow System Schematic

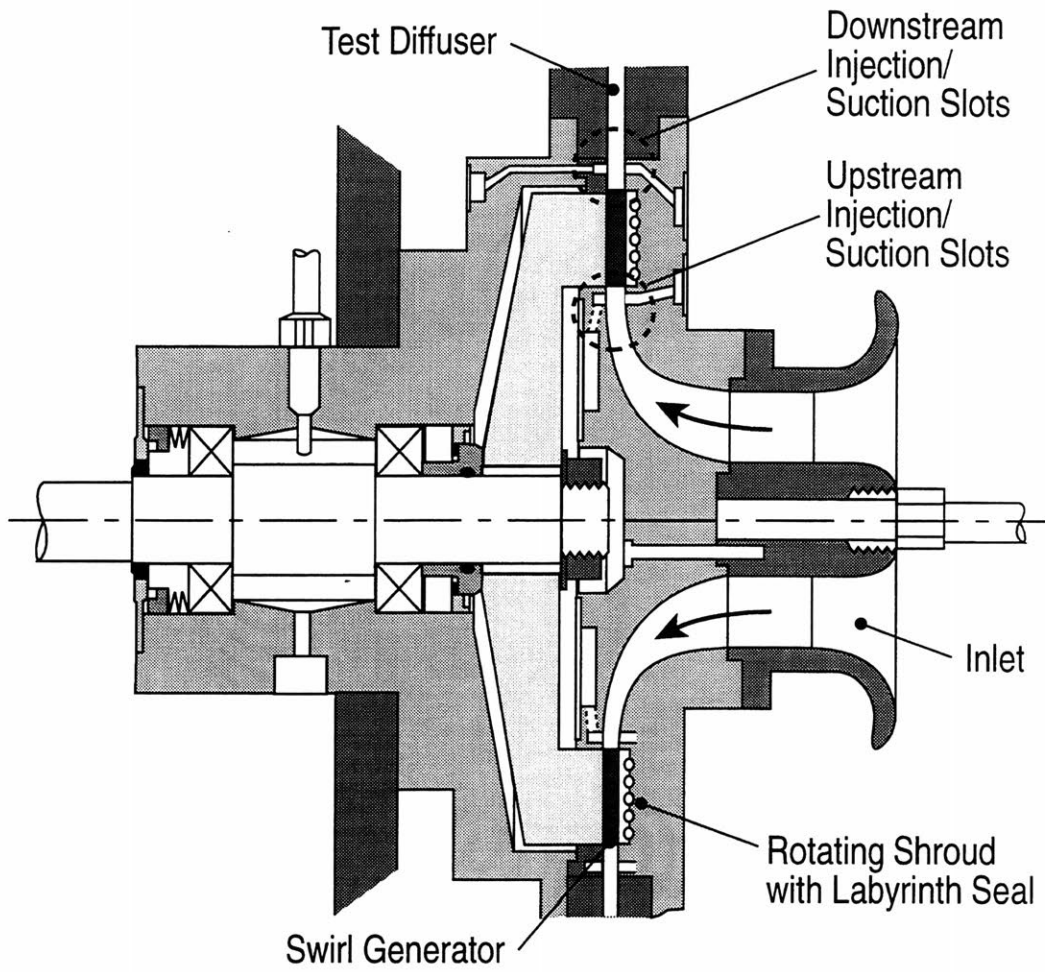
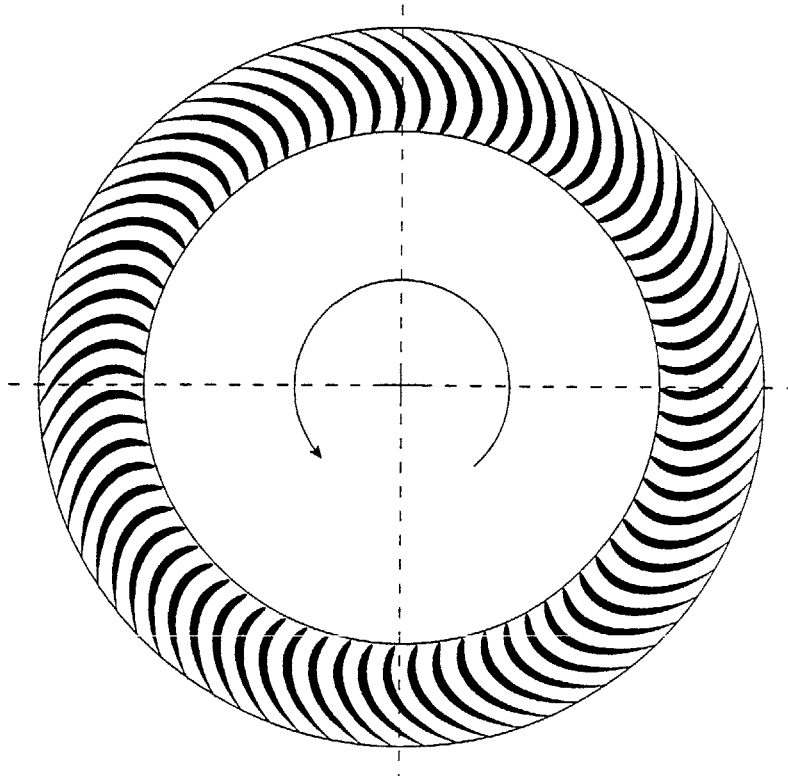


Figure 2.2 Swirl generator mechanical-concept schematic.



Blade Number, $Z_b = 71$

Figure 2.3 Scale Diagram of Swirl Generator Blading

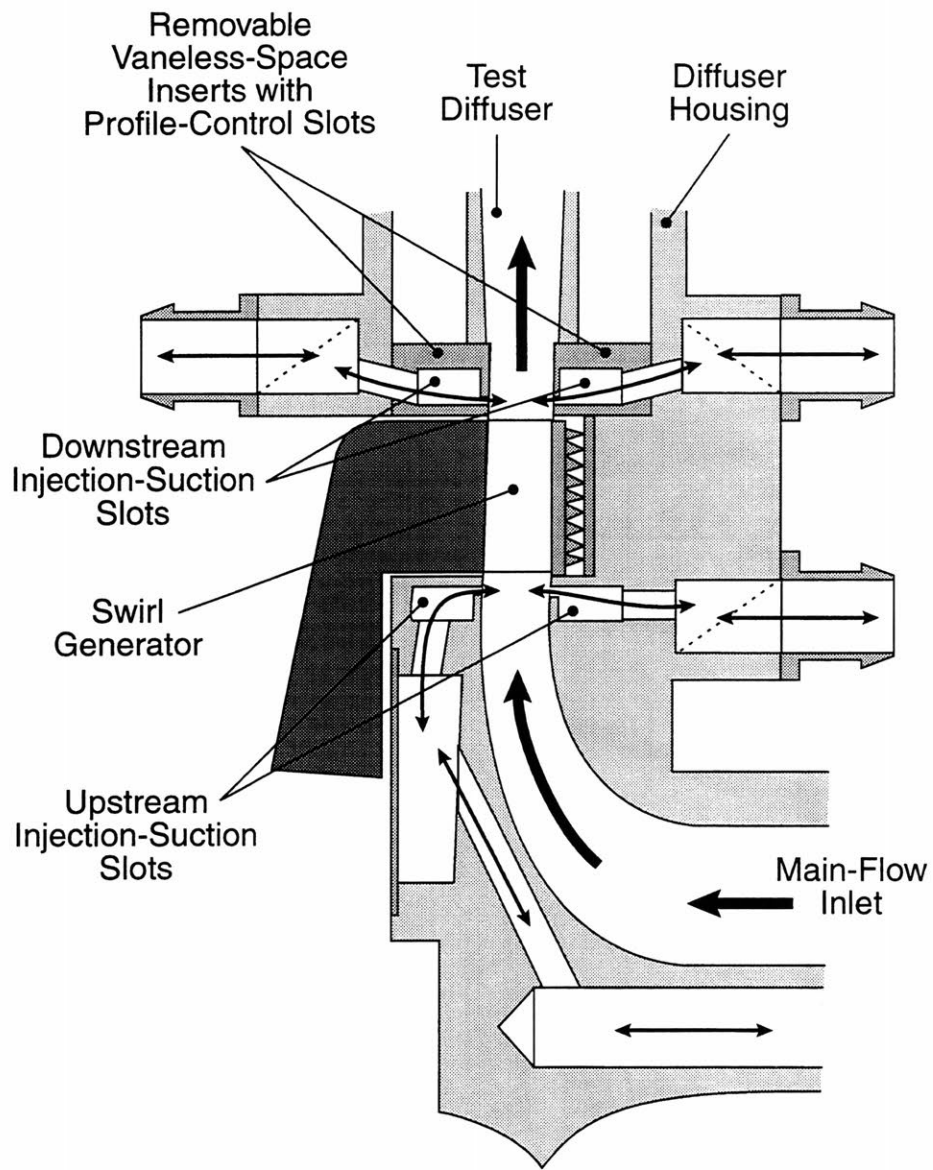


Figure 2.4 Schematic of the velocity profile-control slots and flow passage arrangement.

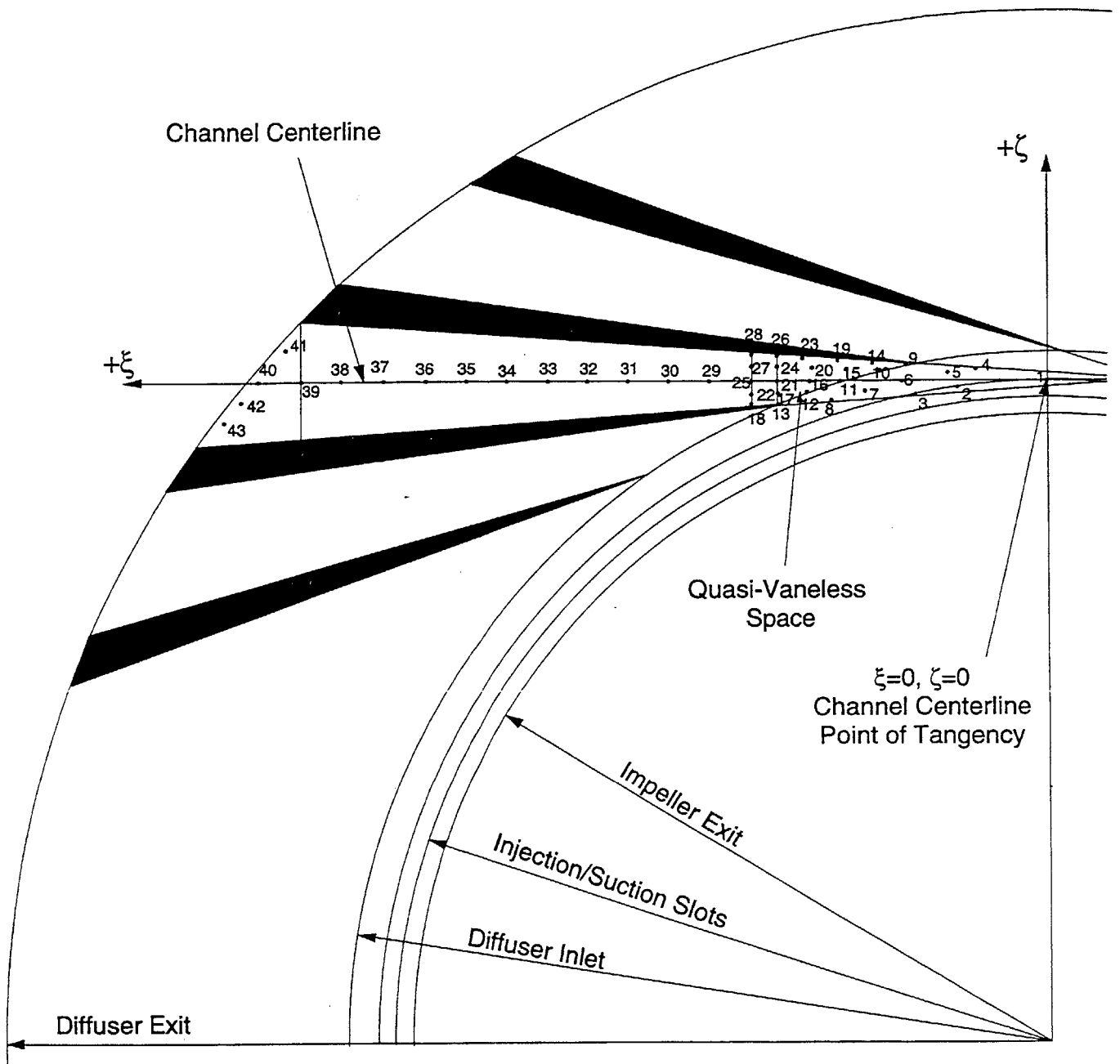


Figure 2.5 Straight-Channel Diffuser Channel Static Pressure Tap Locations

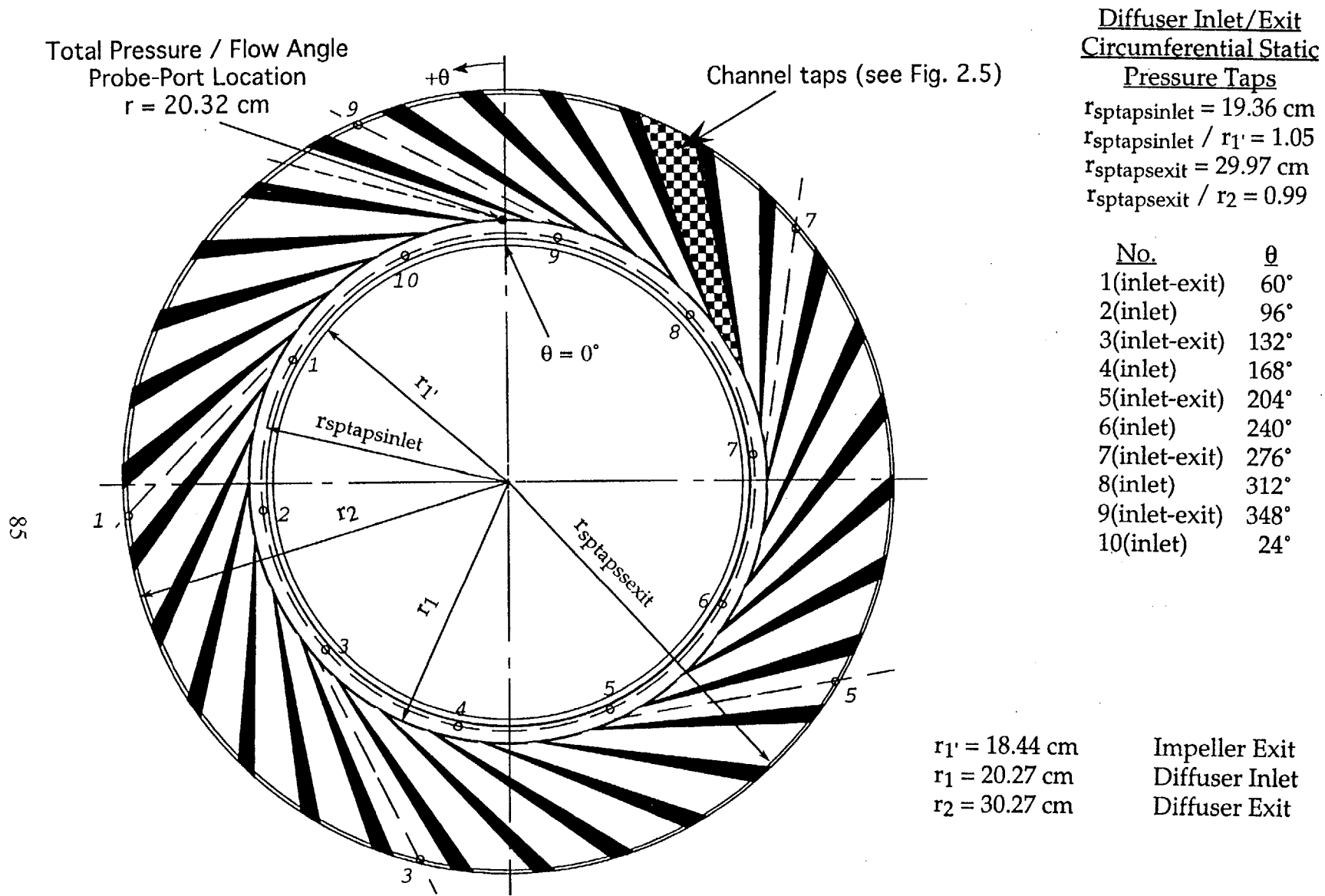


Figure 2.6a Straight-Channel Diffuser Rear Wall Pressure Taps

Diffuser Inlet/Exit
Circumferential Static

Pressure Taps

$r_{\text{sptapsinlet}} = 19.36 \text{ cm}$

$r_{\text{sptapsinlet}} / r_1 = 1.05$

$r_{\text{sptapsexit}} = 29.97 \text{ cm}$

$r_{\text{sptapsexit}} / r_2 = 0.99$

No.	θ
1(inlet-exit)	60°
3(inlet-exit)	132°
5(inlet-exit)	204°
7(inlet-exit)	276°
9(inlet-exit)	348°

$r_1' = 18.44 \text{ cm}$
 $r_1 = 20.27 \text{ cm}$
 $r_2 = 30.27 \text{ cm}$

Impeller Exit
Diffuser Inlet
Diffuser Exit

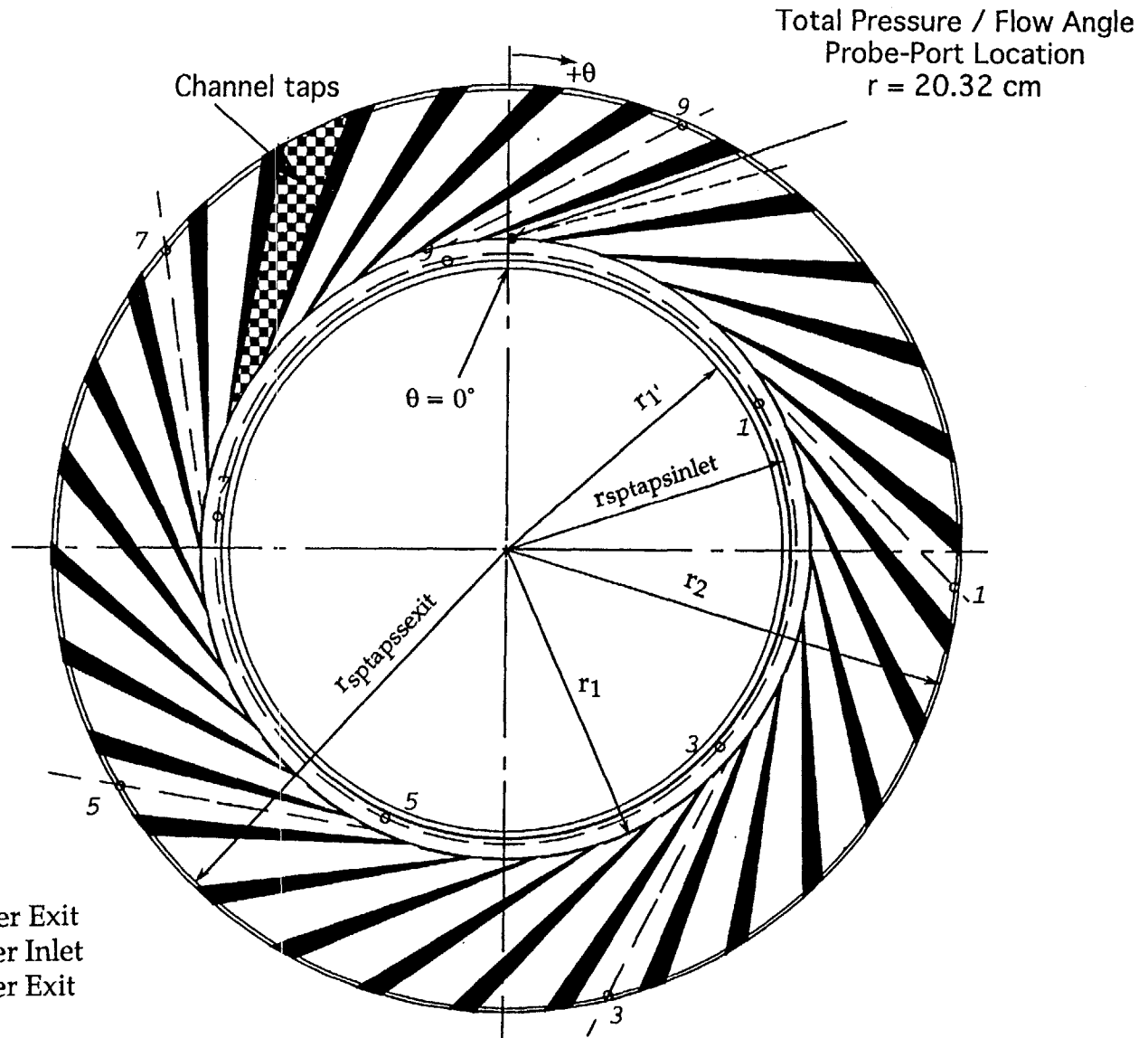


Figure 2.6b Straight-Channel Diffuser Front Wall Pressure Taps

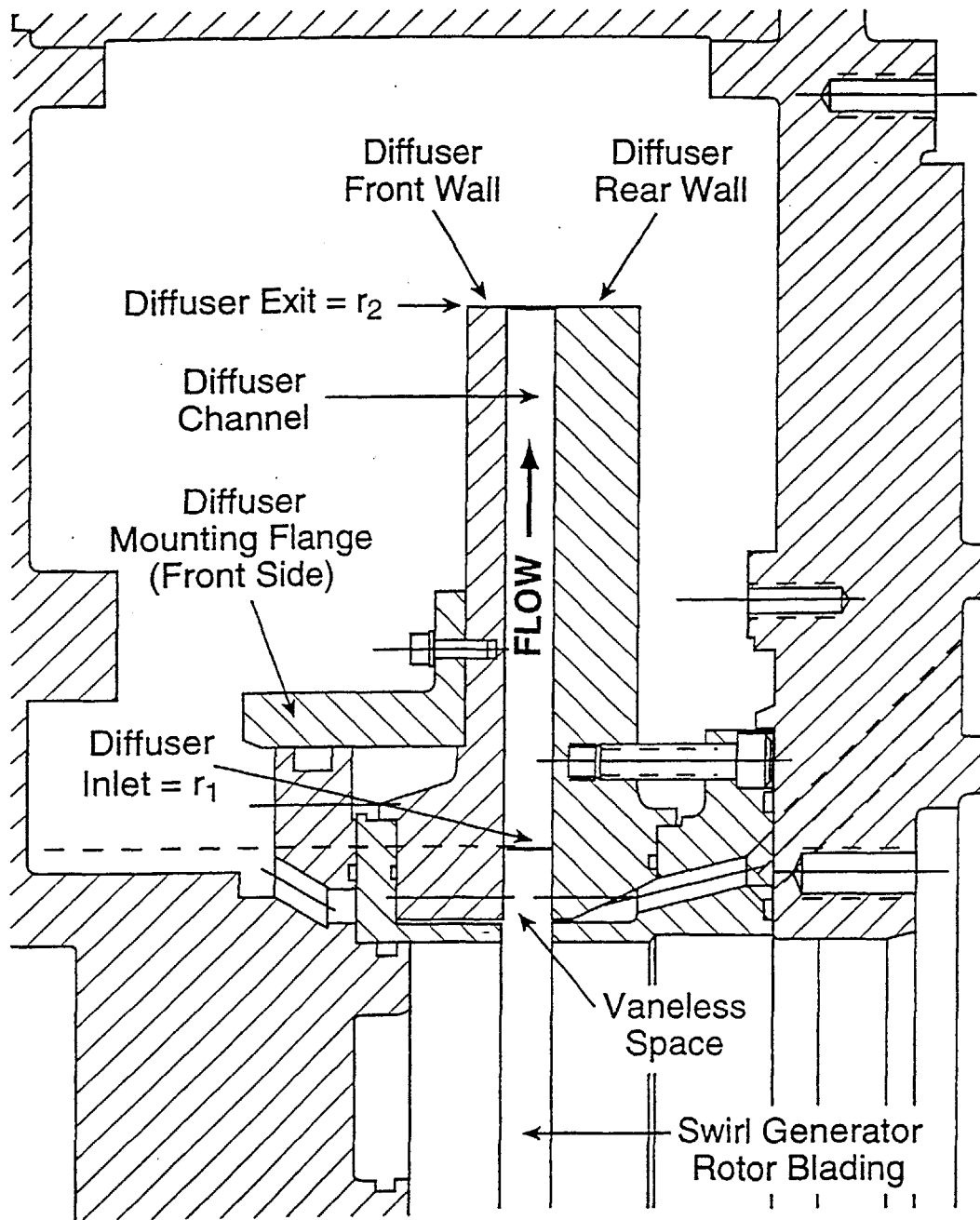


Figure 2.7 Modification of the diffuser test facility and vaneless diffuser mechanical detail

CHAPTER 3

Performance Parameters and Test Plan

3.1 Measured and Derived Quantities

3.1.1 Operating Point Definition

The establishment of an impeller operating point requires the setting of four independent operating parameters: rotor speed, N , diffuser through flow rate, \dot{m} , (or pressure ratio, π), and pressure in the two velocity profile control slot flow distribution chambers.

3.1.1.1 Impeller Rotor Speed

The measured impeller rotor speed, N_{tacho} , was corrected for ambient temperature, T_{amb} .

Corrected impeller speed, N_{corr} ,

$$N_{\text{corr}} = \sqrt{\frac{T_{\text{ref}}}{T_{\text{amb}}}} N_{\text{actual}} \quad (3.1)$$

reference temperature $T_{\text{ref}} = 288.15 \text{ }^\circ\text{K}$ or $T_{\text{ref}} = 518.69 \text{ }^\circ\text{R}$

3.1.1.2 Venturi Mass Flow Rate

The flow through the impeller was expressed conventionally as a corrected mass flow rate, \dot{m}_{corr} .

Corrected mass flow, \dot{m}_{corr} ,

$$\dot{m}_{corr} = \frac{\sqrt{\frac{T_{amb}}{T_{ref}}}}{\frac{P_{amb}}{P_{ref}}} \dot{m}_{actual} \quad (3.2)$$

reference pressure $P_{ref} = 1.013 \text{ bar}$ or $P_{ref} = 14.6958 \text{ psia}$

$$\dot{m}_{actual} = \dot{m}_{venturi} = \dot{m}$$

3.1.1.3 Impeller Performance Ratio

(Pressure-Ratio, π , versus Flow-Rate, \dot{m} , Characteristics)

Constant corrected speed steady state pressure ratio versus flow rate characteristics were determined from pressure measurements at impeller exit (pressure ratio between impeller inlet and impeller exit), diffuser inlet (pressure ratio between impeller inlet and diffuser inlet), diffuser exit (pressure ratio between impeller inlet and diffuser exit) and plenum (pressure ratio between impeller inlet and plenum). "Plane 0" denotes impeller inlet, "Plane 1" denotes impeller exit radii, "Plane 1" denotes diffuser inlet radius, "Plane 2" denotes diffuser exit radius, and "Plane 3" denotes the plenum (see also Figure 1.4). "Plane th" denotes the throat of the diffuser. The axial direction is taken from the front wall, where $x = 0$, to the rear wall, where $x = b$. The positive tangential direction is clockwise aft looking ahead, and zero degree is at top-dead center. The flow angle, α , is defined as the angle from the radial direction, rather than from the tangential direction.

Total to static pressure ratios, π_s , are defined as follows;

$$\pi_{s1'} = \frac{\bar{P}_{s1'}}{P_{amb}} \quad \pi_{s1} = \frac{\bar{P}_{s1}}{P_{amb}} \quad \pi_{s2} = \frac{\bar{P}_{s2}}{P_{amb}} \quad \pi_{s3} = \frac{\bar{P}_{s3}}{P_{amb}} \quad (3.3)$$

where

$P_{amb} = P_0 =$ ambient pressure or impeller inlet pressure.

The different pressures are defined as:

$$\bar{P}_{s1'} = \frac{1}{10} \sum_{n=1}^{10} P_{s1'n}$$

$\bar{P}_{s1'}$ = the absolute static pressure at the impeller exit (1') is the mean value of the pressure readings from the ten vaneless diffuser circumferential static taps at the 1.05 radius ratio

$$\bar{P}_{s1} = \frac{1}{5} \sum_{n=1}^5 P_{s1'n}$$

\bar{P}_{s1} = the absolute static pressure at the diffuser inlet (1) is the mean value of the pressure readings from the five static channel pressure taps at the diffuser inlet radius at the 1.10 radius ratio

$$\bar{P}_{s2} = \frac{1}{4} \sum_{n=1}^4 P_{s2'n}$$

\bar{P}_{s2} = the absolute static pressure at the diffuser exit (2) is the mean value of the pressure readings from the four static channel pressure taps at the diffuser exit radius

\bar{P}_{s3} = the absolute static pressure at the plenum.

The total-pressure/flow-angle traverse data provides, \hat{P}_{t1} , the mass averaged total pressure (see Equation (3.27)) to give the

Total-to-Total Pressure Ratio (of Impeller), π_{t1} , is defined as
$$\pi_{t1} = \frac{\hat{P}_{t1}}{P_{amb}} \quad (3.4)$$

Steady-state operating points were chosen to provide an appropriate range of diffuser inlet Mach numbers, M , and flow angles, α . Each operating point was defined by an impeller corrected speed and an atmosphere to plenum (total-to-static) pressure ratio, π_{s3} .

At each impeller speed, the maximum flow is limited by the choking of either the impeller or the test diffuser. The minimum flow limit was marked by the breakdown of the axisymmetric flow regime in the impeller/diffuser and is signaled by an audible

blowdown of the plenum through the impeller inlet. In more detail as the flow rate through the test diffuser is decreased at a constant impeller speed (resulting in the increase of the diffuser inlet flow angle), the axisymmetric flow through the diffuser and impeller became unstable, resulting in an operating regime characterized by circumferentially-traveling pressure distributions (rotating stall). In all cases, the transition to rotating stall occurred with a single blowdown of the plenum ending at an operating point at which the plenum pressure and through-flow rate was steady (indicated by the output signal from the plenum Kulite pressure transducer), but impeller and diffuser were operating in rotating stall. Filipenco [1991] also showed that surge cycle could be initiated at these same limiting flow rates if the slope of the main collector/plenum discharge-throttle characteristic was adequately increased.

3.1.2 Total-Pressure/Flow-Angle Traverse Probe Data

The diffuser inlet profile was measured over the diffuser depth, b , at one tangential location ($\theta = 0^\circ$) using a total-pressure/flow-angle traverse probe (see Section 2.3.1). At each steady-state operating point, a fifteen point traverse of the diffuser inlet was made and the total pressure, $P_t(x)$, and the flow angle, $\alpha(x)$, distributions were measured. The gradients of the flow-field parameters are larger near the diffuser walls than near the center plane so that closer spacing was used in the former. Pressure from all static pressure taps were also recorded at the same time.

3.1.2.1 Mach Number at the Diffuser Inlet

Diffuser inlet Mach number, M_1 , is defined as:

$$M_1 = \sqrt{\frac{2}{\gamma - 1} \left\{ \left[\frac{P_{t1}}{P_{s1}} \right]^{\frac{\gamma - 1}{\gamma}} - 1 \right\}} \quad (3.5)$$

The Mach number at the diffuser inlet, $M_1(x)$, for the axial location, x , was calculated by using measured total pressure, $P_t(x)$, and static pressure from:

$$M_1(x) = \left[\frac{2}{\gamma - 1} \right]^{\frac{1}{2}} \left[\left[\frac{P_{t1}(x)}{P_{s1}} \right]^{\frac{\gamma-1}{\gamma}} - 1 \right]^{\frac{1}{2}} \quad (3.6)$$

3.1.2.2 Static Temperature at the Diffuser Inlet

Static temperature distribution at the diffuser inlet, $T_{s1}(x)$, is calculated with:

$$T_{s1}(x) = \frac{T_{t1}}{\left(\frac{P_{t1}(x)}{P_{s1}} \right)^{\frac{\gamma-1}{\gamma}}} \quad (3.7)$$

Here T_{t1} is equal to T_{t2} , which is the total temperature measured at the diffuser exit at an axial location $x = b/2$ (see Section 2.3.3)

3.1.2.3 Mass Flow Continuity Verification

To assess the consistency of the data, a comparison can be made between the measured mass flow rate using venturi flow meter (section 3.1.1.2) and the calculated mass flow rate by integrating across the diffuser inlet. The mass flow rate is:

$$\dot{m} = 2\pi r_1 \int_0^b \rho_{s1}(x) V_{r1}(x) dx \quad (3.8)$$

The velocity at the diffuser inlet, V , can be written as,

$$V(x_i) = M(x_i) \sqrt{\gamma R T_s(x_i)} \quad (3.9)$$

and can be separated into the radial and tangential components:

$$V_r = V \sin \alpha \quad V_r(x_i) = M(x_i) \sqrt{\gamma R T_s(x_i)} \cos \alpha(x_i) \quad \text{radial velocity} \quad (3.10)$$

$$V_\theta = V \cos \alpha \quad V_\theta(x_i) = M(x_i) \sqrt{\gamma R T_s(x_i)} \sin \alpha(x_i) \quad \text{tangential velocity} \quad (3.11)$$

Equation (3.8) for mass flow integration can be evaluated as:

$$\dot{m} \approx 2\pi r_1 \sum_{i=1}^{16} \left[\frac{\rho_s(x_i) V_r(x_i) + \rho_s(x_{i-1}) V_r(x_{i-1})}{2} \right]_{r=r_1} (x_i - x_{i-1}) \quad (3.12)$$

($V = 0$ at $x = 0$ and $x = b$)

The result of the comparison was that mass flow difference between the measured venturi mass flow rate and calculated mass flow rate using Equation (3.12) was within $\pm 5\%$. A detailed description of this comparison is given in Appendix A.2.

3.1.3 Diffuser Performance Parameters

3.1.3.1 Performance Parameters for Pressure Recovery

To quantify the diffuser performance we need to define appropriate diffuser performance parameter(s). A widely used diffuser performance parameter is the pressure recovery coefficient, C_p , which is defined as the ratio of the diffuser static pressure rise to the diffuser inlet dynamic pressure. This parameter indicates what fraction of the dynamic pressure at the inlet of the diffuser is converted into static pressure by the diffuser. For an ideal flow (isentropic, one-dimensional), the maximum value of this coefficient can reach unity if the flow is decelerated to zero velocity by the diffuser. For an actual diffuser of finite area ratio, the value of C_p is less than unity. Other factors, such as losses due to viscous effects, flow separation, and mixing can also reduce the diffuser pressure recovery.

Pressure recovery coefficient, C_p , is defined as,

$$C_p = \frac{P_2 - P_1}{P_{t1} - P_1} \quad (3.13)$$

for a compressible fluid. For an incompressible fluid this is reduced to:

$$C_p = \frac{P_2 - P_1}{\rho \frac{V_1^2}{2}} \quad (3.14)$$

The theoretical or ideal pressure recovery coefficient, $C_{p_{id}}$, gives the level of pressure recovery which would be attained in the case of isentropic, uniform, ideal flow in a diffuser of a given area ratio,

$$C_{p_{id}} = 1 - \frac{1}{AR^2} \quad (3.15)$$

for an incompressible fluid. For a compressible fluid and perfect gas it becomes:

$$C_{p_{id}} = \frac{\left(1 + \frac{\gamma-1}{2} M_2^2\right)^{\frac{\gamma}{1-\gamma}} - \left(1 + \frac{\gamma-1}{2} M_1^2\right)^{\frac{\gamma}{1-\gamma}}}{1 - \left(1 + \frac{\gamma-1}{2} M_1^2\right)^{\frac{\gamma}{1-\gamma}}} \quad (3.16)$$

Another useful diffuser performance parameter is the diffuser effectiveness, η_{diff} , which is defined as the ratio of the actual pressure recovery coefficient, C_p , to the theoretical or ideal diffuser pressure recovery coefficient, $C_{p_{id}}$, for that particular geometry:

$$\eta_{diff} = \frac{C_p}{C_{p_{id}}} \quad (3.17)$$

Use of diffuser effectiveness eliminates the direct effect of area ratio, and gives a better indication of fluid dynamic phenomena and losses in the diffuser than pressure recovery. For a diffuser with uniform inlet conditions, there is no ambiguity in the interpretation of the either definitions. With non-uniform inlet conditions an appropriate representation of the diffuser inlet total pressure must be made.

3.1.3.2 Diffuser Inlet Average and Distortion Flow Field Parameters

3.1.3.2.1 Total Pressure at the Diffuser Inlet

The static pressure at the diffuser inlet and exit was quite uniform and the problem of defining the pressure recovery coefficient, C_p , is rather a matter of assigning a relevant value of total pressure to the non-uniform diffuser inlet flow. Previous researchers have presented diffuser pressure recovery performance data based on various different definitions of the diffuser inlet dynamic pressure (see also Section 1.2.6). Masuda et al. [1971] defined the pressure recovery coefficient in terms of diffuser inlet mass-averaged dynamic pressure :

$$\hat{C}_p = \frac{P_{s2} - P_{s1}}{\frac{1}{2} \hat{\rho}_{s1} \hat{V}_1^2} \quad (3.18)$$

Wolf & Johnston [1969] defined the diffuser inlet dynamic pressure based on the area averaged velocity:

$$\tilde{V}_1 = \frac{1}{b} \int_0^b V_1(x) dx \quad (3.19)$$

The pressure recovery coefficient thus becomes:

$$\tilde{C}_p = \frac{P_{s2} - P_{s1}}{\frac{1}{2} \tilde{\rho}_{s1} \tilde{V}_1^2} \quad (3.20)$$

Al Mudhafar et al. [1982] based the definition of pressure recovery coefficient on the diffuser inlet area-averaged dynamic pressure (assuming uniform static pressure across the diffuser inlet):

$$\tilde{P}_{t1} = \frac{1}{b} \int_0^b P_{t1}(x) dx \quad (3.21)$$

$$\tilde{C}_p = \frac{P_{s2} - P_{s1}}{\tilde{P}_{t1} - P_{s1}} \quad (3.22)$$

Bhinder et al. [1984] based the definition of the pressure recovery on the spatially-averaged dynamic pressure. Runstadler et al. [1975] modeled the inlet flow as a potential core with boundary layers and the diffuser recovery coefficient was based on the potential core total pressure which is measured at the diffuser throat centerline:

$$Cp_a = \frac{P_{s2} - P_{s1}}{P_{t1 \max.}(x) - P_{s1}} \quad (3.23)$$

Cp_a is a pressure recovery coefficient based on the peak value of the diffuser inlet dynamic pressure across the diffuser inlet depth, b . Dutton et al. [1986] based the definition of pressure recovery on the diffuser throat centerline total pressure similar to the one proposed by Runstadler et al. [1975]. Baghdadi [1973] used the mass-averaged total pressure at diffuser inlet for the definition of the pressure recovery coefficient.

These different methods of specifying the diffuser performance make interpretation, comparison, and generalization of the data of the different diffuser investigations difficult and in some cases impossible. Filipenco [1991] calculated the pressure recovery coefficient using different averaging methods of diffuser inlet dynamic pressure and argued that a number of these were inappropriate. He proposed a pressure recovery coefficient based on an availability averaged inlet total pressure. Filipenco started his analysis asking the question: given a generally non-uniform flow entering the diffuser, what is the maximum static pressure which can possibly be attained by the flow without any external work or heat interactions? This is the pressure which would be attained in a reversible, adiabatic, zero-work process which ends in a uniform zero-velocity state. Such a process conserves the net thermodynamic availability of the flow and an appropriate designation of the final total pressure attained is the "availability averaged" total pressure (Livesey & Hugh [1966]).

The availability averaged total pressure, $P_{t\psi}$, at the diffuser inlet is defined as:

$$P_{t\psi} = \exp \left[\frac{\int_0^b \ln(P_{t1}) \rho_{s1} V_{r1} 2\pi r_1 dx}{\int_0^b \rho_{s1} V_{r1} 2\pi r_1 dx} \right] \quad (3.24)$$

The availability averaged pressure recovery coefficient then becomes:

$$Cp_{\psi 1} = \frac{P_{s2} - P_{s1}}{P_{t\psi 1} - P_{s1}} \quad (3.25)$$

The denominator of the last equation can be defined as the diffuser inlet availability-averaged dynamic pressure. In the present diffuser tests, where the diffuser inlet profile data is available at discrete points across the diffuser inlet, the integrals for $P_{t\psi}$ are approximated using the trapezoidal rule.

$$P_{t\psi 1} \approx \exp\left(\frac{2\pi r_1}{\dot{m}} \sum_{i=1}^{16} \left[\frac{\ln(P_t(x_i)) \rho_s(x_i) V_r(x_i) + \ln(P_t(x_{i-1})) \rho_s(x_{i-1}) V_r(x_{i-1}))}{2} \right]_{r=r_1} \right) (x_i - x_{i-1}) \quad (3.26)$$

Among these different definitions of Cp mentioned, Cp_{ψ} is the most physically appropriate one to be used as a diffuser pressure recovery performance parameter, because it is based on a comparison of the diffuser pressure recovery to the best possibility which could be achieved by an arbitrary zero-work, adiabatic device with the given inlet flow conditions.

The mass-averaged total pressure at the diffuser inlet, \hat{P}_{t1} is defined as:

$$\hat{P}_{t1} = \frac{\int_0^b P_{t1} \rho_{s1} V_{r1} 2\pi r_1 dx}{\underbrace{\int_0^b \rho_{s1} V_{r1} 2\pi r_1 dx}_0} \quad (3.27)$$

$$\dot{m} = \rho_s V_r A$$

$$\hat{P}_{t1} = \frac{1}{\dot{m}} \int_0^b P_{t1}(x) \rho_{s1}(x) V_{r1}(x) 2\pi r_1 dx \quad (3.28)$$

$$\hat{P}_{t1} \approx \frac{2\pi r_1}{\dot{m}} \sum_{i=1}^{16} \left[\frac{P_t(x_i) \rho_s(x_i) V_r(x_i) + P_t(x_{i-1}) \rho_s(x_{i-1}) V_r(x_{i-1}))}{2} \right]_{r=r_1} (x_i - x_{i-1}) \quad (3.29)$$

The mass-averaged pressure recovery coefficient, $\hat{C}p$, then becomes:

$$\hat{C}_p = \frac{P_{s2} - P_{s1}}{\hat{P}_{t1} - P_{s1}} \quad (3.30)$$

The availability-averaged total pressure is equal to the mass-averaged total pressure for an ideal incompressible fluid. Filipenco [1991] and Johnston [1993] emphasized parameters which are defined in terms of availability; however, this is not really necessary in practical applications. Pressure recovery coefficients based on mass averaged total pressure are roughly equivalent, (1 - 1.5% difference) to availability averaged pressure recovery coefficient. On the other hand, using area averaged inlet total pressure can be inaccurate for the calculation of the pressure recovery coefficient. For the Mach numbers and levels of flow-field non-uniformity in the investigation by Filipenco [1991], the pressure recovery coefficient based on the mass-averaged total pressure was, in the extreme case, 1.6% less than the pressure recovery coefficient based on the availability-averaged total pressure. In the presentation of experimental results in Chapter 4, we will use mass averaged pressure recovery coefficient because it is conceptually simpler than the availability averaged pressure recovery coefficient and very close in value (in our investigations with straight channel diffuser, the maximum difference between both definitions of pressure recovery was 1%). Comparisons between different definitions of diffuser pressure recovery coefficient are given in Figures 4.32 a, b, and c.

The mass averaged pressure recovery coefficient in Equation (3.30) is the overall diffuser pressure recovery coefficient between the diffuser inlet (1) and exit (2). To analyze the pressure rise in different subcomponents of diffuser, we can also define C_p at different stations through the diffuser. One pressure recovery coefficient is based on the pressure rise from the diffuser leading edge to the throat (quasi-vaneless space), and another is from the diffuser throat to the exit (channel part of the diffuser). The former is defined as:

$$\hat{C}_{p_{1-th}} = \frac{P_{sth} - P_{s1}}{\hat{P}_{t1} - P_{s1}} \quad (3.31)$$

where subscript "th" means the diffuser throat. The latter is defined as:

$$\hat{C}P_{th-2} = \frac{P_{s2} - P_{sth}}{\hat{P}_{th} - P_{sth}} \quad (3.32)$$

3.1.3.2.2 Calculation of Ideal Pressure Recovery

The diffuser inlet total pressure, P_{t1} , total temperature, T_{t1} , venturi mass flow, $\dot{m}_{venturi}$ and diffuser exit area determine the ideal exit Mach number, M_{2id} , defined as follows:

$$\dot{m}_{venturi} = \sqrt{\frac{\gamma}{R}} \frac{M_{2id} A_2 P_{t1}}{\sqrt{T_{t1}} \left(1 + \frac{\gamma-1}{2} M_{2id}^2\right)^{\frac{\gamma+1}{2(\gamma-1)}}} \quad (3.33)$$

The ideal Mach number, M_{2id} , (from Equation (3.33)) also defines an ideal static pressure at the diffuser exit, P_{s2id} :

$$P_{s2id} = \frac{P_{t1}}{\left(1 + \frac{\gamma-1}{2} M_{2id}^2\right)^{\frac{\gamma}{\gamma-1}}} \quad (3.34)$$

This in turn implies an ideal pressure recovery coefficient, C_{pid} :

$$C_{pid} = \frac{P_{s2id} - P_{s1}}{P_{t1} - P_{s1}} \quad (3.35)$$

3.1.3.2.3 Flow Angle at the Diffuser Inlet

The diffuser-inlet "average" flow angle, $\hat{\alpha}_1$, is defined in terms of tangential and radial mass-averaged velocities at the diffuser inlet as:

$$\hat{\alpha}_1 = \tan^{-1} \left[\frac{\hat{V}_{\theta 1}}{\hat{V}_{r1}} \right] \quad (3.36)$$

where

$$\hat{V}_{\theta 1} = \frac{\int_0^b \rho_1 V_{r1} V_{\theta 1} 2\pi r_1 dx}{\underbrace{\int_0^b \rho_1 V_{r1} 2\pi r_1 dx}_m} \quad (3.37)$$

$$\hat{V}_{r1} = \frac{\int_0^b \rho_1 V_{r1} V_{r1} 2\pi r_1 dx}{\underbrace{\int_0^b \rho_1 V_{r1} 2\pi r_1 dx}_m} \quad (3.38)$$

Since the tangential and radial mass-averaged velocities represent the tangential and radial momentum of the diffuser inlet flow, the average flow angle given by Equation (3.36) is termed as "momentum averaged" flow angle.

We can also calculate mass averaged flow angle as:

$$\hat{\alpha}_1 = \frac{\int_0^b \alpha_1 \rho_1 V_{r1} 2\pi r_1 dx}{\underbrace{\int_0^b \rho_1 V_{r1} 2\pi r_1 dx}_m} \quad (3.39)$$

$$\hat{\alpha}_1 = \frac{1}{\dot{m}_0} \int_0^b \alpha(x) \rho_s(x) V_r(x) 2\pi r dx \quad (3.40)$$

$$\hat{\alpha}_1 \approx \frac{2\pi r_1}{\dot{m}} \sum_{i=1}^{16} \frac{\alpha(x_i) \rho_s(x_i) V_r(x_i) + \alpha(x_{i-1}) \rho_s(x_{i-1}) V_r(x_{i-1})}{2} (x_i - x_{i-1}) \quad (3.41)$$

In the present experiments differences between the momentum averaged and mass averaged flow angles were smaller than 0.5%. This difference is small but should not be dismissed as completely negligible, since the range of inlet flow angle between maximum flow rate and stall could be only 5°. Relative to such a range, the difference is then maximum 7%.

3.1.3.2.4 Inlet Blockage, Mass, Momentum, and Kinetic Energy Deficit and Skew Parameters

In addition to average diffuser inlet flow quantities, distortion and skew parameter for diffuser inlet mass, momentum, and kinetic-energy flux were defined by Filipenco [1991] to quantify the severity of the inlet flow field non-uniformity. These flow profile

parameters measured the basic level of deviation from the maximum, or mean, of the flow parameter and the axial asymmetry of the parameter. Table 3.1 summarizes these definitions of the distortion parameters.

A mass distortion parameter, mass-flux deficit, σ_m , was used by Filipenco to describe the quality of inlet blockage of the diffuser. σ_m is essentially the displacement thickness at the diffuser inlet and gives the fraction of the mass flow "lost" relative to the mass flow which would have been attained if the profile were uniform at velocity and flow angle values corresponding to the local maximum value of mass flux within the diffuser inlet. Analogous 'deficit' parameters, σ_p and σ_{ke} were also defined for the momentum and kinetic energy flows by Filipenco [1991] and their definitions are given in Table 3.1.

Profile skew parameters were also defined (see Table 3.1) to indicate the extent of asymmetry of the inlet flow field relative to the diffuser radial center plane. These parameters were defined in terms of the axial position which divides the diffuser inlet depth, b , into two equal flows of mass, momentum, or kinetic energy (i.e. the center of mass, momentum, or kinetic energy flow). The offset of these positions relative to the diffuser center plane ($x = b/2$) is expressed as a fraction of the maximum possible offset ($b/2$). The skew parameters have a value of zero for any flow field which is symmetrical about the diffuser center plane and have a value of ± 1.0 in the hypothetical limiting case when all of the flow is concentrated in an infinitesimally thin layer at one of the walls at the diffuser inlet.

Diffuser inlet flow angle non-uniformity and skew parameters were also defined. The flow angle non-uniformity, α_n , can be presented as the root mean square (rms) deviation of the flow angle from the momentum averaged value:

$$\alpha_n = \sqrt{\frac{1}{b} \int_0^b (\alpha - \hat{\alpha})^2 dx} \quad (3.42)$$

The flow angle skew, α_s , can be defined as the difference between the area averaged flow angles computed over half of the diffuser inlet width ($b/2$) on each side of the diffuser center plane:

$$\alpha_s = \frac{2}{b} \left[\int_0^{b/2} \alpha dx - \int_{b/2}^b \alpha dx \right] \quad (3.43)$$

The inlet profiles are described in terms of distortion and skew of: mass, momentum, energy, and flow angle. The distortion parameters, which integrate the profile variation from its maximum value, and the skew parameters, indicating the axial position about which the flow is split, are listed in Table Appendix A1.

For single channel diffusers there is a significant reduction in the diffuser pressure recovery as the thickness of boundary layer, or 'fluid dynamic blockage' is increased at the diffuser inlet. The diffuser inlet blockage, B_1 , is defined as:

$$B_1 = 1 - \frac{A_{effective}}{A_{geometric}} \quad (3.44)$$

Where $A_{geometric}$ is the geometrical area at the diffuser inlet radius and $A_{effective}$ is the area effectively used by the flow. $A_{effective}$ was calculated using the static pressure and the mass averaged total pressure measured at the diffuser inlet. The blockage can be calculated at the diffuser inlet (subscript 1) as well as at diffuser throat (subscript th) using Equation (3.44), if the throat total pressure is known.

3.1.4 Static Pressure Measurements at Different Locations

Using static pressure circumferential taps at the impeller exit a circumferential non-uniformity parameter, $\psi_d(\theta)_{r1}$, can be defined as:

$$\psi_d(\theta)_{r1} = \frac{P_{s1'}(\theta) - \bar{P}_{s1'}}{\hat{P}_{t1,ref} - \bar{P}_{s1'}} \quad (3.45)$$

where $\hat{P}_{t1,ref}$ is the mass averaged total pressure obtained from the axial traverse of the diffuser inlet at circumferential position $\theta = 0^\circ$. Circumferential non-uniformity parameter, $\psi_d(\theta)_{r1}$, is used to determine the circumferential static pressure non-uniformity at impeller exit (see Appendix A3).

Similar to Equation (3.45) a static pressure coefficient for the diffuser channel pressure taps can be defined. This static pressure coefficient for the diffuser centerline, $C_p(y/L)$, is:

$$C_p(y/L) = \frac{P_s(y/L) - \bar{P}_{s1}}{P_{t\psi 1} - \bar{P}_{s1}} \quad (3.46)$$

For the quasi-vaneless space, $C_p(z,\theta)$ is defined as:

$$C_p(z,\theta) = \frac{P_s(z,\theta) - \bar{P}_{s1}}{\hat{P}_{t1} - \bar{P}_{s1}} \quad (3.47)$$

In equations (3.46) and (3.47), \hat{P}_{t1} , is "mass-averaged" diffuser inlet total pressure.

In addition to mass flow-rate, \dot{m} , and pressure recovery coefficient, C_p , the dimensionless flow number, ϕ , and the pressure rise coefficient, D_p , are also used in the open literature, to characterize the flow in turbomachines.

The definition of dimensionless flow number, ϕ , is,

$$\phi = \frac{Q}{\frac{\pi}{4} D^2 U} = \frac{\dot{m} / \rho_s}{\frac{\pi}{4} D^2 U} \quad (3.48)$$

and pressure rise coefficient, D_p , is defined as,

$$D_p = \frac{\Delta P}{\rho_s \frac{U^2}{2}} \quad (3.49)$$

where

$\Delta P = (P_2 - P_1)$ is the static pressure rise at the diffuser and

$U = \pi D N_{\text{corr}}$ is the meridional velocity.

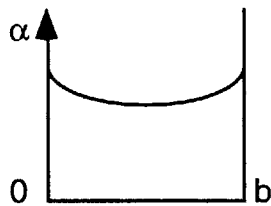
The Reynolds number, Re , is defined by the diffuser depth, b , and total velocity, V_1 , at the diffuser inlet:

$$Re = \frac{V_1 b}{\nu} \tag{3.50}$$

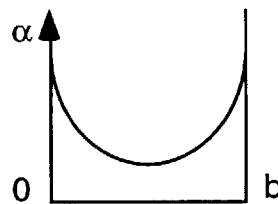
3.2 Scope of Experiments

The measurements addressed the effects of the inlet Mach number, inlet boundary layer blockage, inlet flow asymmetry, and flow angle. Diffuser inlet profiles were controlled by mass injection and suction downstream of the impeller. Testing consisted of throttling the impeller and diffuser at a constant rotor speed with various combinations of axial air injection and/or suction to alter the inlet velocity profile. The general direction of alteration is shown schematically below:

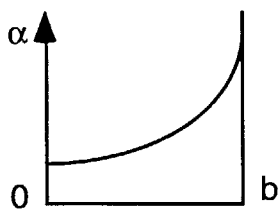
Suction Both Sides



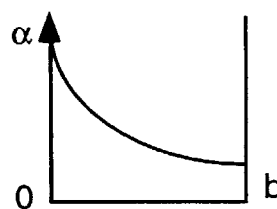
Injection Both Sides



Rear Side injection/Front Side Suction



Rear Side Suction/Front Side Injection



A detailed test matrix is given in Table 3.2 which comprises of the diffuser inlet flow-field parameter range obtained in the measurements of straight channel diffuser.

The first series of measurements (Series I in Table 3.2) were carried out without air injection and suction. For each corrected impeller speed (from 1000 RPM to 6000 RPM) a constant speed characteristic is measured at several operating points from the full valve opening to the 35 - 50% valve opening (onset of instability) depending on the impeller speed. Each valve position corresponds to a different impeller exit (or plenum) to atmosphere static pressure ratio.

Experiments with air injection and/or suction, where an axially distorted flow field was produced using a cross-flow injection and/or suction through the profile control slots in the vaneless space, consist of three data series denoted with the numbers II, III, and IV in the Table 3.2. For data series II and III, two constant impeller speeds were chosen, a low speed $N = 2000$ RPM (Mach number at diffuser inlet $M_1 \approx 0.2$ to 0.4) and a high speed $N = 5000$ RPM (Mach number at diffuser inlet $M_1 \approx 0.7$ to 1.0). For data series II, for a constant impeller speed and valve position, the applied injection and suction rates were at the same amount (maximum 10% of venturi mass flow rate), so that the venturi mass flow rate, \dot{m} , remained nearly constant with and without injection suction. Data series (II) thus did not have a high level of flow non-uniformity at the diffuser inlet (difference of flow angle between front and rear sides of the diffuser was smaller than 10°). In order to maintain high level of distortion at the diffuser inlet, the data series III was obtained and up to 45° difference of flow angle between front and rear sides of the diffuser was achieved.

Data series IV contains three different impeller speeds, one at low speed range $N = 2000$ RPM (Mach number at diffuser inlet $M_1 \approx 0.2$ to 0.4), another in the high speed range $N = 6000$ RPM (Mach number at diffuser inlet $M_1 \approx 0.8$ to 1.2) and one at $N = 4000$ RPM. In the data series IV, not only asymmetrical, highly distorted velocity profiles, but also symmetrical velocity profiles with different boundary layer blockage levels were applied at the diffuser inlet.

The parameter range of the straight channel diffuser investigations can be summarized as follows:

- Diffuser inlet flow angle, α , 62 - 71°
- Diffuser inlet Mach number, M , 0.2 - 1.15
- Velocity profile axial-distortion (uniform and non-uniform profiles)
- Diffuser inlet blockage, B_1 , 2 - 35 %
- Diffuser inlet Reynolds number, Re_1 , $0.5 \cdot 10^5$ - $2.5 \cdot 10^5$

	distortion level	asymmetric skew
mass	$\sigma_m \equiv \frac{\int_0^b [(\rho V_r)_{max} - \rho V_r] 2\pi r_1 dx}{2\pi r_1 b (\rho V_r)_{max}}$	$\xi_m \equiv \frac{x_m^* - b/2}{b/2}; \text{ where } x_m^* \text{ is:}$ $\int_0^{x_m^*} \rho V_r 2\pi r_1 dx = \int_{x_m^*}^b \rho V_r 2\pi r_1 dx$
momentum	$\sigma_p \equiv \frac{\int_0^b [(\rho V_r V)_{max} - \rho V_r V] 2\pi r_1 dx}{2\pi r_1 b (\rho V_r V)_{max}}$	$\xi_p \equiv \frac{x_p^* - b/2}{b/2}; \text{ where } x_p^* \text{ is:}$ $\int_0^{x_p^*} \rho V_r V 2\pi r_1 dx = \int_{x_p^*}^b \rho V_r V 2\pi r_1 dx$
kinetic energy	$\sigma_{KE} \equiv \frac{\int_0^b [(\rho V_r V^2)_{max} - \rho V_r V^2] 2\pi r_1 dx}{2\pi r_1 b (\rho V_r V^2)_{max}}$	$\xi_{KE} \equiv \frac{x_{KE}^* - b/2}{b/2}; \text{ where } x_{KE}^* \text{ is:}$ $\int_0^{x_{KE}^*} \rho V_r V^2 2\pi r_1 dx = \int_{x_{KE}^*}^b \rho V_r V^2 2\pi r_1 dx$
swirl angle	$\alpha_n = \sqrt{\frac{1}{b} \int_0^b (\alpha - \bar{\alpha})^2 dx}$	$\alpha_s = \frac{2}{b} (\int_0^{b/2} \alpha dx - \int_{b/2}^b \alpha dx)$

Table 3.1 Filipenco's [1991] distortion parameter definitions

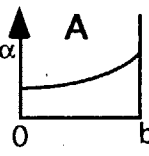
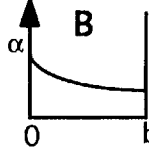
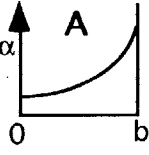
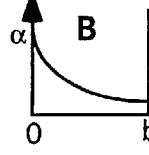
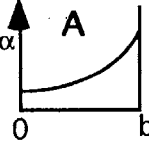
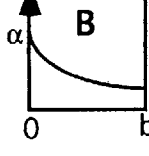
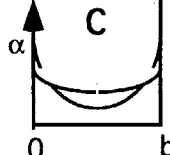
Series	Impeller Speed N [RPM]	Diffuser Inlet Mach Number M_1 [-]	Plenum to Atmosphere Pressure Ratio π_{03} [-]	Throttle Valve Position [%]	Diffuser Inlet Flow Angle α [°]	Inlet Flow Conditions	Diffuser Inlet Velocity (Flow Angle) Profiles
I	1000 to 6000	0.15 to 1.15	0.99 to 1.09	100% (Max. Flow Rate) to 35% - 50% (Stall Begin)	67° to 70.5°	no injection- suction natural distortion	---
II	2000 → 5000 →	0.20 to 0.35 0.70 to 1.0	1.00 to 1.04 1.02 to 1.06	100 / 52 / 38 100 / 59 / 52	68° to 69.5° 68.5° to 70°	with injection-suction applied small distortion	 
III	2000 → 5000 →	0.15 to 0.35 0.65 to 0.95	1.00 to 1.03 1.02 to 1.05	100 / 40 100 / 55	63° to 70° 68° to 70.5°	with injection-suction applied high distortion	 
IV	2000 → 4000 → 6000 →	0.20 to 0.35 0.50 to 0.75 0.75 to 1.15	1.00 to 1.01 1.01 to 1.05 1.01 to 1.06	100 / 52 / 40 100 / 54 / 50 100 / 55	63° to 67.5° 65° to 68° 67° to 71°	with injection-suction applied high distortion and also symmetrical profiles with different blockage levels	  

Table 3.2: Test plan with the diffuser inlet flow-field parameter range obtained

CHAPTER 4

Experimental Results

The results of the experiments carried out with the straight channel diffuser are presented in this chapter. Section 4.1 describes diffuser performance data, obtained without air injection and/or suction at impeller exit, provided that diffuser inlet profile was as uniform as possible. Section 4.2. describes similar data with flow injection and/or suction at the impeller exit. Section 4.3 includes comparisons of the results between straight channel diffuser experiments and discrete passage diffuser results from previous investigations. In Section 4.4 we compare the results with the other varied diffuser investigations available in the open literature.

4.1 Baseline Inlet Flow-Field Data (Data Without Air Injection/Suction)

Figure 4.1a depicts the atmosphere to diffuser inlet pressure ratio versus venturi mass flow rate constant-speed characteristics for several corrected impeller speeds from 1000 to 6000 RPM. A plot of the atmosphere to diffuser exit pressure ratio is shown in Figure 4.1b for the same speeds. Both inlet and exit pressures in the facility loop are atmospheric. The diffuser exit pressure is higher than the atmospheric pressure and, as shown in Figure 4.1b, the diffuser exit pressure ratio, π_{02} , is always greater than unity. There is a pressure drop across the impeller as shown in Figure 4.1a. Since the static pressure rise versus mass flow rate characteristics have negative slope (Fig. 4.1a), the impeller itself shows stable behavior for the flow range of interest. The atmosphere-to-plenum pressure ratio, π_{03} , was used as an operating point reference for some of the data presented in Sections 4.1 and 4.2. There is no pressure rise after the diffuser exit so the measured atmosphere-to-plenum pressure ratio, π_{03} , and atmosphere-to diffuser exit pressure ratio, π_{02} , were very close in value. For every impeller speed in Figure 4.1a and b, the maximum flow rate was limited by the maximum throttle valve opening whereas the minimum flow rate by the onset of flow instability.

The performance map in terms of dimensionless flow coefficient, ϕ , and diffuser pressure rise, D_p , with corrected impeller speed as parameter is shown in Figure. 4.2.

Diffuser inlet flow angle and Mach number axial profiles were measured for every operating point. For the baseline case (no injection/suction) examples of axial distributions of flow angle and Mach number are shown in Figures 4.3a and 4.3b for different corrected impeller speeds from 2000 RPM to 6000 RPM and a fixed atmosphere-to-plenum ratio. The profiles of flow angle and Mach number are fairly symmetrical at the diffuser inlet. The disturbances in flow angle near the front wall ($x/b = 0$) are due to the influence of labyrinth seal leakage. The diffuser inlet Mach number increases as impeller speed increases with maximum achieved Mach number at the diffuser inlet 1.15.

The main performance parameter, the mass averaged overall diffuser pressure recovery coefficient (as defined by Equation 3.30) versus momentum averaged inlet flow angle (as defined by Equation 3.36) is shown in Figure 4.4 for different corrected impeller speeds, from maximum flow rate to the stall. For all speeds the overall diffuser pressure recovery increases slightly with increasing flow angle. The pressure recovery increased from 0.67 to 0.77 as the flow is reduced from maximum ($\alpha \approx 67^\circ$) to the near stall operating point ($\alpha \approx 70.5^\circ$). With injection/suction the lower flow angle boundary shifted to $\alpha = 63^\circ$ (see Figure 4.19) and thus a broader flow angle range could be investigated. For constant impeller speed, lower mass flow rate implies lower radial velocity and, therefore, increasing flow angle at the diffuser inlet. Reducing the mass flow at constant impeller speed, increases the inlet flow angle, and if a critical inlet flow angle is reached rotating stall occurs. The critical flow angle at which rotating stall appeared was between 70° and 70.5° for all impeller speeds investigated.

The effect of inlet Mach number on the mass averaged overall diffuser pressure recovery coefficient is shown in Figure 4.5. In this figure the absolute Mach number as defined in Equation 3.5 varied from 0.2 to 1.15 and did not show any remarkable influence on the mass averaged overall diffuser pressure recovery coefficient.

According to single channel diffuser data, an important fluid dynamic parameter for diffuser performance is blockage at diffuser inlet. Figure 4.6 plots mass averaged overall

diffuser pressure recovery coefficient versus diffuser inlet blockage (as defined in Equation 3.44). For a better comparison with single channel diffuser performance data, the blockage of centrifugal compressor vaned diffusers must be defined at the diffuser throat, because the channel part of the centrifugal compressor vaned diffuser is geometrically similar to single channel diffusers. Since there is no measured data (total pressure) available at diffuser throat, the throat blockage can be defined either by assuming that the flow is isentropic from the diffuser inlet to throat or it can be estimated on a basis of the empirical correlation between throat blockage and pressure recovery coefficient from diffuser inlet to throat, adopting the approach which was first suggested by Kenny [1972]. Calculation of throat blockage for the straight channel diffuser and performance comparisons with single channel diffuser data can be found in Appendix A4.

The variation in the axial velocity distribution at the diffuser inlet can be expressed in terms of the distortion parameters presented in Table 3.1. The effects of flow angle non-uniformity and mass flow non-uniformity at the diffuser inlet on mass averaged overall diffuser pressure recovery are shown in Figures 4.7 and 4.8. For the experiments carried out without injection/suction, the axial velocity distributions at the diffuser inlet were nearly symmetrical and uniform as seen in Figure 4.3a. Therefore, the flow non-uniformity level obtained at the diffuser inlet was not high compared to the investigations with injection/suction. Both Figures 4.7 and 4.8 show no dependence of mass averaged overall diffuser pressure recovery coefficient on flow non-uniformity parameters at diffuser inlet over the range investigated.

Examples of static pressure distributions along the centerline of an individual diffuser channel are shown in Figures 4.9 and 4.10. The static pressure rise in these figures is represented by a local pressure coefficient defined in Equation 3.46. In Figures, 4.9a and b, the corrected impeller speed was varied from 2000 RPM to 6000 RPM, at a constant plenum pressure ratio. Figure 4.10 depicts static pressure distributions along the diffuser centerline at different pressure ratios between maximum flow rate and the stall for a constant impeller speed $N = 3000$ RPM. As seen in these figures, a substantial part of the pressure rise occurs immediately following the diffuser leading edge at the quasi-vaneless space and diffuser throat region. In the channel part of the diffuser, the slope of the pressure rise decreases. Over 55 to 60 % of the overall diffuser pressure

static rise occurs within the first 30% of the diffuser channel length. In addition, the differences in the channel centerline static pressure distributions for different impeller speeds and different pressure ratios are substantial only at the inlet region of straight channel diffuser. These differences almost disappear in the channel diffuser part.

The channel centerline static pressure rise characteristics do not show any significant difference for various impeller speeds in Figures 4.9a and 4.9b, except for the highest impeller speed $N = 6000$ RPM. This high speed (or high Mach number) operating point exhibits no pressure rise at the diffuser inlet region up to the diffuser throat, due to the acceleration of the flow in the diffuser inlet region. For this operating point, the flow angle (incidence) is low with respect to the circumferential direction. The impeller exit flow is accelerated into the diffuser inlet, followed by a rapid diffusion resulting in a steep pressure gradient. There is no pressure rise in quasi-vaneless space but because of high pressure rise in the throat region and after the throat, the overall diffuser pressure rise in this case is almost at the same level compared to the other operating points in Figures 4.9a and 4.9b.

4.2 Influence of Inlet Flow Conditions

(Data With Air Injection/Suction)

The results of the experiments with applied air injection and/or suction are described in this section. Different test series (II, III, and IV see Table 3.2) were carried out with axial profile control injection/suction. Inlet conditions to the diffuser include low and high Mach numbers, symmetric and asymmetric profiles, with high and low distortions and different blockage levels. Typical examples of the shape and the range of axial flow angle and Mach number distributions at the diffuser inlet are shown in Figures 4.11 through 4.18. In the legends of these figures the average values for the flow angle and Mach number distributions are given along with the flow angle non-uniformity, α_n .

The variation of the inlet flow angle profile was from low distortion (Series II) to high distortion levels (Series III and IV). The maximum inlet flow angle variation between rear and front walls of the diffuser was 10° for test Series II (Figures 4.11a, 4.12a, 4.13a and 4.14a). The variation in inlet Mach number versus axial position is shown in Figures

4.11b through 4.14b for the test Series II. In test Series III the inlet distortion was varied from a symmetrical distribution to an asymmetric distribution. There is a 45° change in flow angle across the diffuser depth for the maximum distorted case in Figure 4.15b. In test Series IV the diffuser inlet blockage level was varied with both side injection or suction. An example of the inlet flow angle profile combinations for different blockage levels is presented in Figure 4.18a.

4.2.1 Effect of Inlet Parameters

The parameters that characterize the flow at the diffuser inlet include flow angle, Mach number, Reynolds number, turbulence, blockage, and the parameter expressing non-uniformity of the mass, momentum, kinetic energy, and flow angle. All of these parameters can influence the performance of the diffuser, hence:

$$C_p = f(\alpha, M, Re, Tu, B, \alpha_n, \sigma, \xi, \dots)$$

The effect of these parameters on mass averaged overall diffuser pressure recovery coefficient are presented in Figures 4.19 through 4.24. These figures contain all the operating points measured with and without air injection and/or suction. Since the distortion (σ) and skew (ξ) levels of mass, momentum, and kinetic energy are roughly scaled, in differentiating diffuser performance, only the mass distortion and mass skew parameters as well as the flow angle non-uniformity are presented in diagrams.

Figure 4.19 depicts mass averaged overall straight channel diffuser pressure recovery coefficient as a function of inlet flow angle for various impeller speeds, throttle valve positions and inlet distortion parameter levels. The overall diffuser pressure recovery and operating range depend primarily on inlet flow angle, and the inlet axial flow field distortions affect the performance of the straight channel diffuser to a lesser degree. The onset of rotating stall occurred at a momentum averaged flow angle (70° - 70.5°) independent of the inlet flow field parameters and Mach number, and for all the data series the maximum diffuser pressure recovery was achieved just prior to the rotating stall threshold.

The independence of mass averaged overall diffuser pressure recovery coefficient of the inlet Mach number and Reynolds number can be seen from Figures 4.20 and 4.21. The lower pressure recovery coefficient values in these figures are not the effects of inlet Mach number or Reynolds number, because these points of lower pressure recovery are also points of lower inlet flow angle in Figure 4.19. The Reynolds number range of the investigations for straight channel diffuser was $0.5 \cdot 10^5$ to $2.5 \cdot 10^5$.

Figure 4.22 shows that the effect of diffuser inlet blockage on the mass averaged overall diffuser pressure recovery is minimal, however, a decreasing trend is detectable with increasing inlet blockage.

Flow angle non-uniformity, α_n , and mass flow non-uniformity, σ_m , have similar effects on mass averaged overall diffuser pressure recovery as shown in Figures 4.23 and 4.24. Up to a certain level of these inlet distortion parameters ($\alpha_n < 6$ and $\sigma_m < 0.35$) there is no influence of both non-uniformity parameters on the mass averaged overall pressure recovery, but after these values ($\alpha_n > 6$ and $\sigma_m > 0.35$) for very high distortion levels the mass averaged overall pressure recovery decreases with increasing inlet distortion. This range of very high distortion levels corresponds to inlet flow angle differences of 25° to 45° between front and rear sides of the diffuser. Most of the points with high level of flow non-uniformity and lower pressure recovery in Figures 4.23 and 4.24 have average inlet flow angles of 63° to 66° . (As a consequence of increasing inlet flow angle non-uniformity by applying injection/suction, the mean value of inlet flow angle decreases). These points of low pressure recovery in Figures 4.23 and 4.24 also appear as low pressure recovery points in Figure 4.19 because of the influence of inlet flow angle.

The main trend of the presented Figures from 4.19 to 4.24 is that the performance of the radial diffusers can be correlated using one main parameter, the inlet flow angle. For a given flow angle, mass averaged overall diffuser pressure recovery coefficient is essentially independent of diffuser inlet conditions. In the worst case, there is a maximum 10% difference in pressure recovery at a constant flow angle in Figure 4.19. To isolate the influence of parameters associated with the inlet flow field the data in Figures 4.19 through 4.24 were presented for constant flow angles in Figures 4.25 through 4.28. Figure 4.25 shows the effect of inlet Mach number, Figure 4.26 inlet blockage, Figure 4.27 inlet flow angle non-uniformity, and Figure 4.28 mass flow non-

uniformity as a function of mass averaged overall diffuser pressure recovery coefficient for constant inlet flow angles 67° , 68° , 69° and 70° . In all these figures (4.25 through 4.28) there is no obvious dependence of mass averaged pressure recovery on the inlet Mach number, inlet blockage and flow distortion parameters. The mass averaged overall diffuser pressure recovery coefficient is mainly determined by the momentum averaged inlet flow angle.

4.2.2 Static Pressure Rise in Diffuser Channel

Examples of the static pressure distribution along the centerline of one diffuser channel are shown in Figures 4.29, 4.30, and 4.31 for experiments with injection/suction. In Figure 4.29 for a corrected impeller speed of 6000 RPM, the static pressure rise curves in the diffuser channel are similar for different distortion levels, except for the diffuser inlet region (quasi-vaneless space and throat). At the diffuser inlet region there is either an acceleration or a diffusion depending on the average inlet flow angle. In the channel part of the diffuser there is no significant difference among the pressure rise curves for different inlet distortion levels.

Figure 4.30 is another constant speed case for 4000 RPM with various distortion levels. The bold lines in this figure are the baseline data without injection/suction. Between the bold lines and the curve of lowest pressure rise (line with blank squares) there is a difference in the pressure recovery, however this is an effect of inlet flow angle, since there is a difference of 2.6° in inlet flow angle between both cases.

Figure 4.31 is a low speed ($N = 2000$ RPM) case with three different inlet flow field distortion levels. The average values of inlet flow angles are 63.0° , 64.5° and, 68.5° . There is a substantial difference in the pressure recovery among the three pressure rise curves. The slope of the pressure rise in the channel diffuser part has the same level for three cases (63.0° , 64.5° and, 68.5°) in Figure 4.31 (in fact, the value of the slope in the channel diffuser part is the highest for $\alpha = 63^\circ$, whereas the overall diffuser pressure recovery coefficient is the lowest), but the overall diffuser pressure recovery values achieved are different. This indicates that the reason for different overall diffuser pressure recovery values is the pressure rise of the diffuser inlet region. In Figure 4.31 the highest pressure

recovery is for $\alpha = 68.5^\circ$, which is close to the diffuser design angle. For this inlet flow angle an important pressure rise occurs in the diffuser inlet region immediately after the leading edge. Decreasing the flow angle from $\alpha = 68.5^\circ$ to $\alpha = 64.8^\circ$ lowers the slope of the pressure rise in the diffuser inlet region. If one decreases the inlet flow angle further to $\alpha = 63.0^\circ$, there is no pressure rise at the diffuser inlet region, but rather an acceleration of the flow until the channel diffuser part, resulting in a low overall diffuser pressure recovery in this case of $\alpha = 63.0^\circ$.

4.2.3 Different Definitions of Diffuser Pressure Recovery Coefficient

As discussed in Section 3.1.3.2.1 the overall diffuser pressure recovery coefficient can be calculated using a number of different definitions of inlet dynamic pressure. In the performance diagrams presented for the straight channel diffuser we have used the mass averaged pressure recovery coefficient which is conceptually simpler and differs by roughly 1% from the availability averaged pressure recovery coefficient. Pressure recovery coefficients based on area averaged inlet dynamic pressure and on peak value of the diffuser inlet dynamic pressure have also been calculated for the straight channel diffuser. These definitions of pressure recovery coefficient are often used in the open literature. For purposes of comparison, some examples are shown in Figures 4.32 a, b, and c, which includes calculations of overall diffuser pressure recovery coefficients using different definitions versus momentum averaged inlet flow angle. Figure 4.32a is for a corrected impeller speed of 4000 RPM without injection/suction (from Series I). Figure 4.32b is for a corrected speed of 2000 RPM with injection/suction and includes maximum levels of inlet flow axial non-uniformities achieved during the investigations (from Series III). Figure 4.32c is high speed data for 6000 RPM with injection/suction and includes high blockage levels (from Series IV).

It can be seen in Figures 4.32 a, b, and c that there is only a very small difference between mass averaged and availability averaged pressure recovery coefficients. The pressure recovery coefficient based on the area averaged total pressure is higher and the pressure recovery coefficient based on the inlet maximum total pressure is more than 10% lower than the mass averaged pressure coefficient. Since the maximal inlet total pressure measured across the diffuser depth is higher than the mass averaged inlet total

pressure, the denominator of the equation for the pressure recovery coefficient becomes higher, and therefore the pressure recovery lower if one uses the peak value of the inlet total pressure. Filipenco [1991] also showed that different definitions of pressure recovery coefficient lead to different conclusions regarding the effect of inlet distortion on diffuser performance. An apparent sensitivity of the diffuser pressure recovery performance to axial inlet distortion and Mach number was observed either using area averaged pressure recovery or pressure recovery coefficient based on the maximum inlet total pressure, this is not the case if one uses mass and/or availability averaged pressure recovery coefficient.

Another observation from Figure 4.32 concerns the difference between the ideal and actual overall diffuser pressure recovery coefficients. According to Dawes [1994] or Cumpsty [1989] the performance of a centrifugal impeller is often good but when it is combined with a vaned diffuser the performance of the overall stage is disappointing. Although single channel diffusers may permit 80% static pressure recovery (if the diffuser is long enough and the inlet boundary layer is thin), this has never been achieved in a centrifugal compressor (Japikse [1987]). The ideal pressure recovery coefficient in Figure 4.32 is calculated for an isentropic, and quasi-one-dimensional flow. Typical values for the diffuser ideal pressure recovery are 90 - 95% for an inlet Mach number of $M \approx 1$, and diffuser area ratios of high performance centrifugal compressors. The measured pressure recovery of the straight channel diffuser is in the range of 65 - 75%, which results a diffuser efficiency of ≈ 0.75 . One can separate the overall straight channel diffuser into two diffusers in series with the quasi-vaneless space (diffuser inlet) and channel diffuser part. For the channel diffuser part of a centrifugal compressor vaned diffuser, an efficiency of 0.90 - 0.95 can be achieved (if the divergence angle of the channel diffuser part is not extremely high). This indicates that important part of the losses in centrifugal compressor diffuser occurs in the diffuser inlet region.

4.2.4 Stall Onset Observation

One objective of this research was to determine the effect of inlet flow field distortion on the stable operating range of the straight channel diffuser. Therefore, attention was paid to the diffuser inlet flow field and diffuser channel centerline static pressure distribution

near stall operating points. It was found in Figure 4.19 that the onset of rotating stall occurs at a critical inlet flow angle $70^\circ - 70.5^\circ$ independent of inlet flow field distortion and Mach number.

In addition to changing the axial shape of the diffuser inlet profile, the flow injection/suction system in the vaneless space permitted operation of the radial diffuser over an inlet flow angle range independent of the operating point of the impeller and its characteristics. Control of the diffuser inlet flow angle independent of impeller speed was possible and this allowed the isolation of instability phenomena, specific to either component, diffuser or impeller.

Filipenco [1991] found in his investigations on discrete passage diffuser that the diffuser was the stability limiting element. To demonstrate that the onset of rotating stall is triggered by flow instability in the vaned diffuser and not by the impeller, three operating points with different inlet flow angles were examined corresponding to impeller speeds of 2000 RPM, 4000 RPM and 6000 RPM. The points were approximately 20% far from the rotating stall onset point in mass flow. For these three operating points at which impeller speed and throttle valve position remained constant, different levels of axial injection and suction were applied until rotating stall occurred. In all three cases the onset of rotating stall occurred when the diffuser inlet momentum averaged flow angle reached the values of 69.8° , 70.3° and 70.7° . Since rotating stall occurred for different impeller operating points (the slope of the impeller pressure rise characteristics was also negative for all three operating points), it can be concluded that the onset of rotating stall was triggered by the diffuser.

4.3 Comparison With Discrete Passage Diffuser Results

The discrete passage diffuser, developed by General Electric has a design characterized by straight centerline passages which are circular in cross section from the diffuser inlet up to diffuser throat and acquire a semi-rectangular cross section between the throat and diffuser exit (Figure 4.33). Between the diffuser inlet and the throat, the intersection of the conical passages forms a quasi-vaneless space with highly swept back cusp-like

leading edges. The quasi-vaneless space is designed to diffuse supersonic inlet flow, and the throat area sets the maximum flow rate of the diffuser.

The test results of the investigations (Filipenco [1991], Johnston [1993]) with discrete passage diffusers (30 and 38 passages) showed that if one uses the proper variables, changes in inlet distortion have little effect on pressure recovery of a discrete passage diffuser. The results of the experiments with straight channel diffuser presented in Sections 4.1 and 4.2 show similar behavior and confirm the results of discrete passage diffuser experiments done by Filipenco [1991] and Johnston [1993].

The mass averaged pressure recovery coefficient of the 30 passage discrete passage diffuser (from Filipenco [1991]) is compared in Figure 4.34 with the pressure recovery of the straight channel diffuser (from Figure 4.19) as a function of momentum averaged inlet flow angle. The overall pressure recovery coefficient for both diffusers correlates with the inlet flow angle and is insensitive to axial distortions of the diffuser inlet flow field. If we compare the achieved overall diffuser pressure recovery level of straight channel diffuser to that of discrete passage diffuser in Figure 4.34, the straight channel diffuser shows ca. 10% higher pressure recovery coefficient. At operating points near the design point, the mass averaged pressure recovery coefficient for straight channel diffuser and discrete passage diffuser are 0.65 - 0.78 and 0.60 - 0.70 respectively. The comparison also indicates that the critical inlet flow angle for the onset of rotating stall for the straight channel diffuser is $70^\circ - 70.5^\circ$ and that for the discrete passage diffuser is $73^\circ - 74^\circ$. Although the critical inlet flow angle for the rotating stall onset is lower for straight channel diffuser, we can not conclude that the operating range of the straight channel diffuser is smaller than that of the discrete passage diffuser. According to Figure 4.34 the operating inlet flow angle range for the discrete passage diffuser is ca. 5° and an operating range of 5° is also observed for the straight channel diffuser.

We can also compare the channel centerline pressure rise characteristics of the investigated discrete passage and straight channel diffusers, in terms of the pressure recovery before and after diffuser throat. This kind of comparison must be made with the following cautions:

i) The geometrical position of the throat is different in the two diffusers: The non-dimensional distance from the leading edge to the throat (normalized with the diffuser

length) is longer for the discrete passage diffuser than that for the straight channel diffuser. In other words for the straight channel diffuser the throat is closer to the diffuser inlet radius.

ii) The same value of inlet flow angle means different operating conditions for each diffuser, because each diffuser has different operating ranges of flow angle between maximum flow rate and stall onset (see Figure 4.34).

iii) Although the overall diffuser pressure recovery is not influenced by the inlet flow field distortion, the pressure rise in the diffuser inlet region is. For a direct comparison of the pressure recovery in the diffuser inlet region between the two diffusers, the inlet flow field distortions should be the same, but this is not easy to achieve in practice.

An example of the static pressure distributions along discrete passage diffuser centerline (Figure. 4.35) is chosen for the comparison with the similar distribution data of the straight channel diffuser (see Figures 4.9, 4.10, 4.29, 4.30, and 4.31). Figure 4.35 summarizes Filipenco's [1991] discrete passage diffuser static pressure rise distributions, for an operating point near the rotating stall, at three different impeller speeds (covering inlet Mach number from 0.2 to 1.0) with low and high inlet distortion levels. For all three impeller speeds a pressure rise of 50% of the overall pressure recovery occurs from leading edge to throat in case of low inlet distortion. With higher inlet distortion the overall pressure recovery remains nearly the same for all three speeds, but the pressure rise up to the throat is 55 - 60% of the overall pressure recovery. For the same impeller speeds, low inlet flow field distortion, and an operating point near the onset of rotating stall, the overall pressure recovery of the straight channel diffuser is higher than that of the discrete passage diffuser, but only 40% of this overall pressure rise occurs between leading edge and throat in comparison to 50% of the pressure rise in the discrete passage diffuser inlet region. According to this comparison the pressure rise at the inlet region (quasi-vaneless space and throat) of the discrete passage diffuser is higher than that of the straight channel diffuser, but a lower pressure rise occurs in the channel diffuser part for the discrete passage diffuser resulting in a lower overall discrete passage diffuser pressure recovery.

We note that we do not have complete knowledge of the design criterion of the discrete passage diffuser. The design of the straight channel diffuser was based on maximum pressure recovery and a flow regime without appreciable stall. The geometrical

parameters such as diffuser channel divergence angle, area ratio and length-to-width ratio were chosen according to this criterion from Reneau's diffuser map. The discrete passage diffuser was an engine part and, although its geometrical parameters are given in Table 2.2, they do not indicate the criteria on which the design was based.

4.4 Comparisons With Other Vaned Diffuser Investigations

Comparisons with other vaned diffuser investigations contain two aspects, maximum overall diffuser performance and the influence of inlet flow field conditions on diffuser performance. Most of the radial diffuser investigations available in the open literature (see Section 1.2.6) were carried out in a compressor stage with an impeller upstream and most of the data show stage performance characteristics (overall efficiency and/or pressure ratio versus mass flow rate) with vaned diffusers and not component performance data in the form of separate impeller and diffuser characteristics.

Rodgers [1980] gives typical vaned diffuser static pressure recovery values for high performance centrifugal compressors as 0.65 - 0.78, which is in accordance with Japikse [1996]. Regarding overall diffuser pressure recovery, the only exception we can find in the open literature is Krain's [1984] straight channel diffuser performance. Parameters of Krain's diffuser compared with the straight channel diffuser investigated in this study is shown in the following table:

	<u>Present investigation</u>	<u>Krain's diffuser</u>
2θ	8°	7.54°
AR	2.34	2.51
LWR	9.574	11.46
Throat AS	0.643	1.6
Vane number	30	27
Vaneless space radius ratio	0.10	0.10

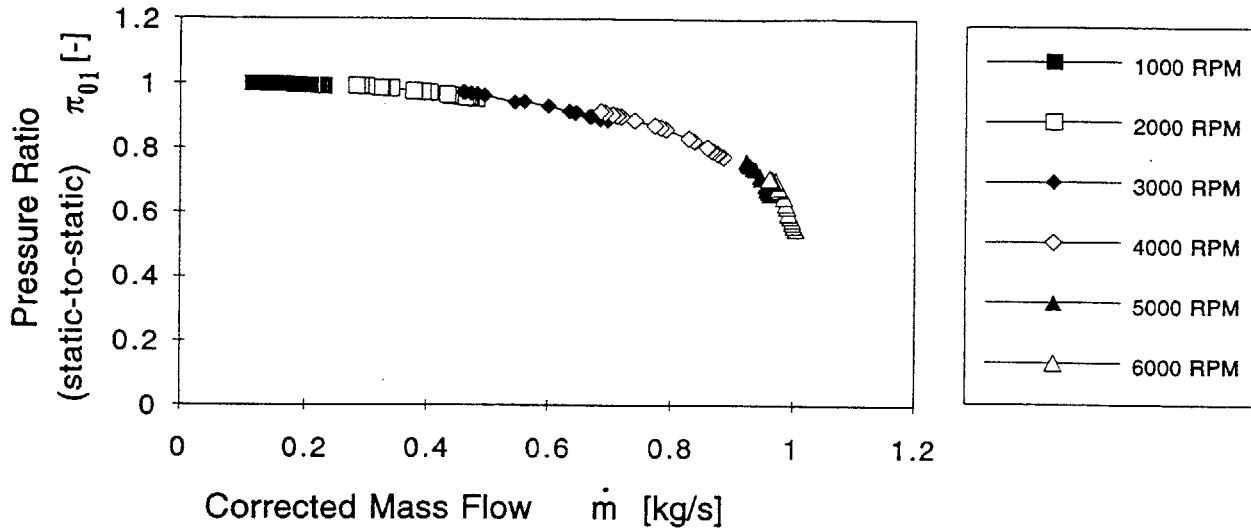
Krain [1984] measured straight channel diffuser overall pressure recovery as 0.80 - 0.87, which is significantly higher than the result of the present investigation (0.65 - 0.77) and also the other straight channel diffuser data in the open literature.

With regard to the influence of inlet conditions, the observed insensitivity of the diffuser pressure recovery to the diffuser inlet Mach number is in accordance with most of the other investigations, such as by Krain [1984] (straight channel diffuser) or Hunziker [1993] (cambered vane diffuser), except by Baghdadi [1973] and Baghdadi & Mc Donald [1975]. In Baghdadi's investigations, the pressure recovery as well as the operating range of the vaned diffusers were strongly Mach number dependent.

Figures 4.36a, and b taken from Hunziker [1993] show diffuser pressure recovery and pressure recovery from impeller exit to the plenum versus inlet flow angle for cambered vane diffusers investigated in a centrifugal compressor test rig. Figure 4.36a is for a cambered vane diffuser with a divergence angle of $2\theta = 15^\circ$ and Figure 4.36b is for a diffuser with $2\theta = 30^\circ$. Both diffusers have 24 vanes and tested with the same impeller. From these figures, it can be seen that diffuser pressure recovery coefficients correlates well with the diffuser inlet flow angle and there is no influence of diffuser inlet Mach number on pressure recovery coefficient. The cambered vane diffuser with a smaller divergence angle (Figure 4.36a) has a higher diffuser pressure recovery (peak value of $C_p = 0.75$ compared to 0.64) than the diffuser with higher divergence angle (Figure 4.36b), but the operating range is smaller. In addition the rotating stall onset for the first diffuser (Figure 4.36a) is at an inlet flow angle of $\alpha = 80^\circ$ and for the second diffuser (Figure 4.36b) at $\alpha = 73^\circ$.

a)

Atmosphere to Diffuser Inlet Pressure Ratio



b)

Atmosphere to Diffuser Exit Pressure Ratio

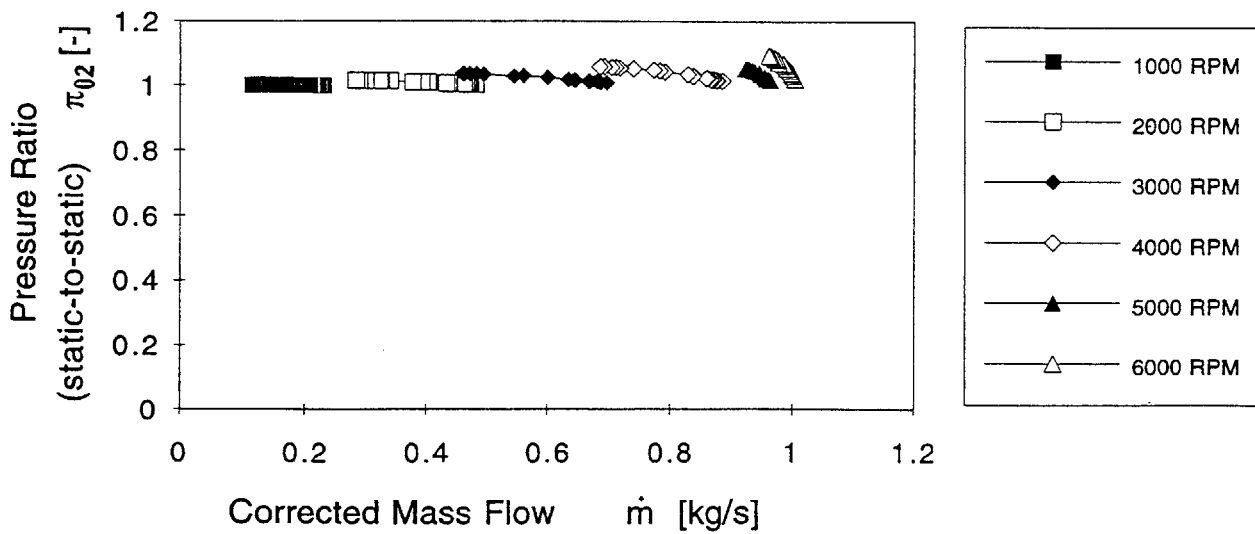


Figure 4.1 Constant speed characteristics, a) Atmosphere to diffuser inlet pressure ratio, π_{01} , versus corrected mass flow, \dot{m} , b) Atmosphere to diffuser exit pressure ratio, π_{02} , versus corrected mass flow, \dot{m}

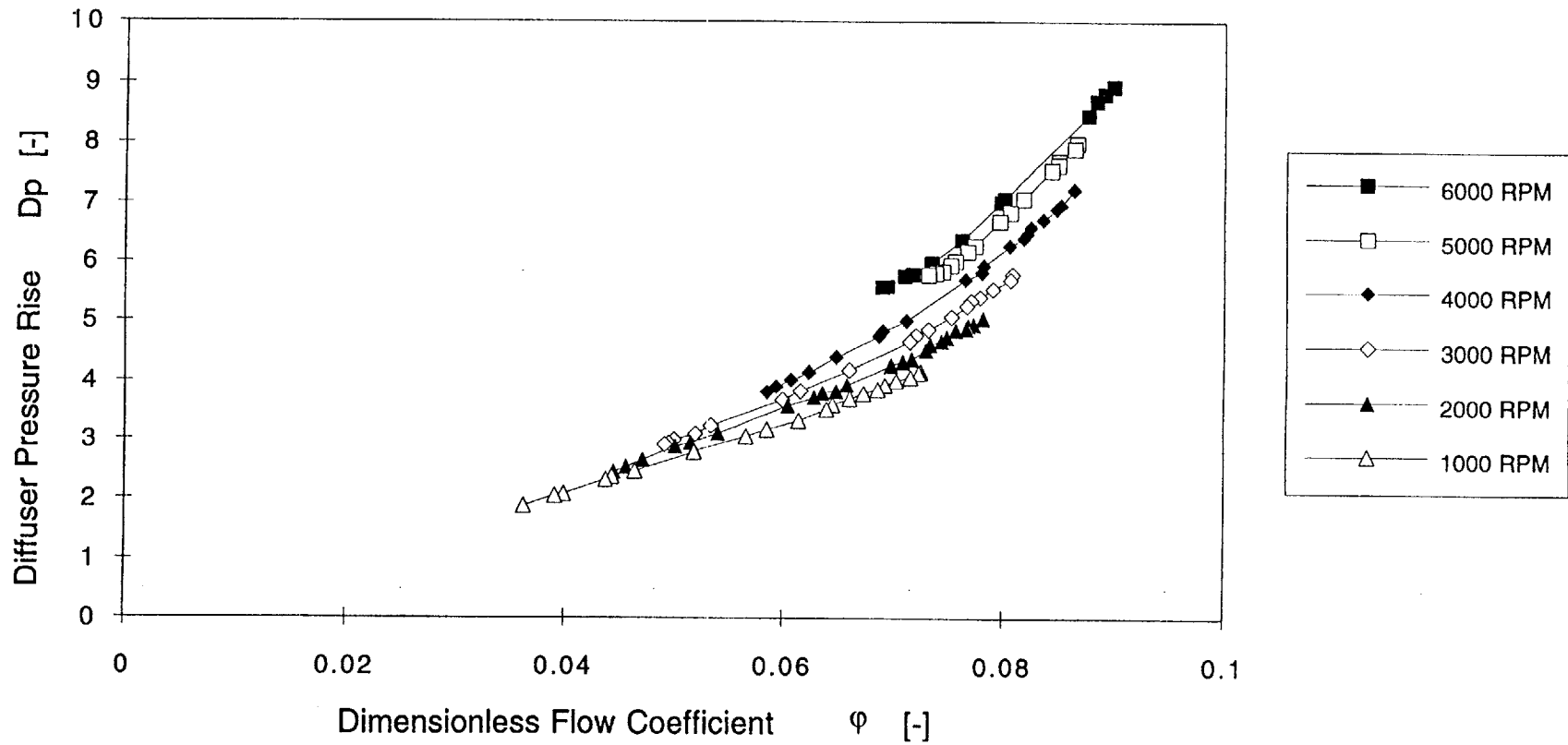
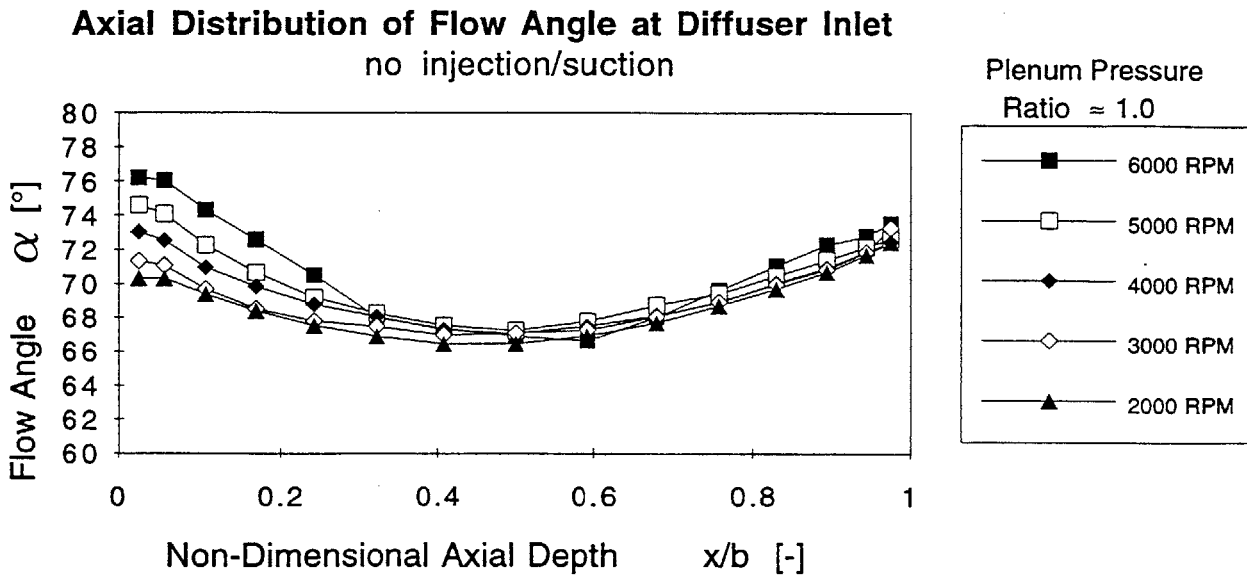


Figure 4.2 Performance map in terms of dimensionless flow coefficient, ϕ , versus diffuser pressure rise, D_p .

a)



b)

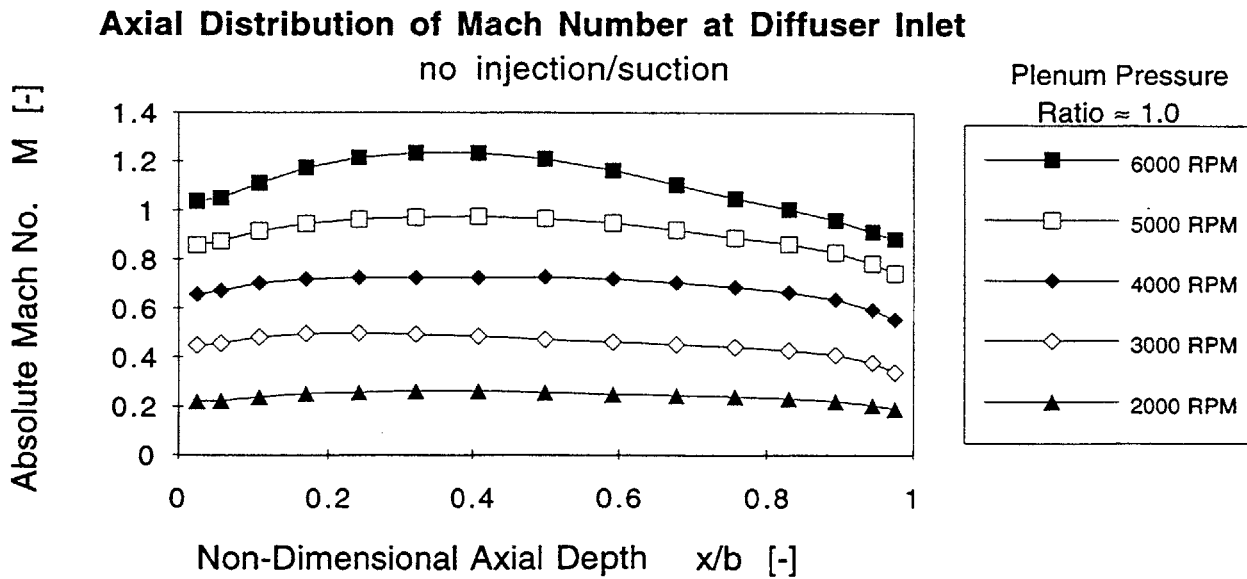


Figure 4.3 (a) Flow angle, α , and (b) absolute Mach number, M , axial distributions at the diffuser inlet achieved without profile control injection/suction for different corrected impeller speeds and for a plenum pressure ratio $\pi_{03} = 1.0$

Overall Straight-Channel Diffuser Pressure Recovery no injection/suction

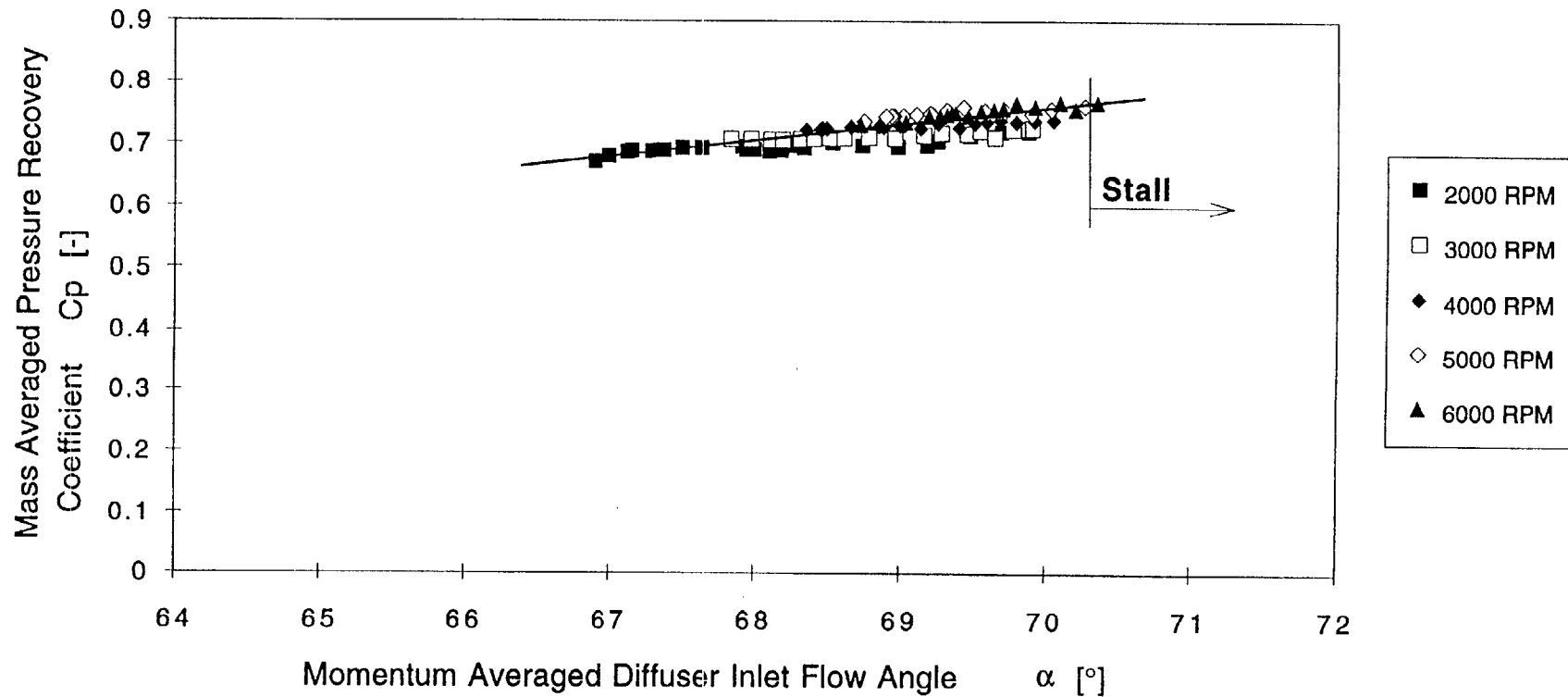


Figure 4.4 Mass averaged overall straight-channel diffuser pressure recovery, C_p , as a function of the diffuser inlet momentum averaged flow angle, α , no injection/suction, different corrected impeller speeds

Effect of Inlet Mach Number on Overall Diffuser Pressure Recovery

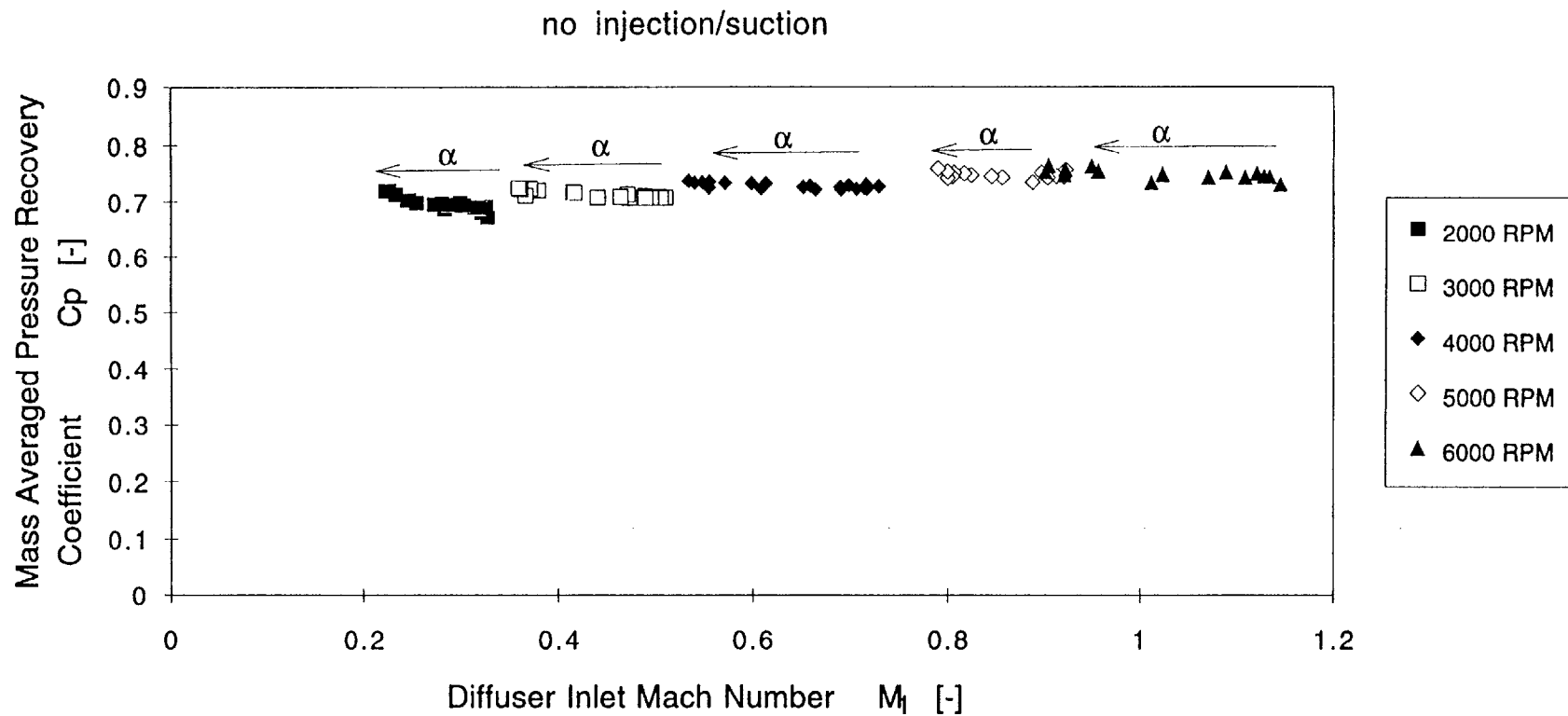


Figure 4.5 Mass averaged overall straight-channel diffuser pressure recovery, C_p , as a function of the diffuser inlet absolute Mach number, M_1 , no injection/suction, different corrected impeller speeds

Effect of Inlet Blockage on Overall Diffuser Pressure Recovery

no injection/suction

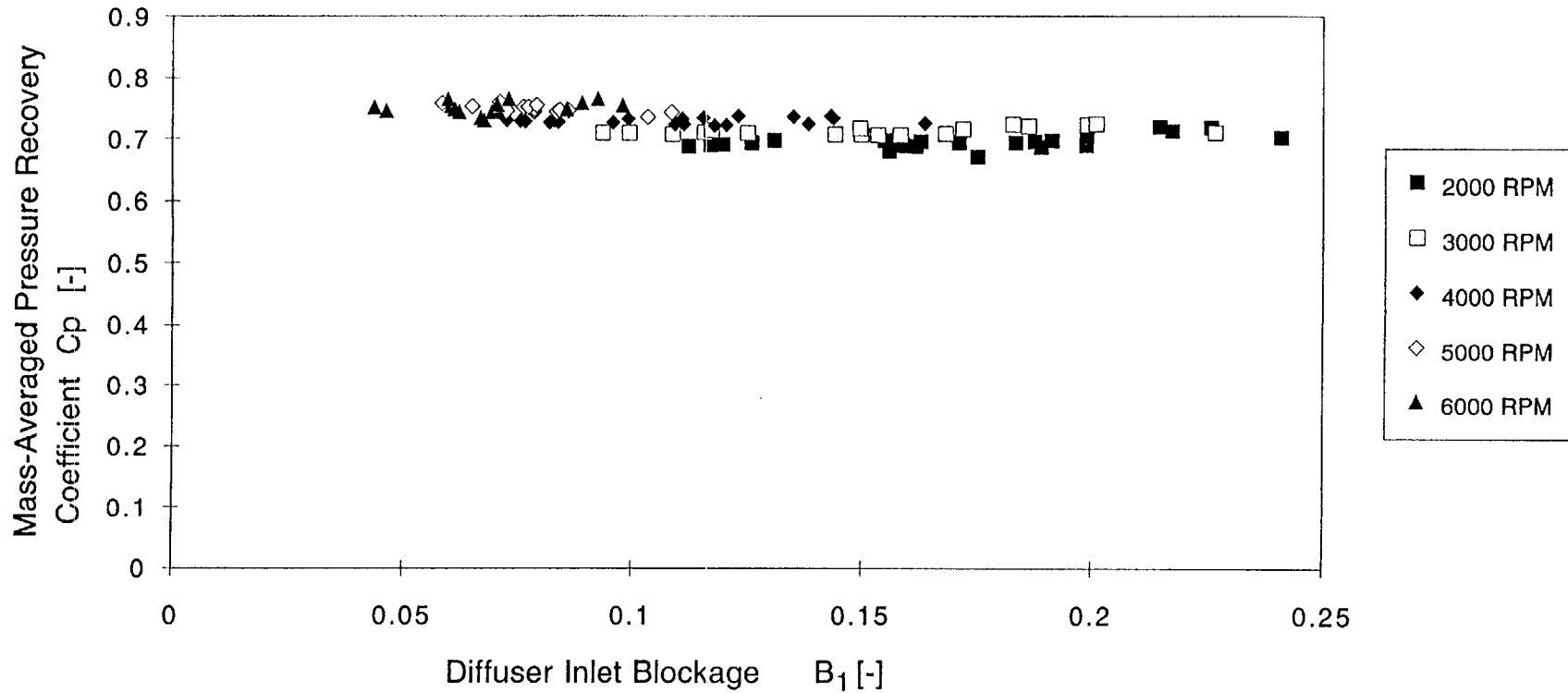


Figure 4.6 Mass averaged overall straight-channel diffuser pressure recovery, C_p , as a function of the diffuser inlet blockage, B_1 , no injection/suction, different corrected impeller speeds

Effect of Flow Angle Non-Uniformity on Overall Diffuser Pressure Recovery

no injection/suction

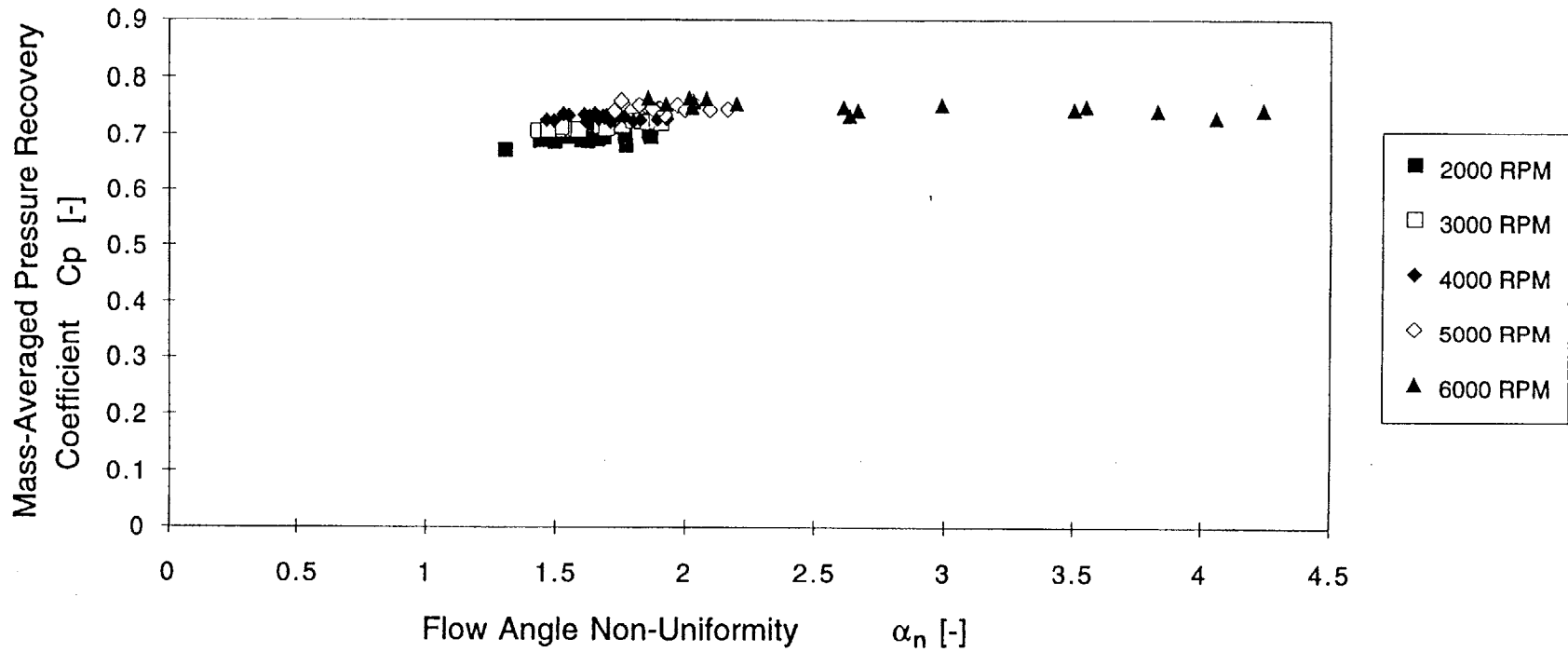


Figure 4.7 Mass averaged overall straight-channel diffuser pressure recovery, C_p , as a function of the diffuser inlet flow angle non-uniformity, α_n , no injection/suction, different corrected impeller speeds

Effect of Mass Flow Non-Uniformity on Overall Diffuser Pressure Recovery

no injection/suction

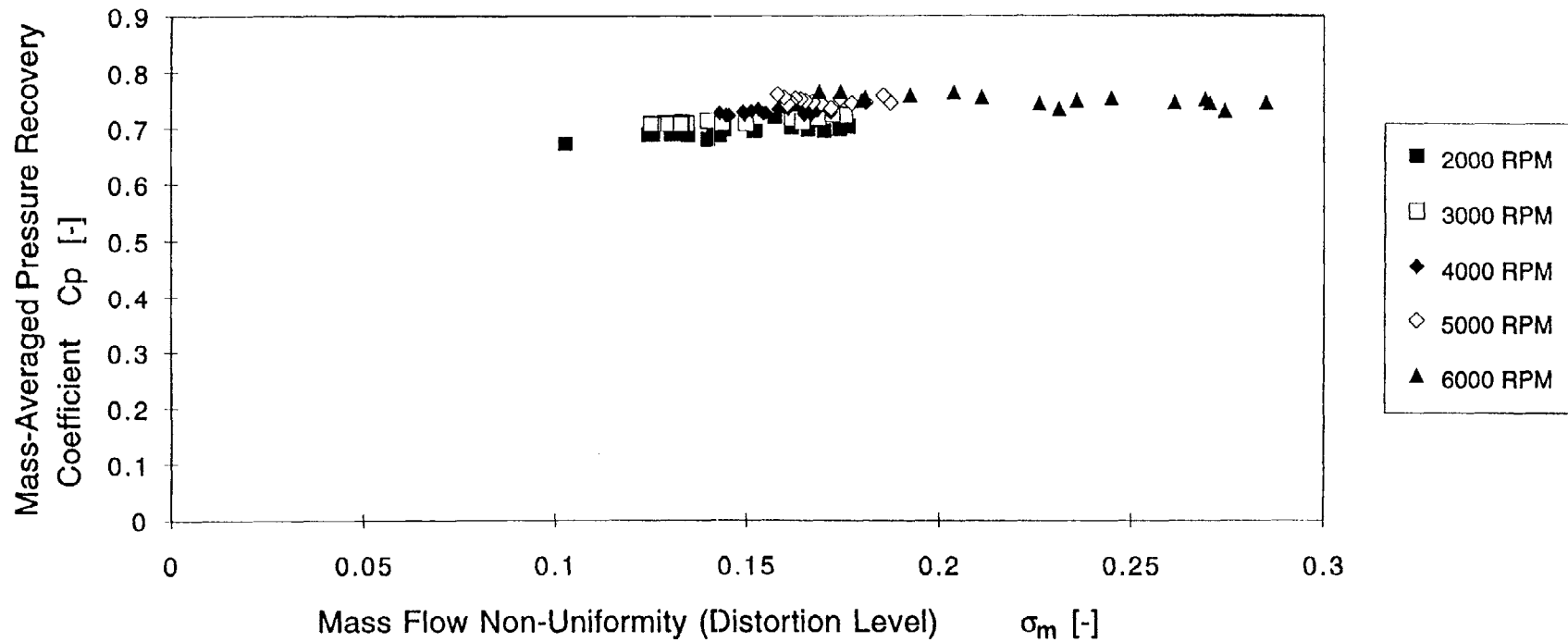
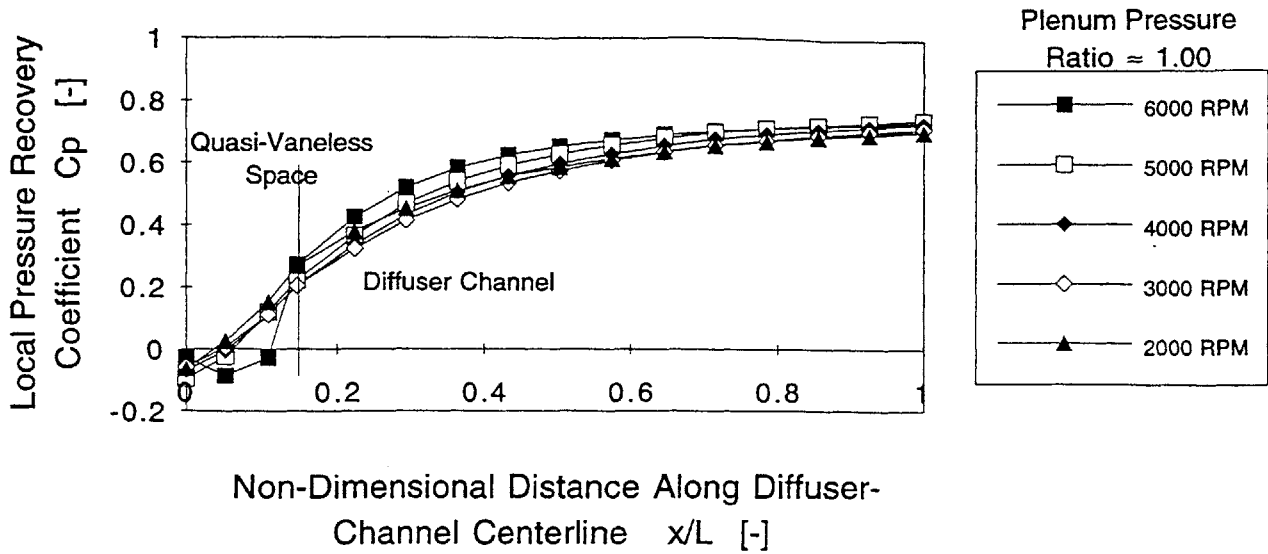


Figure 4.8 Mass averaged overall straight-channel diffuser pressure recovery, C_p , as a function of the diffuser mass flow non-uniformity, σ_m , no injection/suction, different corrected impeller speeds

a) **Static Pressure Distribution within Diffuser Channel**



b) **Static Pressure Distribution within Diffuser Channel**

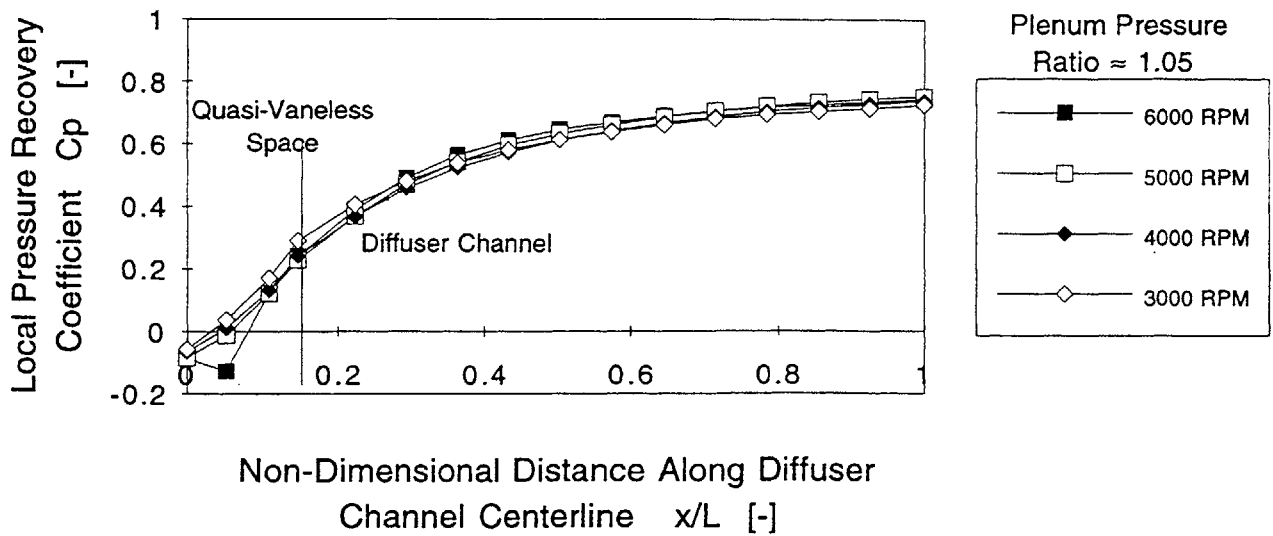


Figure 4.9 Static pressure distribution along the centerline of a diffuser channel for different corrected impeller speeds and a) for the plenum pressure ratio $\pi_{03} = 1.00$ and b) for the plenum pressure ratio $\pi_{03} = 1.05$

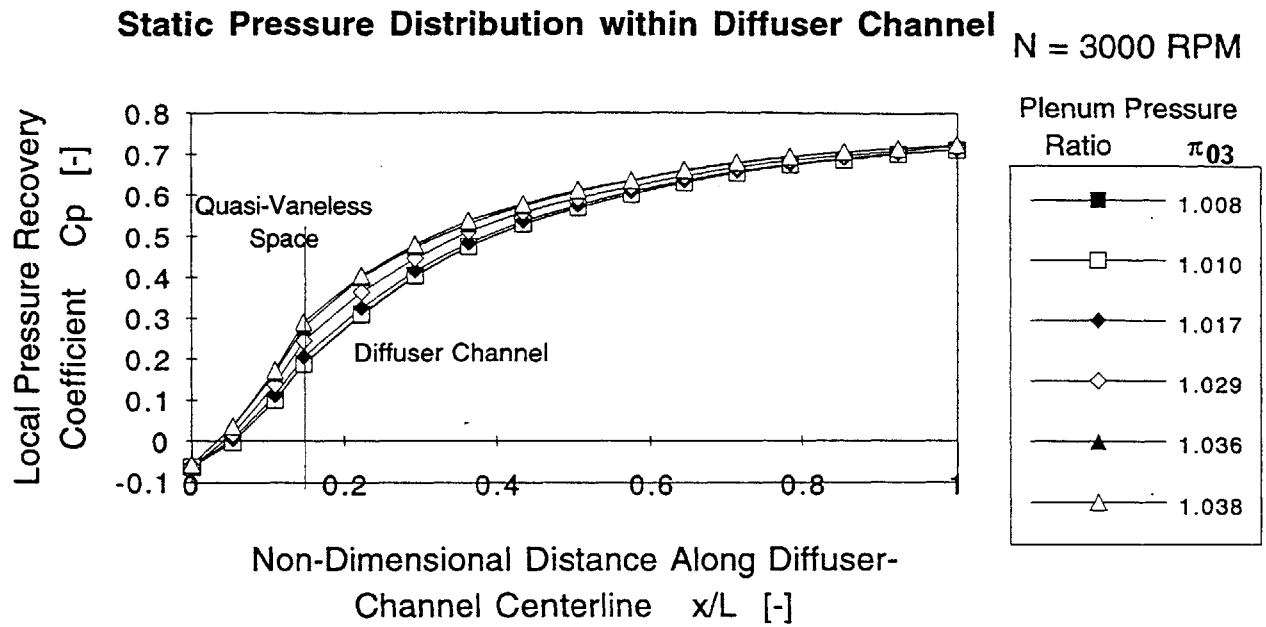
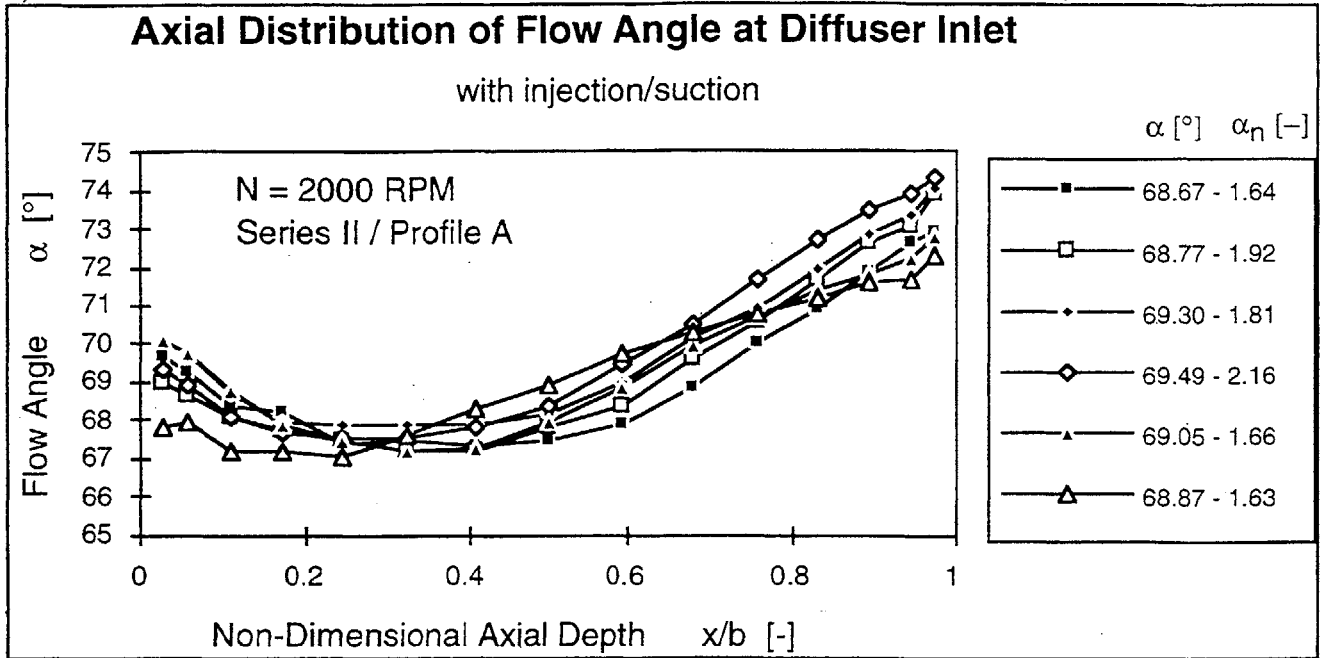


Figure 4.10 Static pressure distribution along the centerline of a diffuser channel for different plenum pressure ratios, π_{03} and for a corrected impeller speed $N = 3000$ RPM

a)



b)

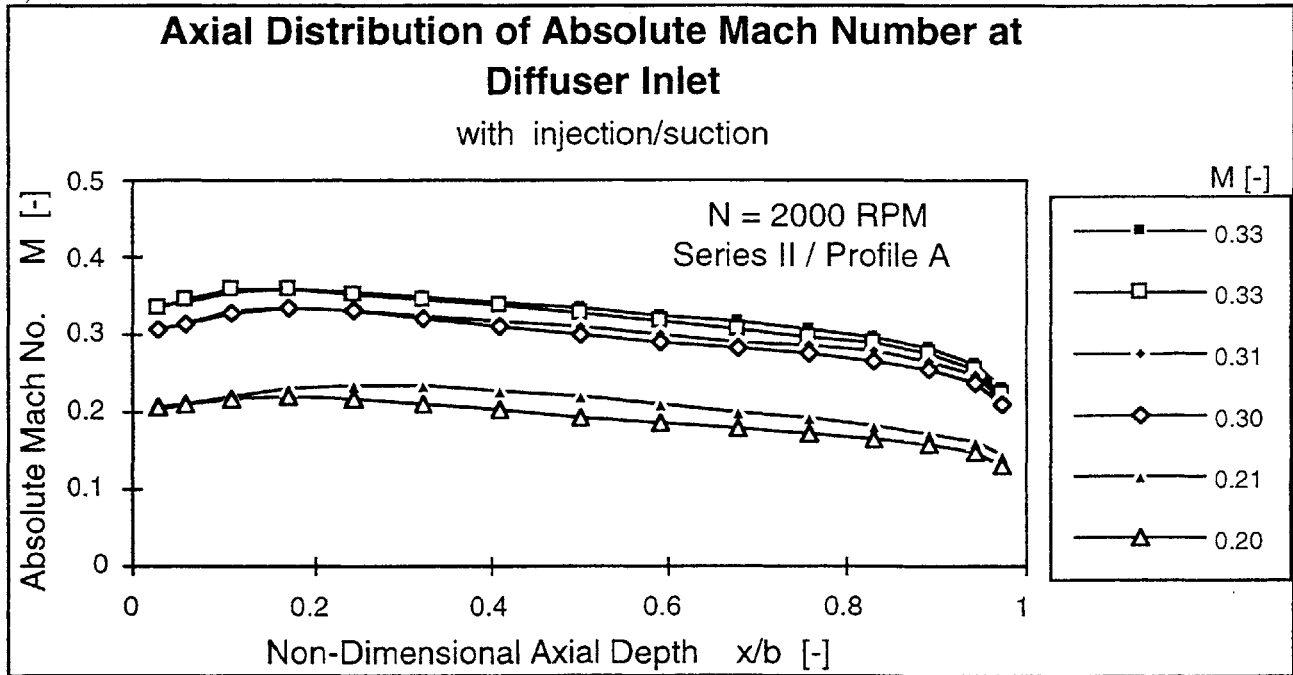
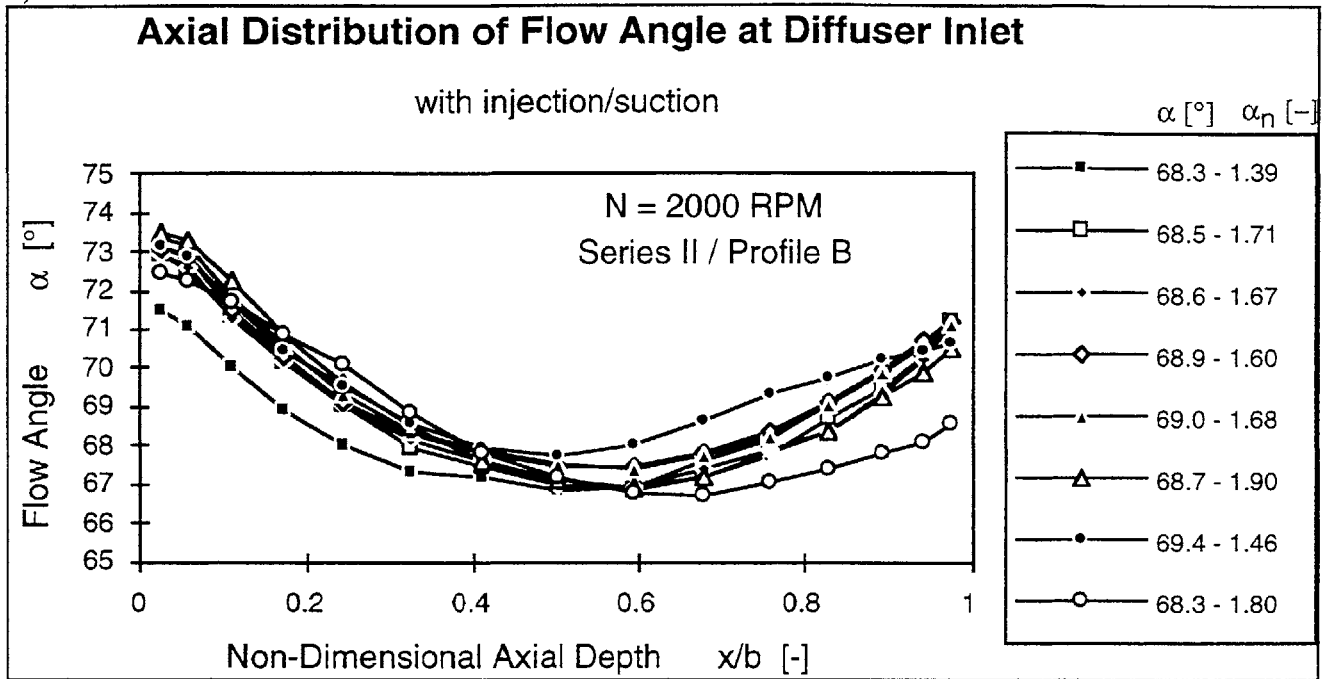


Figure 4.11 (a) Flow angle, α , and (b) absolute Mach number, M , axial distributions at the diffuser inlet achieved with profile control injection/suction (Series II/Profile A/ $N = 2000$ RPM)

a)



b)

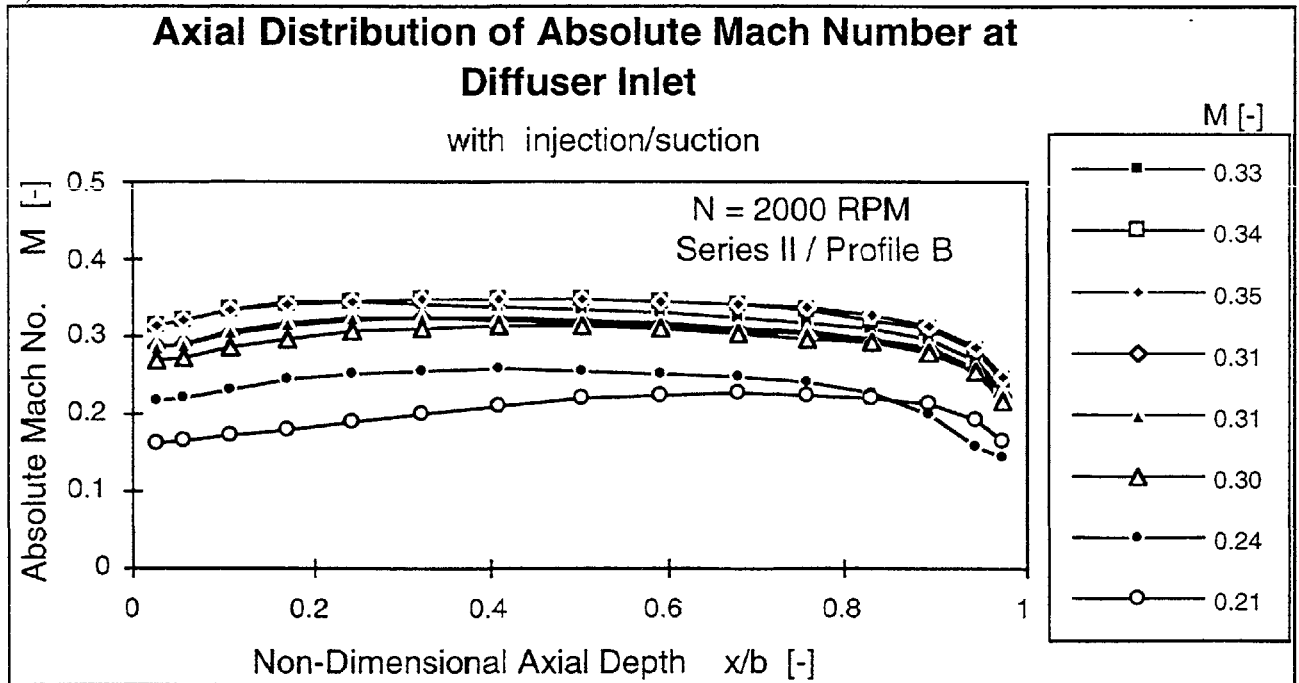
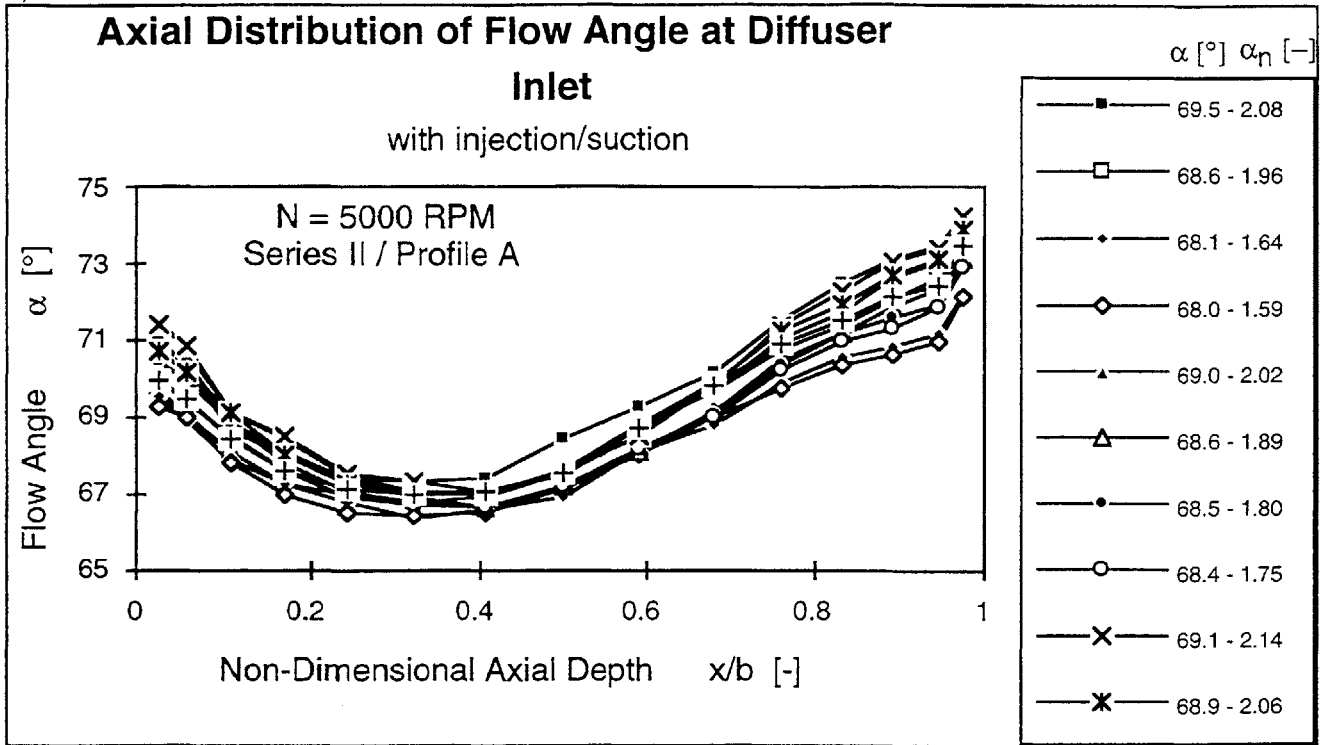


Figure 4.12 (a) Flow angle, α , and (b) absolute Mach number, M , axial distributions at the diffuser inlet achieved with profile control injection/suction (Series II/Profile B/N = 2000 RPM)

a)



b)

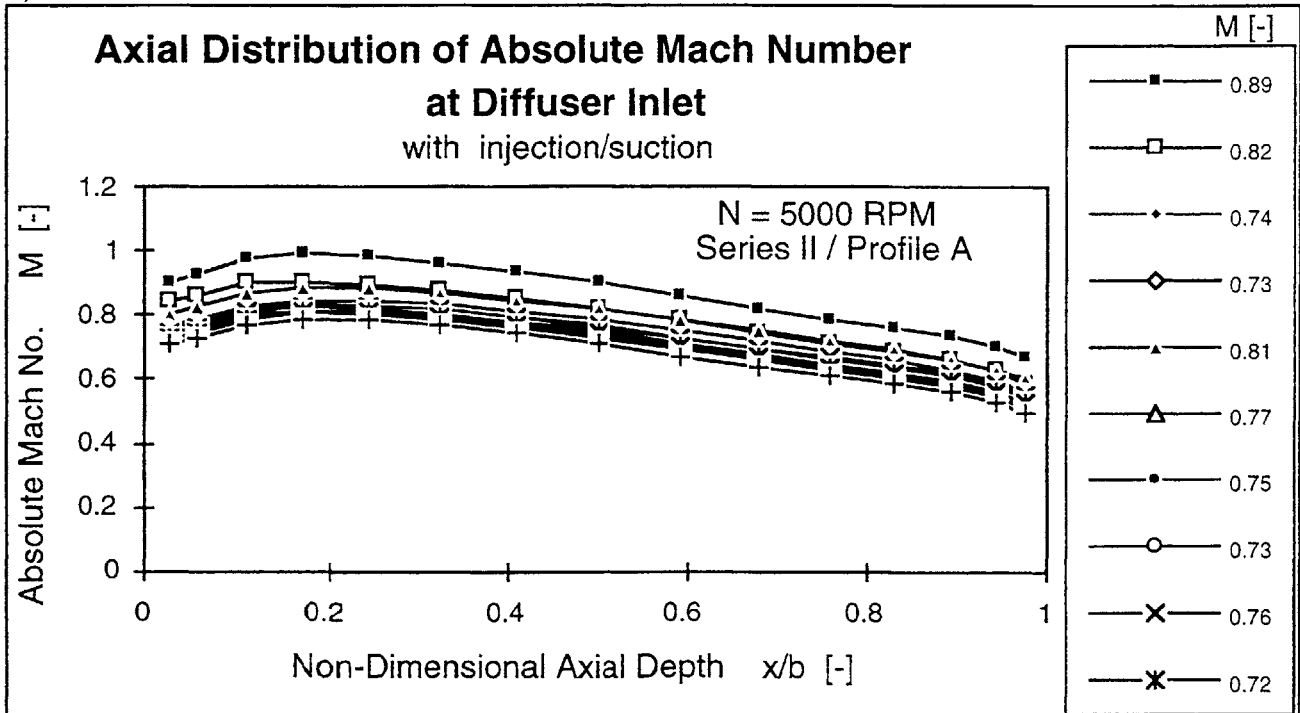


Figure 4.13 (a) Flow angle, α , and (b) absolute Mach number, M , axial distributions at the diffuser inlet achieved with profile control injection/suction (Series II/Profile A/ $N = 5000$ RPM)

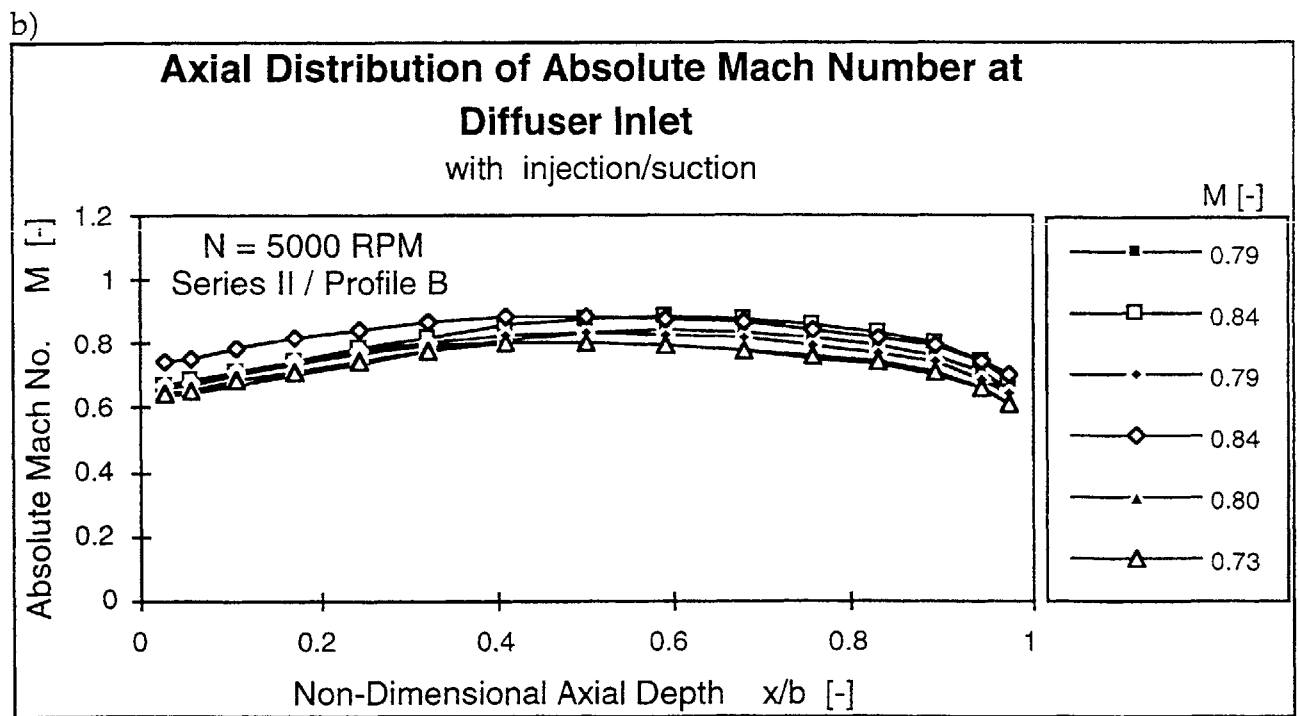
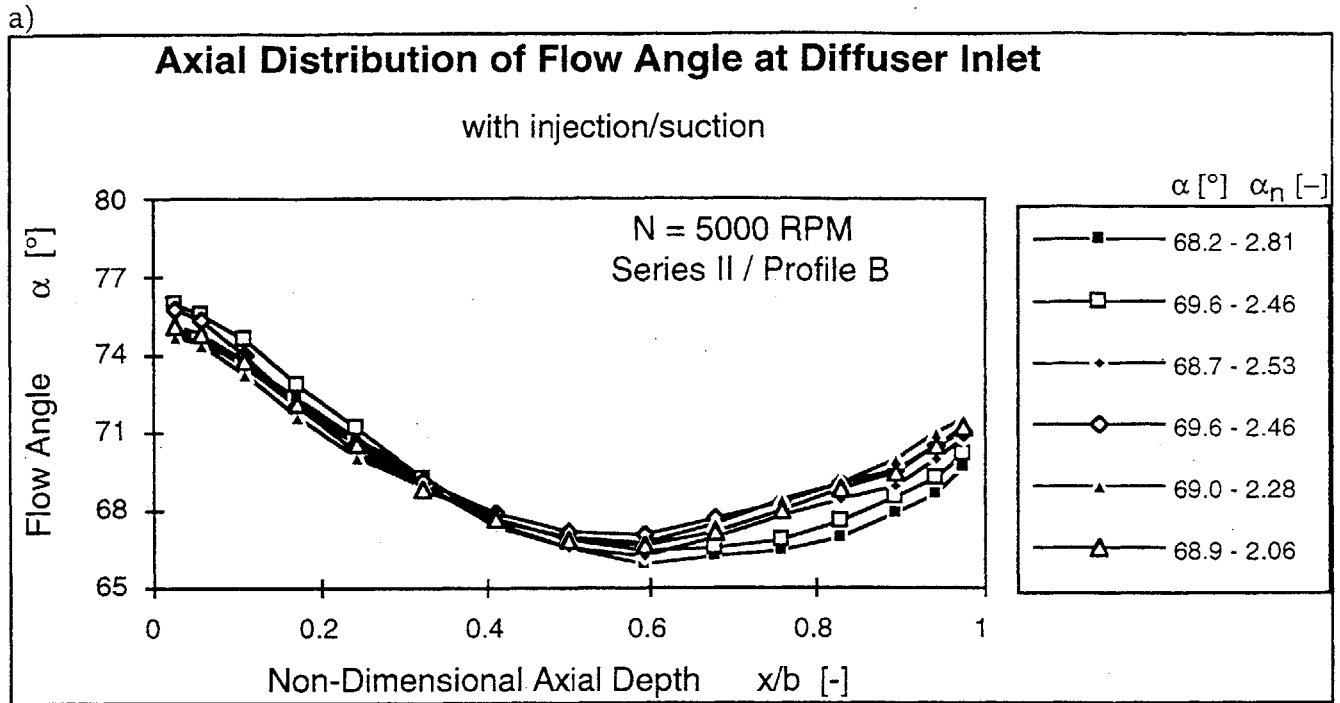
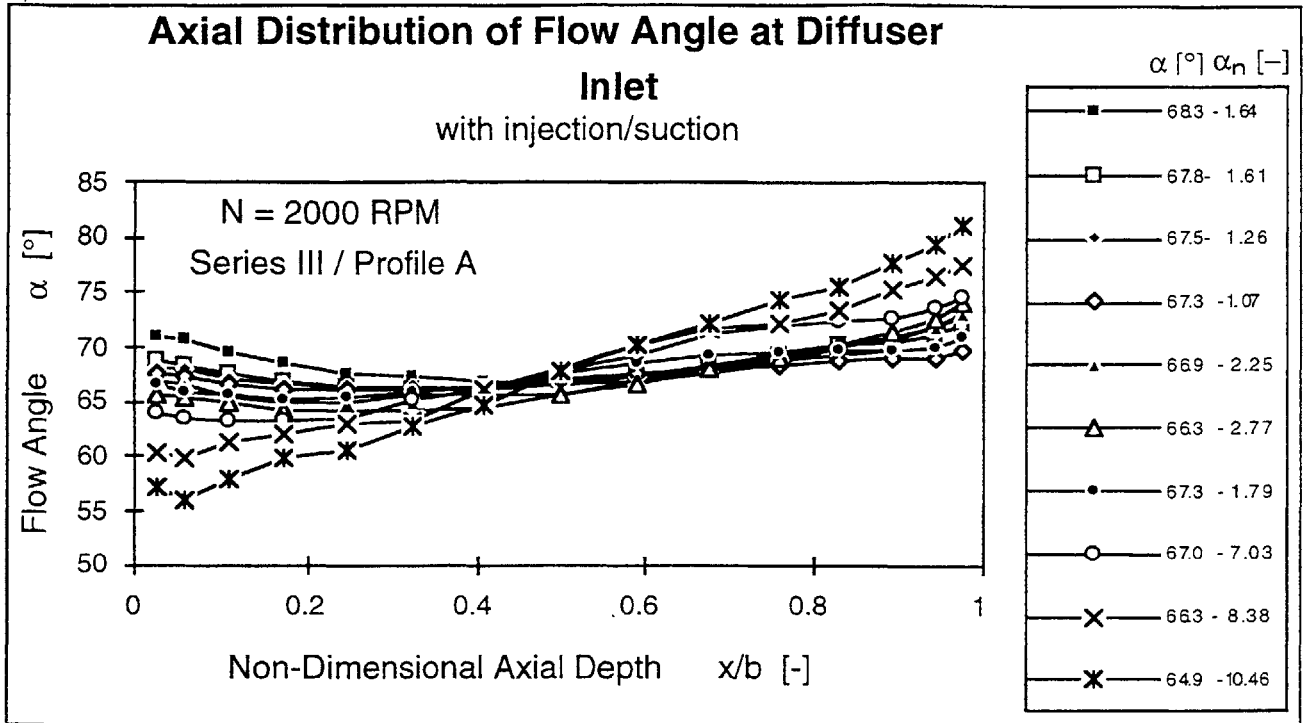


Figure 4.14 (a) Flow angle, α , and (b) absolute Mach number, M , axial distributions at the diffuser inlet achieved with profile control injection/suction (Series II/Profile B/ $N = 5000$ RPM)

a)



b)

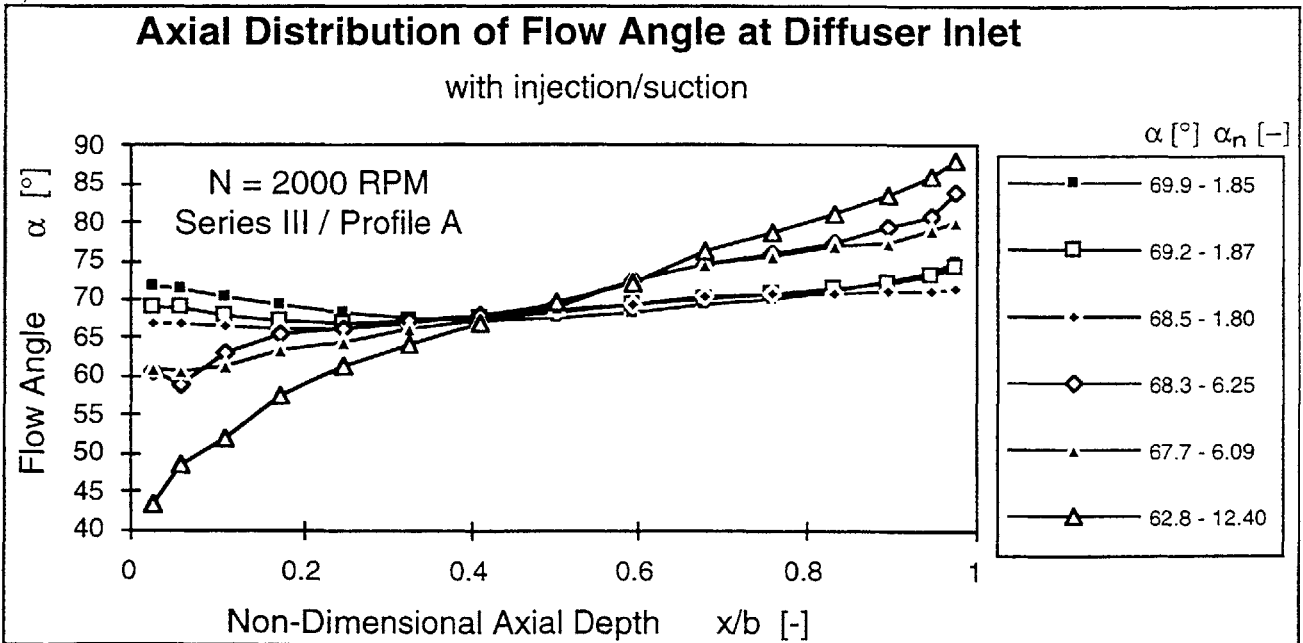
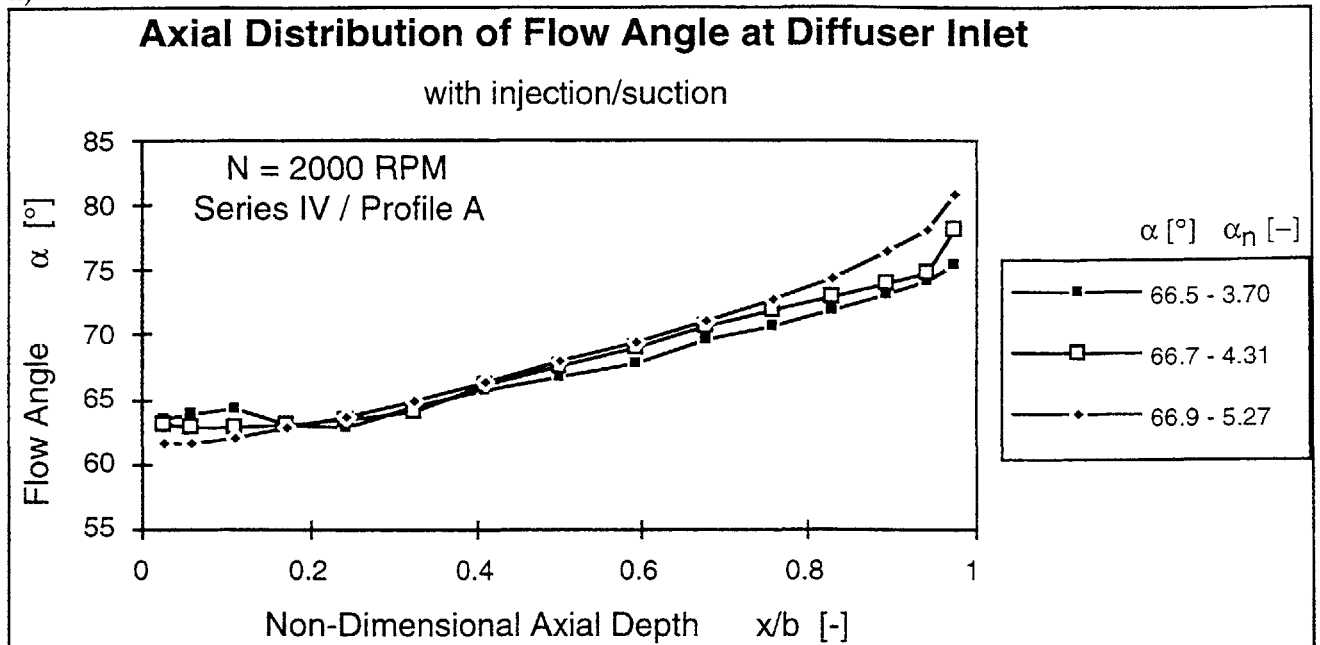


Figure 4.15 Flow angle, α , axial distributions at the diffuser inlet achieved with profile control injection/suction (Series III/Profile A/N = 2000 RPM)

a)



b)

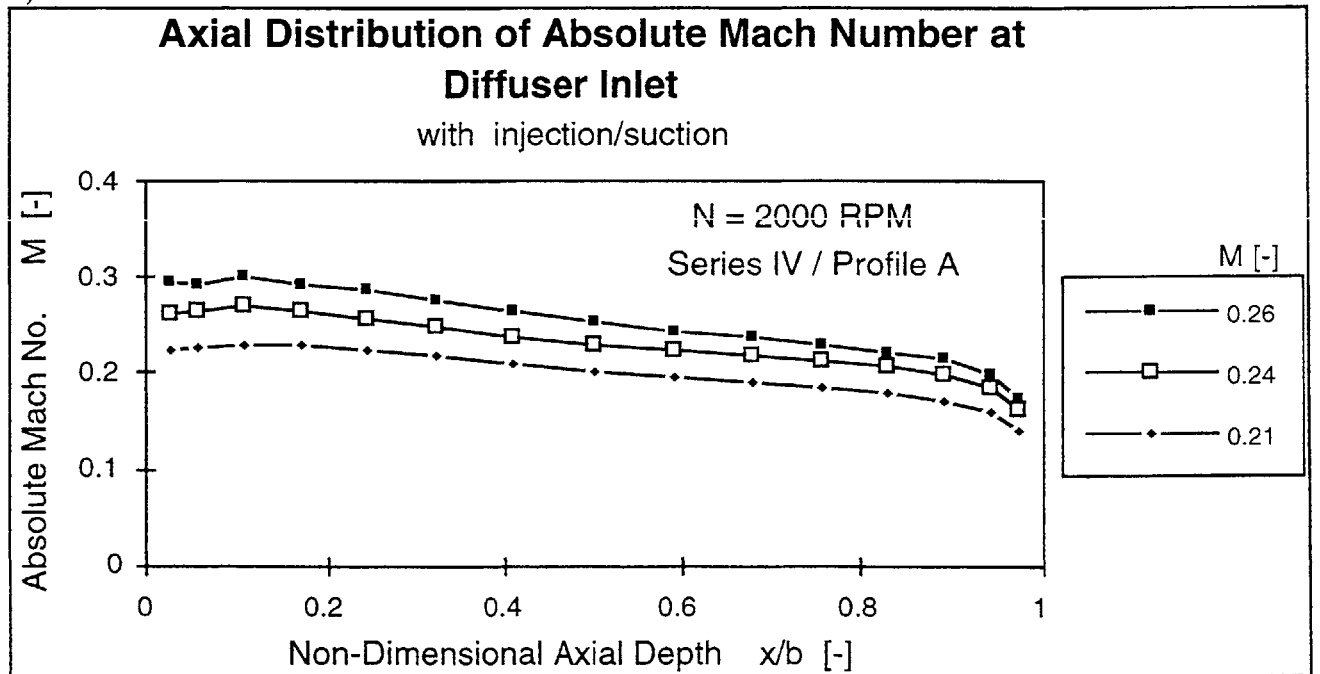
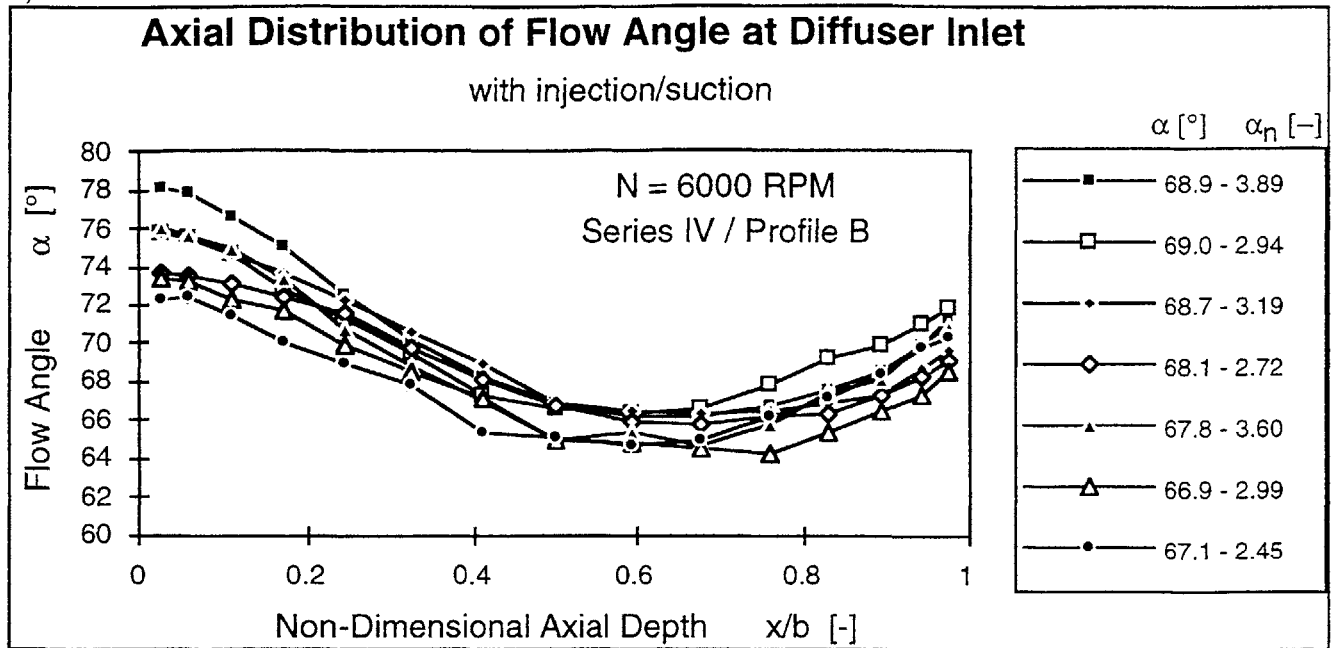


Figure 4.16 (a) Flow angle, α , and (b) absolute Mach number, M , axial distributions at the diffuser inlet achieved with profile control injection/suction (Series IV/Profile A/N = 2000 RPM)

a)



b)

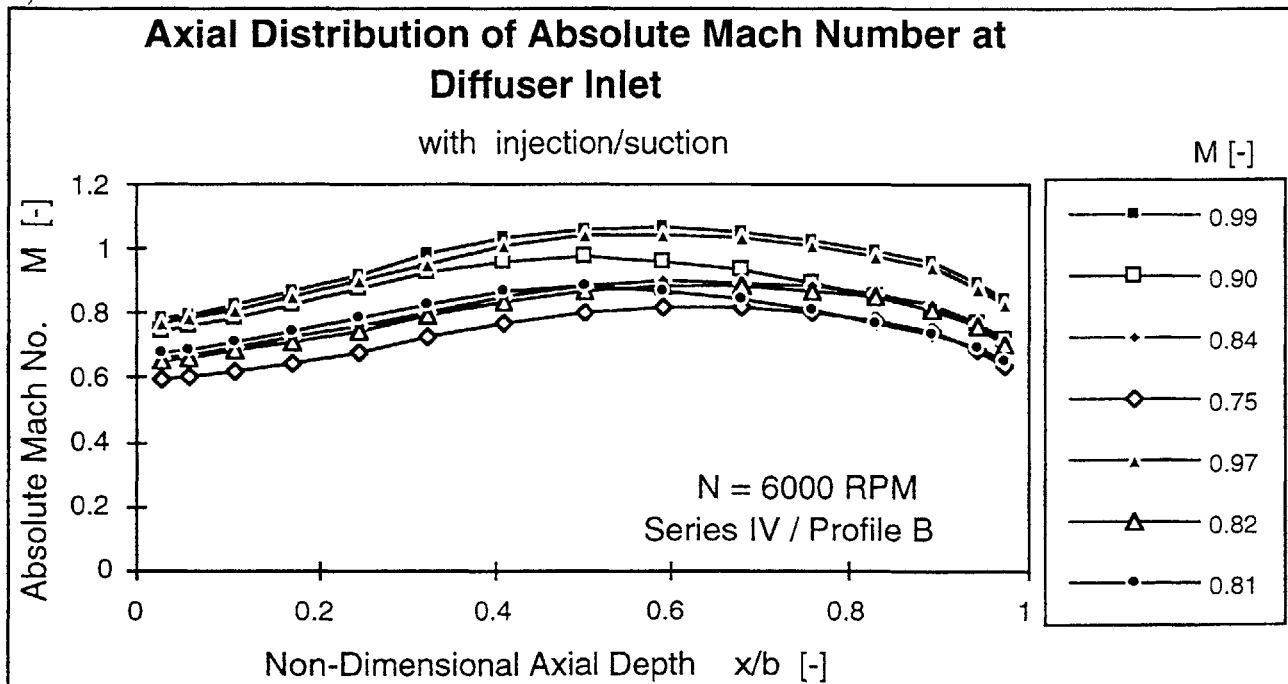


Figure 4.17 (a) Flow angle, α , and (b) absolute Mach number, M , axial distributions at the diffuser inlet achieved with profile control injection/suction (Series IV/Profile B/ $N = 6000$ RPM)

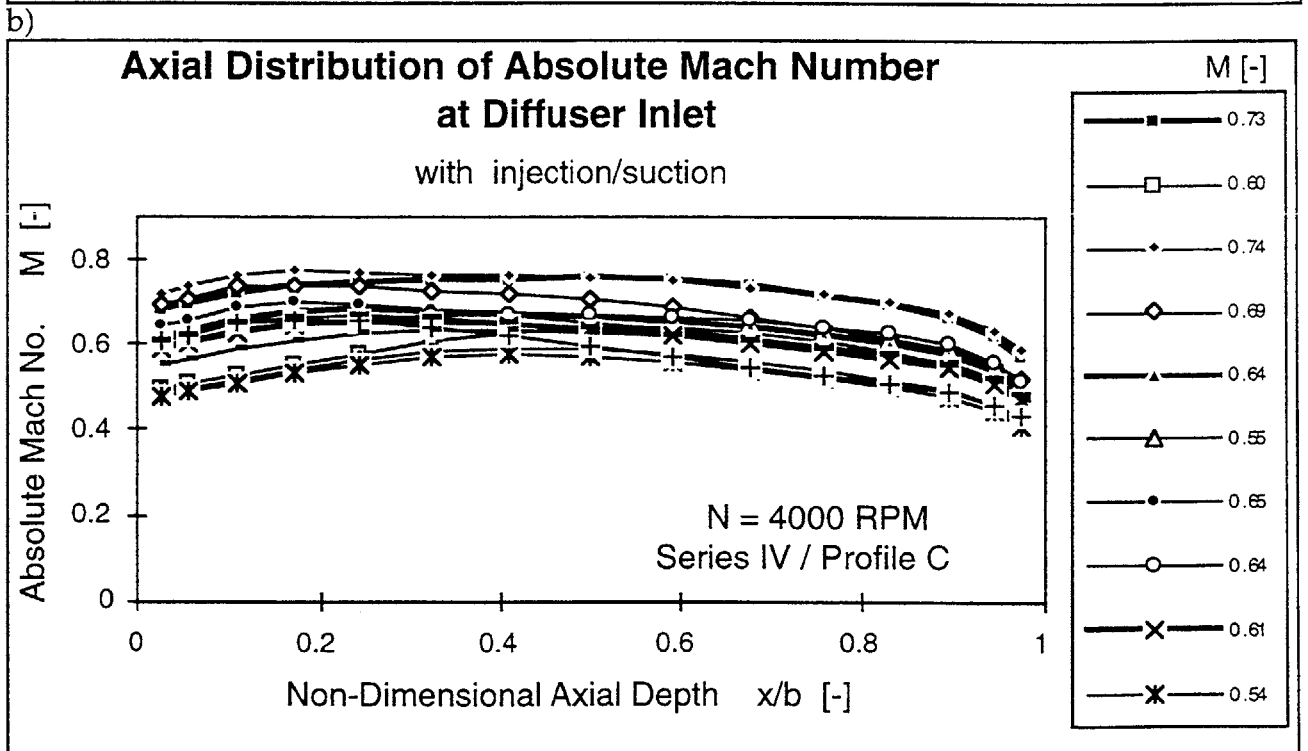
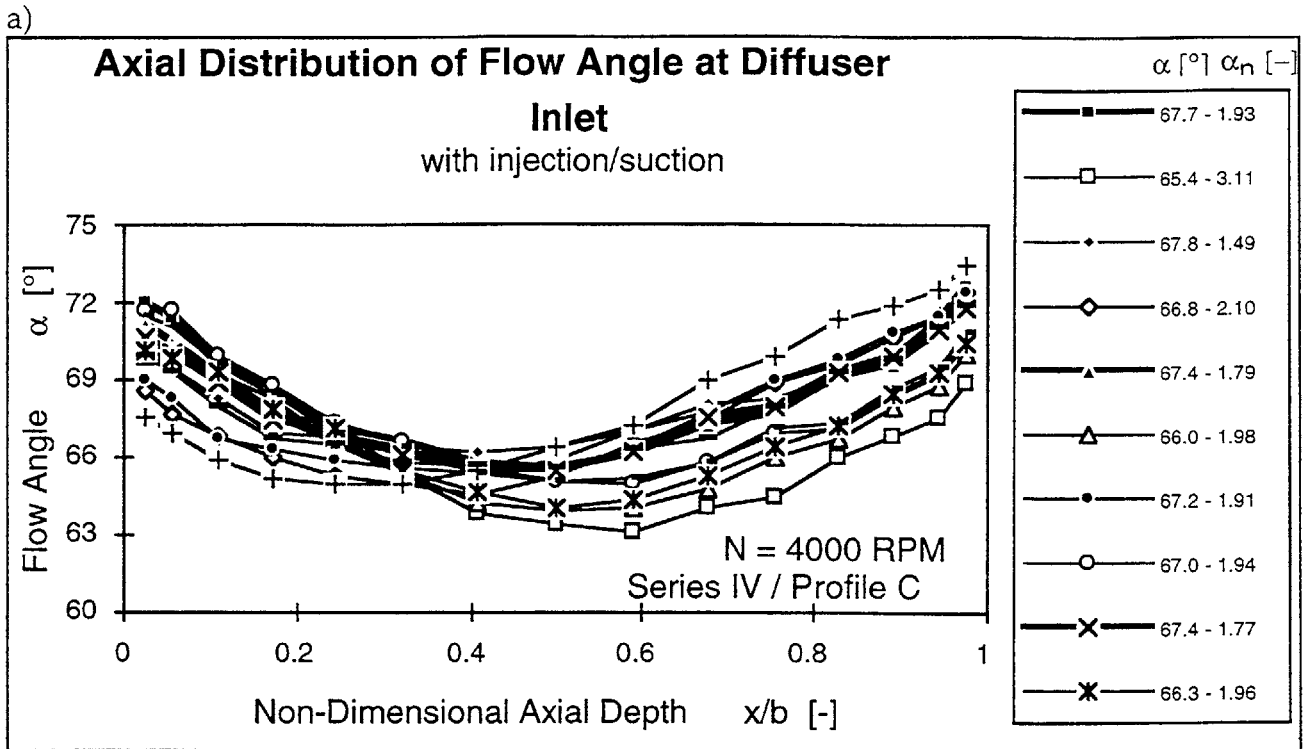


Figure 4.18 (a) Flow angle, α , and (b) absolute Mach number, M , axial distributions at the diffuser inlet achieved with profile control injection/suction (Series IV/Profile C/ $N = 4000$ RPM)

Overall Straight-Channel Diffuser Pressure Recovery

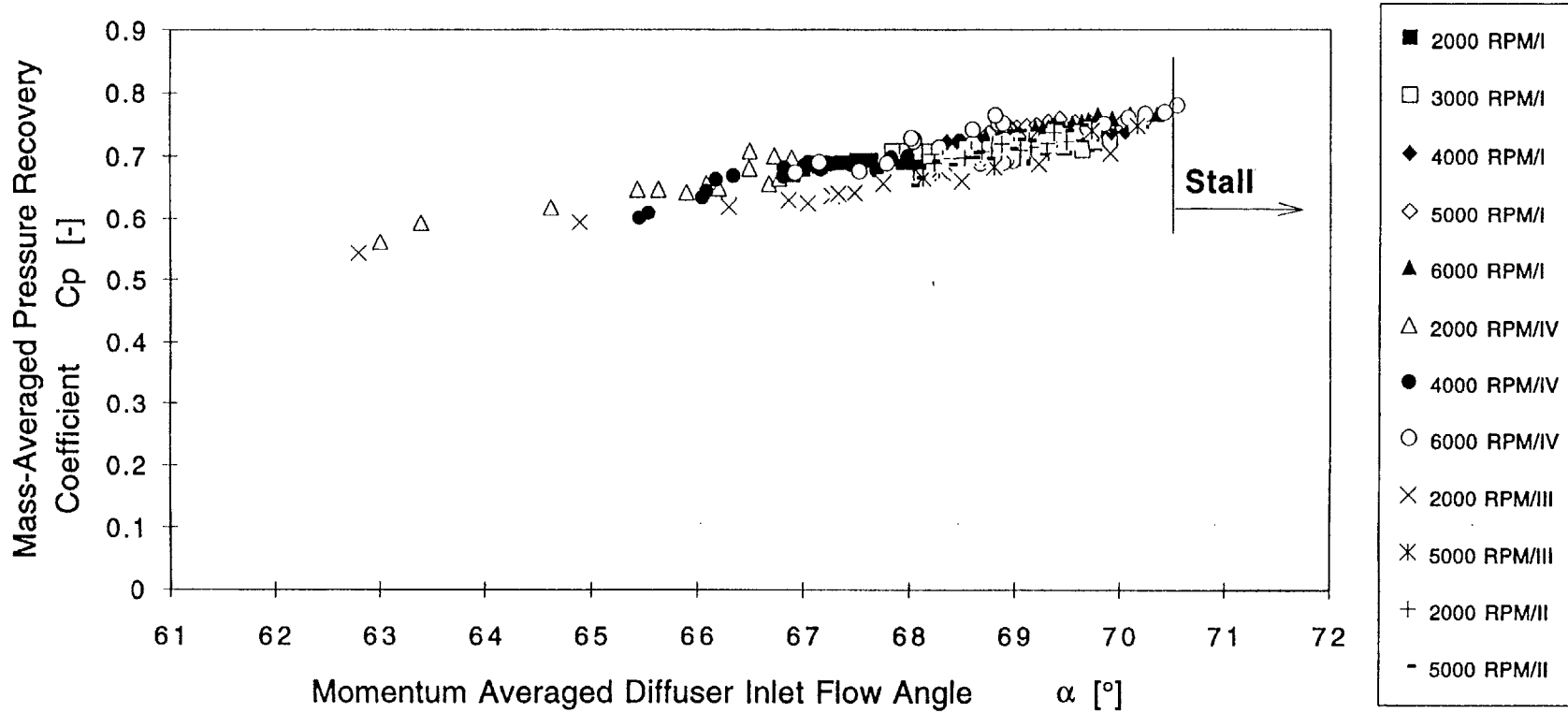


Figure 4.19 Mass averaged overall straight-channel diffuser pressure recovery, C_p , as a function of the diffuser inlet momentum averaged flow angle, α , with (II, III, and IV) and without (I) injection/suction, different corrected impeller speeds

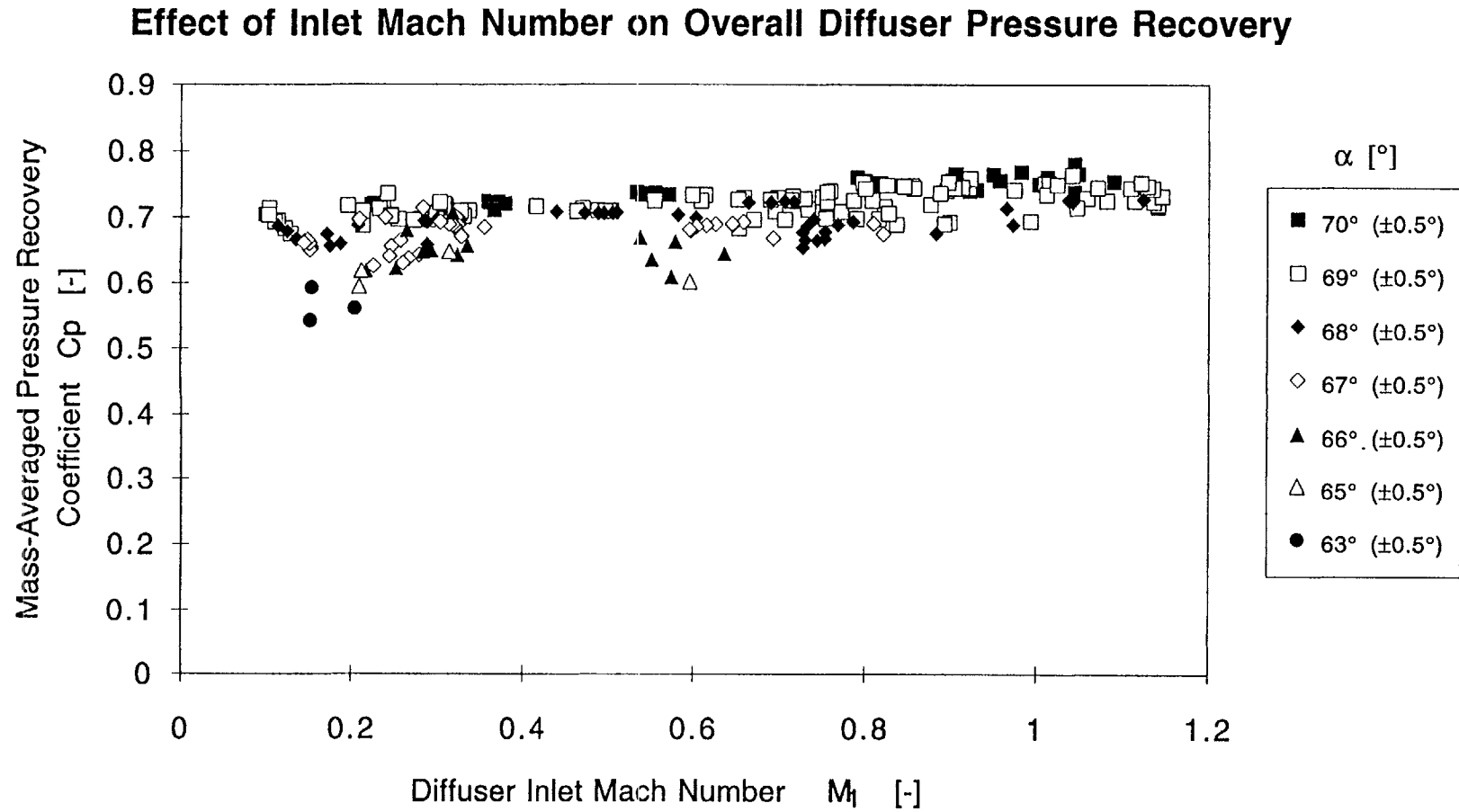


Figure 4.20 Mass averaged overall straight-channel diffuser pressure recovery, C_p , as a function of the diffuser inlet absolute Mach number, M_1 , with and without injection/suction

Effect of Reynolds Number on Overall Diffuser Pressure Recovery

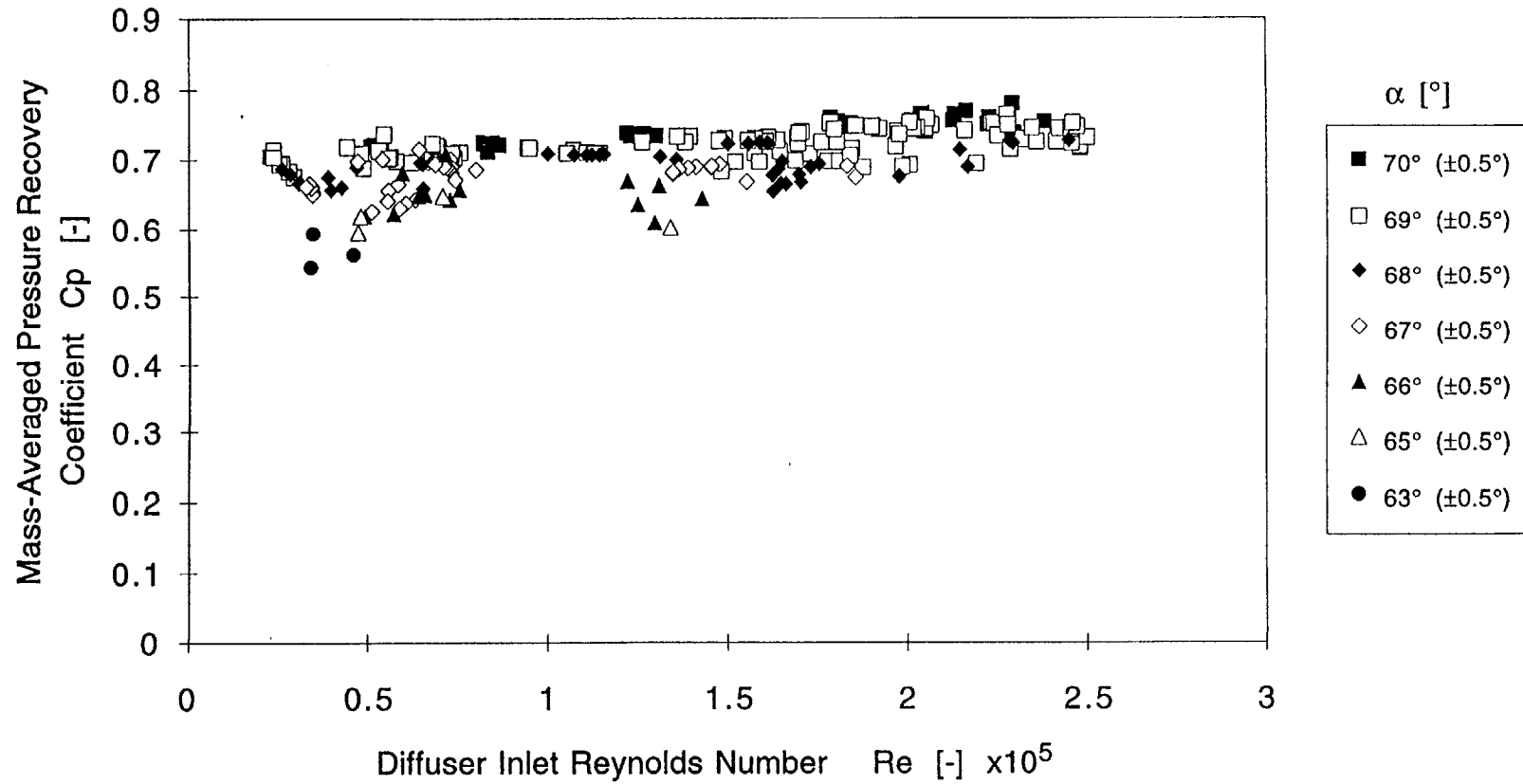


Figure 4.21 Mass averaged overall straight-channel diffuser pressure recovery, C_p , as a function of the diffuser inlet Reynolds number, Re , with and without injection/suction

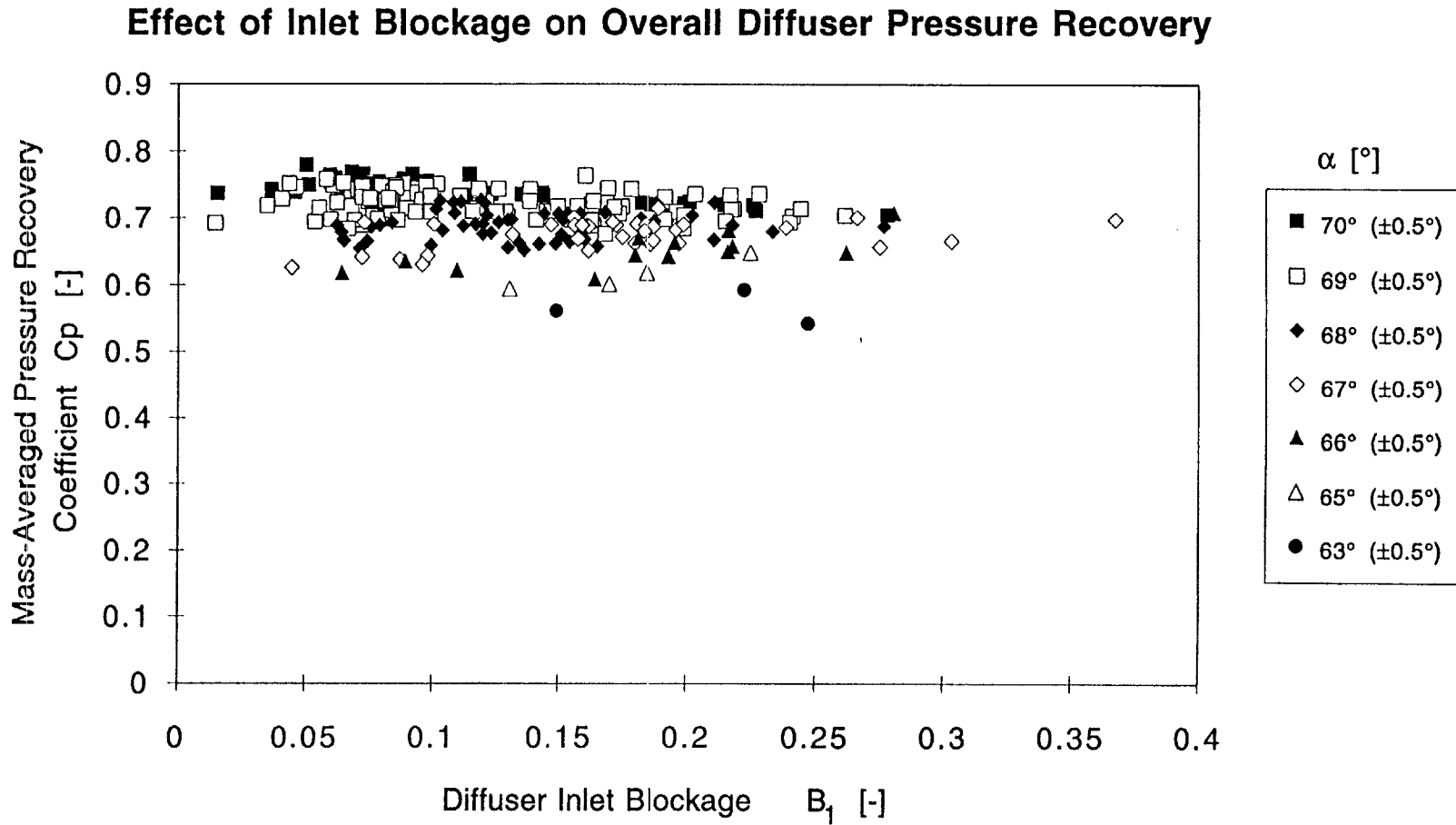


Figure 4.22 Mass averaged overall straight-channel diffuser pressure recovery, C_p , as a function of the diffuser inlet blockage, B_1 , with and without injection/suction

Effect of Flow Angle Non-Uniformity on Overall Diffuser Pressure Recovery

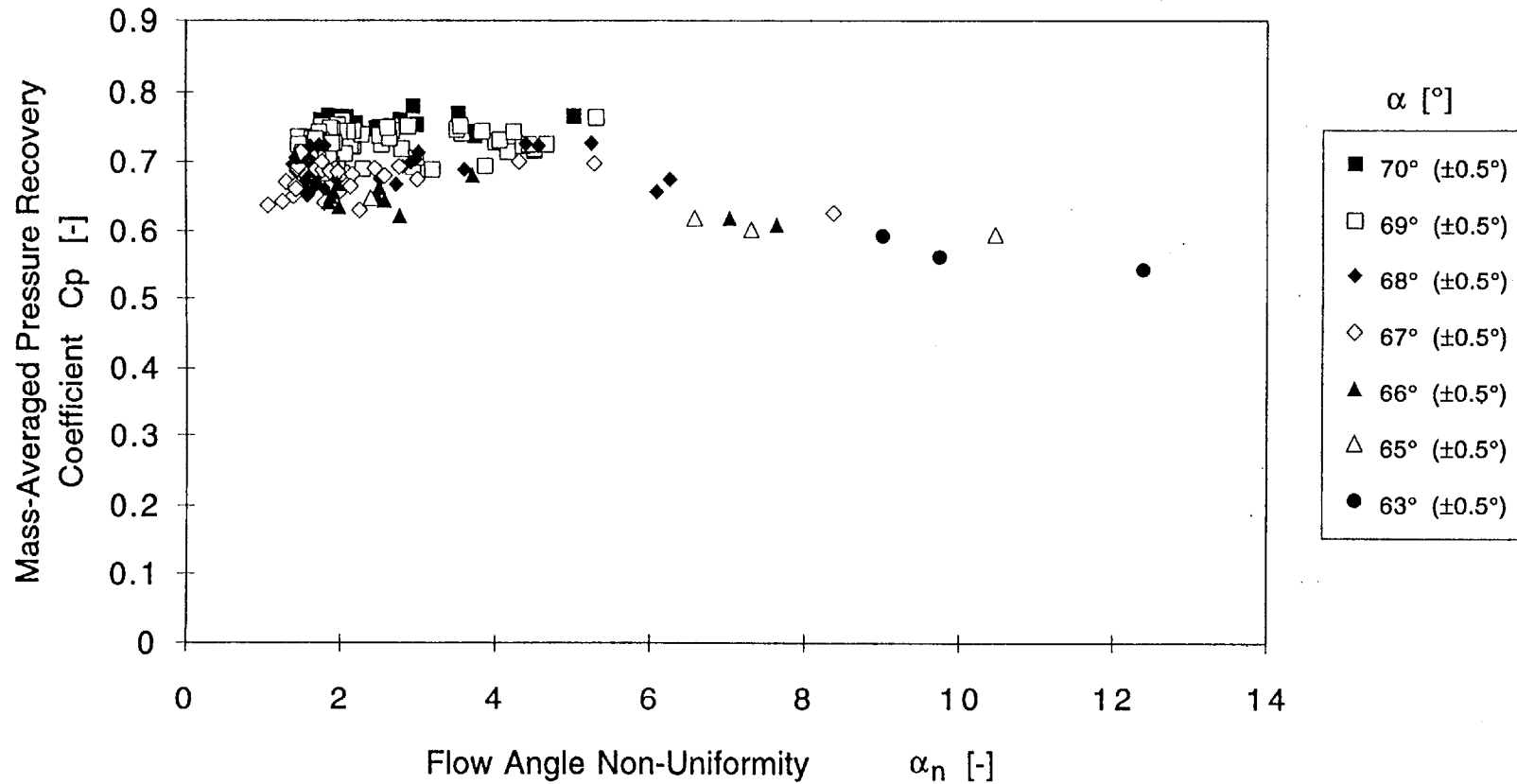


Figure 4.23 Mass averaged overall straight-channel diffuser pressure recovery, C_p , as a function of the diffuser inlet flow angle non-uniformity, α_n , with and without injection/suction

Effect of Mass Flow Non-Uniformity on Overall Diffuser Pressure Recovery

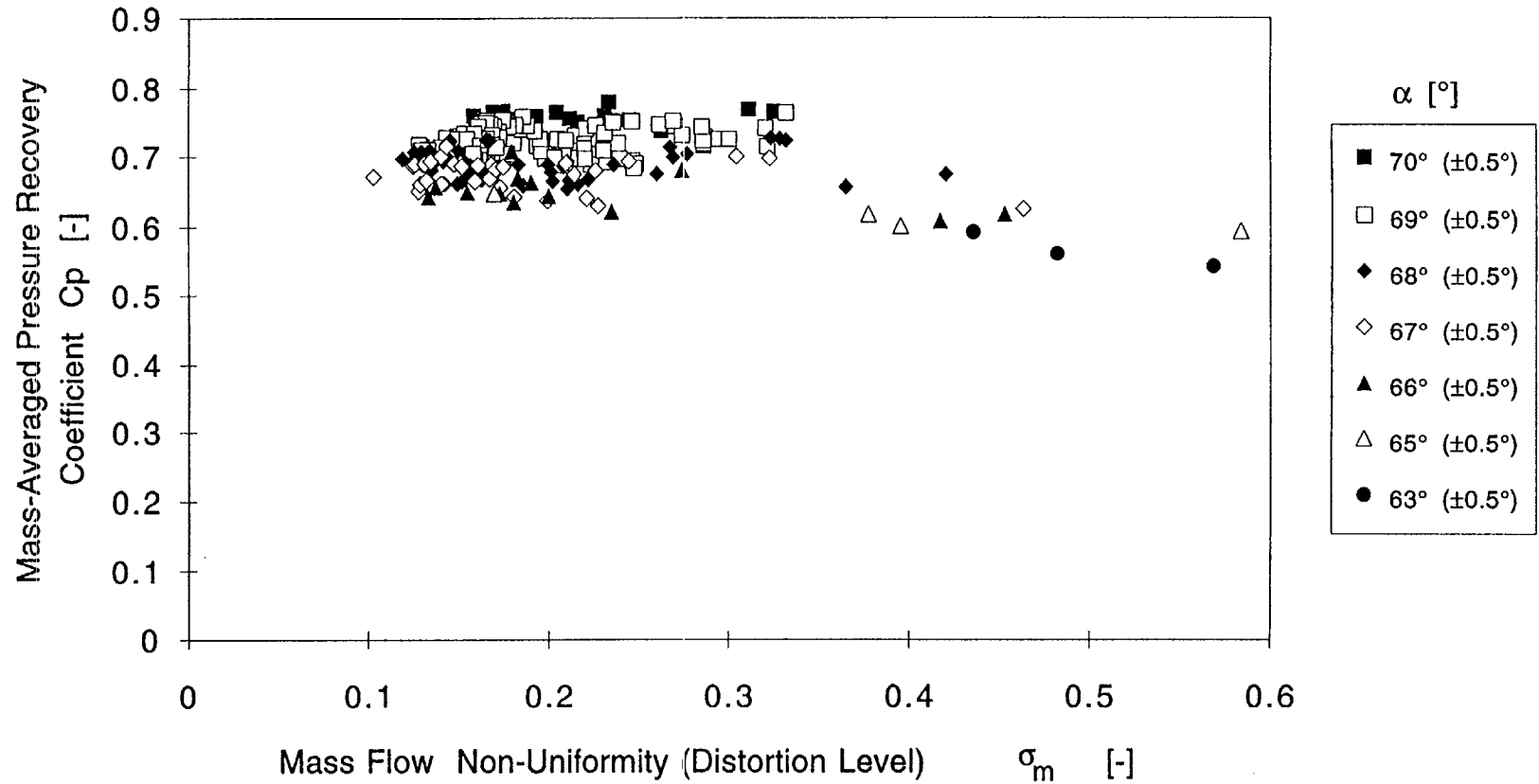


Figure 4.24 Mass averaged overall straight-channel diffuser pressure recovery, C_p , as a function of the diffuser mass flow non-uniformity, σ_m , with and without injection/suction

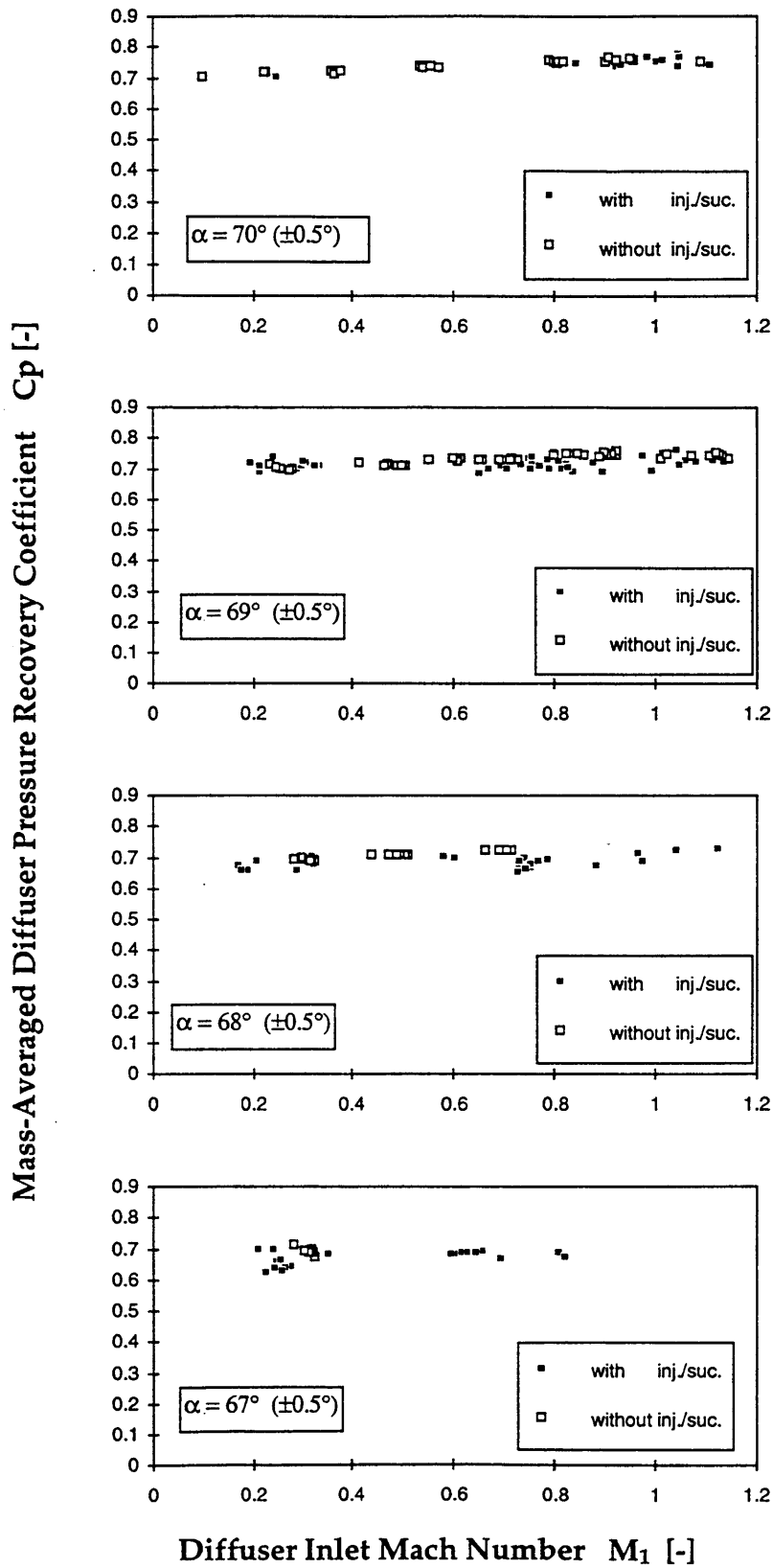


Fig. 4.25 Mass averaged overall diffuser pressure recovery, C_p , as a function of the diffuser inlet absolute Mach number, M_1 , represented for constant inlet flow angles.

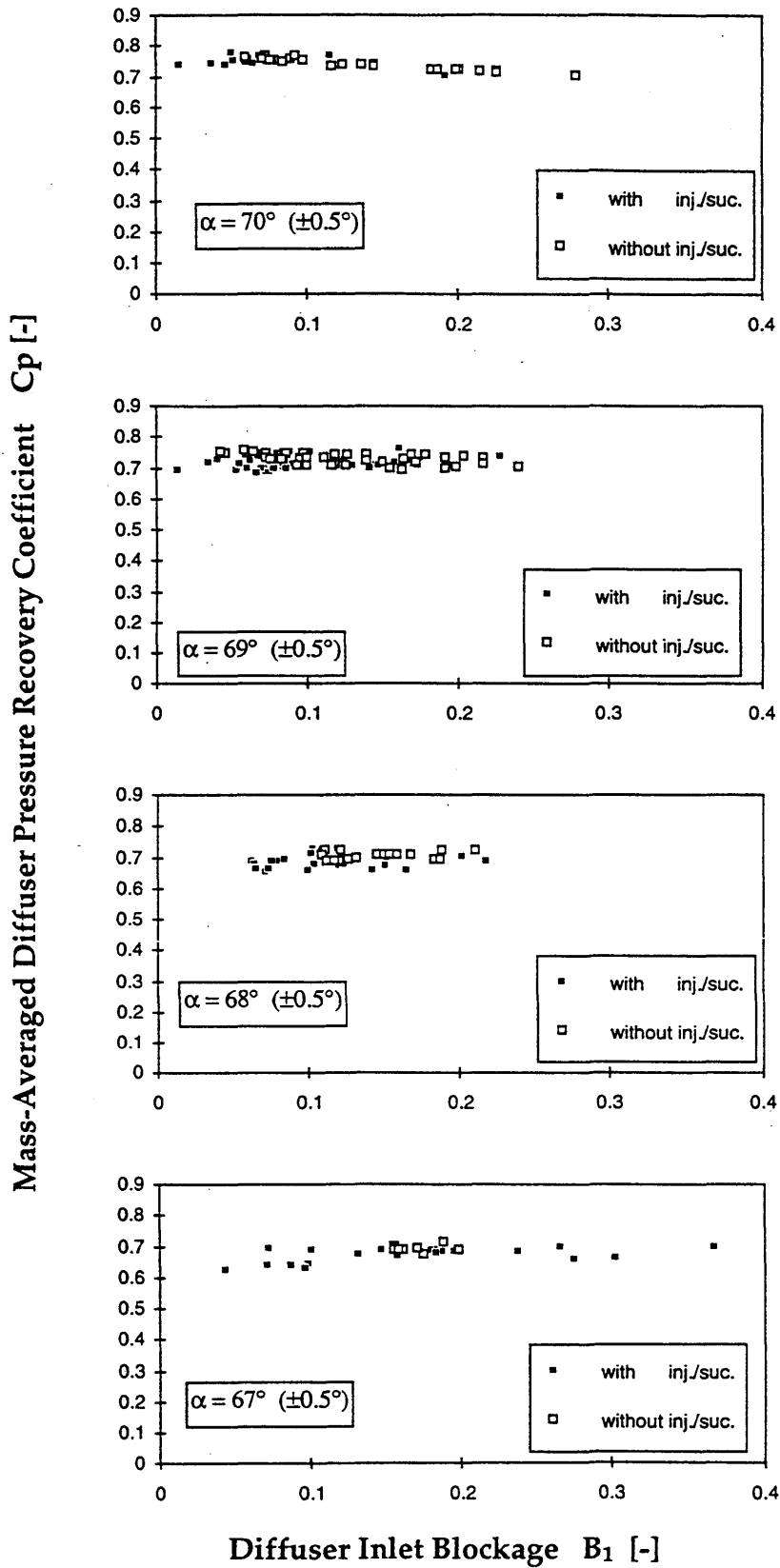


Fig. 4.26 Mass averaged overall diffuser pressure recovery, C_p , as a function of the diffuser inlet blockage, B_1 , represented for constant inlet flow angles.

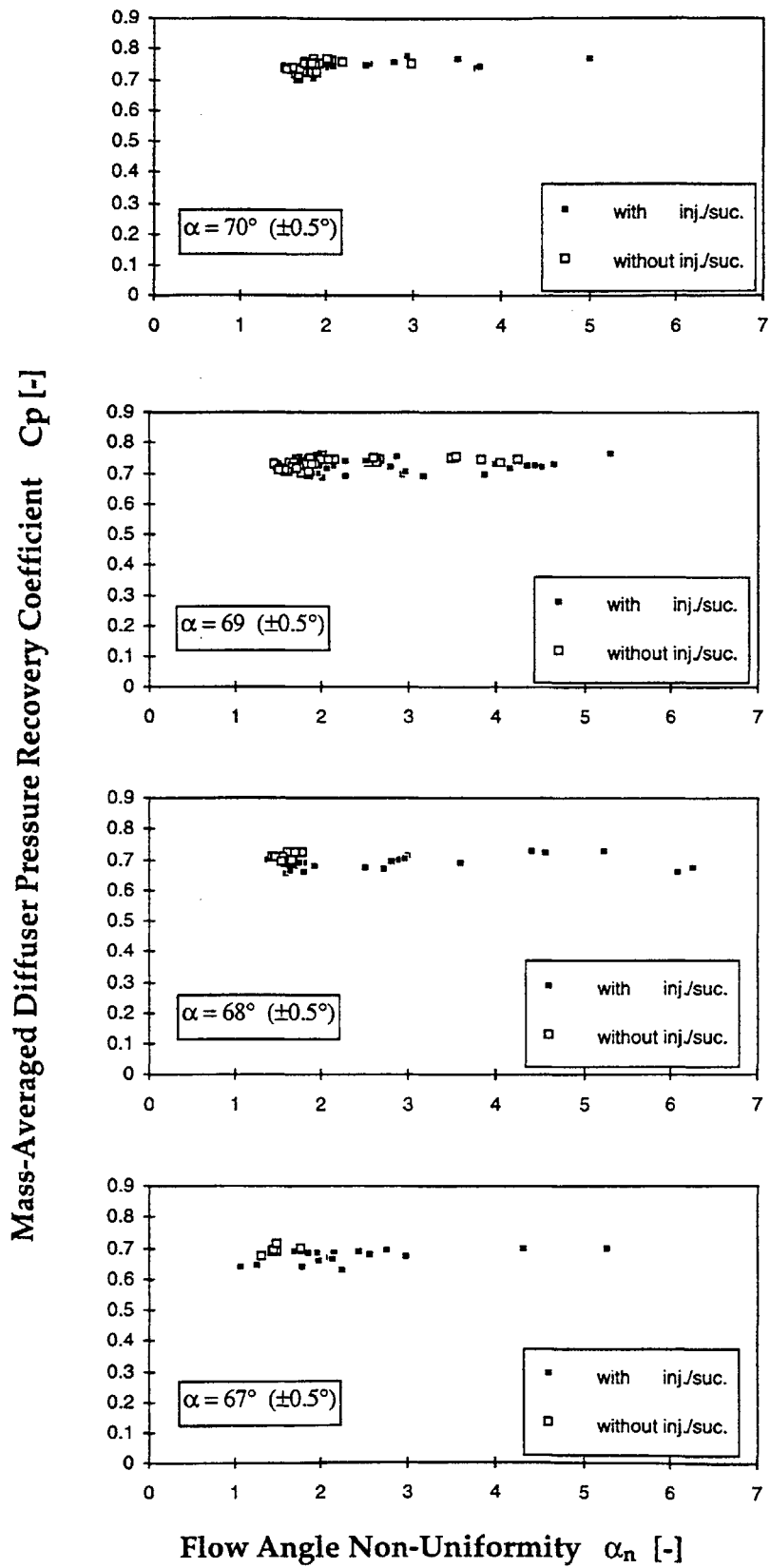


Fig. 4.27 Mass averaged overall diffuser pressure recovery, C_p , as a function of the diffuser inlet flow angle non-uniformity, α_n , represented for constant inlet flow angles.

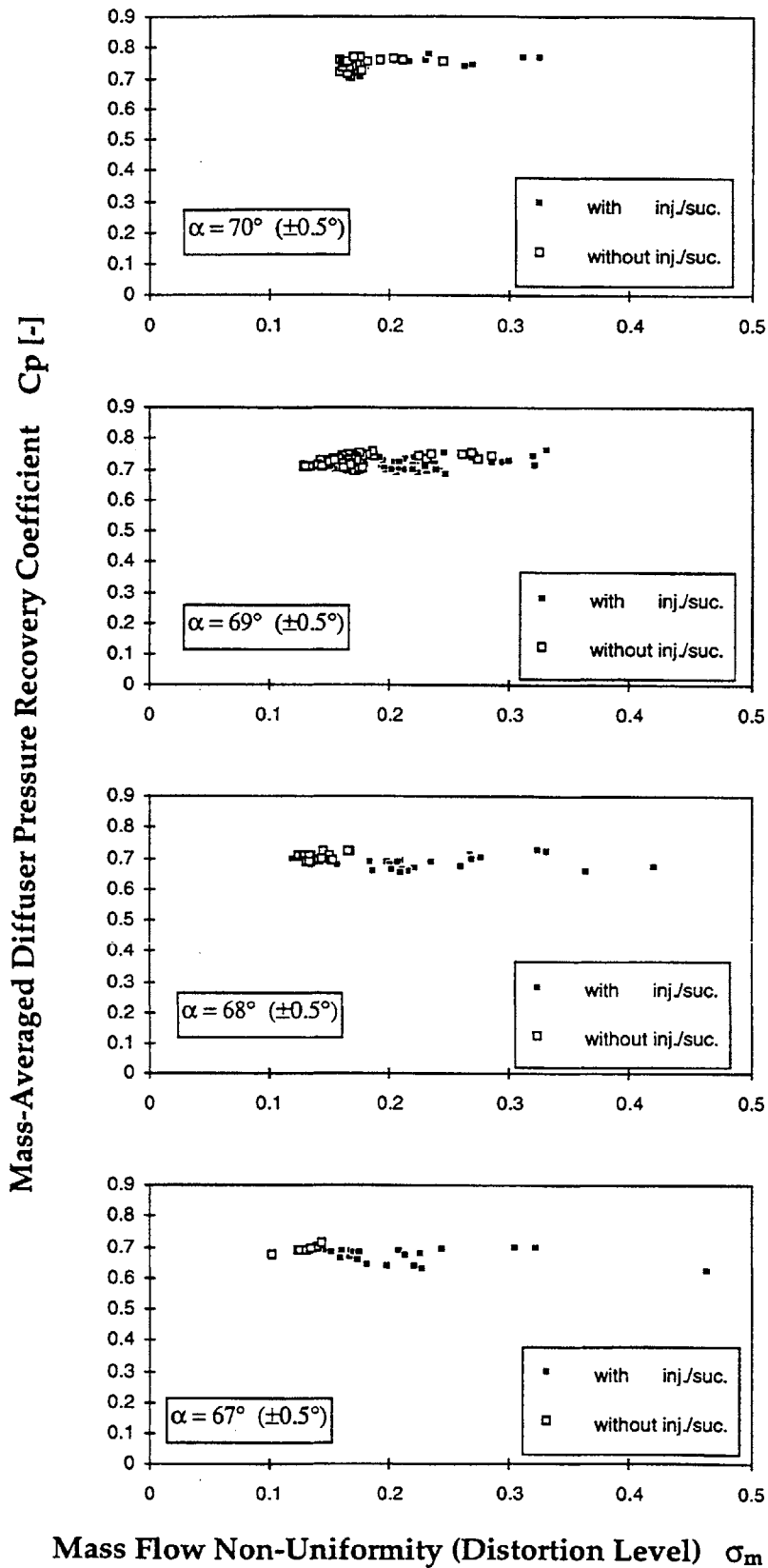


Fig. 4.28 Mass averaged overall diffuser pressure recovery, C_p , as a function of the diffuser mass flow non-uniformity, σ_m , represented for constant inlet flow angles.

Static Pressure Distribution within Diffuser Channel

N = 6000 RPM

153

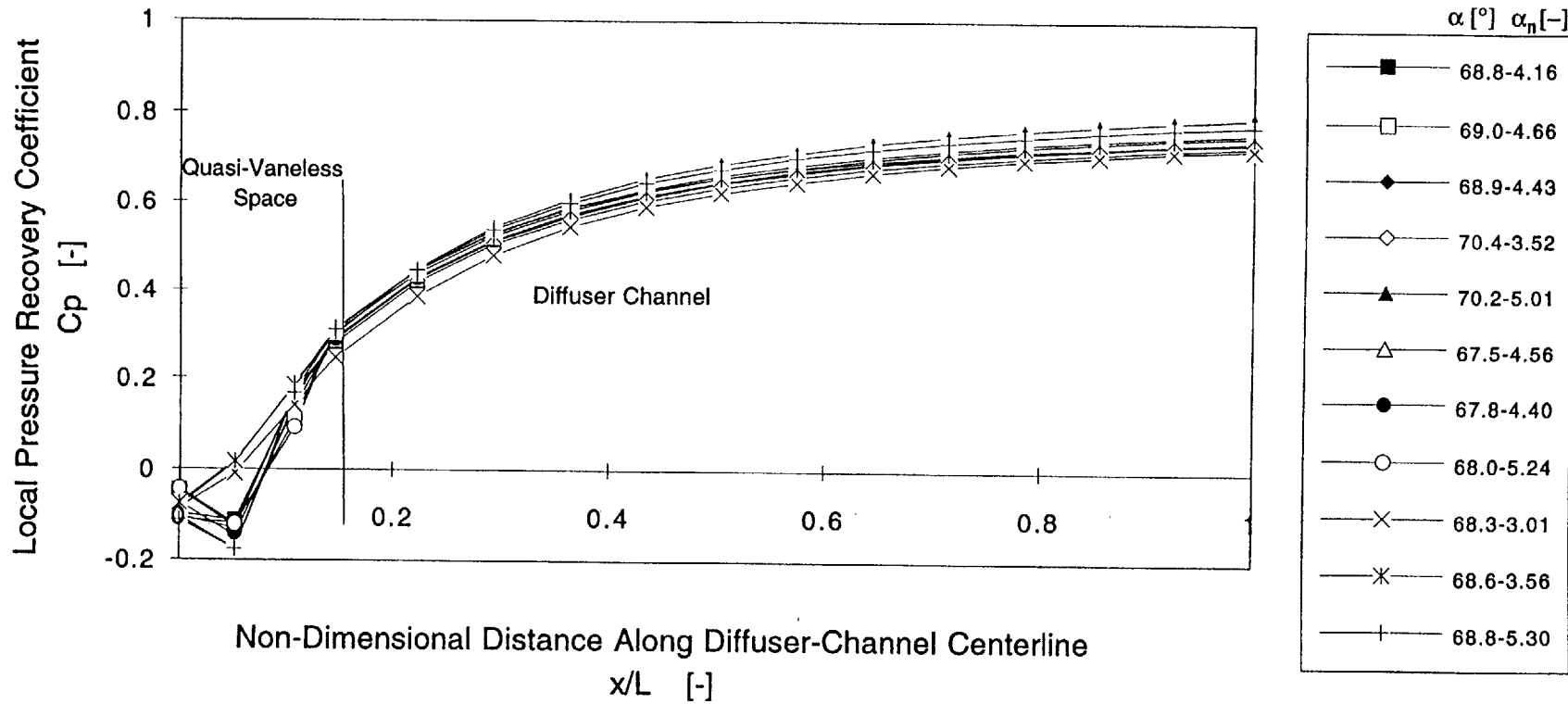


Figure 4.29 Static pressure distribution along the centerline of a diffuser channel for a corrected impeller speed N = 6000 RPM, achieved with injection/suction

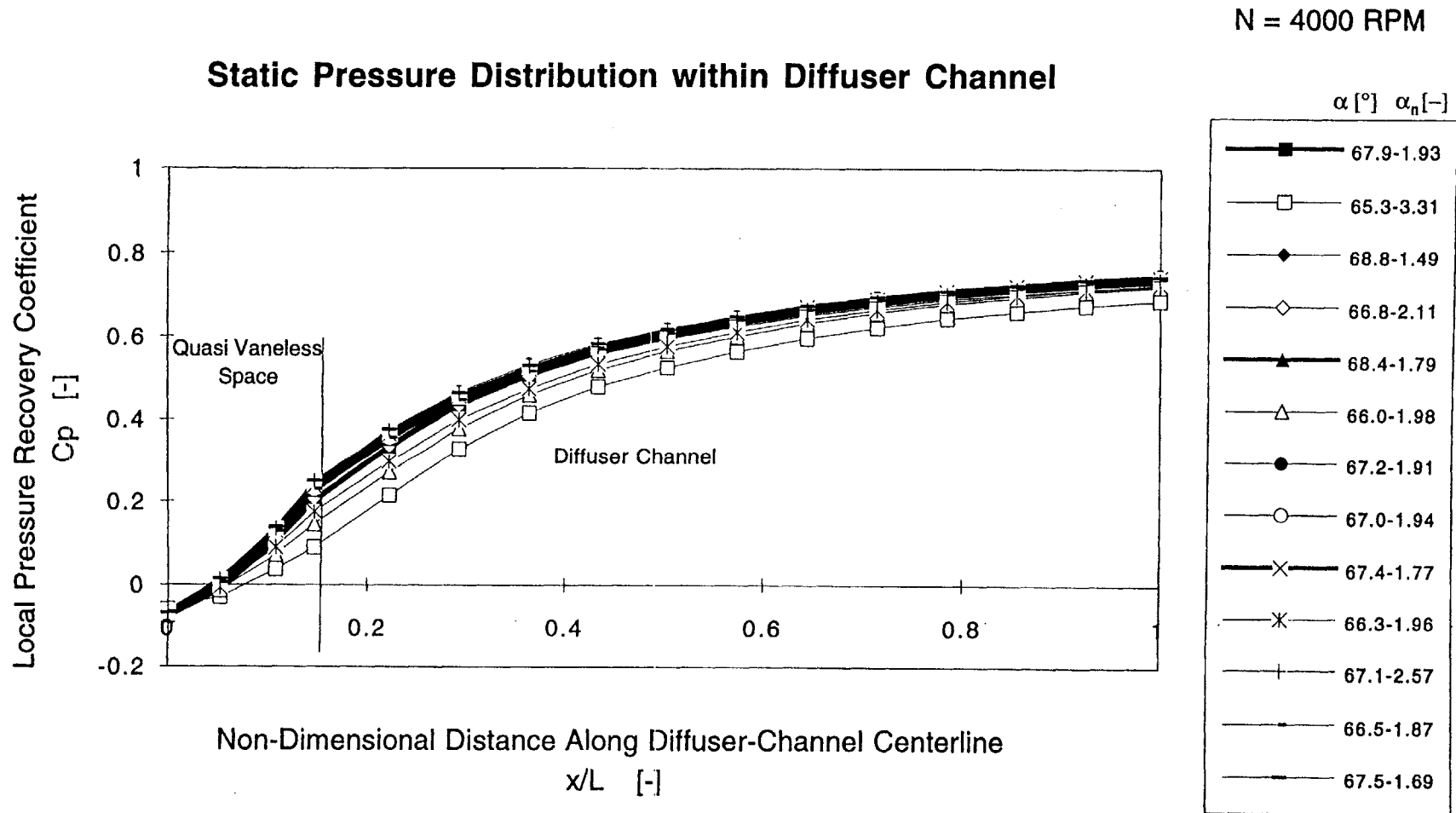


Figure 4.30 Static pressure distribution along the centerline of a diffuser channel for a corrected impeller speed $N = 4000$ RPM, achieved with and without (bold lines) injection/suction

Static Pressure Distribution within Diffuser Channel

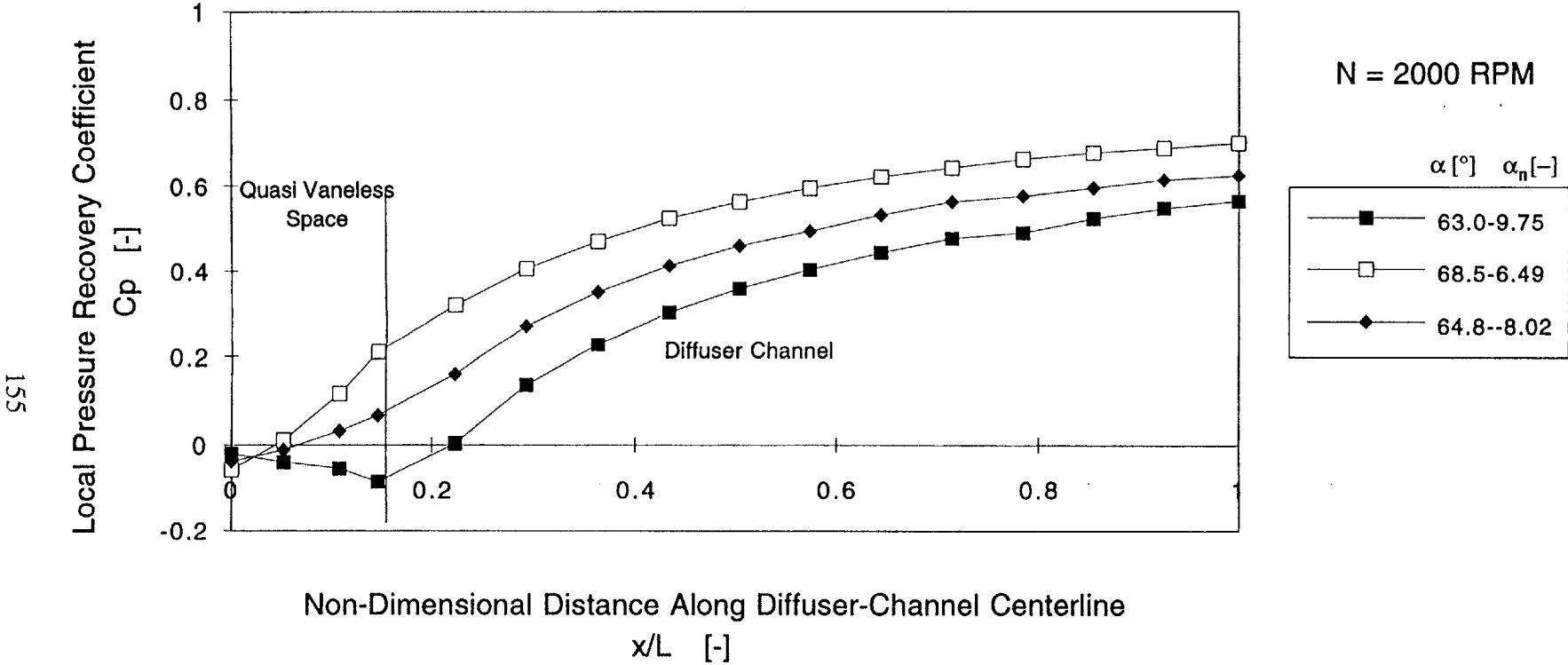


Figure 4.31 Static pressure distribution along the centerline of a diffuser channel for a corrected impeller speed N = 2000 RPM, achieved with injection/suction

Overall Diffuser Pressure Recovery Different Definitions

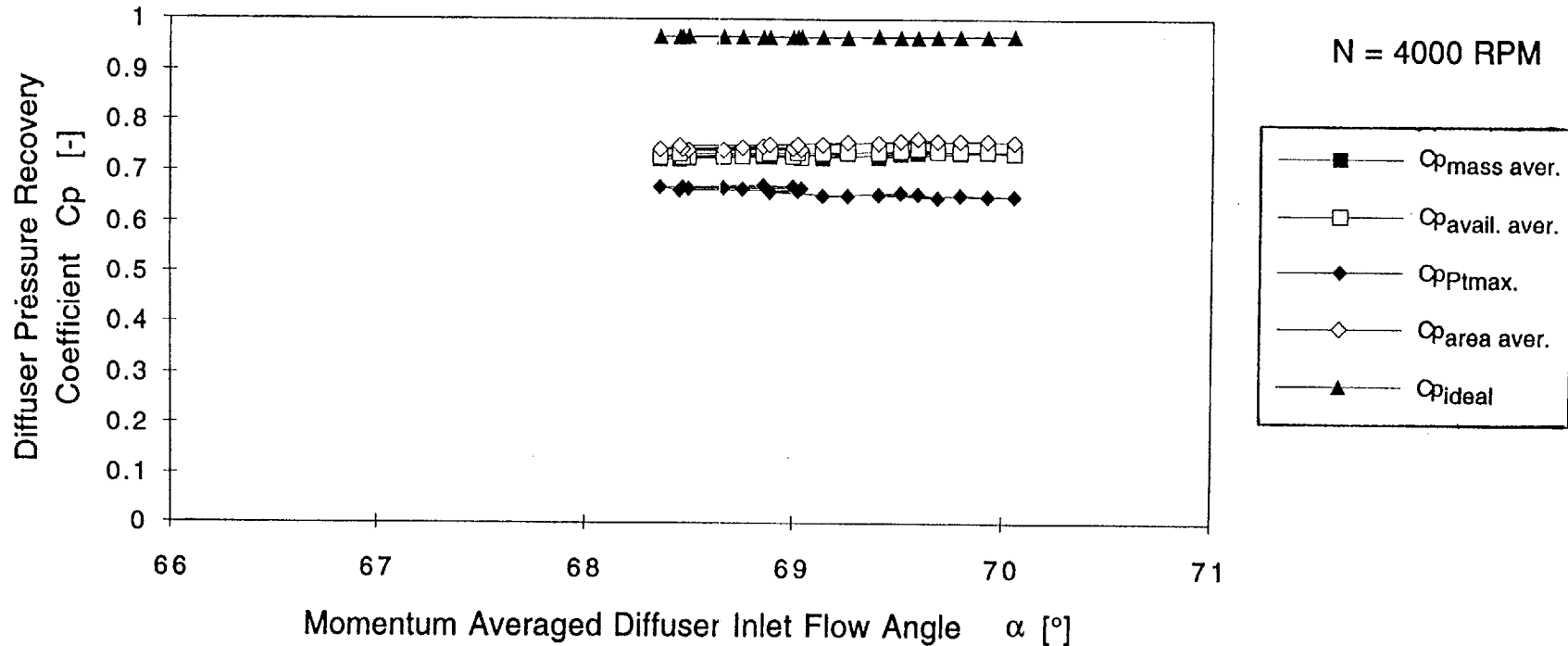
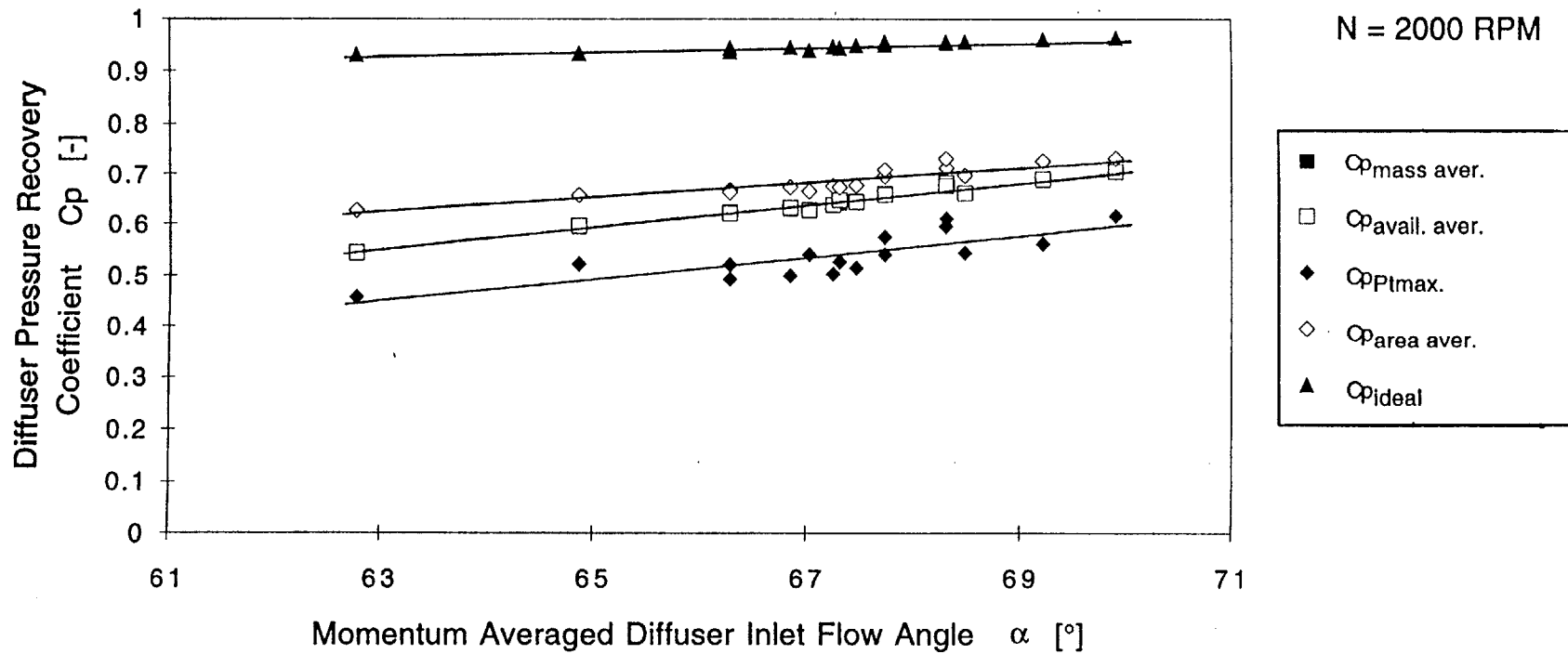


Figure 4.32a Different definitions of overall diffuser pressure recovery coefficient, C_p , as a function of the diffuser inlet momentum averaged flow angle, α , for a corrected impeller speed $N = 4000$ RPM and without injection/suction

Overall Diffuser Pressure Recovery Different Definitions



157

Figure 4.32b Different definitions of overall diffuser pressure recovery coefficient, C_p , as a function of the diffuser inlet momentum averaged flow angle, α , for a corrected impeller speed $N = 2000$ RPM and with injection/suction

Overall Diffuser Pressure Recovery Different Definitions

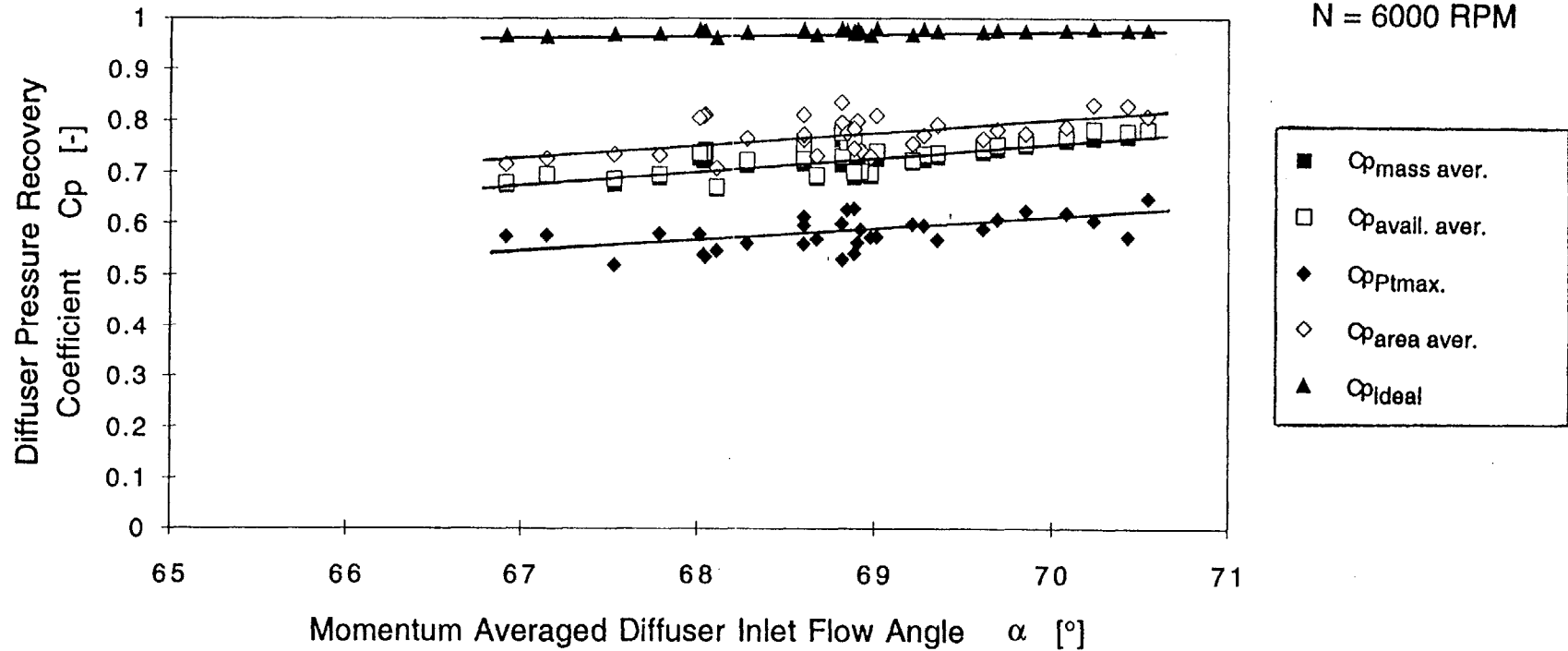


Figure 4.32c Different definitions of overall diffuser pressure recovery coefficient, C_p , as a function of the diffuser inlet momentum averaged flow angle, α , for a corrected impeller speed $N = 6000$ RPM and with injection/suction

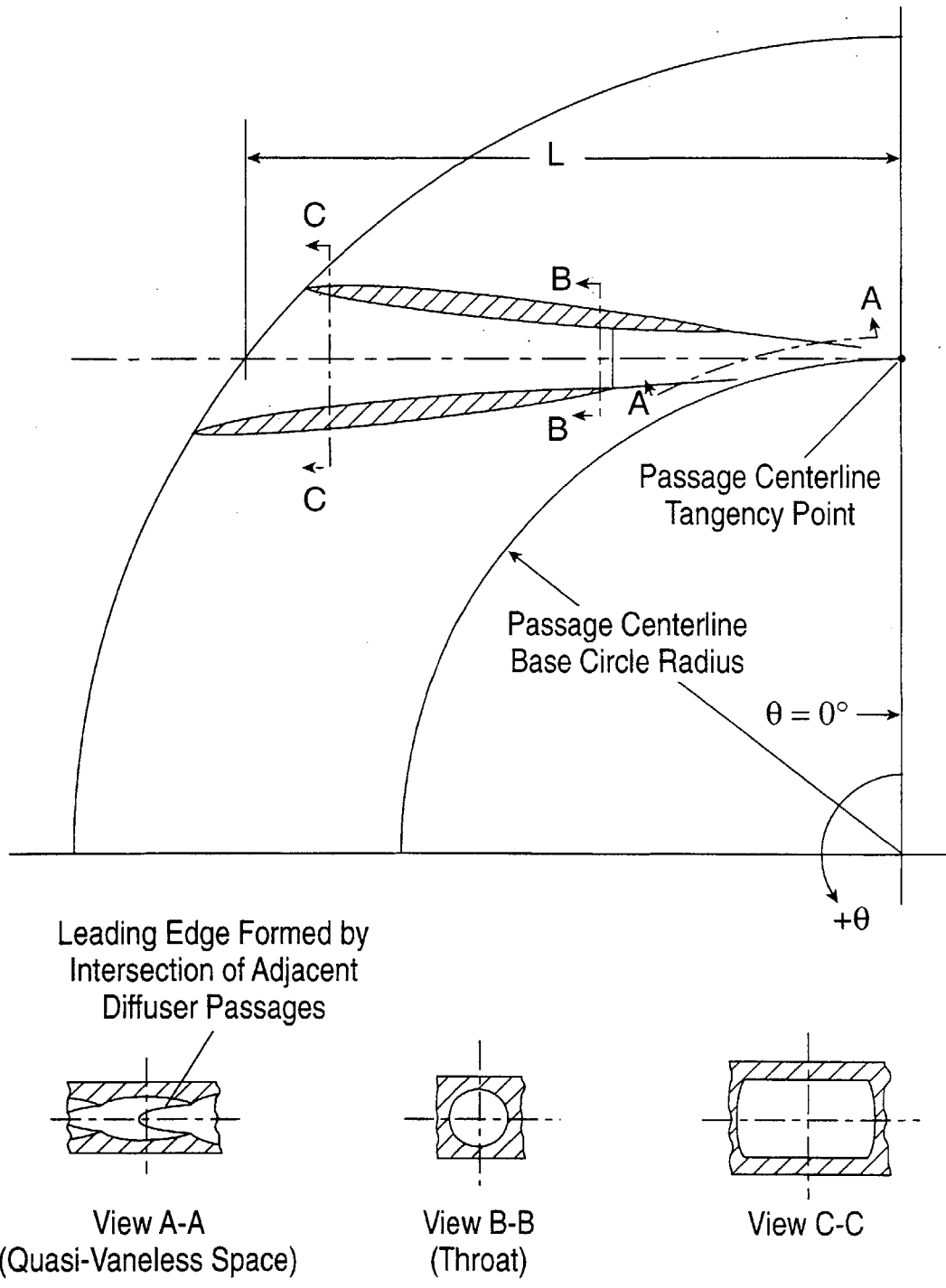


Figure 4.33 Discrete-passage diffuser geometry schematic.

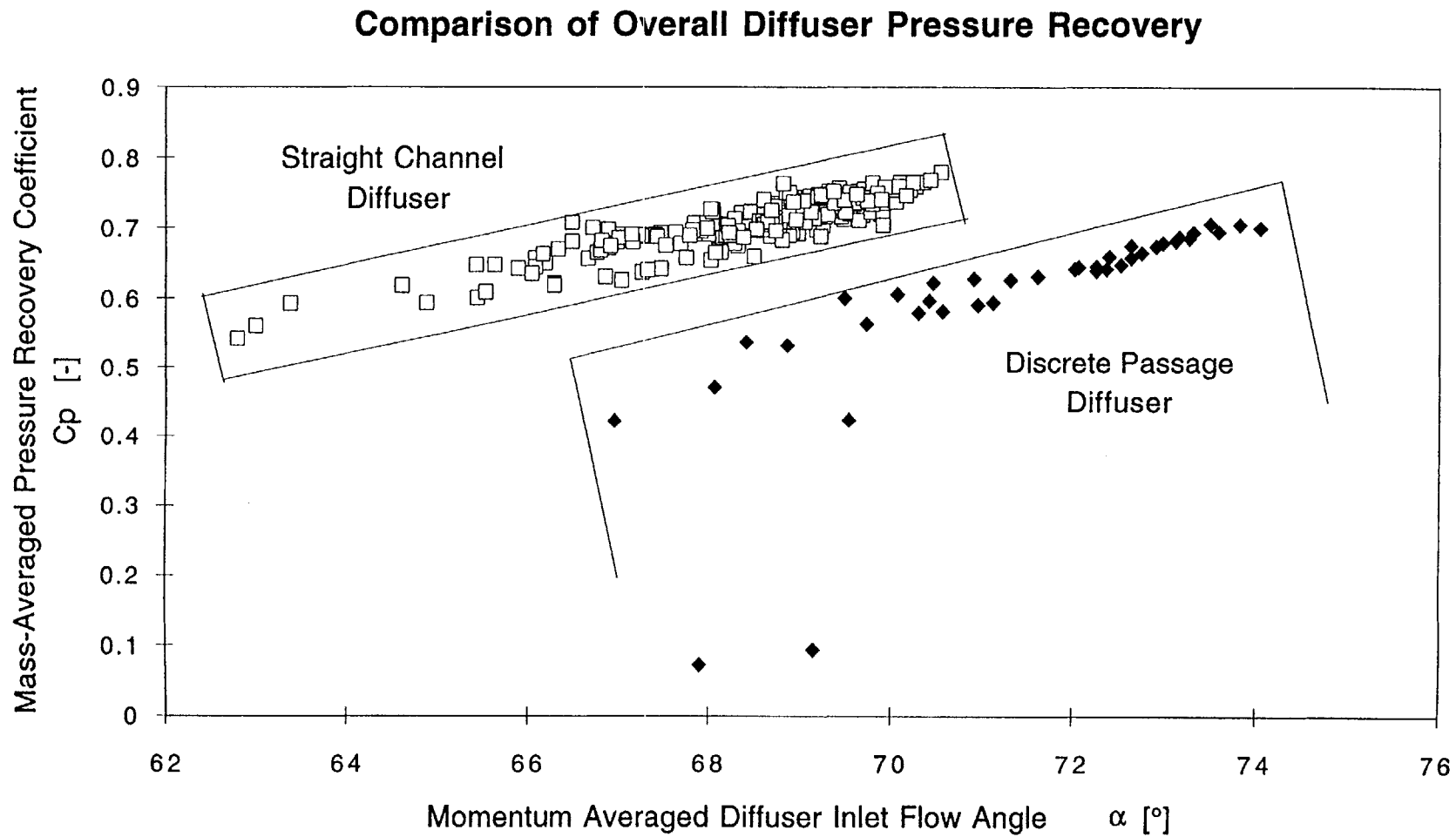
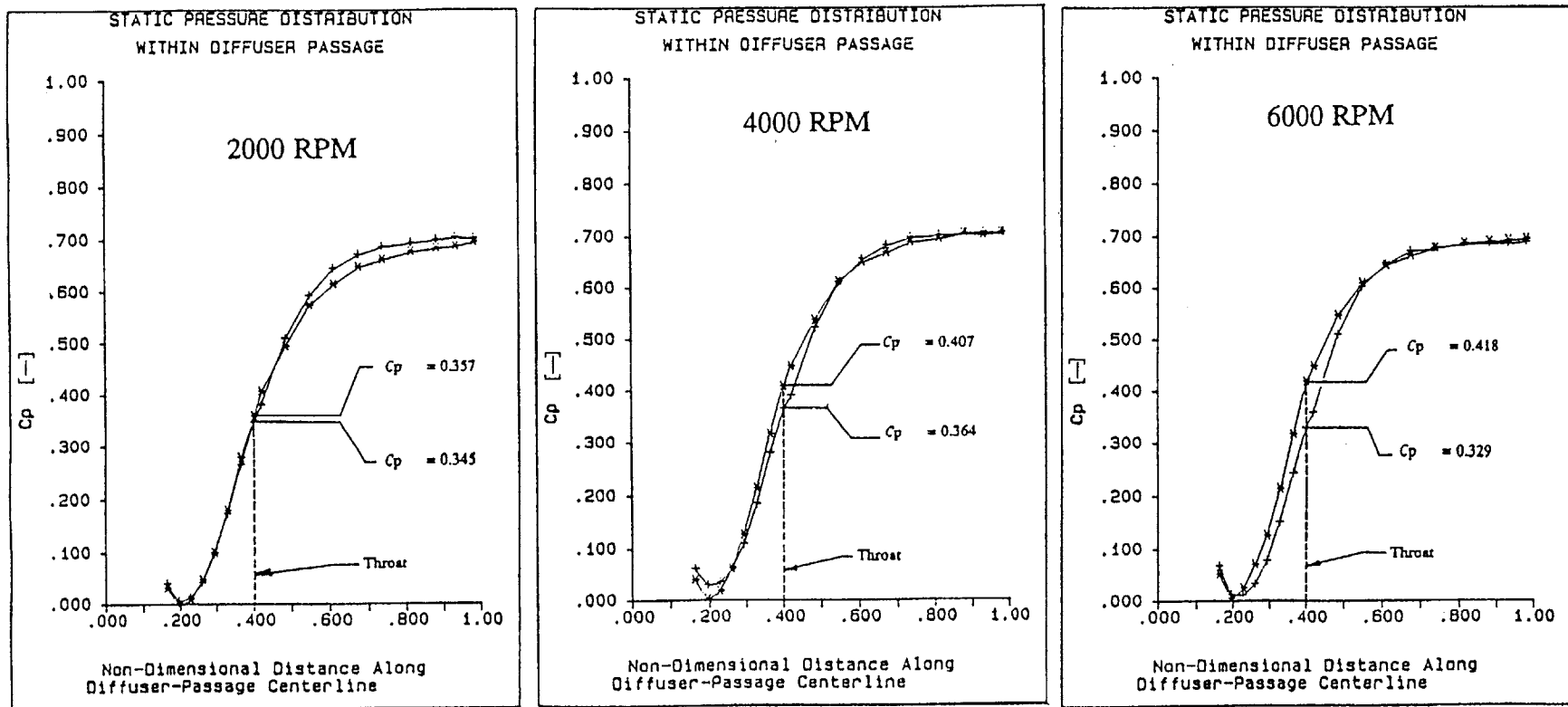
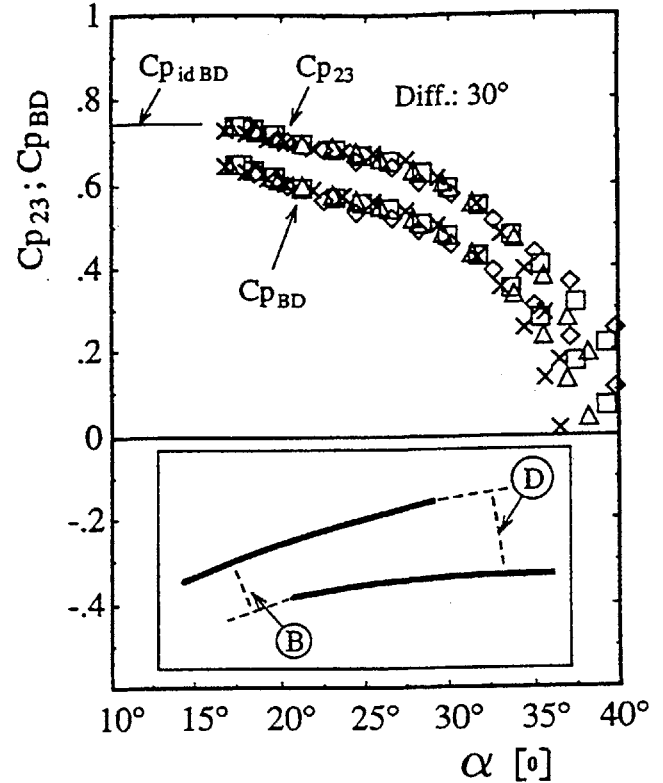
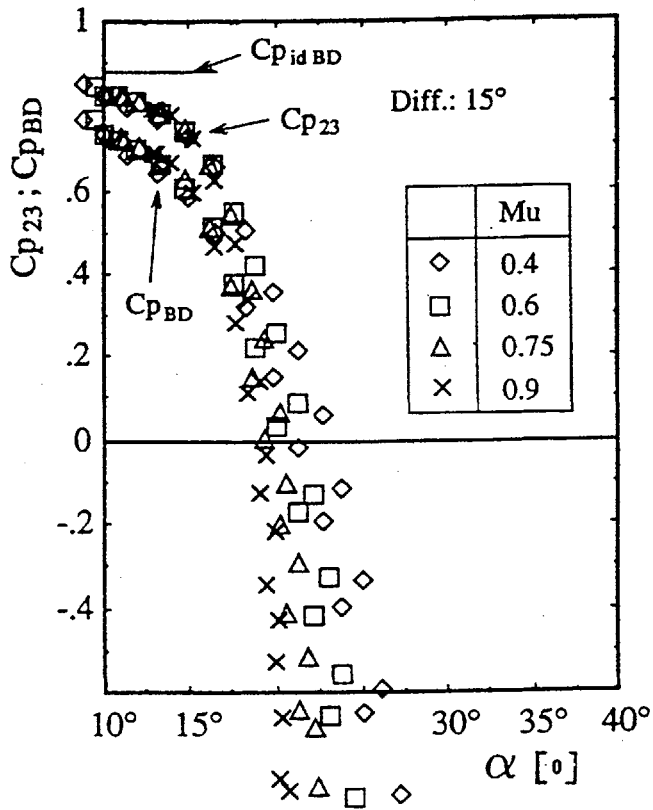


Figure 4.34 Mass averaged overall diffuser pressure recovery, C_p , as a function of the diffuser inlet momentum averaged flow angle, α , for straight channel and discrete passage diffusers



- + Low Inlet Flow Field Distortion
- * High Inlet Flow Field Distortion

Figure 4.35 Static pressure distribution along discrete-passage diffuser centerline with low and high diffuser inlet flow field distortion for three corrected impeller speeds (Filipenco [1991])



a)

b)

Cambered Vane Diffuser

Vane number = 24

C_{pBD} = Pressure recovery coefficient from diffuser inlet to diffuser exit

C_{p23} = Pressure recovery coefficient from impeller exit to plenum

$C_{p_{idBD}}$ = Ideal pressure recovery coefficient from diffuser inlet to diffuser exit

$Mu = U/a$ Mach number

α = Diffuser inlet from angle (measured from tangential)

Figure 4.36 Pressure recovery of cambered vane diffuser as a function of the diffuser inlet flow angle a) for diffuser divergence angle $2\theta = 15^\circ$ and b) for diffuser divergence angle $2\theta = 30^\circ$ (Hunziker [1993])

CHAPTER 5

Summary, Conclusions, and Recommendations for Future Research

5.1 Summary and Conclusions

An experimental investigation has been carried out on performance, operating range, and fluid dynamic phenomena of a straight channel diffuser from high performance centrifugal compressor stages. The influence of inlet flow field conditions, including Mach number, flow angle, fluid dynamic blockage, and flow non-uniformity in axial direction, on the pressure recovery and stability was investigated. The range of diffuser inlet conditions included Mach numbers from 0.2 to 1.1, flow angles from 62° to 71° , blockage levels from 3 to 35%, and high levels of axial flow field distortion, e.g. up to 45° flow angle difference between front and rear walls at the diffuser inlet.

Diffuser pressure recovery and other parameters were calculated from total pressure/flow angle axial traverse measurements made at the inlet of the diffuser. Wall static pressure measurements within a diffuser channel, at the vaneless space, quasi-vaneless space and at the diffuser exit were made to examine the diffuser behavior.

Different averaging methods of the inlet total pressure distributions, together with various definitions of diffuser pressure recovery coefficient for non-uniform diffuser inlet conditions were considered. The main result was that the mass- and/or availability averaged overall diffuser pressure recovery coefficient was a function of diffuser inlet momentum averaged flow angle only, specifically, overall diffuser pressure recovery was insensitive to inlet Mach number, inlet blockage, and flow angle non-uniformity, as also seen in the results of previous investigations on discrete passage diffusers.

The observed onset of the flow instability was diffuser rotating stall. This occurred at a critical diffuser inlet momentum averaged flow angle independent

of the inlet flow field distortion and Mach number, over the parameter range investigated.

The static pressure distribution in the quasi-vaneless space and the static pressure rise along the diffuser centerline were analyzed in detail for different inlet distortion levels and operating points. A substantial part (40 - 50%) of the pressure rise occurs immediately following the diffuser leading edge in the quasi-vaneless space and diffuser throat region. The measurements imply that intensive mixing occurs in this region, and it is hypothesized that the insensitivity of the diffuser performance to inlet distortion is due to this mixing.

The straight channel diffuser was designed for performance comparison similar the discrete passage diffuser previously tested in the same facility. The range of the overall pressure recovery coefficients for the straight channel diffuser and for the discrete passage diffuser were 0.65 - 0.78 and 0.60 - 0.70 respectively, i.e. the straight channel diffuser had a pressure recovery about 10% higher than the discrete passage diffuser. Both diffuser types, straight channel and discrete passage diffuser showed similar behavior regarding the insensitivity of the pressure recovery performance to inlet flow axial distortion.

In addition, both diffuser types showed similar behavior regarding the insensitivity of the onset of instabilities to inlet flow distortion. However, the critical momentum averaged diffuser inlet flow angle for the onset of rotating stall was $\alpha_{crit} = 73^\circ - 74^\circ$ for discrete passage diffuser and $\alpha_{crit} = 70^\circ - 71^\circ$ for the straight channel diffuser.

5.2 Recommendations for Future Research

Some detailed experimental and numerical work has been done to investigate the influence of impeller exit circumferential flow non-uniformity on radial diffuser performance (Inoue & Cumpsty [1984], Dawes [1994]). One important conclusion from these studies was that the circumferential variations in the impeller exit flow mix out very rapidly and seem to have little effect on the performance of the diffuser. The results of the investigations with straight channel and discrete passage diffusers showed that different inlet velocity and flow angle

distributions and inlet blockage levels could be collapsed by using the inlet momentum averaged flow angle. These results still leave unanswered the question of why the flow behaves the way it does. The research in the future should include not only information on the overall performance and stability limit but also information of more local sort (especially for the diffuser inlet region), aimed at understanding not only what the radial diffuser is doing, but why it is doing it so.

The flow at the impeller exit/diffuser inlet region is sensitive to the instrumentation and the use of conventional pneumatic and thermal instrumentation is inadequate for a full understanding of the flow developments in the vaneless and quasi-vaneless spaces and throat region. High frequency anemometry, laser velocimetry and flow visualization are useful means to thoroughly evaluate the fluid dynamic phenomena of this region, between impeller exit and throat. From this viewpoint, the use of a non-intrusive LDA (Laser Doppler Anemometry) system and the use of high-image-density particle image velocimetry (PIV) at the diffuser inlet region might allow characterization of the instantaneous velocity field.

A parallel and supplementary research to the above-mentioned investigation using LDV measurements and flow visualization with PIV should be the numerical investigation of unsteady impeller-diffuser interaction and the analysis of radial diffuser flow phenomena with CFD. This kind of research would not only show the ability of current CFD methods to capture basic flow phenomena in radial diffusers but would elucidate the time averaged effects of unsteady impeller-diffuser interactions on performance and instability.

Rotating stall of a centrifugal compressor stage can be triggered by the diffuser. To increase stable flow range one needs an improved understanding of the basic unsteady flow process that leads to the termination of the stable flow in radial diffuser. Experimental investigation of this process should include both local and global time resolved features (e.g. the frequency content of the disturbance mode, the growth rates, and the spatial structure) of the flow field. Detailed experimental investigation with more high frequency response pressure transducers at the diffuser inlet is required.

To suppress the flow instabilities in form of rotating stall and/or surge in axial and centrifugal compressors, active control techniques have been employed and there is an increasing interest in the implementation of active control schemes to extend the operating range of compressors. A few unsteady flow measurements carried out on centrifugal compressor stages showed that a centrifugal compressor with a vaned diffuser exhibited a much broader spectrum of unstable behavior than those observed in low speed axial compressor investigations. The effective design of active control laws requires detailed understanding of stall inception dynamics in centrifugal compressors with vaned diffusers. This point also emphasizes the necessity of more detailed unsteady measurements.

The present test facility at MIT Gas Turbine Laboratory was proved to be a good investment for the investigation of centrifugal compressor vaned diffuser performance and instability phenomena. Additional radial diffuser configurations such as an airfoil type diffuser (cambered vane or low solidity vaned diffuser) would provide useful performance comparisons with the discrete passage diffuser and/or straight channel diffusers. The application of low solidity vaned diffuser (LSVD) has been popular in last years specially in process and refrigeration industry, but not many performance comparisons between conventional vaned diffusers (e.g. straight channel diffuser) and LSVDs exist. In addition the LSVD does not include a throat between its blades whereas the previously tested discrete passage and straight channel diffusers do have. Comparisons of the results between LSVD and e.g. straight channel diffuser investigations would give insight into the flow phenomena in quasi-vaneless space and throat of the straight channel diffuser in the observed insensitivity of the diffuser performance to the inlet flow field distortion.

The investigations on two discrete passage diffusers with 30 and 38 passages did not show a strong influence of vane number on the performance and instability of the investigated diffusers although one may argue that the difference in passage numbers between 30 and 38 was not high enough to observe any great difference. In some practical applications, radial diffusers with smaller vane numbers e.g. vane island diffuser are in common. The present facility with straight channel diffuser could be easily adopted to a radial diffuser configuration with 10 or 15 vanes.

Regarding the influence of throat blockage on the performance of channel diffuser part, the mass averaged value of throat total pressure is a necessary input. A reliable information of throat total pressure will also give information about the losses occurring between the diffuser inlet and throat. One suggestion to measure throat total pressure could be using a long total pressure probe, which can be installed from the diffuser exit in the diffuser channel centerline instead of diffuser side walls at the throat radius.

REFERENCES

- * **ABDELHAMID, A.N. - HAUPT, U. - RAUTENBERG, M. / 1987** : "Unsteady Flow Characteristics in a Centrifugal Compressor with Vaned Diffuser"
ASME Paper # 87-GT-142,
- * **ABDELHAMID, A.N. / 1983** : "Control of Self-Excited Flow Oscillations in Vaneless Diffuser of Centrifugal Compression Systems"
Canadian Aeronautics and Space Journal, Vol. 29, #4, also ASME Paper # 82-GT-188,
- * **ABDELHAMID, A.N. / 1981** : "Effects of Vaneless Diffuser Geometry on Flow Instability in Centrifugal Compression Systems"
Canadian Aeronautics and Space Journal, Vol. 29, # 3, pp. 259-288, also ASME Paper # 81-GT-10,
- * **ABDELHAMID, A.N. / 1980** : "Analysis of Rotating Stall in Vaneless Diffusers of Centrifugal Compressors"
ASME Paper # 80-GT-184, -
- * **ABDELHAMID, A.N. & BERTRAND, J. / 1980** : "Distinction Between Two Types of Self Excited Gas Oscillations in Vaneless Radial Diffusers"
Canadian Aeronautics and Space Journal, Vol. 26, # 2, also ASME Paper # 79-GT-58,
- * **AL MUDHAFAR, M.M. - ILYAS, M. - BHINDER, F.S. / 1982** : "Investigation of Flows in Rectangular Diffusers with Inlet Flow Distortion"
ASME Paper # 82-GT-67,
- * **ALVERSON, R. & SAGRE, D. / 1994** : Private communication
- * **AMANN, C.A. - NORDENSEN, G.E. - SKELLENGER, G.D. / 1975** : "Casing Modification for Increasing the Surge Margin of Centrifugal Compressor in an Automotive Gas Turbine Engine"
Trans. ASME, Journal of Engineering for Power, Vol. 97, No. 3, pp. 329-336,
- * **AMANN, C.A. & NORDENSEN, G.E. / 1961** : "The Role of the Compressor in Limiting Automotive Gas Turbine Acceleration"
SAE Technical Progress Series, Vol. 3,
- * **AMINENI, N. K. - ENGADA, A. - HOHLWEG, W.C. - BOAL, C.F. / 1996** : "Flow Phenomenon in Low Solidity Vaned Diffusers of a Process Compressor"
ASME Paper # 96-WA/PID-4,

- * AMINENI, N. K. - ENGADA, A. - HOHLWEG, W.C. - DIRENZI, G.L. / 1996 :
 "Performance of Low Solidity and Conventional Diffuser Systems for Centrifugal Compressors"
ASME Paper # 96-GT-155,
- * ARNDT, N. - ACOSTA, A.J. - BRENNEN, C.E. - CAUGHEY, T.K. / 1989 :
 "Experimental Investigation of Rotor-Stator Interaction in a Centrifugal Pump with Several Vaned Diffusers"
ASME Paper # 89-GT-62,
- * BAGHDADI, S. / 1976 : "The Effect of Rotor Blade Wakes on Centrifugal Compressor Diffuser Performance-A Comparative Experiment"
 In 'Centrifugal Compressor and Pump Stability, and Surge' ASME, pp. 121-138, or *Journal of Fluids Engineering Trans. ASME, Vol. 99, #1, (1977-3) pp. 45-52, 1977,*
- * BAGHDADI, S. & McDONALD A.T. / 1975 : "Performance of Three Radial Vaned Diffusers with Swirling Transonic Flow"
Journal of Fluids Engineering, Trans. ASME, June, Vol. 97, pp. 155-173, or ASME Paper # 75-FE-19,
- * BAGHDADI, S. / 1973 : "A Study of Vaned Radial Diffusers Using Swirling Transonic Flow Produced by a Vortex Nozzle"
Ph.D. Thesis, School of Mechanical Engineering, Purdue University,
- * BAMMERT, K. - JANSEN, M. - RAUTENBERG, M. / 1983 : "On the Influence of the Diffuser Inlet Shape on the Performance of a Centrifugal Compressor Stage"
ASME Paper # 83-GT-9,
- * BAMMERT, K. - MOBARAK, A. - RAUTENBERG, M. / 1976 : "Unsteady Flow Measurements in Centrifugal Compressors"
Atomkernenergie, Vol. 27, # 4, pp. 217-229,
- * BARDINA, J. - LYRIO, A. - KLINE, S.J. - FERZIGER, J.H. - JOHNSTON, J.P. / 1981 : "A Prediction Method for Planar Diffuser Flows"
Journal of Fluids Engineering, Trans. ASME, Vol. 103, June, pp. 315-321, or ASME Paper # 81-FE-5,
- * BENVENUTI, E. / 1978 : "Aerodynamic Development of Stages for Industrial Centrifugal Compressors. Part 2: Test Data Analysis, Correlation and Use"
ASME Paper # 78-GT-5 ,

- * **BERENJI, S.G. & RAFFA, C.J. / 1979** : "Variable Area Turbocharger for High Output Diesel Engines"
Society of Automotive Engineers, SAE/SP-79/442,
- * **BHINDER, F.S. - AL MUDHAFAR, M.M. - ILYAS, M. / 1984** : "Further Data on the Performance of a Rectangular Diffuser in Distorted Inlet Flows"
ASME Paper # 84-GT-64,
- * **BHINDER, F.S. & AL MUDHAFAR, M.M. / 1982** : "Development and Application of a Performance Prediction Method for Straight Rectangular Diffuser"
ASME Paper # 82-GT-122,
- * **BLAIR, L.W. & RUSSO, C.J. / 1980** : "Compact Diffusers for Centrifugal Compressors"
Journal of Aircraft, Vol. 19 No. 1, pp. 46-51, AIAA-Paper # 80-1077, June,
- * **BOTROS, K.K. & HENDERSON, J.F. / 1994** : "Developments in Centrifugal Compressor Surge Control - A Technology Assessment"
ASME, Journal of Turbomachinery, Vol. 116, pp. 240-249, also ASME Paper# 93-GT-8,
- * **BROWNELL, R. - FLACK, R. - DAVIS, M. - RICE, J. / 1987** : "Flow Visualization in a Laboratory Vaned Diffuser"
Int. Journal Heat and Fluid Flow, Vol. 8, # 1, March, pp. 37-43,
- * **CAME, P.M. & BELLAMY, A.G. / 1982** : "Design and Performance of Advanced Large Turbochargers"
IMechE, C37/82,
- * **CAME, P.M. & HERBERT, M.V. / 1980** : "Design and Experimental Performance of Some High Pressure Ratio Centrifugal Compressors"
AGARD, CP-282, Paper # 15, May,
- * **CASEY, M.V. - EISELE, K. - ZHANG, Z. - GÜLICH, J. - SCHACHENMANN, A. / 1995a** : "Flow Analysis in a Pump Diffuser, Part 1: LDA and PTV Measurements of the Unsteady Flow"
ASME FED-Vol. 229, Laser Anemometry, pp. 89-100,
- * **CASEY, M.V. - EISELE, K. - MUGGLI, F.A. - GÜLICH, J. - SCHACHENMANN, A. / 1995b**: "Flow Analysis in a Pump Diffuser, Part 2: Validation of a CFD Code for Steady Flow"
ASME FED-Vol. 227, Numerical Simulations in Turbomachinery, pp. 135-143,

- * **CASEY, M.V. - DALBERT, P. - ROTH, P. / 1990** : "The Use of 3D Viscous Flow Calculations in the Design and Analysis of Industrial Centrifugal Compressors"
ASME Paper # 90-GT-2,
- * **CASEY, M. & MARTI, F. / 1986** : "Centrifugal Compressors - Performance at Design and Off-Design"
Proceedings of the Institute of Refrigeration, Session 1985-1986,
- * **CLEMENTS, W.W. & ARTT, D.W. / 1989** : "The Influence of Diffuser Vane Leading Edge Geometry on the Performance of a Centrifugal Compressor"
ASME Paper # 89-GT-163,
- * **CLEMENTS, W.W. / 1987** : "A Theoretical and Experimental Study of Diffusion Levels in Centrifugal Compressor Stages"
Ph. D. Thesis, Faculty of Engineering, University of Belfast,
- * **CLEMENTS, W.W. & ARTT, D.W. / 1987a** : "Performance Prediction and Impeller Diffuser Matching for Vaned Diffuser Centrifugal Compressors"
IMechE, C256/87,
- * **CLEMENTS, W.W. & ARTT, D.W. / 1987b** : "The Influence of Diffuser Channel Geometry on the Flow Range and Efficiency of a Centrifugal Compressor"
Proc. IMechE, Vol. 201, Paper # C41/87, and ASME Paper # 89-GT-163
- * **COCKRELL, D.J. & MARKLAND, E. / 1974** : "Diffuser Behavior - A Review of Past Experimental Work - Relevant To-Day"
Journal of Aeronautical Engineering, Vol. 46, #4, April, pp. 16-26,
- * **CONRAD, O. - RAIF, K. - WESSELS, M. / 1980** : "The Calculation of Performance Maps for Centrifugal Compressors With Vane-Island Diffusers"
Performance Prediction of Centrifugal Pumps and Compressors, ASME Conference, New Orleans, pp. 135-147,
- * **CUMPSTY, NA / 1989** : "Compressor Aerodynamics"
Longman Scientific & Technical,
- * **DALBERT, P. / 1993** : "Turbokompressoren numerisch optimiert"
SULZER Technical Review, Nr. 2, pp. 20- 25,
- * **DALBERT, P. - GYARMATHY, G. - SEBESTYEN, A. / 1993** : "Flow Phenomena in a Vaned Diffuser of a Centrifugal Stage"
ASME Paper # 93-GT-53,

- * **DALBERT, P. - CASEY, M.V. - SCHURTER, M.V. / 1988** : "Development, Testing, and Performance Prediction of Radial Compressor Stages for Multistage Industrial Compressors"
Journal of Turbomachinery, Vol. 110, #3, pp. 283-292, ASME Paper # 88-GT-34,
- * **DAVIS, M.C. & FLACK, R.D. / 1990** : "Laser Velocimetry Measurements in a Laboratory Vaned Diffuser"
Experiments in Fluids, Vol. 9, pp. 33-42, Springer Verlag,
- * **DAWES, W.N. / 1994** : "A Simulation of the Unsteady Interaction of a Centrifugal Impeller with its Vaned Diffuser: Flow Analysis"
ASME Paper # 94-GT-105,
- * **DAWES, W.N. / 1988** : "Development of a 3D Navier-Stokes Solver for Application to all Types of Turbomachinery"
ASME Paper # 88-GT-70,
- * **DEAN, R.C.Jr. & YOUNG, L.R. / 1977** : "The Time Domain of Centrifugal Compressor and Pump Stability and Surge"
Journal of Fluids Engineering, Trans. ASME, Vol. 99, # 1, March, pp. 53-63,
- * **DEAN, R.C.Jr. / 1974** : "Boundary Layers in Centrifugal Compressors"
In 'Fluid Mechanics, Acoustics and Design of Turbomachinery' Part 1, pp. 301-337, NASA SP-304, ed. B. Lakshminarayana,
- * **DEAN, R.C.Jr. / 1973** : "The Fluid Dynamic Design of Advanced Centrifugal Compressors"
Creare, TN-180, August, also Von Karman Institute Lecture Notes,
- * **DEAN, R.C.Jr. / 1971** : "On the Unresolved Fluid Dynamics of the Centrifugal Compressor"
In 'Advanced Centrifugal Compressors', ASME Gas Turbine Division, pp. 1-55,
- * **DEAN, R.C.Jr. - WRIGHT, D.D. - RUNSTADLER, P.W.Jr. / 1970** : "Fluid Mechanics Analysis of High Pressure Ratio Centrifugal Compressor Data"
USAAVLABS (U.S. Army Aviation Material Laboratories)TR-69-76, Feb.,
- * **DEAN, R.C.Jr. & SENOO, Y. / 1960** : "Rotating Wakes in Vaneless Diffusers"
ASME Journal of Basic Engineering, Sept. , Vol. 82, pp. 563-570, Paper # 59-A-104,
- * **DOLAN, F.X. & RUNSTADLER, P.W.Jr. / 1973** : "Pressure Recovery Performance of Conical Diffusers at High Subharmonic Mach Numbers"
Technical Report CR-2299, NASA, August,
- * **DONG, Y. / 1996** : Private communication

- * **DRTINA, P. - DALBERT, P. - RÜTTI, K. - SCHACHENMANN, A. / 1993 :** "Optimization of a Diffuser with Splitter by Numerical Simulation"
ASME Paper # 93-GT-110,
- * **DUTTON, J.C. - PIEMSOMBOON, P. - JENKINS, P.E. / 1986 :** "Flowfield and Performance Measurements in a Vaned Radial Diffuser"
Journal of Fluids Engineering, Vol. 108, June, pp. 141-147,
- * **ECKARDT, D. / 1980 :** "Flow Field Analysis of Radial and Backswept Centrifugal Compressor Impellers Part. 1: Flow Measurements Using a Laser Velocimeter"
Performance Prediction of Centrifugal Pumps and Compressors, ASME, pp. 77-86, ed. Gopalakrishnan,
- * **ECKARDT, D. / 1979 :** "Jet-Wake Mixing in the Diffuser Entry Region of a High -Speed Centrifugal Compressor"
Joint Symposium on Design and Operation of Fluid Machinery Vol. 1, IAHR/ASME/ ASCE, pp. 301-319,
- * **ECKARDT, D. / 1977 :** "Untersuchung der Strahl/Totwasserströmung hinter einem hochbelasteten Radialverdichterlaufrad"
Ph. D. Thesis, R. W. Technische Hochschule Aachen, Germany,
- * **ECKERT, B. & SCHNELL, E. / 1961 :** "Axial- and Radialkompressoren"
Springer Verlag,
- * **ELDER, R.L. & FORSTER, C.P. / 1987 :** "Centrifugal Compressors"
In 'Flow in Centrifugal Compressors' Von Karman Institute for Fluid Dynamics, Lecture Series # 1987-01,
- * **ELDER, R.L. & GILL, M.E. / 1985 :** "A Discussion of the Factors Affecting Surge in Centrifugal Compressors"
Journal of Engineering for Gas Turbines and Power, Vol. 107, pp. 499-506, ASME Paper # 84-GT-194,
- * **ENGADA, A. / 1996 :** "Investigation of Impeller-Diffuser Interaction on the Basis of Three Types of Diffusers"
ASME Paper # 96-WA/PID-5,
- * **FILIPENCO, V.G. / 1991 :** "Experimental Investigation of Flow Distortion Effects on the Performance of Radial Discrete-Passage Diffusers"
M.I.T. - GTL Report # 206, September, Cambridge, Massachusetts, (Ph. D. Thesis,)

- * **FINK, D.A. - CUMPTSY, N.A. - GREITZER, E.M. / 1991** : "Surge Dynamics in a Free-Spool Centrifugal Compressor System"
ASME Paper # 91-GT-31,
- * **FISCHER, F.B. / 1986** : "Development of Vaned Diffuser Compressors for Heavy Duty Diesel Engine Turbochargers"
IMechE, Conference on Turbocharging and Turbochargers, C108/ 86, 1986-4,
- * **FISCHER, E.H. & INOUE, M. / 1981** : "A Study of Diffuser/Rotor Interaction in a Centrifugal Compressor"
Journal of Mechanical Engineering Science, Vol. 23, # 3, pp. 149-156,
- * **FRIGNE, P. & VAN DEN BRAEMBUSSCHE, R. / 1984** : "Distinction Between Different Types of Impeller and Diffuser Rotating Stall in a Centrifugal Compressor With Vaneless Diffuser"
Journal of Engineering for Gas Turbines and Power, Vol. 106, pp. 468-474, ASME Paper # 83-GT-61 ,
- * **FRIGNE, P. & VAN DEN BRAEMBUSSCHE, R. / 1978** : "One Dimensional Design of Centrifugal Compressors Taking Into Account Flow Separation in the Impeller"
Von Karman Institute for Fluid Dynamics, Technical Note 129, June,
- * **GREITZER, E.M. / 1981** : "The Stability of Pumping Systems - The 1980 Freeman Scholar Lecture"
ASME Journal of Fluids Engineering, June Vol. 103, pp. 193-242,
- * **GREITZER, E.M. / 1980** : "Review - Axial Compressor Stall Phenomena"
Journal of Fluids Engineering, Vol. 102, June, pp. 134-151,
- * **GREITZER, E.M. / 1976a** : "Surge and Rotating Stall in Axial Flow Compressors - Part 1: Theoretical Compression System Model"
Journal of Engineering for Power, Vol. 98, Apr., pp. 190-198,
- * **GREITZER, E.M. / 1976b** : "Surge and Rotating Stall in Axial Flow Compressors - Part 2: Experimental Results and Comparison with Theory"
Journal of Engineering for Power, Vol. 98, Apr., pp. 199-217,
- * **GYARMATHY, G. / 1996** : "Impeller-Diffuser Momentum Exchange During Rotating Stall"
ASME Paper # 96-WA/PID-6 ,
- * **GYSLING, D.L. - DUGUNDJI, J. - GREITZER, E.M. - EPSTEIN, A.H. / 1991** : "Dynamic Control of Centrifugal Compressor Surge Using Tailored Structures"
Trans. ASME , Journal of Turbomachinery, Vol. 113, October, pp. 710-722, Paper # 90-GT-122,

- * **HAAK, M. - KRIMPEN, V.J.E. - WORMGOOR, H.J. / 1995** : "Improvement of Centrifugal Compressor Stage Performance by Utilizing of Low Solidity Diffuser"
In 'Symposium Turbomachinery-Fluid Dynamic and Thermodynamic Aspects-Experimental Fluid Dynamics/Special Problems of Turbomachinery' VDI Berichte No. 1186, pp. 327-340,
- * **HAH, C. & KRAIN, H. / 1989** : "Secondary Flows and Vortex Motion in a High Efficiency Backswept Impeller at Design and Off-Design Conditions"
ASME Paper # 89-GT-181,
- * **HAMKINS, C.P. & FLACK, R.D. / 1987** : "Laser Velocimeter Measurements in Shrouded and Unshrouded Radial Flow Pump Impellers"
Journal of Turbomachinery, Vol. 109, pp. 70 - 76 also ASME Paper # 86-GT-129,
- * **HARADA, H. / 1996** : "Study of a Surge-Free Centrifugal Compressor with Automatically Variable Inlet and Diffuser Vanes"
ASME Paper # 96-GT-153,
- * **HARADA, H. & GOTO, M. / 1993** : "Numerical and Experimental Studies of Single and Tandem Low-Solidity Cascade Diffusers in a Centrifugal Compressor"
ASME Paper # 93-GT-108,
- * **HARP, J.L. & OATWAY, T.P. / 1979** : "Centrifugal Compressor Development for a Variable Area Turbocharger"
Society of Automotive Engineers, SAE/SP-79/442,
- * **HASEMANN, H. - HAUPT, U. - JIN, D. - SEIDEL, U. - CHEN, J. - RAUTENBERG, M. / 1991** : "Rotating Stall Flow and Dangerous Blade Excitation of Centrifugal Compressor Impeller - Part II: Case Study of Blade Failure"
ASME Paper # 91-GT-103,
- * **HASS, U. / 1976** : "Zum Strömungsverlauf im schaufellosen Diffusor eines hochbelasteten Radialverdichters"
Ph. D. Thesis, University of Hannover, Germany,
- * **HATHAWAY, M.D. - CHRISS, R.M. - WOOD, J.R. - STRAZISAR, A.J. / 1993** : "Experimental and Computational Investigation of the NASA Low-Speed Centrifugal Compressor Flow Field"
ASME Paper # 92-GT-213, also Journal of Turbomachinery, Vol. 115, pp. 527-542,

* HAUPT, U. - SEIDEL, U. - ABDELHAMID, A.N. - RAUTENBERG, M. / 1988 : "Unsteady Flow in a Centrifugal Compressor with Different Types of Vaned Diffusers"

Journal of Turbomachinery, Vol. 110, # 3, pp. 293-302, ASME Paper # 88-GT-22,

* HAUPT, U. - CHEN, Y.N. - RAUTENBERG, M. / 1987 : "On the Nature of Rotating Stall in Centrifugal Compressors With Vaned Diffusers, Part I: Detection of Reverse Flow"

JSME Paper # 87-TOKYO-IGTC-22, Vol. II, Japan,

* HAYAMI, H. - SENOO, Y. - UTSUNOMIYA, K. / 1989 : "Application of Low-Solidity Cascade Diffuser to Transonic Centrifugal Compressor"

ASME Paper # 89-GT- 66,

* HERBERT, M.V. / 1980 : "A Method of Centrifugal Compressor Performance Prediction"

In 'Performance Prediction of Centrifugal Pumps and Compressors' ASME Conference, New Orleans, March , pp. 171-184,

* HIRSCH, C. - KANG, S. - POINTEL, G. / 1996a : "A Numerically Supported Investigation of the 3D Flow in Centrifugal Impellers, Part 1: The Validation Base"

ASME Paper # 96-GT-151,

* HIRSCH, C. - KANG, S. - POINTEL, G. / 1996b : "A Numerically Supported Investigation of the 3D Flow in Centrifugal Impellers, Part 2: Secondary Flow Structure"

ASME Paper # 96-GT-152,

* HOFFMAN, J.A. & GONZALES, G. / 1984 : "Effects of Small-Scale, High Intensity Inlet Turbulence on Flow in a Two-Dimensional Diffuser"

ASME Journal of Fluids Engineering, Vol. 106, pp. 121-124,

* HOFFMAN, J.A. / 1981 : "Effects of Free-Stream Turbulence on Diffuser Performance"

Journal of Fluids Engineering, Trans. ASME, Vol. 103, September, pp. 385-390,

* HOHLWEG, W.C. - DIRENZI, G.L. - AUNGIER, R.H. / 1993 : "Comparison of Conventional and Low Solidity Vaned Diffusers"

ASME Paper # 93-GT-98,

* HUNZIKER, R. & GYARMATHY, G. / 1993 : "The Operational Stability of a Centrifugal Compressor and its Dependence on the Characteristics of the Subcomponents"

ASME Paper # 93-GT-284,

- * **HUNZIKER, R. / 1993** : "Einfluss der Diffusorgeometrie auf die Instabilitätsgrenze des Radialverdichters"
Ph. D. Thesis, No. 10252, ETH Zurich, Swiss Federal Institute of Technology, Switzerland,
- * **INOUE, M. & CUMPTSY, N.A. / 1984** : "Experimental Study of Centrifugal Impeller Discharge Flow in Vaneless and Vaned Diffusers"
Journal of Engineering for Gas Turbines and Power, Vol. 106, pp. 455-467,
- * **INOUE, M. / 1980** : "Centrifugal Compressor Diffuser Studies"
Ph. D. Thesis, University of Cambridge, England,
- * **JANSEN, M. / 1982** : "Untersuchungen an beschaufelten Diffusoren eines hochbelasteten Radialverdichters"
Ph. D. Thesis, University of Hannover, Germany,
- * **JANSEN, M. & RAUTENBERG, M. / 1982** : "Design and Investigation of a Three Dimensionally Twisted Diffuser for Centrifugal Compressor"
ASME Paper # 82-GT-102,
- * **JANSEN, W. - CARTER, A.F. - SWARDEN, M.C. / 1980** : "Improvements in Surge Margin for Centrifugal Compressors"
In 'Centrifugal Compressors, Flow Phenomena and Performance' AGARD Conference-Proceedings 282, Paper # 19,
- * **JANSEN, W. / 1964a** : "Rotating Stall in a Radial Vaneless Diffuser"
Journal of Basic Engineering, Trans. ASME, Vol. 86, # 4, December, pp. 750-758,
- * **JANSEN, W. / 1964b** : "Steady Fluid Flow in a Radial Vaneless Diffuser"
Journal of Basic Engineering, Trans. ASME, Vol. 86, # 3, September, pp. 607-619,
- * **JAPIKSE, D. / 1996** : "Centrifugal Compressor Design and Performance"
Concepts ETI Inc., Vermont,
- * **JAPIKSE, D. / 1987** : "The Technology of Centrifugal Compressors: A Design Approach and New Goals for Research"
In 'Flow in Centrifugal Compressors' Von Karman Institute, Lecture Notes,
- * **JAPIKSE, D. / 1986** : "Centrifugal Compressor Design and Performance"
Concepts ETI Inc., Norwich, Vermont,
- * **JAPIKSE, D. & OSBORNE, C. / 1986a** : "Optimization of Industrial Centrifugal Compressors; Part 6A: Studies in Component Performance - Eight Design Cases from 1972 to 1982"
ASME Paper # 86-GT-221,

* **JAPIKSE, D. & OSBORNE, C. / 1986b** : "Optimization of Industrial Centrifugal Compressors; Part 6B: Studies in Component Performance - Laboratory Development of Eight Design Cases from 1972 to 1982"
ASME Paper # 86-GT-222,

* **JAPIKSE, D. / 1984a** : "Turbomachinery Diffuser Design Technology"
The Design Technology Series (DTS-1), Concepts ETI Inc., Norwich, Vermont,

* **JAPIKSE, D. / 1984b** : "A Critical Evaluation of Stall Concepts for Centrifugal Compressors and Pumps - Studies in Component Performance , Part 7"
In 'Stability Stall and Surge in Compressors and Pumps' ASME Conference, FED- Vol. 19, pp. 1-10,

* **JAPIKSE, D. / 1982** : "Advanced Diffusion Levels in Turbocharger Compressors and Component Matching"
Turbocharging and Turbochargers, Institution of Mechanical Engineers, April, pp. 143-155,

* **JAPIKSE, D. / 1980** : "The Influence of Diffuser Inlet Pressure Fields on the Range and Durability of Centrifugal Compressor Stages"
AGARD CP-282, Paper # 13, Conference Centrifugal Compressors, Flow Phenomena and Performance, Brussels,

* **JESIONEK, K.J. & WYSZYNSKI, R. / 1979** : "Effect of Entrance Conditions on the Performance of Curved Subsonic Diffusers"
Joint Symposium on Design and Operation of Fluid Machinery Vol. 1, IAHR/ASME/ ASCE, pp. 291-300,

* **JESKE, H.O. & TEIPEL, I. / 1983** : "A Theoretical Investigation of Transonic Flows in Radial Compressor Diffusers"
Journal of Engineering for Power, Vol. 105, pp. 452-456, ASME Paper # 82-GT-227,

* **JIANG, T. & YANG, T.T. / 1982** : "Improved Vane-Island Diffusers at High Swirl"
ASME Paper # 82-GT-68,

* **JIN, D. - HASEMANN, H. - HAUPT, U. - RAUTENBERG, M. / 1994** : "The Flow and Rotation Characteristics of a Centrifugal Compressor During Surge"
ASME Paper # 94-GT-154,

* **JIN, D. - HAUPT, U. - HASEMANN, H. - RAUTENBERG, M. / 1992** : " Blade Excitation by Circumferentially Asymmetric Rotating Stall in Centrifugal Compressors"
ASME Paper # 93-GT-148,

- * **JOHNSON, M.W. & MOORE, J. / 1983a** : "The Influence of Flow Rate on the Wake in a Centrifugal Impeller"
Journal of Engineering for Power, Trans. ASME, Vol. 105, ASME Paper # 82-GT-45,
- * **JOHNSON, M.W. & MOORE, J. / 1983b** : "Secondary Flow Mixing Losses in a Centrifugal Impeller"
Journal of Engineering for Power, Trans. ASME, Vol. 105, ASME Paper # 82-GT-44,
- * **JOHNSTON, J.M. / 1993** : "Stall Onset Observations of a Discrete Passage Diffuser"
MIT - GTL Report # 217, April, Cambridge, Massachusetts, (M. Sc. Thesis)
- * **JOHNSTON, J.P. / 1986** : "Boundary Layers in Internal Flow-Performance Prediction"
Advanced Topics in Turbomachinery Technology Principal Lecture Series, No. 2, ed. D. Japikse,
- * **JOHNSTON, J.P. & DEAN, R.C.Jr. / 1966** : "Losses in Vaneless Diffusers of Centrifugal Compressors and Pumps"
Journal of Engineering for Power, Vol. 8 pp. 49-60, or Journal of Basic Eng. Trans. ASME, Vol. 88, Jan., also ASME Paper # 65-FE-1,
- * **KÄMMER, N. / 1984** : "Untersuchung der Strömung durch eine Radialverdichterstufe im Bereich der Ablösegrenze"
Ph. D. Thesis, University of Hannover, Germany,
- * **KÄMMER, U. & RAUTENBERG, M. / 1982** : "An Experimental Investigation of Rotating Stall Flow in a Centrifugal Compressor"
ASME Paper # 82-GT-82,
- * **KANO, F. - TAZAWA, N. - FUKAO, Y. / 1982** : "Aerodynamic Performance of Large Centrifugal Compressors"
Journal of Engineering for Power, Trans. ASME, Vol. 104, ASME Paper # 82-GT-17,
- * **KENNY, D. / 1984** : "The History and Future of the Centrifugal Compressor in Aviation Gas Turbines"
1st Cliff Garrett Turbomachinery Award Lecture, Society of Automotive Engineers Paper # SAE/SP-804/902,
- * **KENNY, D.P. / 1972** : "A Comparison of the Predicted and Measured Performance of High Pressure Ratio Centrifugal Compressor Diffusers"
ASME Paper # 72-GT-54,

- * **KERREBROCK, J.L. / 1989** : "Aircraft Engines and Gas Turbines"
The MIT Press, Cambridge, Massachusetts,
- * **KIKUYAMA, K. - MURAKAMI, M. - ODA, S. - GOMI, K. / 1987** : "Pressure Recovery of Rotating Diffuser with Distorted Inflows"
ASME Journal of Fluids Engineering, Vol. 109, pp. 114-120,
- * **KLASSEN, H. A. / 1973** : "Performance of a Low Pressure Ratio Centrifugal Compressor with Four Diffuser Designs"
NASA TN D-7237, Mar.,
- * **KLEIN, A. /1981** : "Review: Effects of Inlet Conditions on Conical-Diffuser Performance"
ASME Journal of Fluids Engineering, Vol. 103, June, pp. 250-257,
- * **KLINE, S.C. & JOHNSTON, J.P. / 1986** : "Diffusers-Flow Phenomena and Design"
In 'Advanced Topics in Turbomachinery Technology' Principal Lecture Series # 2, Chapter 6, Concepts ETI, Inc., Norwich, Vt.,
- * **KLINE, S.J. - ABBOTT, D.E. - FOX, R.W. / 1959** : "Optimum Design of Straight-Walled Diffusers"
Journal of Basic Engineering, Trans. ASME, Vol. 81, September, pp. 321-331,
- * **KOSUGE, H. - ITO, T. - NAKANISHI, K. / 1982** : "A Consideration Concerning Stall and Surge Limitations Within Centrifugal Compressors"
Journal of Engineering for Power, Trans. ASME, Vol. 104, ASME Paper # 82-GT-15,
- * **KRAIN, H. / 1984** : "Experimental Observation of the Flow in Impellers and Diffusers"
In 'Flow in Centrifugal Compressors' Von Karman Institute for Fluid Dynamics, Lecture Series # 1984-07,
- * **KRAIN, H. / 1981** : "A Study on Centrifugal Impeller and Diffuser Flow"
Journal of Engineering for Power, Vol. 103, pp. 1-10, ASME Paper # 81-GT-9,
- * **LAWLESS, B.P. & FLEETER, S. / 1993a** : "Rotating Stall Acoustic Signature in a Low Speed Centrifugal Compressor, Part 2. Vaned Diffuser"
ASME Paper # 93-GT-254,
- * **LAWLESS, B.P. & FLEETER, S. / 1993b** : "Active Unsteady Aerodynamic Suppression of Rotating Stall in an Incompressible Flow Centrifugal Compressor with Vaned Diffuser"
AIAA Paper # 91-8198

- * **LE MANARCH, J. & ROBERT, E. / 1958** : "Contribution de la visualisation a l'etude de l'ecoulement a faible vitesse dans des mequettes de compresseurs centrifuges"
La Recherche Aeronautique, No. 67, pp. 21-34,
- * **LENNEMANN, E. & HOWARD, J.H.G. / 1970** : "Unsteady Flow Phenomena in Rotating Centrifugal Impeller Passages"
Journal of Engineering for Power, Vol. 92, Trans. ASME, January, # 1, pp. 65-72,
- * **LIGRANI, P.M. & VAN DEN BRAEMBUSSCHE, R. / 1982** : "Rotating Stall Measurements in the Vaneless Diffuser of a Radial Flow Compressor"
ASME Paper # 82-GT-257,
- * **LIVESEY, J.L. & HUGH, T. / 1966** : "Suitable Mean Values in One-Dimensional Gas Dynamics"
Journal Mechanical Engineering Science, Vol. 8, No. 4, pp. 374-383,
- * **MASUDA, H. - ARIGA, I. - WATANABE, I. / 1971** : "On the Behavior of Uniform Shear Flow in Diffusers and its Effects on Diffuser Performance"
Journal of Engineering for Power, October, pp. 377-385, ASME Paper # 71-GT-5,
- * **McDONALD, A.T. - FOX, R.W. - DEWOESTINE, R.V. VAN / 1971** : "Effects of Swirling Inlet Flow on Pressure Recovery in Conical Diffusers"
AIAA Journal, Vol. 9, # 10, October, pp. 2014-2018,
- * **Mc DONALD, G.B. - LENENMAN, E. - HOWARD, J.H.G. / 1971** : "Measured and Predicted Flow Near the Exit of a Radial Flow Impeller"
ASME, Journal of Eng. for Power, Vol. 93, pp. 441-451,
- * **MIZUKI, S. - HATTORI, T. - ARIGA, I. - WATANABE, I. / 1976** : "Reversed Flow Phenomena within Centrifugal Compressor at Low Flow Rate"
ASME Paper #76-GT-86,
- * **MIZUKI, S. - ARIGA, I. - WATANABE, I. / 1975** : "A Study on the Flow Mechanism within Centrifugal Impeller Channels"
ASME Paper #75-GT-14,
- * **MOORE, J. & MOORE, J.G. / 1980** : "Calculations of Three-Dimensional Viscous Flow and Wake Development in a Centrifugal Impeller"
ASME Paper in ' Performance Prediction of Centrifugal Pumps and Compressors', pp. 61-67, 25th Annual Int. Gas Turbine Conference, New Orleans,

- * MUGGLI, F.A. - WISS, D. - EISELE, K. - ZHANG, Z. - CASEY, M.V.- GALPIN, P. / 1996 : "Unsteady Flow in the Vaned Diffuser of a Medium Specific Speed Pump"
ASME Paper # 96-GT-157,
- * OGATA, M. & ARIGA, I. / 1995 : "An Experimental Study of Rotating Stall in a Radial Vaned Diffuser"
In 'Unsteady Aerodynamics and Aeroelasticity of Turbomachines' Elsevier Science B.V. pp. 625 - 639,
- * OLIVARI, D. & SALASPINI, A. / 1975 : "Measurement of Velocity Distribution at the Impeller Exit of a Radial Compressor"
VKI Technical Note #106, March 1975,
- * OSBORNE, C. & SOROKES, J.M. / 1988 : "The Application of Low Solidity Diffusers in Centrifugal Compressors"
In 'Flows in Non-Rotating Turbomachinery Components' ASME FED-69,
- * PAMPREEN, R.C. / 1993 : "Compressor Surge and Stall"
Concepts ETI, Inc., Vermont,
- * PAMPREEN, R.C. / 1972 : "The Use of Cascade Technology in Centrifugal Compressor Vaned Diffuser Design"
Journal of Engineering for Power, Vol. 94, pp. 187-192, ASME Paper # 72-GT-39,
- * PIEMSOMBOON, P. - DUTTON, J.C. - JENKINS, P.E. / 1984 : "Flowfield and Performance Measurements in a Vaned Radial Diffuser"
ASME Paper # 84-WA/FM-7,
- * PINSLEY, J.E. - GUENETTE, G.R. - EPSTEIN, A.H. - GREITZER, E.M. / 1991 : "Active Stabilization of Centrifugal Compressor Surge"
Trans. ASME, Journal of Turbomachinery, Vol. 113, October, pp. 723-732, ASME Paper # 90-GT-123,
- * RAW, J.A. / 1986 : "Surge Margin Enhancement by a Porous Throat Diffuser"
Canadian Aeronautics and Space Journal, Vol. 32, # 1,
- * RAYAN, M.A. & YANG, T.T. / 1980 : "An Investigation of Vane-Island Diffusers at High Swirl"
ASME Paper # 80-GT-148,
- * REDDY, D.N. / 1990 : "Influence of Inlet Flow Distortion on the Performance of a Radial Vaneless Diffuser of a High Speed Centrifugal Compressor"
In '1. Int. Symposium on Experimental and Computational Aero-thermodynamics of Internal Flows' July 80-12, Beijing, China, pp. 602-607,

- * **REEVES, G.B. / 1977a** : "Estimation of Centrifugal Compressor Stability with Diffuser Loss-Range System"
Journal of Fluid Engineering, Trans. ASME, Vol. 99, or Symposium on Centrifugal Compressor and Pump Stability and Stall and Surge, ASME(1976), pp. 107-119,
- * **REEVES, G.B. / 1977b** : "Design and Performance of Selected Pipe-Type Diffusers"
ASME Paper # 77-GT-104,
- * **RENEAU, L.R. - JOHNSTON, J.P. - KLINE, S.J. / 1967** : "Performance and Design of Straight, Two-Dimensional Diffusers"
Journal of Basic Engineering, Trans. ASME, Vol. 89, March, pp. 141-150,
- * **RIBAUD, Y. & FRADIN, C. / 1989** : "Revaluation of Researches on the Free Rotating Vaneless Diffuser"
ASME Paper # 89-GT-224,
- * **RIBAUD, Y. / 1987** : "Experimental Aerodynamic Analysis to Three High Pressure Ratio Centrifugal Compressors"
ASME Paper # 87-GT-153,
- * **RIBAUD, Y. & AVRAM, P. / 1982** : "Casing Treatments on a Supersonic Diffuser for High Pressure Ratio Centrifugal Compressors"
ASME Paper # 82-GT-85,
- * **RIBI, B. & GYARMATHY, G. / 1995** : "The Behaviour of a Centrifugal Compressor Stage During Mild Surge"
In 'Symposium Turbomachinery-Fluid Dynamic and Thermodynamic Aspects-Experimental Fluid Dynamics/Special Problems of Turbomachinery' VDI Berichte No. 1186, pp. 341-356,
- * **RIBI, B. & GYARMATHY, G. / 1993** : "Impeller Rotating Stall as a Trigger for the Transition from Mild to Deep Surge in a Subsonic Centrifugal Compressor"
ASME Paper # 93-GT-234,
- * **RODGERS, C. / 1993** : "Compact Diffusers for Small Transonic Compressors"
In 'AGARD Meeting on Technology Requirements for Small Gas Turbines' Paper #19, AGARD-CP-537, March,
- * **RODGERS, C. / 1990**: "Centrifugal Compressor Inlet Guide Vanes for Increased Surge Margin"
ASME Paper # 90-GT-158,

- * **RODGERS, C. / 1982a** : "The Performance of Centrifugal Compressor Channel Diffusers"
ASME Paper # 82-GT-10,
- * **RODGERS, C. / 1982b** : "Static Pressure Recovery Characteristics of Some Radial Vaneless Diffusers"
Canadian Aeronautics and Space Institute Int. Symposium on Centrifugal Compressor Design, Toronto, Canada May,
- * **RODGERS, C. / 1980** : "Specific Speed and Efficiency of Centrifugal Impellers"
In 'Performance Prediction of Centrifugal Pumps and Compressors' ASME Conference, New Orleans, March , pp. 191-200,
- * **RODGERS, C. / 1978** : "A Diffusion Factor Correlation for Centrifugal Impeller Stalling"
ASME Paper # 78-GT-61, Journal of Engineering for Power, Vol. 100, # 4, Oct., pp. 592-602,
- * **RODGERS, C. / 1977a** : "Impeller Stalling as Influenced by Diffusion Limitations"
Journal of Fluids Engineering, Trans. ASME, Vol. 99, # 1, March, pp. 84-97,
- * **RODGERS, C. / 1977b** : " Test Evaluation of Stationary and Rotating Diffusers for a High Pressure Ratio Radial Compressor - Final Report"
Solar Turbine International, Report # ER.602, Oct.,
- * **RODGERS, C. & MNEW, H. / 1975** : "Experiments with a Model Free-Rotating Vaneless Diffuser"
Trans. ASME Journal Eng. Power, Vol. 97, # 2, pp. 231-242, also ASME Paper # 74-GT-58,
- * **RODGERS, C. & SAPHIRO, L. / 1972** : "Design Considerations for High Pressure Ratio Centrifugal Compressors"
ASME Paper # 72-GT-91,
- * **RODGERS, C. / 1968** : "Variable Geometry Gas Turbine Radial Compressor"
ASME Paper # 68-GT-63,
- * **ROHNE, K.H. & BANZHAF, M / 1990** : "Investigation of the Flow at the Exit of an Unshrouded Centrifugal Impeller and Comparison with the Classical Jet-Wake Theory"
ASME Paper # 90-GT-124,

- * **RUNSTADLER, P.W.Jr. - DOLAN, F.X. - DEAN, R.C.Jr. / 1975** : "Diffuser Data Book"
Technical Note TN-186, Creare Inc., Hanover, N.H.
- * **RUNSTADLER, P.W.Jr. & DOLAN, F.X. / 1973** : "Further Data of the Pressure Recovery Performance of Straight-Channel, Plane-Divergence Diffusers at High Subsonic Inlet Mach Numbers"
Journal of Fluids Engineering, Vol. 95, ASME Paper # 73-FE-5,
- * **RUNSTADLER, P.W.Jr. & DEAN, R.C.Jr. / 1969** : "Straight Channel Diffuser Performance at High Inlet Mach Numbers"
Journal of Basic Engineering, Trans. ASME, Vol. 91, September, pp. 397-422, ASME Paper # 63-WA/FE-19,
- * **RUSSO, C.J. & BLAIR, L.W. / 1981** : "Effects of Size and Reynolds Number on Centrifugal Diffuser Performance"
ASME Paper # 81-GT-8,
- * **SALVAGE, J.W. / 1996** : "Variable Geometry Pipe Diffusers"
ASME Paper # 96-GT-202,
- * **SEIDEL, U. & RAUTENBERG, M. / 1994** : "Method for Prediction Choke Flow in Vaned Radial Diffusers Based on Thermodynamic and Gas Dynamic Criteria"
ASME Paper # 94-GT-157,
- * **SEIDEL, U. - CHEN, J. - JIN, D. - RAUTENBERG, M. / 1991** : "Experimental Investigation of Rotating Stall Behaviour Influenced by Varying Design and Operation Parameters of Centrifugal Compressors"
1991 Yokohoma Int. Gas Turbine Congress, Yokohoma, Japan,
- * **SENOO, Y. - HAYAMI, H. - UTSONOMIYA, K. / 1989** : "Application of Low-Solidity Cascade Diffuser to Transonic Centrifugal Compressor"
ASME Paper # 89-GT-66,
- * **SENOO, Y. / 1984a** : "Vaned Diffusers"
In 'Flow in Centrifugal Compressors' von Karman Institute for Fluid Dynamics Lecture Series 1984 -07,
- * **SENOO, Y. / 1984b** : "Vaneless Diffusers"
In 'Flow in Centrifugal Compressors' von Karman Institute for Fluid Dynamics Lecture Series 1984 -07,
- * **SENOO, Y. / 1984c** : "Low Solidity Cascade Diffusers"
In 'Flow in Centrifugal Compressors' von Karman Institute for Fluid Dynamics Lecture Series 1984 -07,

- * **SENOO, Y. - HAYAMI, H. - UEKI, H. / 1983** : "Low-Solidity Tandem-Cascade Diffusers for Wide Range Centrifugal Blowers"
ASME Paper # 83-GT-3,
- * **SENOO, Y. - HAYAMI, H. - KINOSHITA, Y. - YAMASAKI, H. / 1979** : "Experimental Study on Flow in a Supersonic Centrifugal Impeller"
Journal of Engineering for Power, Trans. ASME, Vol. 101, ASME Paper # 78-GT-2,
- * **SENOO, Y. & KINOSHITA, Y. / 1978** : "Limits of Rotating Stall and Stall in Vaneless Diffusers of Centrifugal Compressors"
ASME Paper # 78-GT-19,
- * **SENOO, Y. & KINOSHITA, Y. / 1977** : "Influence of Inlet Flow Conditions and Geometries of Centrifugal Vaneless Diffusers on Critical Flow Angle for Reverse Flow"
Journal of Fluids Engineering, Trans. ASME, Vol. 99, # 1, March, pp. 98-103,
- * **SENOO, Y. & NISHI, M. / 1977a** : "Prediction of Flow Separation in a Diffuser by a Boundary Layer Calculation"
Journal of Fluids Engineering, Trans. ASME, June, pp. 379-389,
- * **SENOO, Y. & NISHI, M. / 1977b** : "Deceleration Rate Parameter and Algebraic Prediction of Turbulent Boundary Layer"
Journal of Fluids Engineering, Trans. ASME, June, pp. 391-394,
- * **SENOO, Y. & ISHIDA, M. / 1974** : "Behavior of Severely Asymmetric Flow in a Vaneless Diffuser"
ASME Paper # 74-GT-64, also Journal of Engineering for Power, Vol. 97, pp. 375-387,
- * **SIMON, J.S. - VALAVANI, L. - EPSTEIN, A.H. - GREITZER, E.M. / 1992** : "Evaluation of Approaches to Active Compressor Surge Stabilization"
ASME Paper # 92-GT-182,
- * **SIMON, H. - WALLMAN, T. - MOENK, T. / 1987** : "Improvements in Performance Characteristics of Single-Stage and Multistage Centrifugal Compressors by Simultaneous Adjustments of Inlet Guide Vanes and Diffuser Vanes"
Journal of Turbomachinery, Trans. ASME, Vol. 109, ASME Paper # 86-GT-127,
- * **SMITH, V.J. / 1970** : "A Review of the Design Practice and Technology of Radial Compressor Diffusers"
ASME Paper # 70-GT-116,

- * **SOROKES, J.M. & WELCH, J.P. / 1992** : "Experimental Results on a Rotatable Solidity Vaned Diffuser"
ASME Paper # 92-GT-19,
- * **SOROKES, J.M. & WELCH, J.P. / 1991** : "Centrifugal Compressor Performance Enhancement through the Use of Single Stage Development Rig"
Proceedings of the 20th Turbomachinery Symposium, Texas A&M, pp. 101-112,
- * **SOVRAN, G. & KLOMP, E.D. / 1967** : "Experimentally Determined Optimum Geometries for Rectilinear Diffusers with Rectangular, Conical, or Annular Cross Section"
In 'Fluid Mechanics of Internal Flows' ed. G. Sovran, Amsterdam, Elsevier, pp. 270-319,
- * **STARKE, J. & HERGT, P. / 1985** : "An Experimental Investigation of Flow Patterns in Vaned Diffusers of Centrifugal Pumps Causing Performance Curve Instabilities"
Three Dimensional Fluid Phenomena Fluid Machinery, ASME FED-Vol. 32, pp. 9-18,
- * **STEIN, W. & RAUTENBERG, M. / 1988** : "Analysis of Measurements in Vaned Diffusers of Centrifugal Compressors"
Journal of Turbomachinery, Vol. 110, # 1, pp. 115-121, ASME Paper # 87-GT-170,
- * **STEIN, W. / 1986** : "Beitrag zur Analyse der gegenseitigen Beeinflussung von Laufrad und Diffusorbeschaufelung in Radialverdichtern"
Ph. D. Thesis, University of Hannover, Germany,
- * **STEIN, W. & RAUTENBERG, M. / 1985** : "Flow Measurements in Two Cambered Vane Diffusers with Different Passage Widths"
ASME Paper # 85-GT-46,
- * **TEIPEL, I. - WIEDERMANN, A. - EVERS, W. / 1992** : "Viscous Flows in Centrifugal Compressor Diffusers at Transonic Mach Numbers"
Proceedings Int. Gas Turbine & Aeroengine Congress and Exposition, ASME Paper # 92-GT-48,
- * **TEIPEL, I. & WIEDERMANN, A. / 1990** : "Viscous Flow Field Calculations in High-Loaded Centrifugal Compressor Diffusers"
ASME Paper # 90-GT-77,
- * **TEIPEL, I. & WIEDERMANN, A. / 1986** : "Three-Dimensional Flowfield Calculation of High-Loaded Centrifugal Compressor Diffusers"
ASME Paper # 86-GT-187,

- * **TEIPEL, I. & WIEDERMANN, A. / 1984** : "The Influence of Different Geometries for a Vaned Diffuser on the Pressure Distribution in a Centrifugal Compressor"
ASME Paper # 84-GT-68,
- * **TOYAMA, K. - RUNSTADLER, P.W. Jr. - DEAN, R.C.Jr. / 1977** : "An Experimental Study of Surge in Centrifugal Compressors"
Journal of Fluids Engineering, Trans. ASME, Vol. 99, #1, March, pp. 115-131,
- * **TRAUPEL, W. / 1977** : "Thermische Turbomaschinen"
Bd.1, Auflage 3, Springer,
- * **UBALDI, M. - ZUNINO, P. - BARIGOZZI, G. - CATTANEI, A. / 1994** : "An Experimental Study of Stator Induced Unsteadiness on Centrifugal Impeller Outflow"
ASME Paper # 94-GT-5,
- * **UBALDI, M. - ZUNINO, P. - CATTANEI, A. / 1992** : "Relative Flow and Turbulence Measurements Downstream of a Backward Centrifugal Impeller"
ASME Paper # 92-GT-212,
- * **UBALDI, M. & ZUNINO, P. / 1990** : "Experimental Investigation of the Stalled Flow in a Centrifugal Pump-Turbine with Vaned Diffuser"
ASME Paper # 90-GT-216,
- * **VAN DEN BRAEMBUSSCHE, R.A. / 1984** : "Surge and Stall Phenomena in Centrifugal Compressors"
Von Karman Institute Lecture Series 1984-07, Flow in Centrifugal Compressors,
- * **VERDONK, G. / 1978a** : "Vaned Diffuser Inlet Flow Conditions for a High Pressure Ratio Centrifugal Compressor"
ASME Paper # 78-GT-50,
- * **VERDONK, G. / 1978b** : "Theoretical and Experimental Investigation of the Flow at the Inlet of the Vaned Diffuser for a High Pressure Ratio Centrifugal Compressor"
Von Karman Institute, Technical Note 125,
- * **WAITMAN, B.A. - RENEAU, L.R. - KLINE, S.J. / 1961** : "Effects of Inlet Conditions on Performance of Two-Dimensional Subsonic Diffusers"
Journal of Basic Engineering, Trans. ASME, Vol. 83, September, pp. 349-360,

- * **WHITFIELD, A. - WALLACE, F.J. - ATKEY, R.C. / 1976** : "The Effect of Variable Geometry on the Operating Range and Surge Margin of a Centrifugal Compressor"
ASME Paper # 76-GT-98,
- * **WILSON, D.G. / 1984** : "The Design of High - Efficiency Turbomachinery and Gas Turbines"
The MIT Press, Cambridge, Massachusetts,
- * **WOLF, S. & JOHNSTON, J.P. / 1969** : " Effects of Nonuniform Inlet Velocity Profiles on Flow Regimes and performance in Two-Dimensional Diffusers"
Journal of Basic Engineering, Trans. ASME, Vol. 91, September, pp. 462-474, ASME Paper # 68-WA/FE-25,
- * **WYSOCKI, W. & KAZIMIERSKI, Z. / 1986** : "Analysis of Subsonic Transitory Stalled Flows in Straight Walled Diffusers"
Journal of Fluids Engineering, June, pp. 222-226,
- * **YAMANE, T. & NAGASHIMA, T. / 1995** : "Flow Choking and Shock Wave Structure at Diffuser Vanes in a High Speed Centrifugal Compressor"
12. International Symposium on Air Breathing Engines, September 10-15, Australia Volume 1, pp. 135-145,
- * **YOSHIDA, Y. - MURAKAMI, Y. - TSURUSAKI, H. - TSUJIMOTO, Y. / 1991** : "Rotating Stalls in Centrifugal Impeller/Vaned Diffuser Systems"
ASME FED-Vol. 107, General Topics in Fluids Eng., ASME 1991
- * **YOSHINAGA, Y. - GYOBU, I. - MISHINA, H. - KOSEKI, F. - HISHIDA, N. / 1980** : "Aerodynamic Performance of a Centrifugal Compressor with Vaned Diffusers"
Journal of Fluids Engineering, Trans. ASME, Vol. 102, pp. 486-493,

APPENDIX

Appendix 1

Result Summary Tables

The following Table A1.1 summarizes all of the traverse data taken during the straight channel diffuser experiments. It contains results obtained with and without injection/suction, including operating point characteristics, diffuser inlet flow field and diffuser performance parameters.

In this table:

- Column II lists corrected impeller speed, N_{corr} (see Eq. 3.1)
- Column III shows whether air injection and/or suction is applied or not. Here "i" stands for injection, "s" suction and "0" for no injection and/or suction. The first character designates the front wall, and the second character, the rear wall of the diffuser.
- Column IV lists corrected mass flow rate, \dot{m}_{corr} (see Eq. 3.2)
- Column V lists impeller pressure ratio, π_{01} (see Eq. 3.3)
- Column VI lists plenum pressure ratio, π_{03} (see Eq. 3.3)
- Column VII lists momentum averaged inlet flow angle, α (see Eq. 3.36)
- Column VIII lists diffuser inlet Mach number, M_1 (see Eq. 3.5)
- Column IX lists diffuser inlet Blockage, B_1 (see Eq. 3.44)
- Column X lists mass averaged overall diffuser pressure recovery coefficient, \hat{C}_p (see Eq. 3.30)
- Column XI lists overall diffuser efficiency, η_{diff} (see Eq. 3.17)
- Column XII lists dimensionless diffuser flow number, φ (see Eq. 3.48)
- Column XIII lists diffuser pressure rise coefficient, D_p (see Eq. 3.49)
- Column XIV lists inlet flow angle non-uniformity, α_n (see Eq. 3.42)
- Column XV lists inlet flow angle skew, α_s (see Eq. 3.43)
- Column XVI lists mass-flux deficit (distortion level), σ_m (see Table 3.1)
- Column XVII lists mass-flux skew, ξ_m (see Table 3.1)

I	II	III	IV	V	VI	VII	VIII	IX	X	XI	XII	XIII	XIV	XV	XVI	XVII
Data No.	N [RPM]	Inlet Flow Condition	\dot{m}_{corr} [kg/s]	$\pi_{01'}$ [-]	π_{03} [-]	α [°]	M_1 [-]	B_1 [-]	\hat{C}_p [-]	η_{diff} [-]	ϕ [-]	D_p [-]	α_n [-]	α_s [-]	σ_m [-]	ξ_m [-]
513/100	2000	0 - 0	0.481	0.953	1.003	67.94	0.32	0.12	0.690	0.724	0.078	5.02	1.66	-0.24	0.13	-0.51
515/100	2000	0 - 0	0.472	0.954	1.003	68.10	0.32	0.11	0.688	0.721	0.077	4.91	1.62	-0.25	0.13	-0.49
499/100	2000	0 - 0	0.471	0.955	1.004	66.90	0.33	0.18	0.671	0.702	0.077	4.93	1.30	-0.14	0.10	-0.35
513/75	2000	0 - 0	0.471	0.955	1.004	68.0	0.32	0.12	0.691	0.724	0.077	4.87	1.62	-0.27	0.13	-0.53
498/100	2000	0 - 0	0.470	0.954	1.004	66.98	0.32	0.16	0.680	0.713	0.077	4.95	1.77	0.15	0.14	0.12
500/100	2000	0 - 0	0.471	0.955	1.004	67.15	0.32	0.16	0.688	0.721	0.077	4.94	1.49	-0.22	0.13	-0.56
504/100	2000	0 - 0	0.468	0.956	1.004	67.29	0.32	0.16	0.690	0.719	0.075	4.81	1.44	-0.13	0.12	-0.40
504/80	2000	0 - 0	0.466	0.956	1.004	67.34	0.32	0.16	0.688	0.721	0.074	4.75	1.45	-0.13	0.13	-0.42
515/72	2000	0 - 0	0.462	0.957	1.004	68.18	0.32	0.12	0.690	0.722	0.075	4.76	1.59	-0.27	0.13	-0.52
504/70	2000	0 - 0	0.438	0.958	1.005	67.37	0.32	0.20	0.689	0.718	0.070	4.64	1.45	-0.10	0.13	-0.39
504/60	2000	0 - 0	0.438	0.963	1.007	67.50	0.30	0.17	0.693	0.724	0.069	4.37	1.46	-0.09	0.13	-0.34
515/58	2000	0 - 0	0.437	0.963	1.007	68.33	0.30	0.13	0.693	0.726	0.070	4.37	1.68	-0.28	0.14	-0.48
513/55	2000	0 - 0	0.433	0.965	1.008	68.28	0.30	0.13	0.697	0.730	0.070	4.29	1.66	-0.25	0.14	-0.46
501/50	2000	0 - 0	0.403	0.971	1.011	67.12	0.28	0.19	0.686	0.717	0.065	3.93	1.49	-0.22	0.14	-0.63
502/50	2000	0 - 0	0.403	0.971	1.011	67.63	0.29	0.18	0.693	0.724	0.065	3.93	1.57	-0.15	0.15	-0.27
504/50	2000	0 - 0	0.402	0.972	1.010	67.91	0.28	0.19	0.695	0.725	0.064	3.85	1.55	-0.13	0.15	-0.29
513/48	2000	0 - 0	0.392	0.973	1.011	68.73	0.28	0.16	0.697	0.727	0.063	3.75	1.76	-0.34	0.16	-0.42
515/46	2000	0 - 0	0.377	0.975	1.012	68.98	0.27	0.16	0.695	0.724	0.060	3.56	1.86	-0.34	0.17	-0.40
513/42	2000	0 - 0	0.341	0.982	1.014	68.18	0.25	0.19	0.697	0.725	0.054	3.10	1.86	-0.33	0.17	-0.38
515/40	2000	0 - 0	0.325	0.984	1.014	69.25	0.25	0.20	0.704	0.731	0.052	2.94	1.85	-0.31	0.18	-0.35
504/50	2000	0 - 0	0.322	0.985	1.015	68.53	0.24	0.24	0.702	0.727	0.050	2.87	1.62	-0.16	0.16	-0.22
513/38	2000	0 - 0	0.299	0.988	1.015	69.47	0.23	0.22	0.712	0.738	0.047	2.64	1.71	-0.34	0.17	-0.39
515/37	2000	0 - 0	0.289	0.989	1.016	69.89	0.23	0.21	0.720	0.746	0.046	2.53	1.65	-0.22	0.16	-0.35
513/37	2000	0 - 0	0.283	0.990	1.016	69.98	0.22	0.23	0.719	0.744	0.045	2.45	1.64	-0.36	0.16	-0.40
513/100	3000	0 - 0	0.697	0.886	1.008	68.31	0.51	0.11	0.707	0.737	0.081	5.80	1.57	-0.19	0.13	-0.43
515/100	3000	0 - 0	0.697	0.888	1.008	68.51	0.50	0.09	0.709	0.740	0.081	5.69	1.50	-0.13	0.13	-0.41
515/75	3000	0 - 0	0.685	0.893	1.010	68.61	0.50	0.10	0.709	0.740	0.079	5.53	1.50	-0.17	0.13	-0.42
505/100	3000	0 - 0	0.685	0.890	1.011	67.83	0.51	0.15	0.706	0.735	0.078	5.66	1.43	-0.10	0.12	-0.36
505/80	3000	0 - 0	0.680	0.896	1.012	67.97	0.50	0.14	0.707	0.736	0.077	5.44	1.46	-0.09	0.13	-0.34
513/65	3000	0 - 0	0.670	0.899	1.013	68.78	0.49	0.12	0.710	0.741	0.077	5.34	1.57	-0.22	0.13	-0.44
505/70	3000	0 - 0	0.667	0.900	1.013	68.10	0.49	0.15	0.706	0.735	0.075	5.29	1.45	-0.11	0.13	-0.35
505/60	3000	0 - 0	0.646	0.911	1.017	68.19	0.47	0.16	0.706	0.735	0.072	4.95	1.43	-0.14	0.13	-0.33
515/58	3000	0 - 0	0.643	0.910	1.017	69.16	0.47	0.12	0.713	0.743	0.073	4.96	1.52	-0.21	0.14	-0.43
513/55	3000	0 - 0	0.634	0.915	1.019	68.96	0.46	0.13	0.709	0.738	0.071	4.81	1.58	-0.25	0.14	-0.42

Table A1.1 Data for Straight Channel Diffuser (see page 193 for the definitions of the parameters in row 2)

I	II	III	IV	V	VI	VII	VIII	IX	X	XI	XII	XIII	XIV	XV	XVI	XVII
Data No.	N [RPM]	Inlet Flow Condition	\dot{m}_{corr} [kg/s]	$\pi_{01'}$ [-]	π_{03} [-]	α [°]	M_1 [-]	B_1 [-]	\hat{C}_p [-]	η_{diff} [-]	φ [-]	D_p [-]	α_n [-]	α_s [-]	σ_m [-]	ξ_m [-]
505/50	3000	0-0	0.600	0.931	1.025	68.40	0.44	0.17	0.708	0.736	0.066	4.23	1.47	-0.16	0.15	-0.29
513/45	3000	0-0	0.600	0.944	1.030	69.28	0.42	0.15	0.717	0.745	0.061	3.86	1.75	-0.25	0.17	-0.34
515/46	3000	0-0	0.544	0.943	1.029	69.45	0.42	0.17	0.716	0.743	0.060	3.88	1.67	-0.25	0.16	-0.35
513/40	3000	0-0	0.494	0.963	1.035	69.54	0.38	0.19	0.720	0.746	0.053	3.22	1.90	-0.29	0.18	-0.33
515/39	3000	0-0	0.482	0.967	1.036	69.88	0.37	0.18	0.723	0.749	0.052	3.09	1.85	-0.26	0.17	-0.32
505/40	3000	0-0	0.472	0.969	1.037	69.64	0.37	0.20	0.710	0.735	0.050	2.99	1.69	-0.18	0.16	-0.21
513/38	3000	0-0	0.462	0.970	1.037	69.77	0.36	0.20	0.722	0.748	0.050	2.93	1.83	-0.23	0.18	-0.30
515/38	3000	0-0	0.458	0.972	1.038	69.90	0.36	0.20	0.724	0.749	0.049	2.90	1.80	-0.20	0.17	-0.29
514/100	4000	0-0	0.887	0.775	1.015	68.75	0.73	0.08	0.728	0.754	0.086	7.20	1.92	-0.10	0.17	-0.17
515/100	4000	0-0	0.879	0.782	1.014	69.03	0.72	0.07	0.731	0.757	0.085	6.93	1.76	-0.10	0.17	-0.18
506/100	4000	0-0	0.879	0.784	1.018	68.49	0.72	0.21	0.723	0.749	0.084	6.92	1.79	0.02	0.17	0.09
514/75	4000	0-0	0.877	0.786	1.018	68.66	0.71	0.08	0.726	0.753	0.085	6.88	1.82	-0.09	0.17	-0.18
506/80	4000	0-0	0.872	0.792	1.020	68.46	0.71	0.11	0.723	0.750	0.082	6.69	1.72	0.01	0.17	0.14
515/72	4000	0-0	0.868	0.795	1.019	68.99	0.70	0.08	0.729	0.756	0.083	6.60	1.73	-0.10	0.15	-0.21
514/65	4000	0-0	0.863	0.803	1.023	68.85	0.69	0.08	0.727	0.754	0.082	6.44	1.89	-0.14	0.15	-0.27
506/70	4000	0-0	0.861	0.803	1.023	68.35	0.69	0.19	0.722	0.748	0.081	6.41	1.71	-0.03	0.14	-0.18
506/60	4000	0-0	0.839	0.822	1.030	68.45	0.66	0.12	0.723	0.749	0.077	5.96	1.61	-0.02	0.14	-0.17
515/58	4000	0-0	0.838	0.824	1.030	69.01	0.66	0.08	0.729	0.757	0.078	5.89	1.69	-0.06	0.15	-0.22
514/55	4000	0-0	0.830	0.832	1.034	68.88	0.65	0.10	0.727	0.754	0.076	5.74	1.66	-0.05	0.14	-0.24
515/50	4000	0-0	0.791	0.859	1.043	69.25	0.61	0.10	0.732	0.760	0.071	5.08	1.63	-0.06	0.15	-0.22
506/50	4000	0-0	0.783	0.865	1.046	69.13	0.61	0.14	0.725	0.751	0.069	4.96	1.49	-0.15	0.15	-0.24
514/47	4000	0-0	0.774	0.871	1.048	69.51	0.60	0.11	0.733	0.760	0.069	4.83	1.68	-0.07	0.16	-0.22
514/45	4000	0-0	0.741	0.889	1.053	69.59	0.57	0.12	0.734	0.761	0.065	4.41	1.55	-0.14	0.16	-0.26
515/44	4000	0-0	0.719	0.899	1.054	69.68	0.56	0.12	0.737	0.763	0.062	4.14	1.53	-0.17	0.16	-0.27
506/45	4000	0-0	0.714	0.902	1.057	69.40	0.55	0.16	0.725	0.751	0.061	4.09	1.46	-0.19	0.15	-0.25
514/43	4000	0-0	0.706	0.906	1.057	69.92	0.55	0.13	0.736	0.762	0.060	4.01	1.61	-0.16	0.16	-0.27
514/42	4000	0-0	0.694	0.911	1.058	69.79	0.54	0.14	0.734	0.760	0.059	3.88	1.69	-0.16	0.17	-0.26
515/42	4000	0-0	0.686	0.915	1.059	70.05	0.53	0.14	0.737	0.763	0.058	3.79	1.65	-0.13	0.17	-0.24
514/100	5000	0-0	0.964	0.660	1.017	69.02	0.92	0.07	0.744	0.766	0.087	7.90	2.16	-0.16	0.19	-0.04
516/100	5000	0-0	0.962	0.659	1.019	69.43	0.92	0.06	0.757	0.763	0.086	7.97	2.03	-0.16	0.19	-0.06
507/100	5000	0-0	0.960	0.668	1.022	69.11	0.91	0.08	0.746	0.758	0.084	7.67	1.89	-0.15	0.18	-0.03
514/75	5000	0-0	0.958	0.672	1.021	68.95	0.90	0.18	0.744	0.763	0.085	7.62	2.09	-0.17	0.18	-0.05
516/72	5000	0-0	0.957	0.677	1.025	69.31	0.89	0.07	0.753	0.766	0.084	7.55	1.97	-0.15	0.18	-0.06

Table A1.1 Data for Straight Channel Diffuser (see page 193 for the definitions of the parameters in row 2)

I	II	III	IV	V	VI	VII	VIII	IX	X	XI	XII	XIII	XIV	XV	XVI	XVII
Data No.	N [RPM]	Inlet Flow Condition	\dot{m}_{corr} [kg/s]	π_{01} [-]	π_{03} [-]	α [°]	M_1 [-]	B_1 [-]	\hat{C}_p [-]	η_{diff} [-]	ϕ [-]	D_p [-]	α_n [-]	α_s [-]	σ_m [-]	ξ_m [-]
507/70	5000	0 - 0	0.954	0.688	1.029	63.75	0.89	0.20	0.735	0.759	0.082	7.24	1.92	-0.13	0.17	-0.33
514/60	5000	0 - 0	0.948	0.709	1.035	63.94	0.86	0.12	0.743	0.769	0.081	6.83	2.00	-0.18	0.17	-0.08
516/58	5000	0 - 0	0.946	0.718	1.040	69.22	0.85	0.07	0.746	0.774	0.080	6.69	1.90	-0.12	0.17	-0.07
514/55	5000	0 - 0	0.939	0.736	1.046	69.20	0.83	0.10	0.748	0.767	0.077	6.26	1.87	-0.08	0.17	-0.06
516/54	5000	0 - 0	0.935	0.741	1.049	69.58	0.82	0.08	0.751	0.777	0.077	6.24	1.84	-0.10	0.16	-0.08
516/53	5000	0 - 0	0.930	0.749	1.052	69.71	0.81	0.08	0.752	0.777	0.076	6.07	1.82	-0.08	0.16	-0.08
514/52	5000	0 - 0	0.928	0.751	1.052	69.89	0.81	0.08	0.747	0.773	0.075	5.99	1.87	-0.08	0.16	-0.06
507/55	5000	0 - 0	0.927	0.758	1.054	63.90	0.80	0.14	0.743	0.767	0.073	5.83	1.72	-0.01	0.16	-0.02
516/52	5000	0 - 0	0.926	0.755	1.054	70.03	0.80	0.08	0.755	0.777	0.075	5.96	1.76	-0.08	0.16	-0.11
516/51	5000	0 - 0	0.924	0.762	1.055	70.27	0.79	0.07	0.759	0.771	0.074	5.76	1.75	0.01	0.16	0.08
527/100a	6000	0 - 0	1.004	0.550	1.021	69.27	1.11	0.13	0.743	0.761	0.086	8.21	3.83	-0.07	0.27	-0.03
527/60a	6000	0 - 0	1.001	0.561	1.042	69.64	1.09	0.06	0.753	0.770	0.083	8.04	2.99	-0.16	0.24	0.01
527/60b	6000	0 - 0	0.999	0.570	1.042	69.46	1.07	0.17	0.744	0.762	0.082	7.87	2.66	-0.49	0.23	0.01
511/100	6000	0 - 0	0.999	0.581	1.020	63.72	1.15	0.19	0.731	0.747	0.090	8.93	4.06	-0.08	0.27	-0.02
527/100b	6000	0 - 0	0.997	0.590	1.021	69.19	1.14	0.07	0.745	0.760	0.086	8.61	4.24	-0.14	0.29	-0.03
515/100a	6000	0 - 0	0.993	0.599	1.017	69.31	1.13	0.05	0.746	0.763	0.088	8.78	3.50	-0.18	0.26	-0.02
515/100b	6000	0 - 0	0.993	0.601	1.018	69.55	1.12	0.04	0.751	0.768	0.088	8.56	3.55	-0.05	0.27	-0.06
511/55	6000	0 - 0	0.991	0.620	1.054	69.03	1.01	0.22	0.734	0.753	0.079	7.00	2.63	-0.09	0.23	-0.09
527/50	6000	0 - 0	0.989	0.630	1.072	69.70	0.96	0.07	0.755	0.775	0.073	6.23	2.20	-0.16	0.21	-0.07
515/60	6000	0 - 0	0.986	0.651	1.040	69.35	1.02	0.06	0.749	0.768	0.080	7.16	2.61	-0.14	0.24	-0.10
515/50	6000	0 - 0	0.978	0.673	1.068	69.79	0.95	0.06	0.764	0.784	0.073	6.16	2.08	-0.03	0.20	-0.06
527/47	6000	0 - 0	0.977	0.680	1.087	69.92	0.92	0.09	0.758	0.778	0.069	5.69	2.03	-0.16	0.19	0.04
511/47	6000	0 - 0	0.973	0.696	1.086	69.37	0.92	0.09	0.749	0.770	0.071	5.76	2.02	-0.07	0.18	-0.04
527/46	6000	0 - 0	0.971	0.701	1.092	70.20	0.90	0.10	0.755	0.775	0.067	5.39	1.92	-0.16	0.18	0.02
515/47	6000	0 - 0	0.966	0.705	1.083	70.09	0.91	0.07	0.766	0.787	0.069	5.57	1.85	-0.01	0.17	0.03
511/46	6000	0 - 0	0.962	0.709	1.089	70.35	0.90	0.09	0.765	0.786	0.069	5.56	2.01	-0.05	0.17	-0.04
517/100/1	2000	0 - 0	0.475	0.954	1.004	68.32	0.32	0.10	0.680	0.713	0.078	4.95	1.64	-0.22	0.13	-0.46
517/100/2	2000	b - 0	0.442	0.965	1.003	67.75	0.29	0.10	0.658	0.693	0.071	3.77	1.61	-0.29	0.19	-0.36
517/100/3	2000	b - 0	0.433	0.968	1.003	67.47	0.28	0.09	0.642	0.677	0.070	3.42	1.26	-0.30	0.18	-0.34
517/100/4	2000	b - 0	0.425	0.971	1.003	67.26	0.27	0.09	0.637	0.673	0.068	3.14	1.07	-0.11	0.20	-0.23
517/100/5	2000	b - 0	0.418	0.973	1.002	66.86	0.26	0.10	0.630	0.667	0.067	2.92	2.25	-0.39	0.23	-0.29
517/100/6	2000	b - 0	0.409	0.975	1.002	66.29	0.25	0.11	0.622	0.659	0.066	2.71	2.77	-0.43	0.23	-0.29
517/100/7	2000	b - 0	0.397	0.978	1.002	67.32	0.24	0.07	0.640	0.679	0.063	2.41	1.79	-0.08	0.22	-0.17
517/100/8	2000	b - 0	0.383	0.981	1.002	67.03	0.23	0.04	0.625	0.666	0.061	2.03	8.37	-0.07	0.46	-0.14

Table A1.1 Data for Straight Channel Diffuser (see page 193 for the definitions of the parameters in row 2)

I	II	III	IV	V	VI	VII	VIII	IX	X	XI	XII	XIII	XIV	XV	XVI	XVII
Data No.	N [RPM]	Inlet Flow Condition	\dot{m}_{corr} [kg/s]	π_{01}' [-]	π_{03} [-]	α [°]	M_1 [-]	B_1 [-]	\hat{C}_p [-]	η_{diff} [-]	ϕ [-]	D_p [-]	α_n [-]	α_s [-]	σ_m [-]	ξ_m [-]
517/100/9	2000	b - 0	0.372	0.983	1.001	66.29	0.22	0.06	0.619	0.660	0.059	1.82	7.03	-0.06	0.45	-0.09
517/100/10	2000	b - 0	0.353	0.986	1.002	64.88	0.21	0.13	0.594	0.636	0.056	1.53	10.46	-0.06	0.58	-0.07
518/40/1	2000	0 - 0	0.325	0.985	1.015	69.91	0.25	0.19	0.704	0.730	0.051	2.93	1.86	-0.26	0.17	-0.32
518/40/2	2000	b - s	0.298	0.991	1.012	69.22	0.21	0.16	0.689	0.717	0.047	2.11	1.87	-0.37	0.21	-0.31
518/40/3	2000	b - s	0.275	0.994	1.010	68.49	0.19	0.14	0.660	0.691	0.043	1.58	1.80	-0.03	0.22	-0.18
518/40/4	2000	b - s	0.250	0.996	1.008	68.31	0.17	0.15	0.674	0.705	0.039	1.15	6.25	-0.07	0.42	-0.09
518/40/5	2000	b - s	0.258	0.996	1.009	67.74	0.18	0.17	0.657	0.688	0.040	1.25	6.09	-0.02	0.36	-0.08
518/40/6	2000	b - s	0.242	0.997	1.008	62.79	0.15	0.25	0.543	0.583	0.038	1.01	12.40	-0.17	0.57	-0.16
531/100/4	2000	s - b	0.474	0.952	1.003	68.31	0.33	0.13	0.696	0.728	0.075	5.01	1.39	0.10	0.12	0.05
531/100/1	2000	0 - 0	0.472	0.955	1.036	68.20	0.32	0.12	0.703	0.737	0.075	5.52	1.44	-0.03	0.13	-0.47
531/100/5	2000	s - b	0.472	0.948	1.003	68.55	0.34	0.14	0.710	0.741	0.075	5.39	1.71	0.22	0.13	0.29
531/100/6	2000	s - b	0.472	0.948	1.003	68.58	0.34	0.15	0.710	0.740	0.075	5.44	1.67	0.27	0.13	0.32
531/100/2	2000	b - s	0.471	0.951	1.003	68.67	0.33	0.13	0.702	0.733	0.075	5.15	1.63	-0.37	0.16	-0.48
531/100/3	2000	b - s	0.465	0.951	1.003	68.77	0.33	0.13	0.709	0.741	0.074	5.12	1.92	-0.41	0.17	-0.42
531/52/1	2000	0 - 0	0.417	0.969	1.010	68.52	0.29	0.14	0.697	0.728	0.065	3.92	1.55	-0.09	0.15	-0.36
531/52/4	2000	s - b	0.417	0.963	1.009	68.94	0.31	0.17	0.715	0.743	0.066	4.53	1.60	0.26	0.13	0.28
531/52/5	2000	s - b	0.417	0.962	1.009	68.99	0.31	0.17	0.717	0.745	0.067	4.63	1.68	0.29	0.13	0.26
531/52/6	2000	s - b	0.410	0.965	1.009	68.69	0.30	0.17	0.707	0.735	0.064	4.26	1.90	0.32	0.15	0.20
531/52/2	2000	b - s	0.414	0.962	1.009	69.30	0.31	0.16	0.720	0.748	0.065	4.59	1.81	-0.34	0.18	-0.38
531/52/3	2000	b - s	0.406	0.963	1.010	69.50	0.30	0.17	0.723	0.750	0.064	4.46	2.16	-0.31	0.20	-0.29
531/38/4	2000	s - b	0.308	0.986	1.016	69.37	0.24	0.23	0.736	0.761	0.048	2.89	1.46	0.28	0.17	0.28
531/38/1	2000	0 - 0	0.308	0.987	1.015	69.15	0.24	0.22	0.714	0.739	0.047	2.69	1.59	-0.10	0.16	-0.28
531/38/2	2000	b - s	0.289	0.991	1.014	69.05	0.21	0.20	0.709	0.736	0.044	2.16	1.66	-0.13	0.20	-0.24
531/38/5	2000	s - b	0.282	0.992	1.013	68.23	0.21	0.22	0.689	0.715	0.043	1.99	1.80	0.36	0.18	0.15
531/38/3	2000	b - s	0.279	0.993	1.012	68.87	0.20	0.16	0.718	0.749	0.043	1.84	1.63	-0.13	0.22	-0.18
520/100/1	2000	0 - 0	0.478	0.954	1.004	65.88	0.32	0.19	0.642	0.674	0.077	4.90	1.85	-0.38	0.13	-0.60
526/100/3	2000	s - b	0.472	0.949	1.003	66.07	0.33	0.22	0.657	0.686	0.076	5.38	1.91	0.19	0.14	0.30
526/100/6	2000	s - s	0.462	0.940	1.003	67.15	0.36	0.24	0.685	0.712	0.076	6.33	1.97	-0.44	0.17	-0.42
526/100/4	2000	s - b	0.452	0.956	1.003	65.42	0.31	0.22	0.674	0.678	0.073	4.66	2.39	0.22	0.17	0.15
520/100/2	2000	b - s	0.375	0.966	1.001	66.48	0.26	0.22	0.681	0.711	0.060	3.46	3.70	-0.24	0.27	-0.15
526/100/5	2000	b - b	0.360	0.985	1.001	63.00	0.20	0.15	0.561	0.602	0.057	1.57	9.75	-0.16	0.48	0.02
520/52/1	2000	0 - 0	0.421	0.967	1.009	66.19	0.29	0.22	0.649	0.679	0.067	4.05	1.88	-0.32	0.15	-0.49
526/52/5	2000	s - s	0.407	0.956	1.009	66.49	0.32	0.28	0.708	0.733	0.066	5.21	1.42	-0.50	0.18	-0.34

Table A1.1 Data for Straight Channel Diffuser (see page 193 for the definitions of the parameters in row 2)

I	II	III	IV	V	VI	VII	VIII	IX	X	XI	XII	XIII	XIV	XV	XVI	XVII
Data No.	N [RPM]	Inlet Flow Condition	\dot{m}_{corr} [kg/s]	π_{01} [-]	π_{03} [-]	α [°]	M_1 [-]	B_1 [-]	\hat{C}_p [-]	η_{diff} [-]	φ [-]	D_p [-]	α_n [-]	α_s [-]	σ_m [-]	ξ_m [-]
526/52/3	2000	s - b	0.390	0.515	1.008	65.62	0.28	0.26	0.648	0.675	0.062	3.81	2.48	0.26	0.17	0.14
526/52/4	2000	b - b	0.340	0.407	1.005	64.61	0.21	0.18	0.618	0.653	0.054	1.86	6.57	0.15	0.38	0.04
520/52/2	2000	b - s	0.318	0.400	1.004	66.72	0.24	0.27	0.700	0.727	0.050	2.91	4.31	-0.22	0.30	-0.13
520/40/1	2000	0 - 0	0.327	0.437	1.015	66.67	0.25	0.28	0.656	0.681	0.051	2.90	1.99	-0.29	0.17	-0.38
526/40/3	2000	s - b	0.323	0.454	1.014	66.76	0.26	0.30	0.664	0.687	0.051	3.21	2.13	0.26	0.16	0.21
526/40/4	2000	b - b	0.247	0.301	1.008	63.38	0.15	0.22	0.593	0.627	0.039	0.99	9.01	-0.15	0.43	-0.07
520/40/2	2000	b - s	0.239	0.342	1.007	66.88	0.21	0.37	0.697	0.717	0.037	2.20	5.27	-0.24	0.32	-0.16
521/100/1	4000	0 - 0	0.891	0.775	1.015	67.68	0.73	0.12	0.677	0.702	0.086	7.09	1.93	-0.14	0.16	-0.26
521/100/2	4000	b - s	0.888	0.807	1.011	67.47	0.66	0.07	0.692	0.723	0.084	5.90	2.76	-0.22	0.24	-0.18
525/100/6	4000	s - s	0.876	0.766	1.015	67.82	0.74	0.15	0.697	0.720	0.085	7.46	1.49	-0.30	0.13	-0.46
525/100/7	4000	b - s	0.875	0.797	1.015	66.80	0.69	0.16	0.667	0.693	0.082	6.34	2.11	-0.26	0.17	-0.36
525/100/4	4000	s - b	0.839	0.832	1.014	66.07	0.64	0.18	0.644	0.670	0.076	5.09	2.57	0.26	0.20	0.10
525/100/5	4000	b - b	0.834	0.855	1.014	65.44	0.60	0.17	0.601	0.628	0.074	4.35	7.31	-0.07	0.40	-0.01
521/100/3	4000	s - b	0.804	0.866	1.012	65.53	0.57	0.16	0.609	0.637	0.072	3.98	7.64	0.21	0.42	0.08
525/54/4	4000	b - b	0.852	0.885	1.032	66.03	0.55	0.09	0.635	0.669	0.074	3.91	1.98	0.02	0.18	0.04
521/54/1	4000	0 - 0	0.830	0.834	1.036	67.41	0.64	0.15	0.689	0.716	0.076	5.62	1.79	-0.10	0.15	-0.27
525/54/5	4000	b - s	0.820	0.835	1.035	67.24	0.65	0.17	0.688	0.713	0.074	5.63	1.91	-0.29	0.17	-0.33
525/54/6	4000	s - b	0.818	0.835	1.035	67.04	0.65	0.18	0.690	0.715	0.074	5.62	1.94	0.17	0.15	0.17
525/54/3	4000	s - b	0.777	0.875	1.032	66.16	0.58	0.20	0.662	0.689	0.068	4.31	2.50	0.24	0.19	0.10
521/54/2	4000	b - s	0.742	0.850	1.028	67.98	0.60	0.18	0.700	0.724	0.067	4.93	2.91	-0.13	0.27	-0.09
525/50/7	4000	s - s	0.800	0.852	1.044	67.21	0.63	0.18	0.689	0.714	0.071	5.27	1.70	-0.23	0.15	-0.36
521/50/1	4000	0 - 0	0.796	0.858	1.043	67.43	0.62	0.16	0.687	0.713	0.071	5.07	1.77	-0.07	0.16	-0.26
525/50/6	4000	s - b	0.786	0.865	1.044	67.00	0.60	0.19	0.685	0.711	0.069	4.85	1.87	0.13	0.15	0.18
525/50/5	4000	b - s	0.777	0.868	1.042	67.16	0.60	0.18	0.679	0.705	0.068	4.73	2.57	-0.28	0.23	-0.22
525/50/3	4000	s - b	0.775	0.869	1.042	66.81	0.59	0.20	0.681	0.707	0.068	4.70	2.15	0.14	0.17	0.10
525/50/4	4000	b - b	0.747	0.898	1.039	65.33	0.54	0.18	0.669	0.697	0.064	3.73	1.96	0.045	0.18	0.06
521/50/2	4000	b - s	0.710	0.866	1.034	68.21	0.58	0.20	0.703	0.727	0.063	4.56	2.97	-0.13	0.28	-0.09
518/100/1	5000	0 - 0	0.976	0.659	1.018	69.74	0.92	0.04	0.739	0.761	0.087	7.95	2.04	-0.11	0.18	-0.04
518/100/2	5000	b - 0	0.975	0.729	1.020	68.78	0.82	0.05	0.715	0.740	0.081	5.94	1.93	-0.08	0.19	-0.20
518/100/3	5000	b - 0	0.969	0.752	1.019	68.55	0.79	0.06	0.698	0.723	0.078	5.32	1.81	-0.09	0.20	-0.21
518/100/4	5000	b - 0	0.966	0.767	1.019	68.32	0.77	0.06	0.689	0.715	0.077	4.94	1.68	-0.08	0.20	-0.19
518/100/5	5000	b - 0	0.959	0.778	1.018	68.28	0.75	0.06	0.678	0.704	0.075	4.67	1.70	-0.15	0.20	-0.21
518/100/6	5000	b - 0	0.953	0.794	1.018	68.13	0.73	0.07	0.665	0.692	0.073	4.27	1.65	-0.14	0.21	-0.19

Table A1.1 Data for Straight Channel Diffuser (see page 193 for the definitions of the parameters in row 2)

I	II	III	IV	V	VI	VII	VIII	IX	X	XI	XII	XIII	XIV	XV	XVI	XVII
Data No.	N [RPM]	Inlet Flow Condition	\dot{m}_{corr} [kg/s]	π_{01} [-]	π_{03} [-]	α [°]	M_1 [-]	B_1 [-]	\hat{C}_p [-]	η_{diff} [-]	ϕ [-]	D_p [-]	α_n [-]	α_s [-]	σ_m [-]	ξ_m [-]
518/55/1	5000	0 - 0	0.929	0.745	1.052	70.16	0.81	0.08	0.747	0.770	0.075	6.15	1.85	-0.07	0.17	-0.07
518/55/2	5000	b - 0	0.918	0.792	1.053	69.45	0.75	0.08	0.731	0.755	0.071	4.99	2.14	-0.11	0.21	-0.14
518/55/3	5000	b - 0	0.911	0.812	1.052	69.13	0.72	0.08	0.725	0.751	0.069	4.48	2.03	-0.14	0.22	-0.15
518/55/4	5000	b - 0	0.906	0.830	1.050	68.87	0.70	0.07	0.709	0.735	0.067	4.05	1.98	-0.15	0.23	-0.14
518/55/5	5000	b - 0	0.897	0.846	1.049	68.77	0.67	0.07	0.696	0.723	0.066	3.68	1.96	-0.13	0.24	-0.12
518/55/6	5000	b - 0	0.886	0.857	1.048	68.80	0.65	0.07	0.683	0.710	0.064	3.42	2.03	-0.11	0.25	-0.11
530/100/1	5000	0 - 0	0.968	0.655	1.020	69.89	0.93	0.06	0.740	0.781	0.084	7.95	2.08	-0.23	0.18	-0.08
530/100/3	5000	b - s	0.966	0.735	1.020	68.59	0.82	0.08	0.698	0.721	0.078	5.67	1.96	-0.27	0.21	-0.23
530/100/7	5000	s - b	0.966	0.727	1.020	68.60	0.83	0.08	0.705	0.729	0.078	5.90	2.98	0.39	0.21	0.19
530/100/5	5000	b - s	0.980	0.797	1.020	68.02	0.73	0.07	0.654	0.680	0.072	4.15	1.59	-0.16	0.21	-0.21
530/100/6	5000	s - b	0.965	0.754	1.020	68.21	0.79	0.08	0.692	0.717	0.076	5.18	2.81	0.33	0.21	0.15
530/100/4	5000	b - s	0.965	0.785	1.020	68.07	0.74	0.07	0.665	0.690	0.073	4.43	1.64	-0.16	0.20	-0.22
530/100/2	5000	b - s	0.965	0.675	1.020	69.48	0.90	0.07	0.740	0.761	0.083	7.36	2.08	-0.18	0.22	-0.17
530/59/3	5000	b - s	0.958	0.772	1.040	69.64	0.77	0.08	0.708	0.733	0.074	5.13	1.87	-0.10	0.19	-0.20
530/59/7	5000	s - b	0.956	0.719	1.039	69.62	0.84	0.07	0.748	0.771	0.079	6.52	2.46	0.41	0.18	0.18
530/59/2	5000	b - s	0.956	0.746	1.040	69.03	0.81	0.07	0.725	0.749	0.076	5.80	2.02	-0.09	0.20	-0.17
530/59/6	5000	s - b	0.956	0.759	1.040	68.68	0.79	0.08	0.725	0.750	0.075	5.44	2.53	0.31	0.19	0.12
530/59/1	5000	0 - 0	0.955	0.712	1.039	69.23	0.86	0.08	0.747	0.770	0.079	6.72	1.85	-0.23	0.16	-0.10
530/59/4	5000	b - s	0.953	0.785	1.039	68.52	0.75	0.08	0.698	0.724	0.073	4.81	1.80	-0.12	0.20	-0.21
530/59/5	5000	b - s	0.950	0.800	1.038	68.37	0.73	0.08	0.686	0.712	0.071	4.43	1.75	-0.19	0.21	-0.22
530/52/2	5000	b - s	0.931	0.791	1.057	69.12	0.76	0.08	0.723	0.748	0.071	5.02	2.14	-0.14	0.28	-0.18
530/52/1	5000	0 - 0	0.930	0.758	1.057	69.37	0.80	0.09	0.752	0.775	0.073	5.82	1.76	-0.14	0.28	-0.10
530/52/5	5000	s - b	0.929	0.785	1.056	69.03	0.76	0.08	0.739	0.764	0.071	5.15	2.28	0.24	0.48	0.09
530/52/3	5000	b - s	0.925	0.806	1.055	68.95	0.73	0.08	0.711	0.736	0.069	4.62	2.06	-0.14	0.28	-0.17
530/52/6	5000	s - b	0.923	0.786	1.056	68.92	0.76	0.09	0.738	0.763	0.070	5.09	2.51	0.30	0.59	0.12
530/52/4	5000	b - s	0.917	0.824	1.054	68.73	0.71	0.09	0.696	0.722	0.067	4.18	1.89	-0.20	0.40	-0.19
528/100/7	6000	b - b	1.049	0.694	1.024	68.98	0.90	0.02	0.692	0.715	0.075	4.86	2.94	-0.18	0.23	-0.20
523/100/6	6000	b - b	0.996	0.535	1.019	68.60	1.14	0.07	0.716	0.732	0.089	8.83	4.50	-0.02	0.29	-0.07
523/100/4	6000	s - b	1.033	0.646	1.022	67.78	0.97	0.08	0.689	0.709	0.080	5.93	3.60	0.22	0.24	0.10
528/100/3	6000	s - b	1.030	0.633	1.022	68.92	0.99	0.05	0.694	0.714	0.079	6.16	3.87	0.33	0.25	0.18
528/100/6	6000	b - b	1.027	0.594	1.022	69.61	1.04	0.02	0.737	0.756	0.084	7.18	3.73	-0.18	0.26	-0.02
528/100/9	6000	b - 0	1.019	0.589	1.022	69.35	1.06	0.04	0.729	0.750	0.084	7.30	4.00	-0.16	0.29	-0.08
528/100/8	6000	0 - 0	1.008	0.555	1.021	69.70	1.11	0.04	0.743	0.760	0.086	8.22	3.76	-0.10	0.27	-0.03

Table A1.1 Data for Straight Channel Diffuser (see page 193 for the definitions of the parameters in row 2)

I	II	III	IV	V	VI	VII	VIII	IX	X	XI	XII	XIII	XIV	XV	XVI	XVII
Data No.	N [RPM]	Inlet Flow Condition	\dot{m}_{corr} [kg/s]	π_{01} [-]	π_{03} [-]	α [°]	M_1 [-]	B_1 [-]	\hat{C}_p [-]	η_{diff} [-]	φ [-]	D_p [-]	α_n [-]	α_s [-]	σ_m [-]	ξ_m [-]
523/100/1	6000	0 - 0	0.996	0.535	1.019	68.60	1.14	0.08	0.719	0.735	0.089	8.83	4.51	-0.01	0.29	-0.07
528/100/1	6000	0 - 0	0.994	0.537	1.020	69.27	1.14	0.06	0.723	0.739	0.087	8.66	4.36	-0.19	0.29	-0.01
528/100/2	6000	b - s	0.983	0.589	1.020	68.81	1.05	0.09	0.714	0.731	0.080	7.22	4.16	-0.28	0.32	-0.11
523/100/3	6000	b - s	0.976	0.590	1.019	68.04	1.04	0.10	0.726	0.744	0.082	7.31	4.40	-0.30	0.33	-0.10
523/100/2	6000	b - s	0.973	0.588	1.019	68.03	1.04	0.11	0.723	0.740	0.082	7.36	4.56	-0.20	0.33	-0.07
523/100/5	6000	s - s	0.960	0.538	1.017	68.01	1.12	0.12	0.727	0.743	0.086	8.73	5.24	-0.33	0.33	-0.16
528/100/5	6000	s - s	0.940	0.564	1.018	68.90	1.08	0.12	0.724	0.740	0.080	7.92	4.43	-0.42	0.29	-0.21
528/100/4	6000	s - s	0.933	0.544	1.018	69.01	1.11	0.12	0.725	0.740	0.080	8.44	4.67	0.35	0.30	0.18
524/55/5	6000	b - 0	1.031	0.727	1.057	67.52	0.88	0.12	0.675	0.696	0.071	4.70	2.52	-0.14	0.26	-0.10
529/55/8	6000	b - b	1.030	0.720	1.059	69.21	0.88	0.03	0.718	0.742	0.072	4.87	2.79	-0.13	0.24	-0.05
529/55/3	6000	b - 0	1.030	0.721	1.059	68.88	0.89	0.07	0.689	0.710	0.071	4.79	2.29	-0.11	0.25	-0.11
524/55/3	6000	b - s	1.025	0.664	1.058	68.28	0.97	0.10	0.713	0.733	0.076	6.05	3.01	-0.08	0.27	-0.07
524/55/7	6000	b - b	1.024	0.765	1.056	67.14	0.81	0.10	0.690	0.716	0.068	4.01	2.45	-0.04	0.21	-0.07
529/55/4	6000	s - b	1.011	0.752	1.056	68.67	0.84	0.07	0.688	0.711	0.067	4.18	3.19	0.28	0.22	0.15
524/55/6	6000	s - b	1.009	0.762	1.054	66.91	0.82	0.13	0.674	0.697	0.067	4.04	2.99	0.23	0.21	0.10
529/55/6	6000	0 - b	1.004	0.810	1.055	68.11	0.75	0.07	0.668	0.693	0.063	3.19	2.72	-0.20	0.22	-0.08
529/55/9	6000	0 - 0	0.999	0.628	1.056	69.85	1.00	0.05	0.750	0.769	0.077	6.86	2.50	-0.24	0.22	-0.05
529/55/1	6000	0 - 0	0.986	0.620	1.054	70.08	1.01	0.06	0.759	0.777	0.076	6.94	2.77	-0.16	0.23	-0.06
524/55/2	6000	b - s	0.986	0.622	1.054	68.84	1.01	0.10	0.750	0.769	0.077	6.97	2.66	-0.03	0.24	-0.09
524/55/1	6000	0 - 0	0.985	0.620	1.053	68.88	1.01	0.10	0.750	0.769	0.077	7.02	2.87	0.02	0.25	0.07
529/55/5	6000	s - 0	0.979	0.600	1.053	70.54	1.04	0.05	0.779	0.797	0.078	7.49	2.94	-0.32	0.23	-0.01
524/55/4	6000	b - s	0.972	0.644	1.051	68.60	0.97	0.12	0.741	0.760	0.074	6.42	3.56	-0.08	0.32	-0.02
529/55/2	6000	b - s	0.970	0.638	1.052	70.43	0.98	0.07	0.768	0.787	0.074	6.51	3.52	-0.15	0.31	-0.05
529/55/7	6000	s - s	0.914	0.582	1.046	70.23	1.05	0.11	0.765	0.781	0.074	7.78	5.01	-0.38	0.32	-0.21
524/55/8	6000	s - s	0.913	0.591	1.045	68.81	1.04	0.16	0.763	0.779	0.073	7.58	5.30	0.32	0.33	0.17

Table A1.1 Data for Straight Channel Diffuser (see page 193 for the definitions of the parameters in row 2)

Appendix 2

Mass Flow Continuity Control

Figure A2.1 shows a comparison between the mass flow rate as calculated by integration across the diffuser inlet (see Eq. 3.12) and the mass flow rate as measured by venturi flow meter at different corrected constant impeller speeds.

Consistency between the calculated and measured mass flow rates was within $\pm 5\%$ in all of the operating range of the impeller without injection/suction, except for the impeller speeds 2000 and 6000 RPM where the deviation went up to $\pm 10\%$ (Figure A2.1).

The causes of this deviation could be:

- The accuracy of mass flow measurements using venturi flow meter decreases at low impeller speeds, such as 2000 RPM,
- The mass flow was calculated from the traverse probe data. This data include only 15 points across the diffuser depth, b ,
- Temperature, T_t , is not uniform across the diffuser inlet, and
- For the high speed case ($N = 6000$ RPM) a Mach number effect is possible.

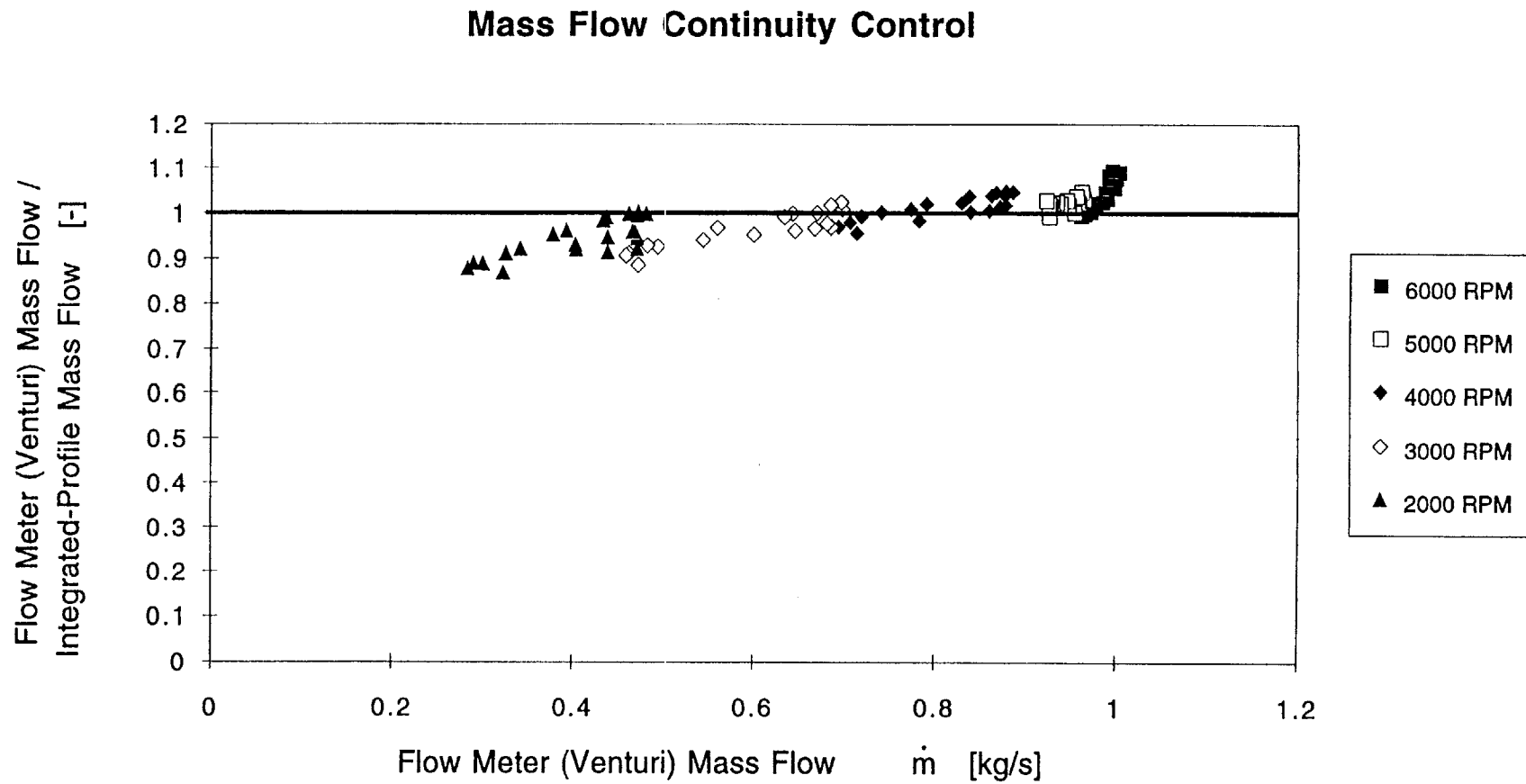


Figure A 2.1 Mass flow continuity control for different corrected impeller speeds

Appendix 3

Circumferential Distortion at the Straight Channel Diffuser Inlet and Exit

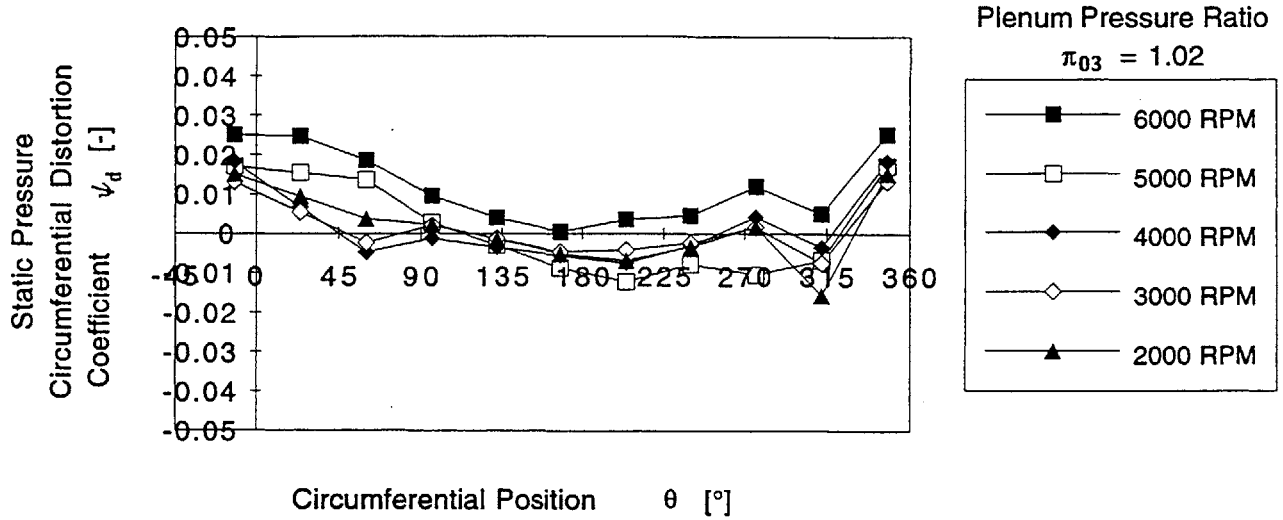
The main objective of this research is to investigate the effect of axial distortion of the diffuser inlet flow field on straight channel diffuser performance and operating range. Therefore, the diffuser inlet flow field should ideally be axisymmetric. This allows the parameters of the straight channel diffuser inlet flow field to be quantified by an axial traverse of the diffuser inlet at one circumferential position.

The axisymmetry of the flow can be addressed by comparing the pressure measured at the diffuser inlet and exit circumferences. The circumferential non-uniformity was measured by using circumferentially distributed static pressure wall taps in the vaneless space and on the diffuser exit radius at both front and rear walls (see Fig. 3.6a and b). A non-dimensional, local pressure distortion coefficient (see Eq. 3.45) was used as a measure of the circumferential static pressure variation. Figures A 3.1 and A 3.2 show the static pressure circumferential distortion coefficient at the impeller (Fig. A 3.1) and diffuser exits (Fig. A 3.2) on the rear and front walls.

According to Figures A 3.1a and b, maximum circumferential variation of the static pressure at the impeller exit over the entire operating range of the impeller without injection/suction was 2% of the diffuser inlet dynamic pressure, except for the rear wall case at the highest impeller speed, 6000 RPM where the maximum distortion was 3%. This indicates a slightly higher axial asymmetry of the flow between rear and front walls at the diffuser inlet for this highest investigated impeller speed. The circumferential static pressure variation became smaller at the diffuser exit (1% at least) at both walls (Fig. A 3.2a and b).

a)

Static Pressure Circumferential Distortion at Impeller Exit (Rear Wall)



b)

Static Pressure Circumferential Distortion at Impeller Exit (Front Wall)

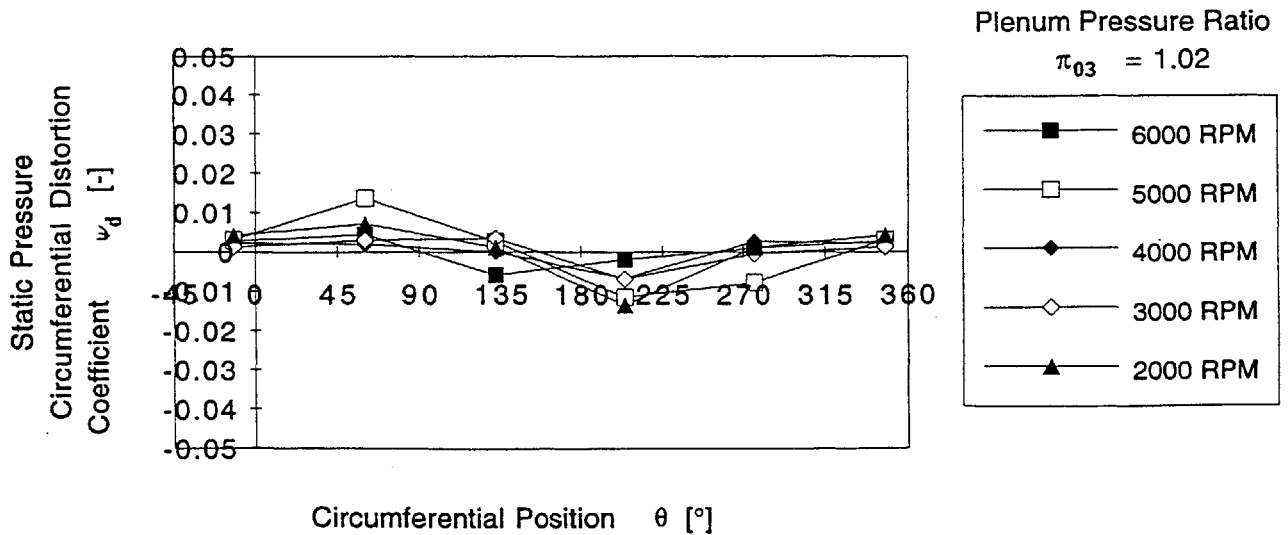
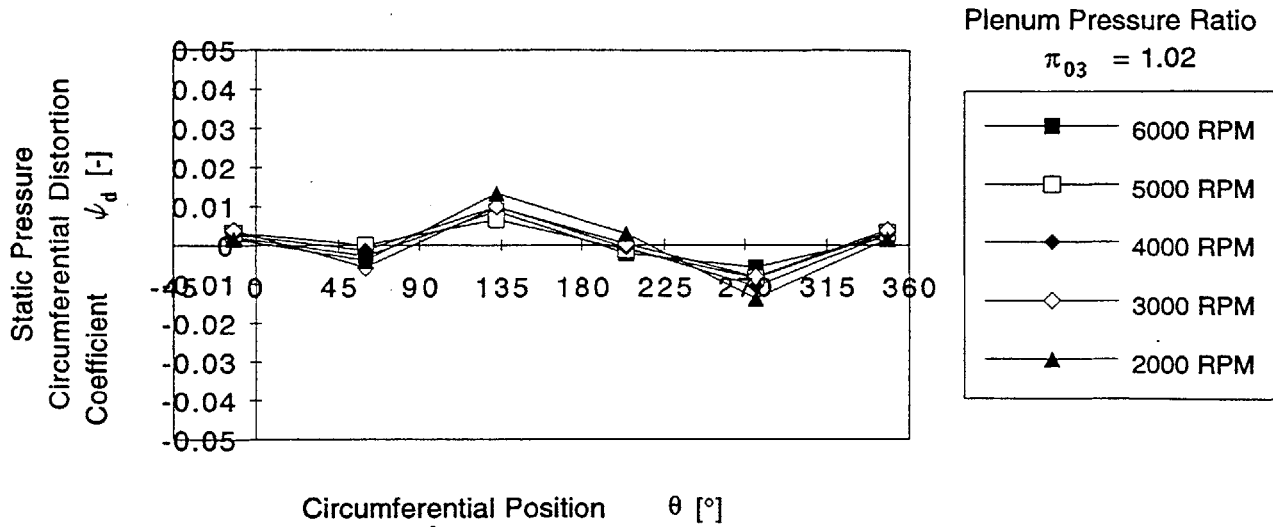


Figure A 3.1 Static pressure circumferential distribution at impeller exit at (a) rear wall and (b) front wall for different corrected impeller speeds

a)

Static Pressure Circumferential Distribution at Diffuser Exit (Rear Wall)



b)

Static Pressure Circumferential Distortion at Diffuser Exit (Front Wall)

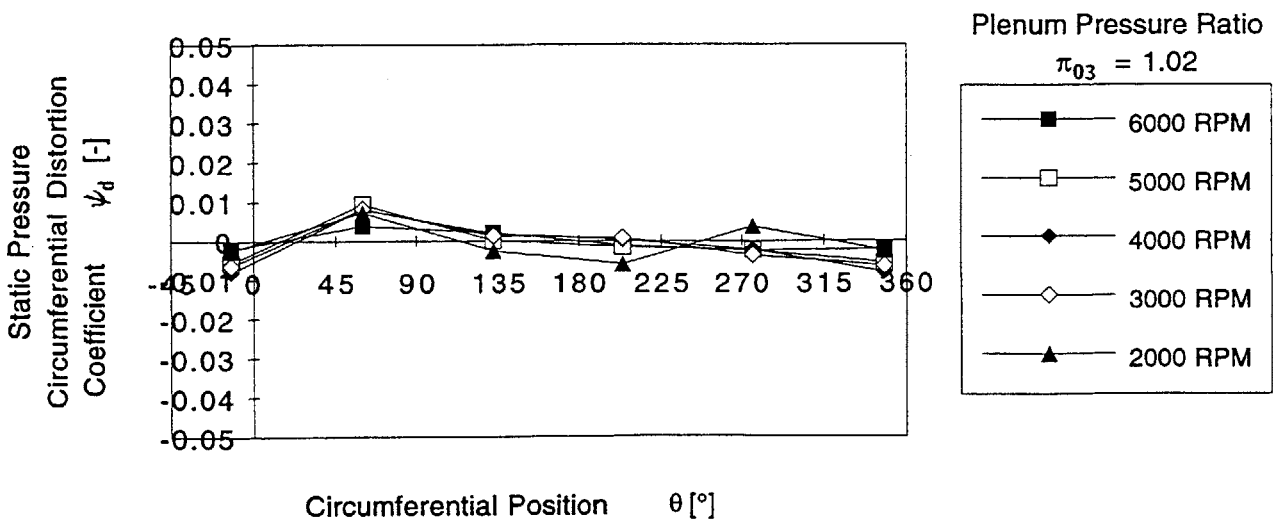


Figure A 3.2 Static pressure circumferential distribution at diffuser exit at (a) rear wall and (b) front wall for different corrected impeller speeds

Appendix 4

Influence of Throat Blockage on Radial Diffuser Performance

The dependence of overall radial diffuser and channel part performance on fluid dynamic blockage is discussed in this section. Blockage is generally considered to be an important factor in determining pressure recovery for a radial diffuser based on information from single channel diffuser investigations, where it is found that pressure recovery decreases as inlet blockage increases. An important difference between a single channel diffuser and a radial diffuser is that the former does not have an entry region (from the impeller exit to the throat), whereas the latter does.

The flow characteristics of a radial diffuser can be understood using two diffusers in series: the inlet region (vaneless diffuser and quasi-vaneless space) and the following channel part. The inlet region, where a large part of the diffuser pressure rise (ca. 40% of the overall diffuser pressure recovery) takes place (see Fig. 4.9 or 4.10), is also a critical region regarding the stability of the stage. The pressure recovery in this region is considered to be the critical controlling parameter for stage stall or surge by many investigators.

The region between impeller exit and diffuser throat is widely regarded as a complex flow field, which involves shock structures at sufficiently high Mach numbers. Various approaches have been used to relate conditions between impeller exit and diffuser throat (Japikse [1984a]). One popular approach is to correlate the development of boundary layer displacement thickness (blockage) with pressure recovery coefficient between the impeller exit and the diffuser throat. Examples of measured blockage at throat versus pressure recovery coefficient from the diffuser leading edge and/or impeller exit to the diffuser throat, for different radial diffuser types, can be found in several publications (Dean et al. [1970], Kenny [1972], Dean [1973], Conrad et al. [1980], Japikse [1982], Rodgers [1982a], Kano et al. [1982], Stein [1986], Clements [1987], Hunziker & Gyarmathy [1993]). An example is given in Figure A 4.1. For the

correlation between throat blockage and pressure recovery at the diffuser inlet region, boundary-layer calculation models also exist as can be found in Kenny [1972], Conrad et al. [1980], Herbert [1980], Kano et al. [1982], Clements [1987]. These calculations are in good agreement with the measured correlation between throat blockage and pressure recovery at the diffuser inlet region. Frigne & Van Den Braembussche [1978] adopted the empirical correlation of Kenny [1972] to calculate the throat blockage directly from the predicted static pressure recovery between the diffuser leading edge and the throat. Only Japikse [1987] and Japikse & Osborne [1986b] found a different trend from the general above-stated one in some investigated radial diffuser-impeller configurations. (The authors explained this odd trend by either a special impeller-diffuser interaction or a possible flow separation region at the diffuser inlet occurred in these studies).

Correlations such as Figure A 4.1 have been used with some success, so that it appears that the geometrical parameters such as vaneless space radius ratio or vane leading edge geometry and unsteady impeller exit flow, velocity distribution, and mixing process in the diffuser inlet region do not have strong influences. However, the correlations are based on a limited amount of data and must, therefore, be applied with caution (Japikse [1987]). As an example, the pressure recovery at the diffuser inlet region versus throat blockage correlation diagrams by Kenny [1972] (Figure A 4.2) showed an influence of diffuser inlet Mach number and diffuser type (pipe diffuser and cambered vane diffuser). To take impeller exit flow into consideration Kenny later correlated the throat blockage with leading edge incidence angle for pipe diffusers. (Leading edge incidence angle is the difference of mean flow angle and the stagger angle of the bisector of the leading edge wedge of the pipe diffuser at the apex of the intersection scallop). He observed that throat blockage increased with increasing diffuser inlet flow angle.

For centrifugal compressor design, the blockage has been considered in connection with the mass flow capacity of the throat of the vaned diffuser, but it is also believed that the throat blockage has another influence on the performance of the channel diffuser part. At high mass flow rates (near choke) there is an acceleration of the flow between impeller exit and diffuser throat (see Fig. 4.9a and b), the boundary-layer development at the diffuser

inlet region is small, and there is low blockage at the diffuser throat. At low and intermediate mass flow rates the diffuser inlet region has an increasing pressure, boundary-layer growth, and therefore high blockage levels at diffuser throat.

According to single channel diffuser investigations, in addition to the diffuser geometry, inlet blockage is an essential fluid dynamic parameter governing diffuser performance. Extensive experimental data of flat and conical channel diffuser performance have been published by Runstadler et al. [1975]. Runstadler et al. [1975] claimed that the single most important parameter governing the channel diffuser recovery is the boundary layer blockage at the throat. These results are today often used for diffuser design. A precise throat blockage prediction, however, is necessary for a reasonable application of these data. This is particularly unfortunate to the compressor performance prediction analysis because the blockage is particularly controlled by the impeller discharge flow and mixing process at the diffuser inlet region.

Figure A 4.3 from Runstadler et al. [1975] shows the dependence of single channel diffuser pressure recovery on inlet blockage. A 10% increase in inlet blockage causes a 20 - 25% decrease of the diffuser pressure recovery. (It should be noted that the diffuser pressure recovery coefficient of Runstadler is based on the measured diffuser inlet centerline total pressure, not on an inlet traverse of total pressure. If one calculates the pressure recovery coefficient based on mass-averaged diffuser inlet total pressure, the dependence of pressure recovery on inlet blockage is much less according to Dong's [1996] measurements). If there is a large pressure rise between the impeller exit and the diffuser throat there will be a large blockage at the diffuser throat; if there is a large blockage at the throat there will be only a small pressure rise in the channel diffuser downstream of the throat. Sovran & Klomp [1967] considered the blockage effect to be the principal cause for poor diffuser performance rather than the increase in losses associated with flow separation and mixing of the flow.

The relation between throat blockage and pressure recovery in the channel part of the radial diffuser has been investigated by several researchers, first by Kenny [1972], with the objective of demonstrating that the performance of a

centrifugal compressor diffuser could be related to single channel diffusers. Kenny's results and those from some of the radial diffuser investigations (Dean et al. [1970], Dean & Young [1977], Verdonk [1978b], Kenny [1984], Clements [1987], Stein [1986], Japikse & Osborne [1986b]) show similar trends for the channel part of radial diffuser to single channel diffusers. The level of channel pressure recovery found in radial diffuser studies, is approximately the same level observed in single channel diffuser performance data.

One difficulty in direct comparison is that the geometrical parameters and blockage levels of the single channel diffuser data do not match with corresponding values of typical centrifugal compressor diffusers. In Figures A 4.4, A 4.5 and A 4.6 small blockage values for centrifugal compressor diffusers belong to the operation points with high mass flow rates. To apply single channel diffuser data to centrifugal compressor diffusers, Herbert [1980] derived appropriate corrections for the diffuser area ratio, AR, length, LWR, aspect ratio, AS, and throat blockage to produce corresponding values for a "two dimensional equivalent" diffuser. Some of the presented data in the open literature imply that blockage level at the throat is critical in determining the pressure rise in the diffuser channel. As an example, the results of Stein [1986] in Figure A 4.4b indicated that increasing blockage at the diffuser throat results in a pressure recovery decrease in the following channel part.

Other investigations, however, (e.g. some diffusers investigated by Japikse & Osborne [1986b], Clements [1987], and Hunziker [1993]) do not show similar behavior to the single channel diffuser data. In these examples, the pressure recovery at the channel part of the diffuser is nearly independent of the throat blockage and even increases slightly as the blockage increases (Figures A 4.4a, A 4.5 and some diffusers in Figure A 4.6). An explanation for this different behavior, by Hunziker [1993], is that the pressure recovery in the diffuser channel part is not only due to diffusion process but also to the influence of diffuser blades on the flow field (Hunziker [1993] used in his investigations cambered vane diffusers with blades). There is a pressure difference between pressure and suction sides of the blades and, hence, diffuser blades in the channel diffuser part influence the diffuser flow field and pressure recovery. Japikse tried to explain this deviation from the trend observed by single

channel diffuser investigations with a possible influence of diffuser inlet velocity profile and turbulence intensity. Both fluid dynamic parameters are considerably different in centrifugal compressor diffusers than the ones in the single channel diffuser investigations. These parameters may be responsible for maintaining high levels of channel pressure recovery, even at fairly high levels of blockage at diffuser throat according to Japikse.

In most cases calculation of the radial diffuser channel pressure recovery (from diffuser throat to diffuser exit) is based on the measured total pressure at diffuser inlet rather than the diffuser throat (e.g. Clements [1987], Clements & Artt [1987], Hunziker [1993]). This assumes that the throat centerline total pressure is the same as the inlet centerline total pressure. However, the mass-averaged total pressure at the diffuser throat is not equal to the mass-averaged total pressure at the diffuser inlet. For example, in the study by Dolan & Runstadler [1973] losses in the order of 20 - 30% of the impeller exit kinetic energy were reported to have been experienced between the impeller exit and diffuser throat. Some part of these losses was in the vaneless space and another part was due to the shock structure which existed at the vane leading edge, but nevertheless a non-negligible portion of the loss between the diffuser inlet and throat occurred due to the mixing process of the flow. Data regarding the loss process at the diffuser inlet region are limited. Japikse & Osborne [1986b] also observed substantial losses (20 - 25%) in total pressure between impeller exit and diffuser throat. These losses are more than one would anticipate from simple boundary-layer calculations. Therefore, to calculate pressure recovery of the channel part the determination of the mass-averaged total pressure at the diffuser throat is necessary. Japikse & Osborne [1986b] measured the throat total pressure, but they did not measure the impeller exit total pressure. (Kano et al. [1982] and Rodgers [1982a] showed data for the throat stagnation pressure, but they did not have traverse measurements and, therefore, could not provide mass-averaged values of diffuser throat pressure).

In the present set of experiments, we measured the mass-averaged total pressure at the diffuser inlet, but not at the diffuser throat. The throat total pressure is a necessary input to calculate pressure recovery for channel part of the diffuser. At the diffuser throat, we have experimental information about

static pressure, mass flow, geometrical area and total temperature. The throat blockage can be estimated on a basis of the empirical correlation between throat blockage, B_{th} , and pressure recovery coefficient, C_{p1-th} , from leading edge to throat, adopting the approach which was first suggested by Kenny [1972] and later confirmed by other investigators for different radial diffuser geometries (Figure A 4.1). The pressure recovery coefficient from the diffuser leading edge (1) to the throat (th) is defined as:

$$\hat{C}_{p1-th} = \frac{P_{sth} - P_{s1}}{\hat{P}_{t1} - P_{s1}} \quad (A 4.1)$$

Figure A 4.7 shows throat blockage versus pressure recovery coefficient from diffuser leading edge to throat for straight channel diffusers. The correlation curves are taken from Kano et al. [1982], Dean [1974] and Rodgers [1993], which are all straight channel diffuser investigations. Although the trends are similar, there are quantifiable differences between the results of the three investigations. From this figure we have chosen a correlation, whose diffuser geometry is most similar to our investigated straight channel diffuser. A curve fit for the experimental correlation between throat blockage and C_{p1-th} has the following form:

$$B_{th} = 5.891C_{p1-th}^4 - 0.642C_{p1-th}^3 - 0.356C_{p1-th}^2 + 0.12C_{p1-th} + 0.087 \quad (A 4.2)$$

Using the experimental data for C_{p1-th} and the curve fit (Eq. A 4.2) we can calculate throat blockage, B_{th} . The throat blockage is defined as:

$$B_{th} = 1 - \frac{\dot{m}_{venturi}}{\dot{m}_{throat ideal}} \quad (A 4.3)$$

We can calculate $\dot{m}_{throat ideal}$, as we know the measured venturi mass flow. $\dot{m}_{throat ideal}$ is a function of total pressure, P_{tth} , and Mach number, M_{th} , at the throat:

$$\dot{m}_{throat\ ideal} = \sqrt{\frac{\gamma}{R}} \frac{P_{tth}}{T_{tth}} \frac{M_{tth} A_{th}}{\left(1 + \frac{\gamma-1}{2} M_{tth}^2\right)^{\frac{\gamma+1}{2(\gamma-1)}}} \quad (\text{A 4.4})$$

Using the following equation:

$$\frac{P_{tth}}{P_{sth}} = \left(1 + \frac{\gamma-1}{2} M_{tth}^2\right)^{\frac{\gamma}{\gamma-1}} \quad (\text{A 4.5})$$

the total pressure at the diffuser throat, P_{tth} , can be calculated.

We will show the influence of throat blockage on straight channel diffuser channel pressure recovery in Figures A 4.8 and A 4.9 and will also compare straight channel diffuser channel part pressure recovery with single channel diffuser data from Reneau et al. [1967] and Runstadler et al. [1975]. In Figure A 4.8 the pressure recovery coefficient (from the throat to the diffuser exit), $C_{p_{th-2}}$, for the channel part of the straight channel diffuser is calculated based on the total pressure at diffuser inlet, P_{t1} , assuming the total pressures at the diffuser inlet and throat are equal. This calculation method for diffuser channel pressure recovery is mostly used in the open literature.

$$\hat{C}_{p_{th-2}} = \frac{P_{s2} - P_{sth}}{\hat{P}_{t1} - P_{sth}} \quad (\text{A 4.6})$$

Figure A 4.8 shows that the pressure recovery coefficient of the straight channel diffuser channel part as defined in this manner is nearly constant and does not depend on the throat blockage. This trend shown is similar to the ones observed by Clements [1987], Hunziker [1993] and Japikse & Osborne [1987b] (see Figures A 4.4a, A 4.5 and 4.6), but does not conform to either single channel diffuser or to some other radial diffuser investigations.

Figure A 4.9 is a similar plot to Figure A 4.8, but the pressure recovery coefficient of the channel part, in this case, is based not on the total pressure at the diffuser inlet but on the calculated total pressure at throat (Eq. A 4.5) . Using the calculated throat total pressure, the pressure recovery coefficient of

the channel part, i.e. the part from the throat to the exit of the diffuser is defined as:

$$\hat{C}_{P_{th-2}} = \frac{P_{s2} - P_{sth}}{\hat{P}_{th} - P_{sth}} \quad (\text{A } 4.7)$$

Figure A 4.9, which gives $C_{p_{th-2}}$ versus throat blockage, shows that the trend of the results agrees with that for the single channel diffuser data, particularly with the single channel diffuser data of Runstadler et al. [1975]. When throat blockage increases, the pressure recovery coefficient of the channel part decreases. It must be mentioned that the calculation of $C_{p_{th-2}}$ using the throat total pressure was based on one experimental correlation in Figure A 4.7, in which case the diffuser geometry is the most similar to the one investigated in this study. Using a different curve from this figure will yield different values for the throat blockage and consequently different values for $C_{p_{th-2}}$.

Another question is how the diffuser throat blockage is related to diffuser inlet blockage and inlet flow parameters. A comparison of the inlet blockage to throat blockage shows that throat blockage increases with increasing inlet blockage, but the correlation between the two parameters for the investigated straight channel diffuser is poor. The relation of the inlet flow field distortion parameters to the throat blockage is also weak. In Figure A 4.10 the mass-averaged pressure recovery coefficient from leading edge to throat is plotted versus the momentum averaged diffuser inlet flow angle. The pressure recovery from leading edge to throat tends to increase with increasing inlet flow angle, but there is a big scatter around the main trend. The scatter is somewhat smaller for the data points without injection/suction. Since the throat blockage increases with the pressure recovery from the leading edge to the throat, it can be concluded that the throat blockage of a straight channel diffuser depends mainly on momentum averaged inlet flow angle, rather than inlet blockage.

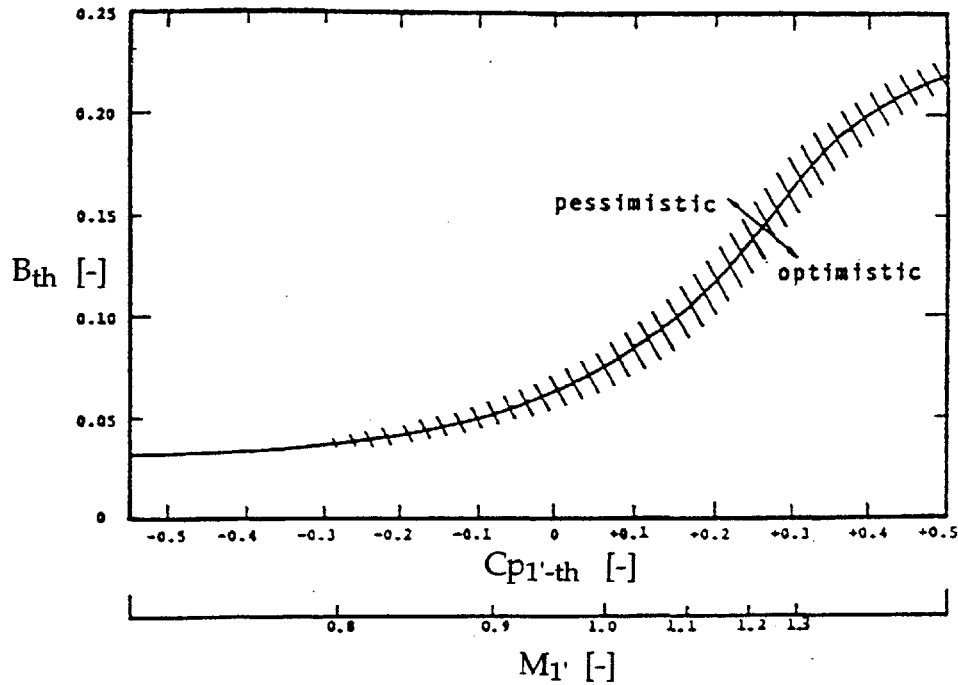


Figure A 4.1 Diffuser throat blockage, B_{th} , versus pressure rise coefficient from impeller exit to throat, $C_{p1'-th}$, (Kenny [1972] and Dean [1973])

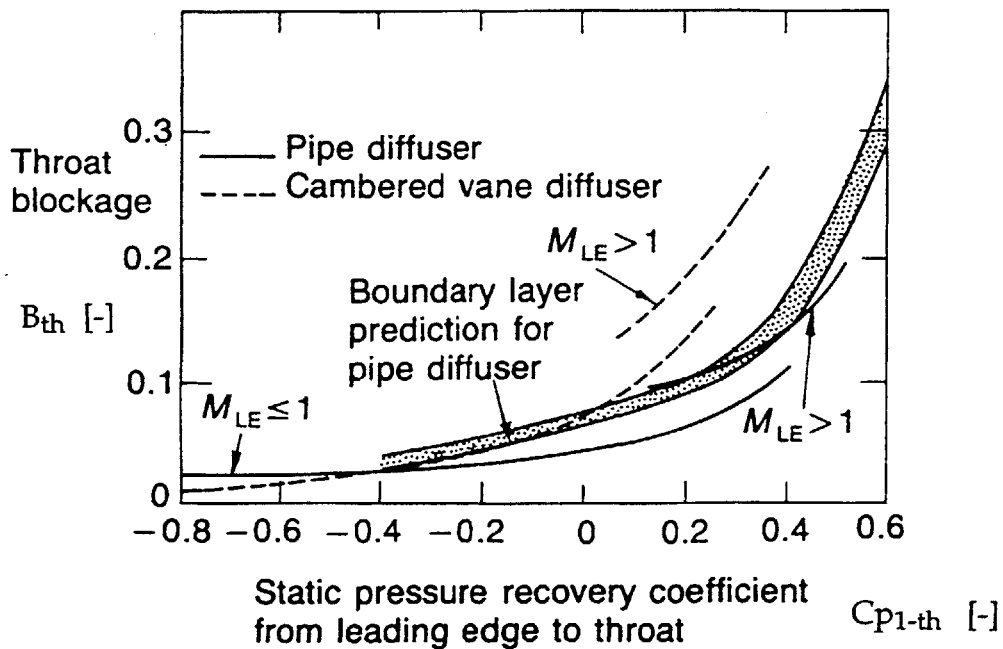


Figure A 4.2 Correlations of throat blockage, B_{th} , versus pressure recovery from vane leading edge to throat, C_{p1-th} . M_{LE} refers to Mach number at vane leading edge (Kenny [1972])

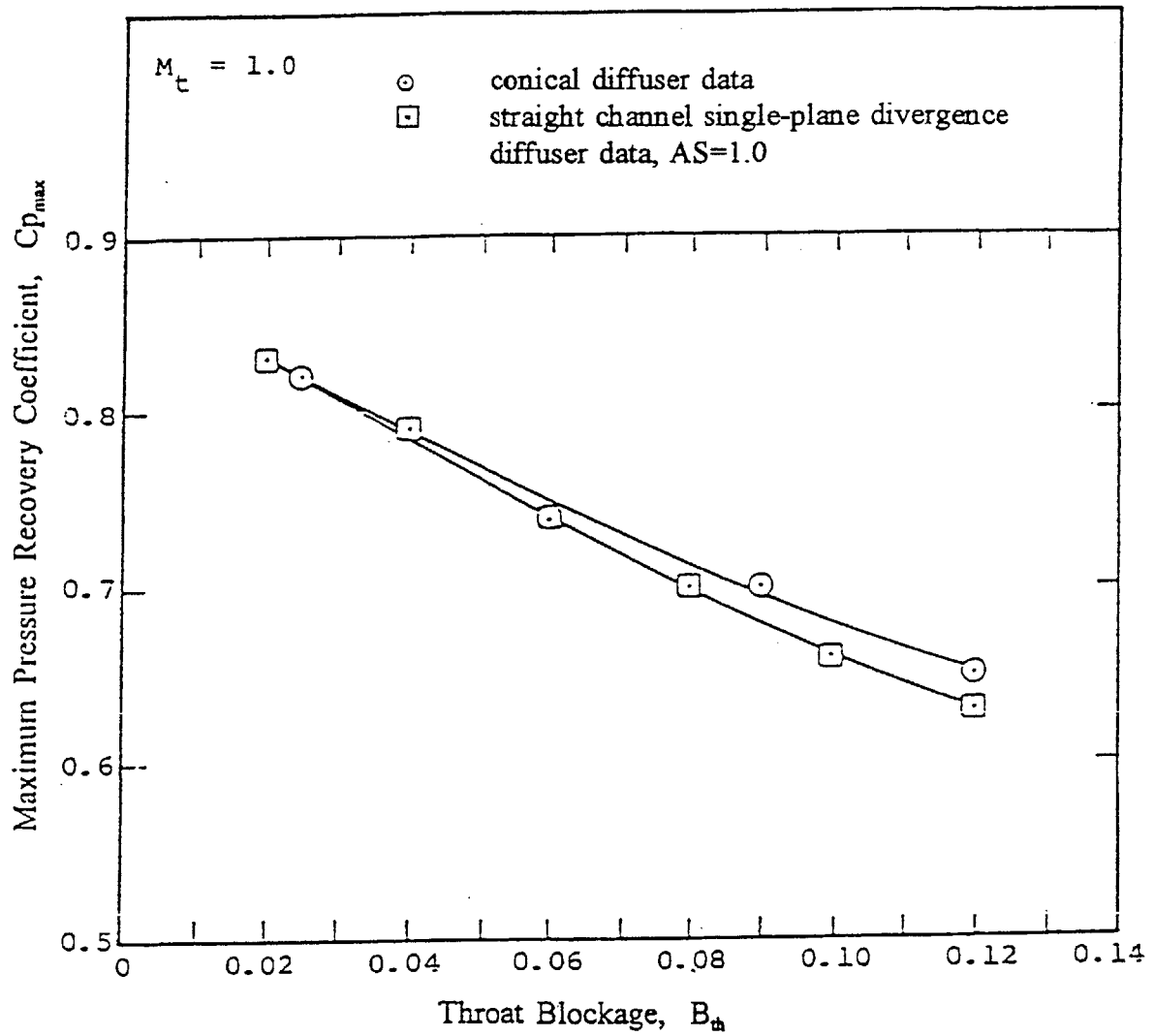


Figure A 4.3 Maximum pressure recovery of conical and square throat, two dimensional diffusers versus blockage (Runstadler et al. [1975])

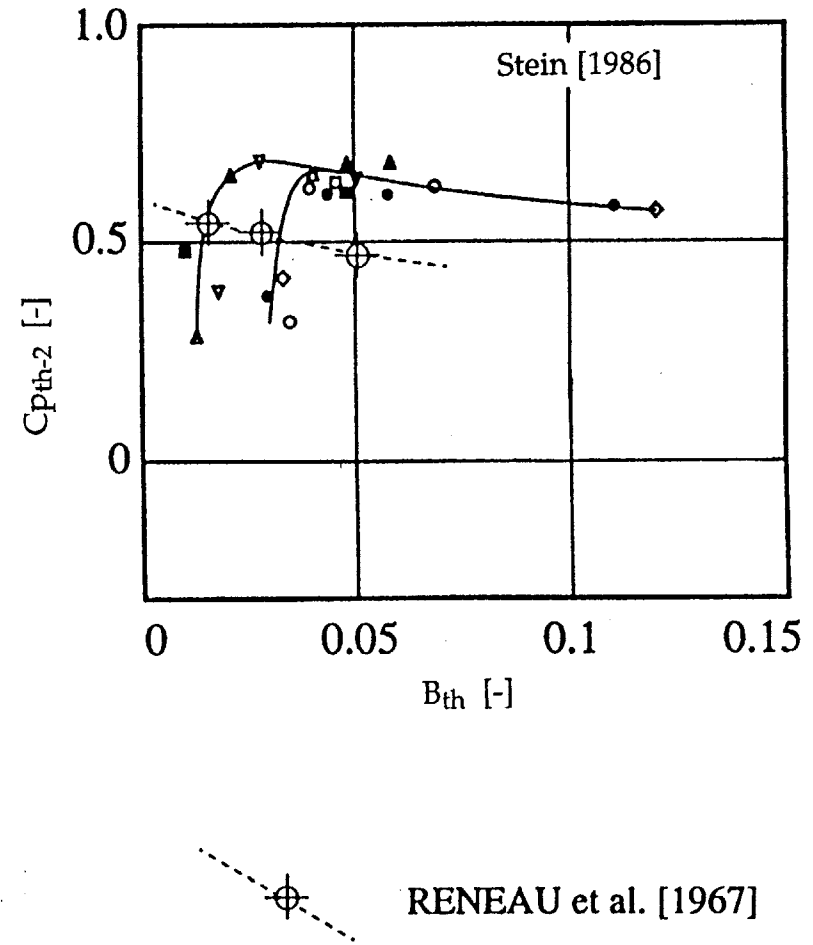
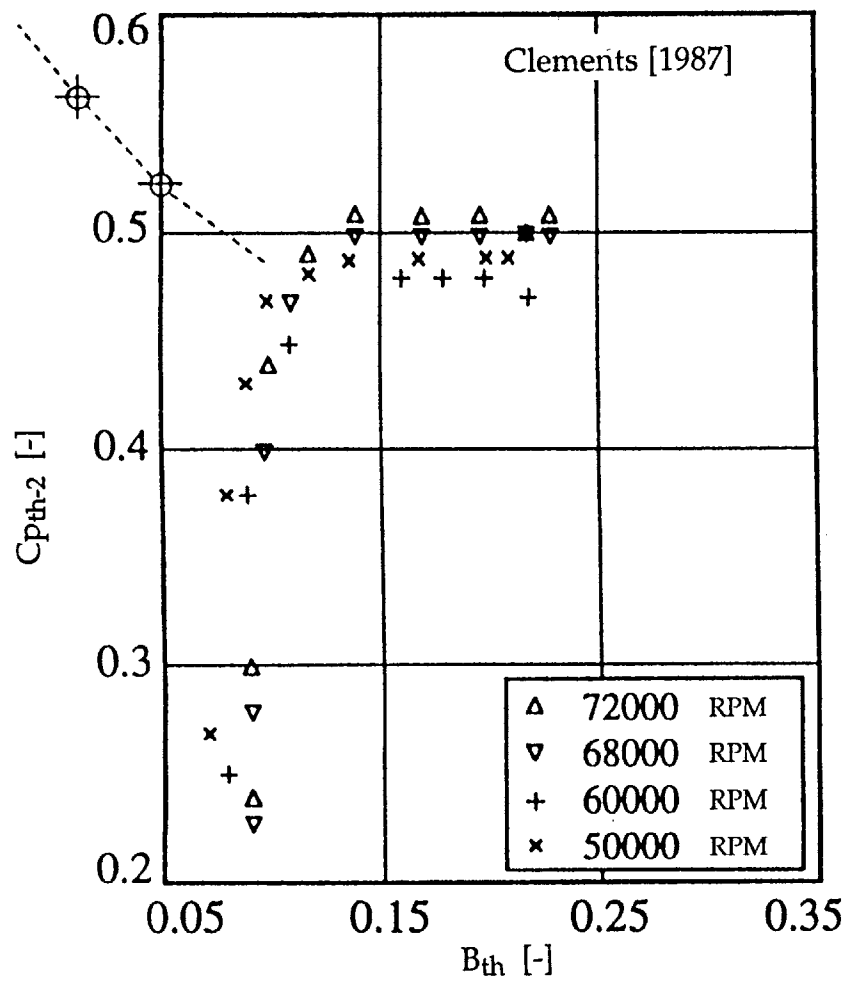


Figure A 4.4 Channel diffuser pressure recovery, $C_{p_{th-2}}$, versus throat blockage, B_{th} , from (a) Clements [1987] and (b) Stein [1986], compared with single channel diffuser data of Reneau et al. [1967] (from Hunziker [1993])

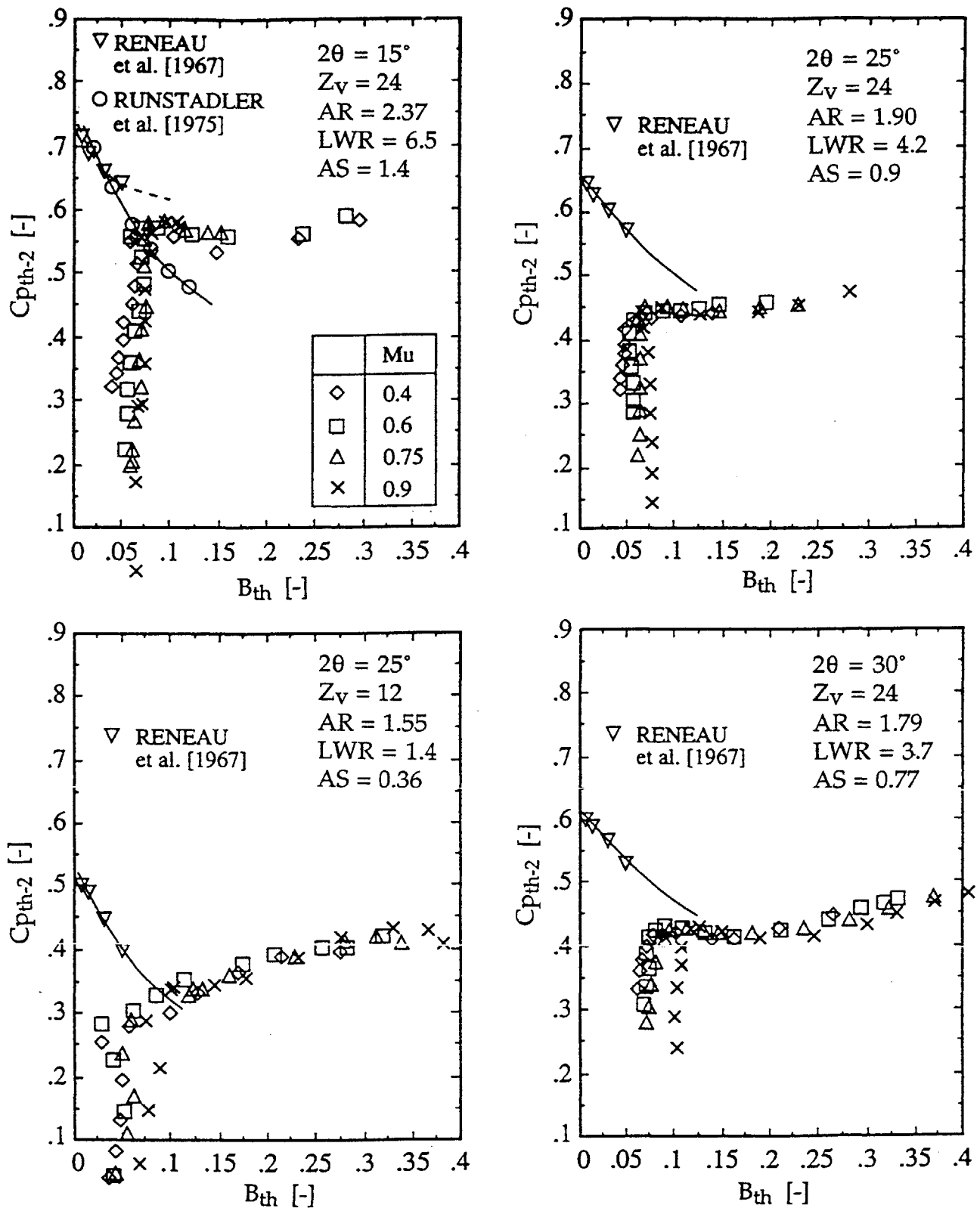


Figure A4.5 Channel diffuser pressure recovery, $C_{p_{th-2}}$, versus throat blockage, B_{th} for different cambered vane diffuser geometries, compared with single channel diffuser data from Reneau et al. [1967] and Runstadler et al. [1975]. Mu refers to Mach number at impeller exit (Hunziker [1993])

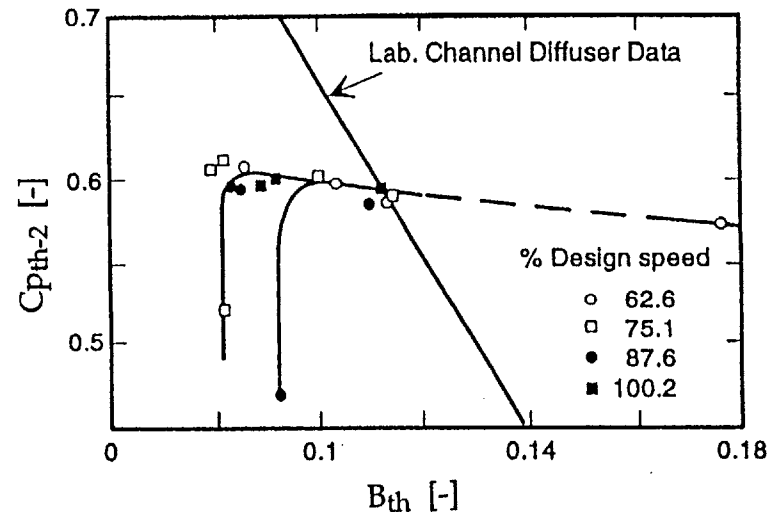
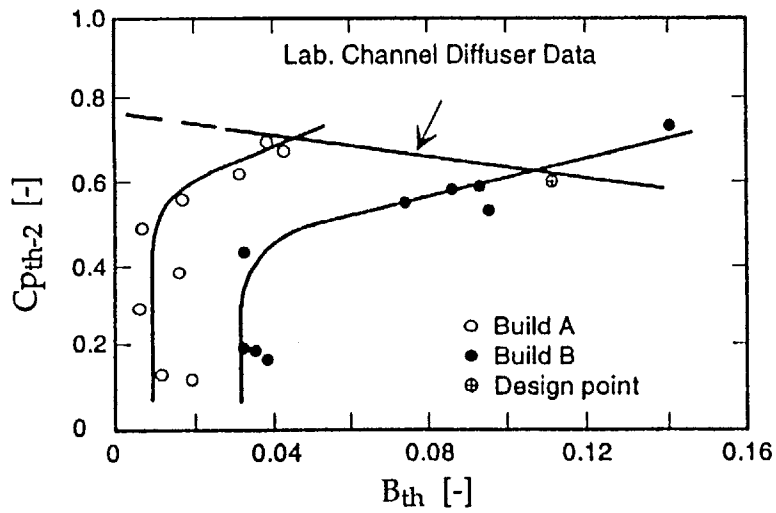
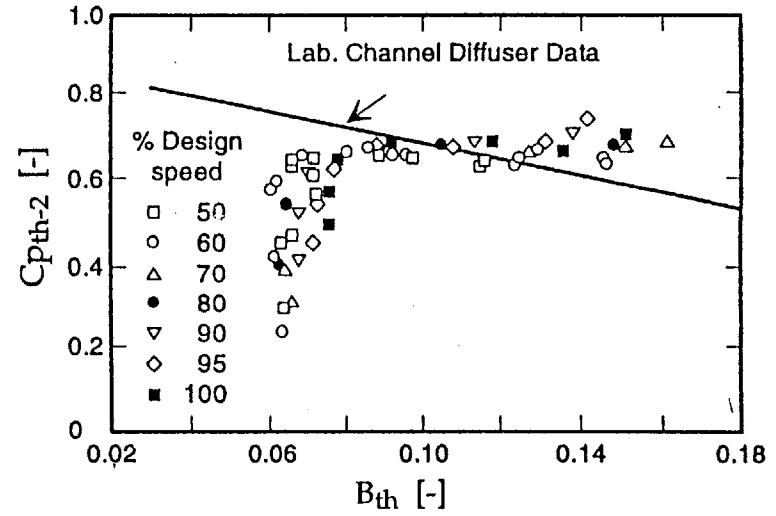
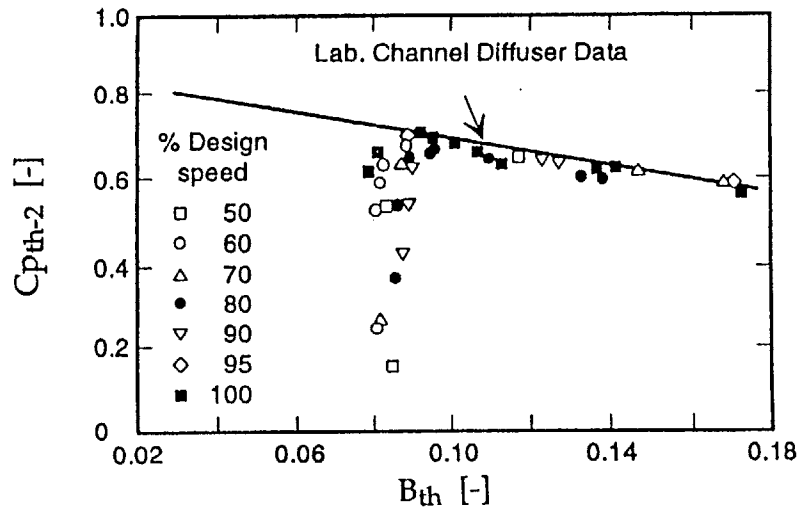


Figure A 4.6 Channel diffuser pressure recovery, $C_{p_{th-2}}$, versus throat blockage, B_{th} for different design cases, builds and vaned diffusers, compared with single channel diffuser data (Japikse & Osborne [1986b])

Straight Channel Diffuser Throat Blockage versus Pressure Recovery from Diffuser Leading Edge to Throat

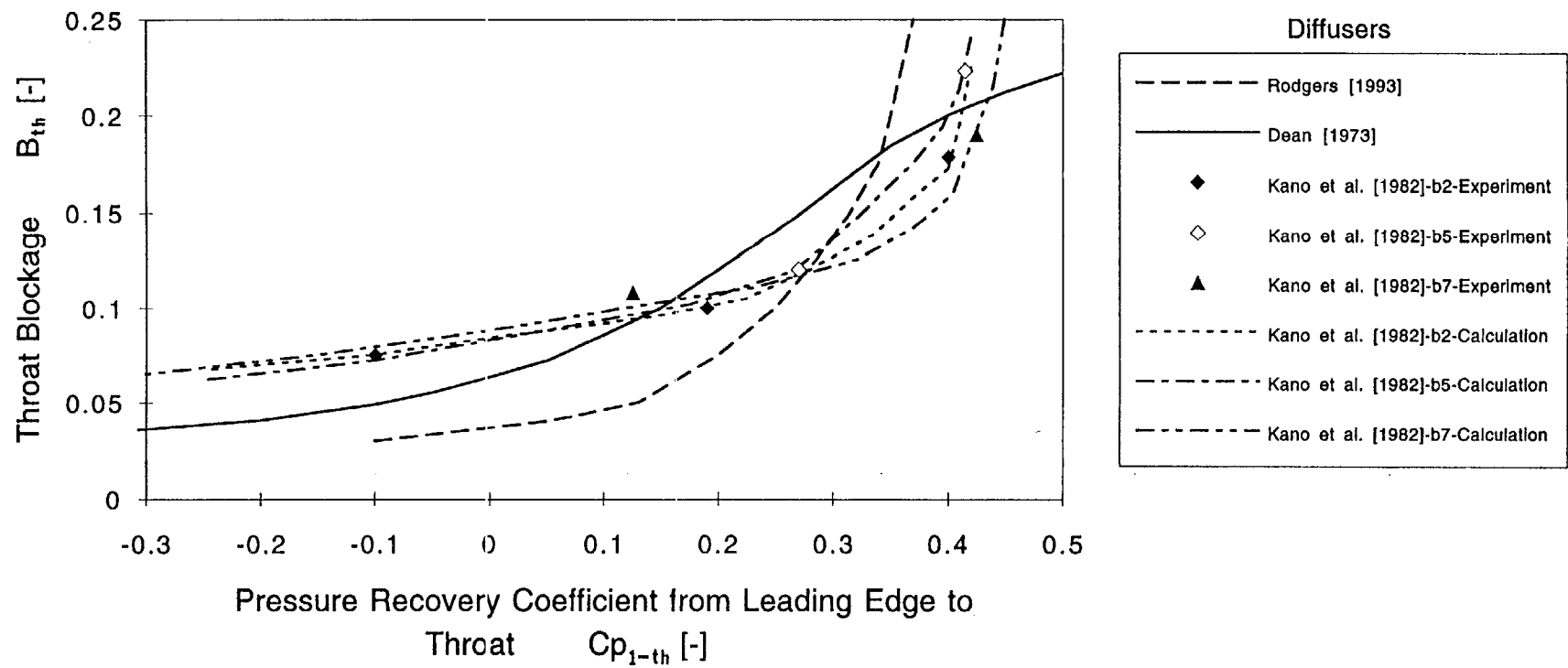


Figure A 4.7 Correlations of throat blockage, B_{th} , versus pressure recovery from leading edge to throat, Cp_{1-th} , for different straight channel diffusers

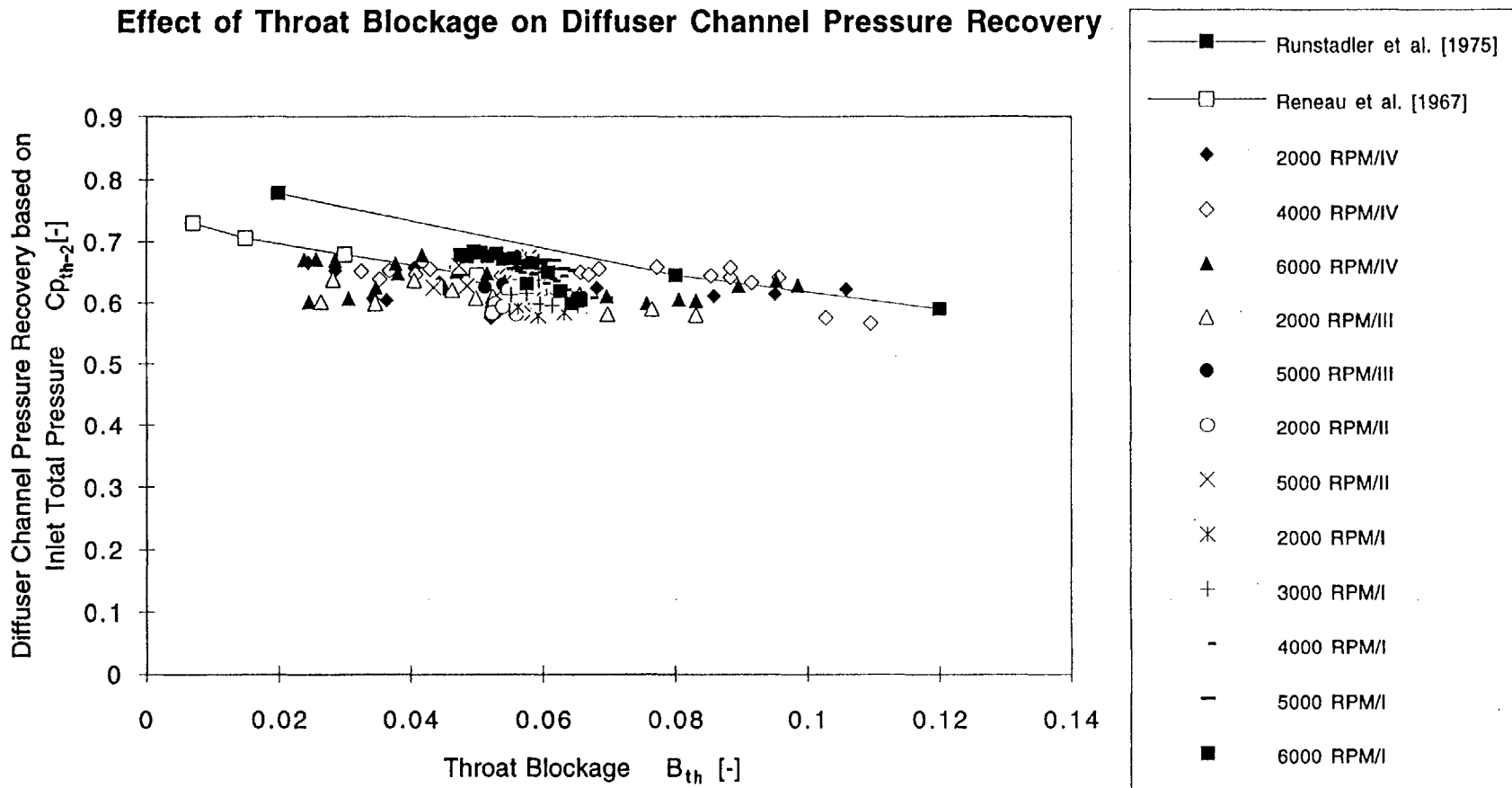


Figure A 4.8 Straight channel diffuser channel part pressure recovery, $C_{p_{th-2}}$, based on diffuser inlet total pressure versus throat blockage, B_{th} , for different corrected impeller speeds and inlet distortion levels, compared with single channel diffuser data from Reneau et al. [1967] and Runstadler et al. [1975]

Effect of Throat Blockage on Diffuser Channel Pressure Recovery

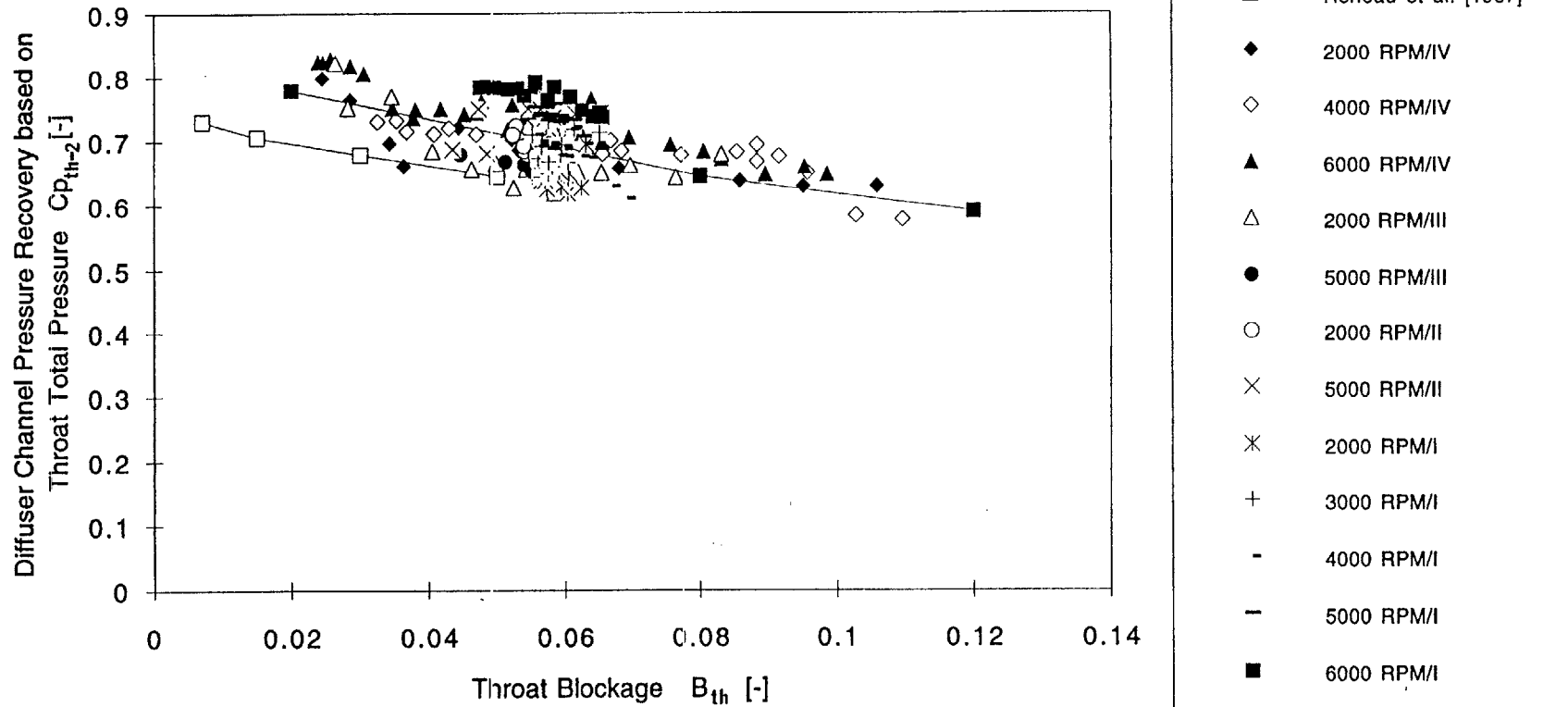


Figure A 4.9 Straight channel diffuser channel part pressure recovery, $C_{p_{th-2}}$, based on computed throat total pressure versus throat blockage, B_{th} , for different corrected impeller speeds and inlet distortion levels, compared with single channel diffuser data from Reneau et al. [1967] and Runstadler et al. [1975]

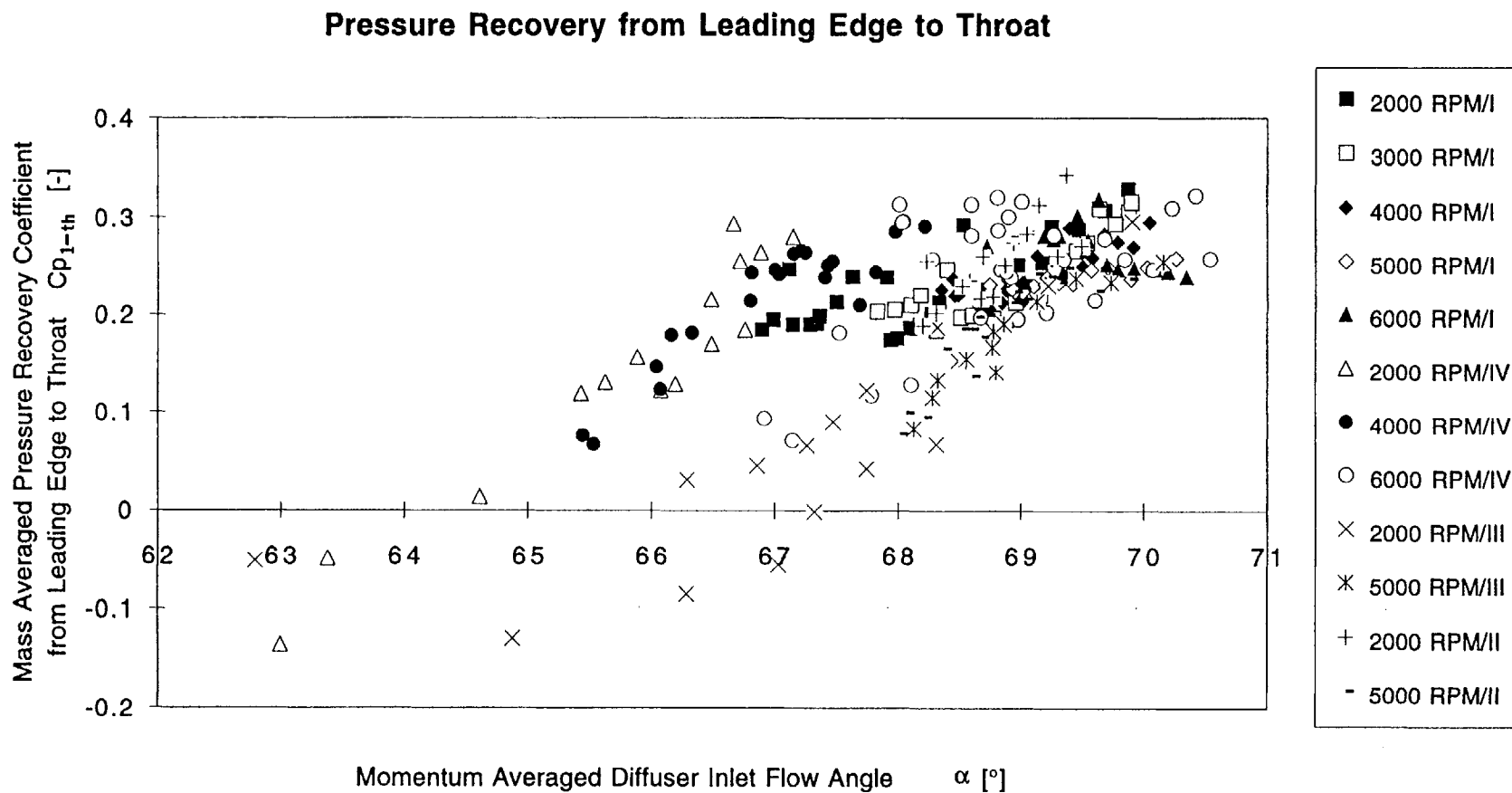


Figure A 4.10 Mass averaged straight channel diffuser pressure recovery from leading edge to throat, C_{p1-th} , as a function of momentum averaged diffuser inlet from angle, α , for different corrected impeller speeds and inlet distortion levels

Appendix 5

Static Pressure Distribution in Quasi-Vaneless Space

In order to analyze the flow field of the diffuser inlet region in more detail, additional wall static pressure taps were located in the quasi-vaneless space of one diffuser channel. The quasi-vaneless space data presented here, consist of static pressure measurements from the diffuser leading edge radius to the throat. The location of the quasi-vaneless space static pressure taps is shown in Figure 2.5.

The static pressure distribution in the quasi-vaneless space for the straight channel diffuser is plotted in Figure A5.1, for different corrected impeller speeds (or inlet Mach numbers) and inlet flow angles, which cover the operating range of the diffuser from rotating stall onset to maximum throttle valve opening. In Figure A5.1 only the data without air injection-suction are shown. The static pressure measurements in the quasi-vaneless space are represented in the form of a local pressure recovery coefficient C_p (as defined in Equation 3.47) as a function of circumferential, θ , and diffuser channel centerline directions. The first column of Figure A.5.1 is for the corrected impeller speed of $N = 2000$ RPM, the second column is for $N = 4000$ RPM and the third column is for $N = 6000$ RPM. The bottom row corresponds to the diffuser inlet flow angles very close to rotating stall onset ($\alpha = 70.2^\circ$ to 70.6°), the second row corresponds to the diffuser inlet flow angles near the diffuser design flow angle ($\alpha = 68.9^\circ$ to 69.2°) and the top row corresponds to the diffuser inlet flow angles for maximum throttle valve openings (or maximum flow rates for a constant corrected impeller speed without using the slave compressor downstream). In this case the diffuser inlet flow angles were smaller than the diffuser design flow angle ($\alpha = 67.8^\circ$ to 68.3°)

The main conclusion of Figure A5.1 is that the wall static pressure distribution in the quasi-vaneless space of the straight channel diffuser is rather a function of diffuser inlet flow angle than the impeller speed (or Mach number). At the diffuser leading edge radius the pressure loading or the static pressure distribution between suction and pressure sides of the diffuser channel changes as the inlet flow angle increases with reduced mass flow. This behavior can be best observed for the high speed case of $N =$

6000 RPM (third column), where there is a reversal of loading at the diffuser leading edge radius from maximum throttle valve opening to rotating stall threshold.

Negative values of C_p means no pressure rise or the acceleration of the flow. For high inlet flow angles near rotating stall there is a strong gradient between suction and pressure sides of the diffuser channel at the diffuser leading edge radius. The maximum pressure recovery at the throat is achieved for operating points near rotating stall onset (bottom row) and the minimum pressure recovery value at the throat is observed for operating points corresponding to maximum valve opening (top row).

The wall static pressure distribution in the quasi-vaneless space for measurements with air injection-suction is not presented for the straight channel diffuser. The reason for this is that the wall static pressure distributions in quasi-vaneless space for the cases with air injection-suction were not distinguishably different from the cases without air injection-suction. An example is given for the previously investigated discrete passage diffuser in Figure A5.2, which compares the distribution of the local static pressure recovery coefficient in the quasi-vaneless space at the rotating stall threshold for three corrected impeller speeds. Here 'Undistorted' indicates measurements without air injection-suction and 'Distorted' indicates measurements with air injection-suction. The shapes of the static pressure distributions are very similar for with and without air injection-suction cases as illustrated in Figure A5.2.

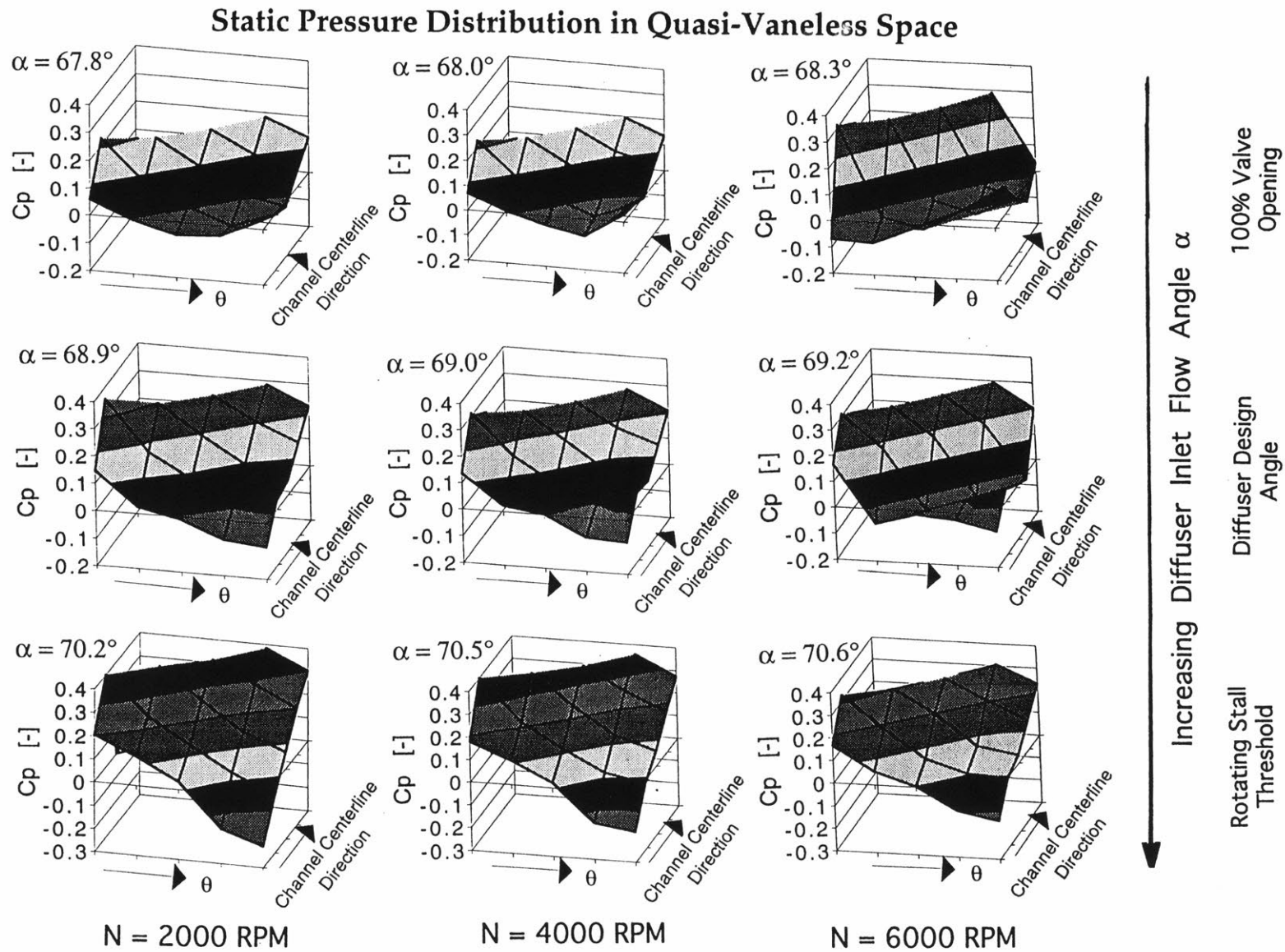


Figure A5.1 Static pressure distribution in the quasi-vaneless space (for straight channel diffuser) for three corrected impeller speeds and increasing diffuser inlet flow angles without injection/suction

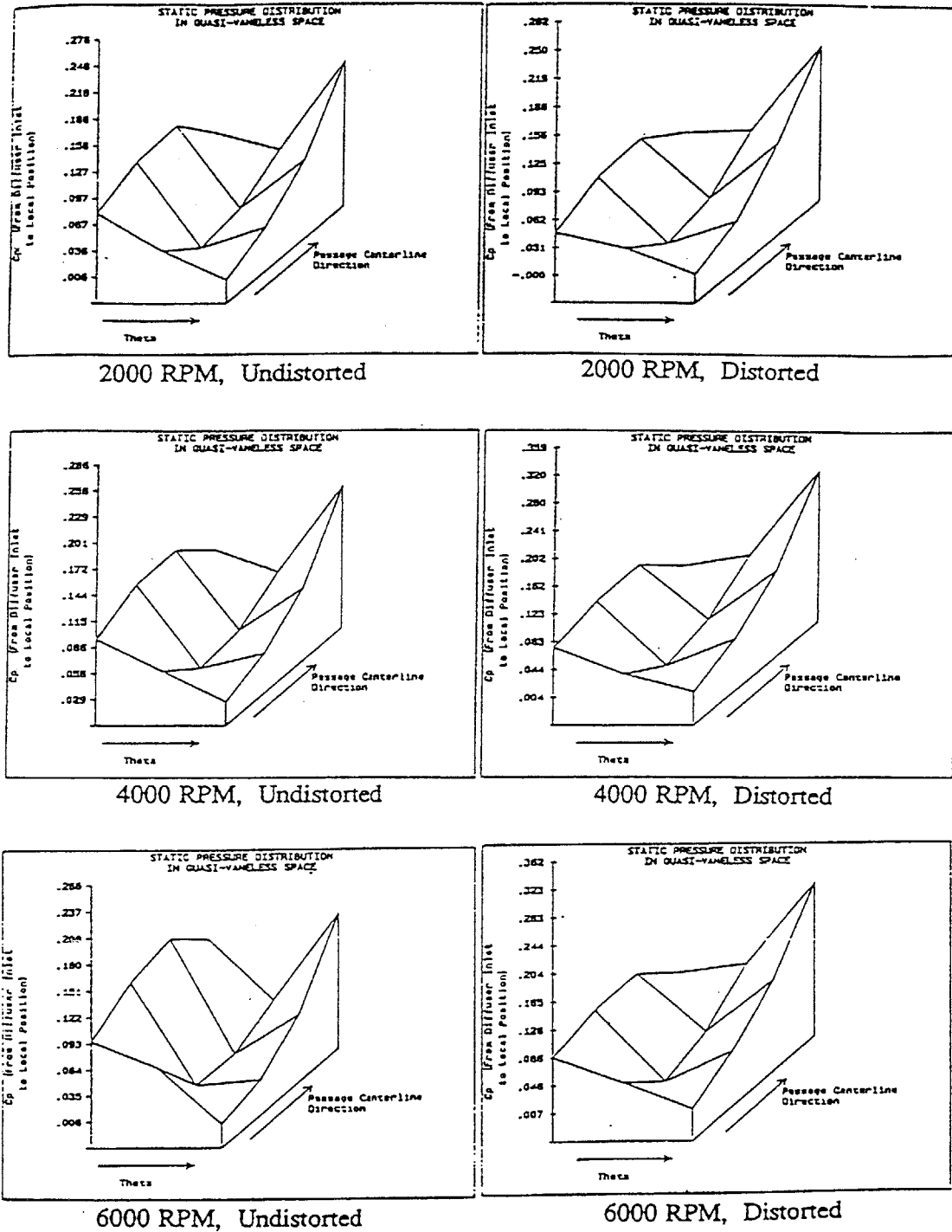


Figure A5.2 Static pressure distribution in the quasi-vaneless space (for discrete passage diffuser) for three corrected impeller speeds at the rotating stall threshold with undistorted (without injection/suction) and distorted (with injection/suction) inlet flow field